OPTIMISATION OF HIGH VOLTAGE ELECTRICAL SYSTEMS FOR AEROSPACE APPLICATIONS

A THESIS SUBMITTED TO THE UNIVERSITY OF MANCHESTER

FOR THE DEGREE OF DOCTOR OF PHILOSOPHY

IN THE FACULTY OF ENGINEERING AND PHYSICAL SCIENCES

2011

By

Ilias Christou

School of Electrical and Electronic Engineering

TABLE OF CONTENTS

List of Tables

List of Figures

List of Abbreviations

AC----------*Alternate Current*

AWG----------*American Wire Gauge*

BD----------*Balanced Detection*

CC----------*Cable to Cable*

Cc----------*Cross correlation*

CEF----------*Calculated Electric Field*

CF----------*Correction Factor*

CG----------*Cylindrical Ground*

CV----------*Cable Voids*

DC----------*Direct Current*

FEA----------*Finite Element Analysis*

GP----------*Grounded Plane*

HP----------*High Pressure*

Ku+ve----------*Kurtosis of Positive Half Cycle*

Ku-ve----------*Kurtosis of Negative Half Cycle*

LP----------*Low Pressure*

MEA----------*More Electric Aircraft*

PCB----------*Printed Circuit Board*

PD----------*Partial Discharge*

PDEV----------*Partial Discharge Extinction Voltage*

PDIV----------*Partial Discharge Inception Voltage*

RMS----------*Root Mean Square*

RR----------*Repetition Rate*

SD----------*Straight Detection*

SMEF----------*Simulated Electric Field*

SOV----------*Safe Operating Voltage*

SOV_{CC}----------*Safe Operating Voltage based on a Cable to Cable Airgap Discharge*

SOV_{CG}----------*Safe Operating Voltage based on a Cable to Ground Airgap Discharge*

$SOV_{TGAirgap}$----------*Safe Operating Voltage based on a Trace to Ground Airgap Discharge*

SOV_{TGVoid}----------*Safe Operating Voltage based on Trace to Ground Void Discharge*

SOV_{TTVoid}----------*Safe Operating Voltage based on Trace to Trace Void Discharge*

SOV_{CV} *or* SOV_{Void}----------*Safe Operating Voltage based on a Void Discharge*

STDEV----------*Standard Deviation*

Sk+ve----------*Skewness of Positive Half Cycle*

Sk-ve----------*Skewness of Negative Half Cycle*

TGAirgap----------*Trace to Ground Airgap Discharge*

TGVoid----------*Trace to Ground Void Discharge*

TTVoid----------*Trace to Trace Void Discharge*

TW----------Twisted Wire

UB----------Unscreened Cable with Added Braid

List of Symbols

α = *Townsend's first ionization coefficient*

α_T = *Temperature dependency coefficient*

γ_E = *Field dependency coefficient*

γ = *Townsend's secondary ionization coefficient*

$tan\ (\delta)$ = *Dissipation factor*

ε_o = *Permittivity of free space* = $8.85418782 \times 10^{-12}$ ($m^{-3}\ kg^{-1}\ s^4\ A^2$ *or* Fm^{-1})

ε_r = *Relative Permittivity of the insulation material*

$\varepsilon_{1,2}$ = *Relative permittivity in insulation layer 1 and 2 respectively*

ε_{r1}, ε_{r2} = *Relative permittivity of insulation for cable 1 and cable 2 respectively*

$\varepsilon(r)$ = *Relative permittivity as a function of the radius in the insulation layers*

η = *Electron attachment coefficient*

θ =*Temperature (K or* ^oC)

$\Delta\theta$ = *Temperature difference (K or* ^oC)

K = *Electric field enhancement factor*

λ = *Factor relating* i_{TB} *(insulation thickness between trace) and* i_{TT} *(insulation thickness between traces)*

λ_e = *Mean free path of an electron (m)*

μ_e = *Electron mobility, also noted as "b", (* $m^2V^{-1}s^{-1}$)

ρ = *Resistivity (Ωm)*

ρ_o= *Resistivity of insulation when temperature coefficient = 0 (Ωm)*

ρ_s = *Free surface charge per unit area (surface charge density)*

ρ_T =*Thermal resistivity* (KmW^{1})

$\rho(r)$ = *Space charge density* (Cm^{-3})

σ = *Conductivity* (Sm^{-1})

τ (= RC) = *Time constant of the charging voltage across the cavity*

φ = *Phase angle* (^{o})

C = Capacitance of insulation (F)

C_b = *Capacitance in series with the cavity (F)*

C_C = *Capacitance of the cavity (F)*

CEF = Calculated electric field (Vm^{-1})

CF = Ratio of simulated electric field to calculated electric field (SMEF/CEF)

CSA = Cross sectional area (m^2)

c= Mean thermal velocity (ms^{-1})

D = Electric displacement (Cm^{-2})

d = Airgap distance (m)

d_{WW} =*Clearance/Shortest distance between two cables in duct (m)*

d_{WG} =*Clearance/Shortest distance between cables and the duct (m)*

E = Electric field (Vm^{-1})

E_i = *Electric field within the insulation material* (Vm^{-1})

E_0 = *Peak electric field* (Vm^{-1})

E_c = Electric field through a cavity in the insulation (Vm^{-1})

E_α = (Vm^{-1})

$E_{(1,2)}$ = Electric field in Insulation layer 1 and 2 respectively (Vm^{-1})

E_V or E_{Brk} = Electric field causing breakdown as from Paschen's Law data (Vm^{-1})

E_{Void} = Electric field in the void (Vm^{-1})

e = Electronic charge = $1.60217646 \times 10^{-19}$ (C)

f = Frequency (Hz)

f_{crit} = Critical frequency (Hz)

f_{PD} or RR = Discharge repetition rate (1/min or 1/s)

$fract_{(Vd)}$ = Fraction of the voltage across the airgap

G & F = Theoretical constants for air ($G = 11335x10^{22}$ Vm^2 & $F = 378.9x10^{22}$ m^2)

h = Planck's constant (6.626068×10^{-34} m^2 kg / s)

$h(q)$ = Probability density of discharges (1/pC)

I = Current (A or Amps)

I_o = Initial current before any ionization or de-ionization occurs (A or Amps)

I_U = Percentage of Current Utilisation for each AWG conductor size (%)

i =Insulation thickness (mm)

i_1, i_2 = Insulation thicknesses of cable 1 and cable 2 respectively (mm)

i_{TB} = Insulation thickness between trace and outer insulation – airgap boundary (mm)

i_A = Total cross sectional area of insulation as in the three phase round conductor duct system (mm^2)

L = Void size (mm)

m = Mass (kg)

N = *Number density of molecules* (m^{-3})

P_{NEW} = *Adjusted pressure (Pa)*

P_{OLD} =*Initial pressure (Pa)*

P = *Pressure (Pa)*

P_{MAX} = *Maximum power transfer*

P_f = *Factor representing how many small duct systems of certain AWG conductor size are required to achieve the same power as a bigger duct system*

PCB_t = *PCB thickness (mm)*

PCB_W = *PCB width (mm)*

Q = *Charges per unit area* (qm^{-2})

Q_m = *Momentum transfer cross section* (m^2)

q_{+ve} = *Charge of the positive ion* ($1.6x10^{-19}$ *C)*

q = *Discharge magnitude (pC)*

$\overline{q_{suc/pre}}$ = *Average magnitude of the successor/predecessor discharge (pC)*

R_C = *Conductor resistance (Ω or Ohms)*

R_b = *Resistance of the insulation in series with the cavity (Ω or Ohms)*

R_C = *Surface resistance of the cavity (Ω or Ohms)*

R_o = *External radius of Insulation (mm)*

R_i = *Internal radius of Insulation (mm)*

R, R_C, R_S *or* r = *Conductor radius (mm)*

R_{pos} = *Void Position radius from the conductor centre to the outer insulation surface (mm)*

$(R-r) = i$ =*Insulation thickness (mm)*

r_C = *Cable radius (mm)*

r_{Duct} = *Duct radius (mm)*

r_{WG} = *Clearance/ Shortest distance between cables and duct (m)*

r_1, r_2 = *Internal and external cable radius respectively (mm)*

S = *Insulation thickness (mm)*

SOV_{CG} = *Safe operating voltages for cable to ground (CG) PD (V)*

SOV_{CV} = *Safe operating voltages for cable void (CV) PD (V)*

SOV_{CC} = *Safe operating voltages for cable to cable (CC) PD (V)*

SOV_{RMS} = *RMS safe operating voltage for the cable system (V)*

SOI_{RMS} = *RMS safe operating current (V)*

SOV_{peak} = *Peak single phase safe operating voltage for the cable system (V)*

$SOV_{TGAirgap}$ = *Safe operating voltage based on PCB trace to ground airgap PD (V)*

SOV_{TGVoid} = *Safe operating voltage based on PCB trace to ground void PD (V)*

SOV_{TTVoid} = *Safe operating voltage based on PCB trace to trace void PD (V)*

SOV_{Void} = *Safe operating voltage based on Trace to trace or trace to ground void PD (V)*

$SMEF$ = *FEA simulated electric field* ($kVmm^{-1}$)

θ_A = *Ambient temperature (K or* ^oC)

T = *Duct radius (mm)*

$(T - R) = d_{WG}$ = *Cable to ground airgap distance (mm)*

T_{R_Total} = *Total thermal resistance: insulation + air* (KmW^{-1})

T_R = *Thermal resistance* (KmW^{-1})

t_R = *Recovery time (s)*

T_w = *Trace width (mm)*

T_t =*Trace thickness (mm)*

t_L = *average statistical time lag, the time it takes for a PD initiating electron to appear*

(T-R) = d_{WG} =*shortest airgap distance between cable and duct (mm)*

$\overline{\Delta t_{suc/pre}}$ = *Average time in seconds to the successor/predecessor discharge (s)*

$T_{R\_Insulation}$ = *Thermal resistance of insulation* (KmW^{-1})

T_{R_Air} = *Thermal resistance of air* (KmW^{-1})

V_{brk} = *Breakdown voltage of air (V)*

$V_{Inception}$ = *Supply voltage which is required to ignite PD (V)*

V or V_S = *Supply voltage (V)*

V_G = *Volume* (m^3)

V_{min} = *Minimum breakdown voltage (V)*

V_r = *Residual voltage across the cavity after a PD (V)*

V_I = *Voltage across the cavity at which PD is initiated (V)*

V_{con} = *Maximum voltage that would be seen across the void if no PD occurred (V)*

V_d = *Voltage across airgap (V)*

V_i = *Voltage across insulation (V)*

V_{inst} = *Instantaneous voltage (V)*

Vi_{TT} =*PD Inception voltage between traces (V)*

Vi_{TB} = *PD Inception voltage between trace and ground (V)*

W_C = *Conductor power losses per unit length* (Wm^{-1})

$W_{dielectric}$ = *Power dissipated in the dielectric per unit length* (Wm^{-1})

ΔW = *Average energy gained between collisions (J)*

W_e = *Drift velocity* (ms^{-1})

Abstract

Increased electrical power demands are being experienced on the new generation of aircraft due to an increased reliance on electrical technology of systems such as air conditioning, de-icing systems and electrical flight control actuation. Distribution of power at higher AC and DC voltages is therefore now being seen in modern aircraft to avoid the penalties incurred due to high cable weights. Voltages have increased past the minimum of Paschen's law resulting in a risk that life limiting partial discharge (PD) damage can occur in the insulation systems. This thesis uses a theoretical analysis backed by PD experimental results to investigate the optimal operating voltage of a cabling system. In addition, it proposes a methodology for optimizing the operating voltage level based on an analysis of the power carrying capability of cabling within a fixed and a non-fixed volume system and the derivation of the cable weight as a function of voltage. Furthermore the power carrying capability of a certain round cable system is compared with an insulated flat conductor system as in a printed circuit board (PCB). An initial assessment has been carried out to determine whether more power can be delivered via insulated flat solid conductors as in a PCB, instead of using round cables. The reason why there is a need to investigate this aspect, is because using new PCB technology can offer several advantages over traditional cabling harnesses. The work done has shown that the optimal operating point (e.g. maximum power to weight ratio) for an aircraft power system, does not improve after certain voltage levels. A tradeoff between cable weight and power transfer is required and furthermore the use of DC systems can result in higher power transfers than conventional three phase/400Hz AC systems. The PCB maximum power transfer assessment has also shown that insulated flat conductor systems can offer higher power transfer efficiencies. In addition, experimental AC and DC PD tests on certain unscreened aerospace cables (laid out in different configurations), have shown that the theoretical analysis employed to determine cable safe operating voltages gives conservative results.

Declaration

No portion of the work referred to in this thesis has been submitted in support of an application for another degree or qualification of this or any other university or other institute of learning.

Copyright

Acknowledgements

Bare acknowledgements are inadequate but I wish to express my appreciation to Ian Cotton, Professor of High Voltage Technology at The University of Manchester, for his guidance and assistance without which the production of this report would have been impossible. I also wish to thank Rolls-Royce plc, in particular Dr. Graham Bruce, Mr. Mark Husband and Hew Edwards of the Strategic Research Centre (SRC) Derby, for their helpful support and cooperation during the work that is associated with this report.

Finally but not least I would like to thank seven very good friends, Dr. Antwnios Tzimas, Dr. Sinisa Durovic, Dr. Kostas Kopsidas, Dr. Sanjay Bahadoorsingh, Dr. Vidyadhar Peesapati, Mr. Riccardo Giussani and Mr. Mathaios Panteli, for their helpful encouragement throughout the period of my PhD.

Chapter 1

The More Electric Aircraft

This chapter describes the idea of the more electric aircraft giving a historical overview of the advancement of operating voltage levels used in aircraft electrical power systems. The reasons why the operating voltage levels have increased throughout the years and the accompanied issues are discussed, together with methods used in the past to reduce aircraft cabling weight. The factors that need to be taken into account for the selection of an optimal voltage level are listed and explained.

1.1 Introduction

It is now clear that the aircraft industry should look towards more advanced electrical systems to reduce the overall weight of an aircraft and consequently minimize fuel consumption and operational costs [1]. Relevant research indicates that in order to achieve the aims of MOET (More Open Electrical Technologies) the power optimized aircraft must be redesigned at a system level. One of the major issues in this respect is the re-evaluation of aircraft operating voltages to reduce cabling weight. Therefore the optimal transmission voltage in cables has to be determined and this must be done in coordination with the capabilities of all aircraft equipment. Higher voltages affect the weight of cable systems, the volume they occupy and also the size and design of the connected equipment, since extra insulation is required to maintain the voltage level increase. This suggests that aircraft electrical system optimization has to be performed taking into account not only electrical but also mechanical and civil requirements and constraints.

1.2 History of Aircraft Electrical Systems

Historically increases in aircraft power demand lead to the increase in the operating voltage of aircraft electrical systems. However early aircraft engines generated power at low voltage as this provided a safe and reliable means of energy transport. For example the total power produced in aircrafts in year 1936 was 1425 Watts and was delivered from two 50 Amp and 14.25 VDC generators [2]. Load demand increased through the years and in year 1946, new standard generators were introduced on aircrafts that provided 28 VDC [2]. Eventually three phase systems of 115/200 VAC at 400 Hz were adopted as they offered a lighter electrical system. These three phase systems are still used in commercial and military aviation today. Following a further increase in power demand the system voltage was increased in year 1980 to 270 VDC for the military providing an even lighter solution compared to the 400 Hz system [3]. Finally in modern commercial aircrafts different load applications require the use of different voltage levels that have been used in the past, for example the 28 VDC, 115 VAC/400Hz and 270 VDC.

1.3 Voltage Increases and Accompanied Issues

Coming back to the reason why voltages have increased through the years, a certain amount of current and hence power can be transferred along the cables depending on conductor size. *"For a 28 VDC system the maximum current per channel that can be carried is 400 Amps which gives a power transfer of about 12 kW whereas a larger commercial aircraft requires power in the range 20 - 90 kVA per channel and even more"* [3]. The 28 VDC systems cannot cope with this higher power demand. Moving to More-Electric-Aircrafts (MEA) [1] will offer a better weight solution, whilst increasing the power demand to the drive in order to eliminate heavy mechanical systems such as air-starter pipe work and hot-air anti-ice systems. The replacement of such systems with electrical alternatives will reduce aircraft weight. There are also clear environmental benefits in relation to the increased use of electrical power within the aircraft and the removal of the alternative mechanical based systems in terms of aircraft fuel consumption

over its lifetime. The difference between a conventional and a more electric aircraft can be observed in Figure 1.1 below.

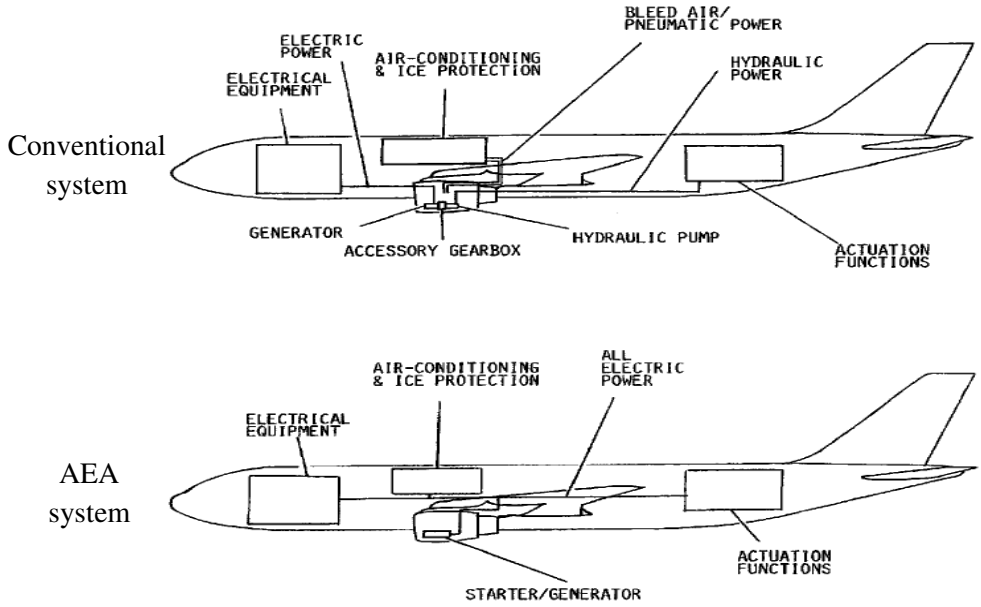

Figure 1.1: Conventional and All Electric Aircraft (AEA) comparison [61]

As it can be observed from Figure 1.1, the accessory gearbox and the hydraulic pump are not present in an AEA system. The hydraulic power driving different actuation functions, as well as bleed air/pneumatic power driving air conditioning and ice protection, have been replaced with all electric power.

However more power demand would mean that larger currents and thus larger conductors will be needed. Even though heavy mechanical and pneumatic parts will be removed from the system, heavier cables will be used and this might counterbalance the reduction in weight. One solution would be to increase the voltage levels and/or the operating frequency to transfer more power around the aircraft, whilst keeping the same conductor sizes and if possible to reduce them. This would lead to an increase in the insulation thickness of cables and the weight of the insulation, triggering an increase in the overall system's volume. These factors in combination with mechanical considerations, limit how much the conductor size can be reduced and thus how much the system voltage can be raised.

Another issue arising with increasing the operating voltage is that "utilisation equipment" has to be redesigned to cope with the new operating voltages and obviate all forms of electrical discharges. These might cause damage to equipment insulation in the long term and even cause immediate failure if insulation breakdown occurs.

Electrical discharges can be disruptive or partial. The former involves the complete breakdown of a gas contained between two conductors having a significant voltage across them. As a result the two conductors are unwittingly joined and a significant current can flow. For this type of event a protective device would be required such as a fuse or a circuit breaker and in the worst case one of the generators would have to be switched off, in order to limit the fault current. An example of where a disruptive discharge can occur is between two uninsulated conductors or between two pins of a connector. In comparison, a partial discharge also occurs between two conductors having a significant voltage across them. However the gas breaks down partially, specifically at a localised region where the electric field is large. Outside this localised region of high electric field, the electric field is reduced below the breakdown field of the gas contained in the gap. Thus, full fault current flow from one conductor to the other is prevented. In this case the system can continue operating normally since very small current flows (partial discharges are usually measured in Pico-coulombs). Examples of where partial discharges can occur are between two insulated unscreened cables installed in a bundle, or in voids or cavities within an insulation material. These types of discharges lead to insulation degradation over time and can cause premature failure of the insulation system. An excellent description of electrical and mechanical modes of failure of aircraft cables can be found in [4, 5].

Currently the 28 VDC and 270 VDC electrical systems that are used in aircraft, offer a relatively safer electrical system as far as electrical discharge (partial discharges) is concerned, since the values are below Paschen's minimum, as it will be explained in this thesis. However these low voltage systems will not be able to cope with MEA's increased power demand. For example the electrical system of the MEA is more likely to consist of two engines, each having two generators and each producing 250 kVA. In addition it would include an APU with another two generators of 225 kVA each. An example is the new Boeing 787 [6]. This means that the total power to be generated for a commercial

aircraft is 1000 kVA excluding the APU generators. At the moment, the "first generation of more electric aircrafts (MEA)" which uses high powers, is Airbus 380 which uses about 415 kVA. Consequently low voltage systems will not be able to cope with these large power demands. The "next generation" MEA like the Boeing 787 and the A350 are using about 1450 kVA and 800 kVA respectively. That is the reason why the generated AC voltage has increased from 115 VAC at 400Hz (currently used in conventional aircrafts), to 230 VAC at 360-800 Hz for the Boeing 787 [6]. This voltage is further rectified using power electronic converters to produce +/- 270 VDC (540 VDC).

As mentioned previously, the operating frequency of the AC system has also increased in order to reduce the weight of the transformers used. However, as a result cable reactance has increased as well. If the power factor is already low due to non linear loads, according to the electrical system design, "*reactive voltage drops become a limitation rather than resistive*" [7].

A comparison of a traditional Boeing aircraft and the new Boeing 787 electrical system can be made by using Figure 1.2.

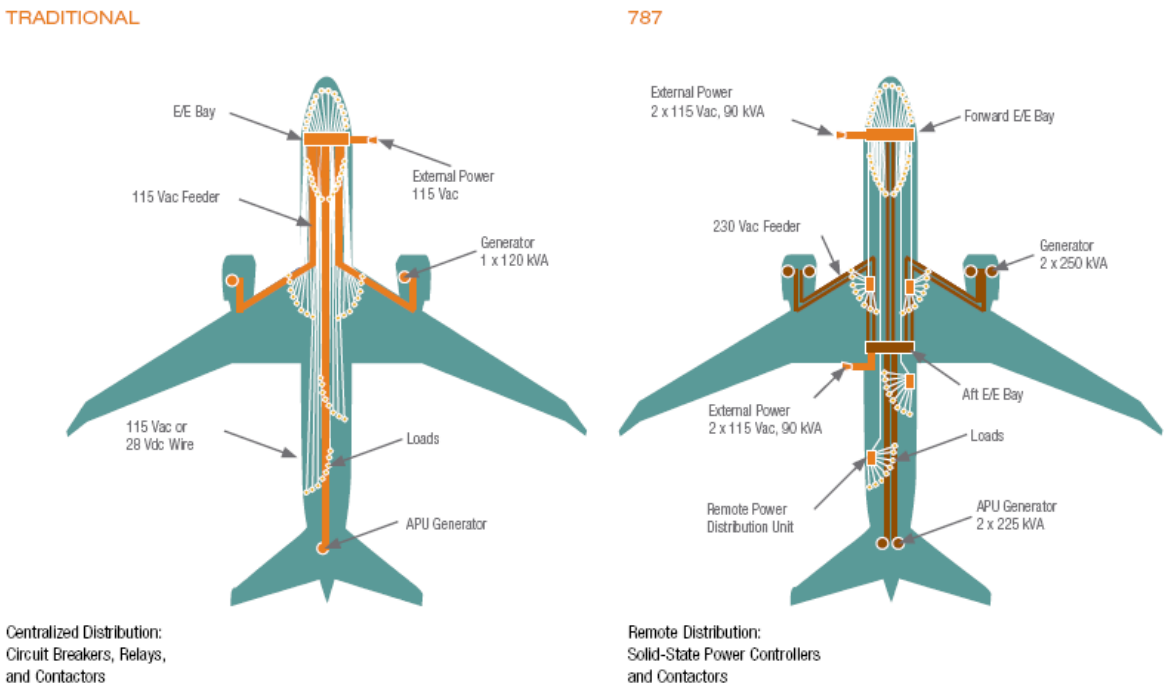

Figure 1.2: Traditional Boeing and 787 Boeing electrical generation and distribution systems [6]

Concluding an increase to higher voltages while welcome in terms of prospective weight savings, must be treated with caution owing to the ability of relatively low voltages to cause electrical discharges at low pressure and high temperatures [8-10]. Therefore an understanding of electrical discharges with respect to their inception and severity within the aircraft environment is essential, since they are extremely important in terms of ensuring safe and reliable operation. According to [11], up to a voltage level of 240 Volts RMS there is no risk of partial discharge *"PD"* (a form of electrical discharge), between cabling and grounded surfaces as well as in cavities in the insulation. Thus the amount of insulation required is determined only by mechanical considerations and "surface discharges" that can cause tracking especially at the connectors' terminals. Nevertheless, the continued use of low voltages is unsustainable as conductor size, transmission losses and weight would continue to increase with increase in load. Moving to higher voltages is unavoidable even though electrical insulation design will become more critical, as this would allow conductor weights and sizes to be dramatically reduced. For voltages higher than the "Paschen's minimum", [11] provides RMS corona inception voltages at different environmental conditions (altitude and temperature). Corona is a type of PD. These conditions affect greatly the optimal transmission voltage as it will be described later on.

1.4 Environmental Conditions

Environmental factors also have an effect on the current rating of cables. The ambient temperature of a cable system might vary from a very low temperature at high altitudes (if the cables are exposed to the outside surrounding atmosphere, approximately -60°C at an altitude of 40,000 feet up to 60,000 feet) [12]), to a high temperature of approximately 400°C (if the cables are installed near electrical systems giving out a lot of heat. An example could be the novel idea of embedded generators installed at the core of an aircraft engine. The cables connecting the generators would be exposed to approximately 400°C). Likewise the pressure might be equal to the atmospheric if the cables are inside the aircraft where the environment is controlled and monitored, or it can be exposed to the outside low pressure atmosphere, or even at relatively high pressures within the fan case of the engine when it is running.

1.5 Optimal Electrical Power Distribution System

Research performed in 1961 [13], examined the use of higher voltages to replace large AWG size conductors with smaller ones, considering the weight, current density, voltage drop and utilisation of cables but neglecting the effect of partial discharges. According to [13], it is stated that after carrying out optimum weight analysis, the voltages to be used are not high enough so that discharge phenomena would become an issue. Based on a specific study case for the historical WF-2 aircraft model, only a third of the total weight of all cables would be affected by increasing the voltage. This is due to the fact that the remaining electrical system was made of cables already being used at their minimum size. This part of the system would remain unchanged since the load would still be the same and an increase in voltage would affect negatively the current utilisation of the cables. Only primary distribution voltages would be changed and a calculation procedure is carried out by the author so as to minimize the reduction in current utilisation and increase in average voltage drop for each cable and to determine cable weight changes with increasing voltage.

A more general research article [14], describes the main factors in selecting the appropriate cable size to be used in an electrical power system. These factors consider the following:

- Ampacity
- Allowable voltage drop
- Short circuit requirements
- Over-current protective devices
- Economic requirements
- Type and design of insulation materials

The information required to determine each factor is listed and explained. Even though a total system analysis, including all the factors listed above, is required to define optimum voltages for use in the aerospace environment, each factor has to be looked at separately. After obtaining a clear understanding of how each factor drives the operating voltage and the weight of the system, an optimal solution can be computed.

Investigating an optimal electrical power transmission system would thus require knowledge of the size, length, voltage drops of cables and equipment connected to it, volume they occupy, frequency of operation, conductor utilisation, power losses, short circuit requirements, aircraft operation data, the surrounding atmospheric environment as well as the economic issues affecting the whole aircraft design.

1.6 Project Objectives

It has to be mentioned that this project was supported by the "Strategic Research Centre of Rolls-Royce plc." The project aims were:

- To calculate the partial discharge inception voltage (PDIV) for different cable sizes using theoretical approximation models. The PDIV has been used to determine the optimal voltage to be used in the MEA.

- To calculate the optimal power transfer based on the current ratings of different AWG conductor sizes obtained from [11]. Each cable has been assumed to be fully utilised according to AS50881. Unlike previous research, specific cable systems are analysed assuming different fixed sized conduits in which the maximum cable size is calculated. For each AWG conductor size the insulation thickness is computed from which the maximum voltage that can be used to avoid partial discharges (PD) is evaluated. By comparing the results for all AWG cable sizes, the best voltage level can be chosen after taking into account all the factors described by [13, 14].

- The development of a reverse methodology to evaluate the required insulation thickness, once the aircraft operating voltage levels are provided.

- To examine the possibility of replacing a round cable system with an insulated flat conductor system, like for example a Printed Circuit Board system (PCB), in an attempt to achieve a higher power transfer. This was done taking into consideration the maximum voltage that can be applied so that no PD occurs.

- To examine experimentally the partial discharge inception voltages (PDIVs) under AC and DC conditions.
- To perform a comparison of the measured PDIV results with the calculated ones using theoretical models.

This study can become the basis for optimal voltage level /insulation thickness selection to be used in future aircraft electrical systems. The thesis begins by carrying out a literature review on partial discharges occurring on aircraft cables.

Chapter 2

Partial Discharges on Aircraft Cable

A partial discharge (PD) is an electrical discharge that partially bridges a gap between a high voltage conductor and a low voltage conductor. What causes these discharges is the localised breakdown of the gas molecules in the gap, due to a significant voltage across it which leads to particle ionization. The voltage causing gas particle breakdown is a function of the pressure and gap distance product. This relationship is described by the famous "Paschen's Law", when the electric field is distributed uniformly between two spherical conductors. A literature review on PD and its effect on aircraft cables are carried out in this chapter.

2.1 Introduction

As it was discussed in Chapter 1 there are two types of electrical discharges. These can be disruptive or partial. This thesis is focused on partial discharges which is actually the localised breakdown of air molecules to form positive and negative ions in which the positive are attracted to a cathode electrode whereas the negative to an anode electrode. Even though there is a temporally charge movement (pulse current), the charges cannot bridge the gap, since the electric field is reduced beyond a certain point. The temporally localised pulses of current flow are a result of the movement of charges and the recombination of negative and positive charges that precede [15]. The magnitude of the supply voltage at which this breakdown of the gas-air (partial discharge) occurs, is called the "inception voltage" and it is stated as 'PDIV' throughout this report.

2.1.1 Different Types of Partial Discharges (PD)

Overall the factors that settle the type of a partial discharge (PD) in a gas and the magnitude of the partial discharge inception voltage (PDIV) are listed below:

- Gas pressure (gas density)
- Electrode shape (conductor, insulation and ground shape)
- Airgap distance (i.e. geometry)
- Polarity of voltage applied
- Type of system (DC or AC conditions and at high / low frequency)
- Impulse voltage
- Cable material properties
- Duration of applied voltage (for how long the voltage is applied on the cable conductor)
- Current ageing state of the cable [16].

Types of partial discharges are such as gaseous discharges, gas-insulator surface discharges, liquid discharges, liquid-insulator interface discharges and solid discharges. This thesis will be focusing on void and gas-insulator surface PD, specifically the ones most likely to occur in an aerospace cable environment. All types of PD are shown below in Figure 2.1 as described by [17].

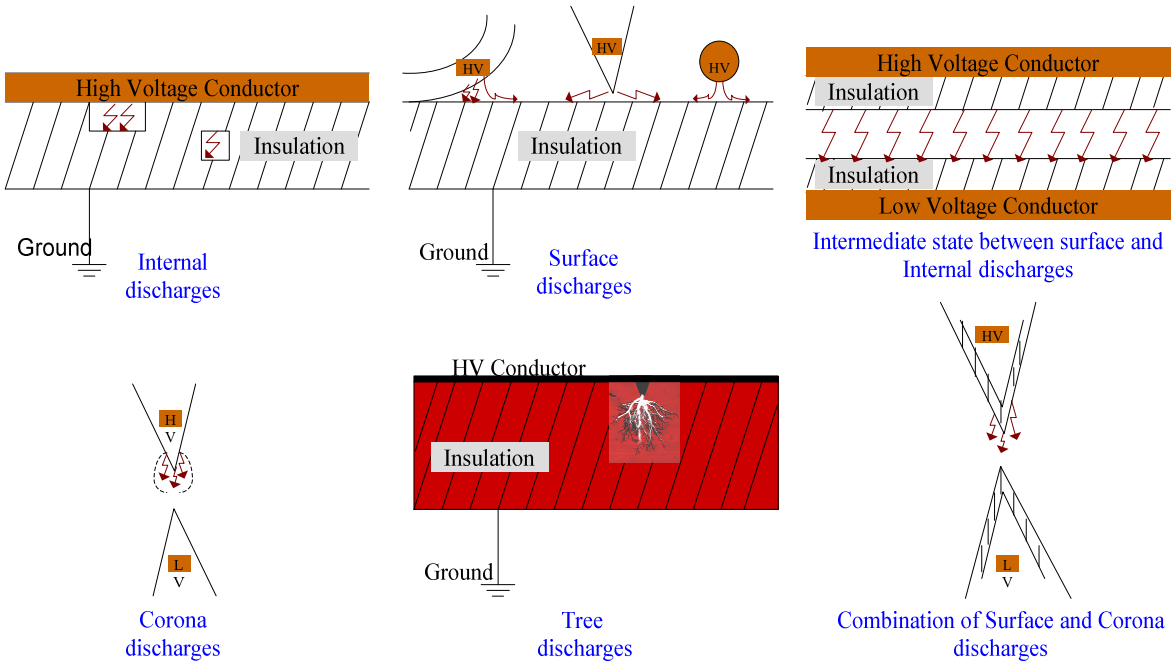

Figure 2.1: Types of gas-insulator surface discharges

2.1.2 Gas Breakdown in a Void in the Insulation

When a voltage is applied to a cable conductor, an electric field *'E'* will appear across the insulation. This electric field is a vector quantity having a magnitude and a direction and it will cause polarisation of the insulation dielectric. This field can be distorted by many parameters which will be described later on. It is therefore important to investigate these parameters since the PDIV and thus the voltage rating of cables, is dependent upon them. Furthermore PD has to be avoided to achieve the highest possible voltage rating.

Polarisation is the effect of charge separation which results in the positive charges being attracted to the cathode electrode and the negative to the anode electrode [18]. The direction of the electrostatic field is shown below in Figure 2.2. We can picture positive charges orientating themselves facing the conductor-insulation surface, whereas negative charges will orientate in the opposite direction. These charges are prohibited to break free and move towards the conductors, because polarization is only the effect on molecules or electrons in atoms to orientate themselves to the direction of the field. If the charges are

able to break free from the molecular or atomic bonds and start moving towards the electrodes, this would be the result of dielectric breakdown.

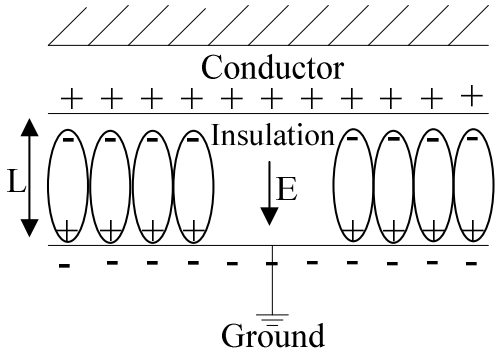

Figure 2.2: Polarization of molecules in an insulation dielectric

The magnitude of the uniform electric field can be calculated by *'E = V/L'* where *'V'* is the supply voltage applied on the conductor and *'L'* is the separation distance of the conductor and the ground. It should be noted that *E* is a vector quantity with a magnitude and a direction. Due to the presence of the insulation dielectric, the capacitance between the conductor and the ground is increased because of the polarisation that takes place. Polarisation produces *"dipole moments which in effect increase the field in the area in which they are located"* [18]. This means that more charges can be stored on the conductor and the ground for the same supply voltage than in the case if the space taken by the dielectric was a vacuum. This implies that different materials will give rise to a different capacitance due to the fact that their degree of molecular polarisation is different.

If the space between the conductor and the dielectric was a vacuum, then the charge per unit area *'Q'* would be as follows according to [19]:

$$Q = \varepsilon_o E \quad (C/m^2) \tag{2.1}$$

ε_o = *Permittivity of free space which is equal to* 8.85×10^{-12} Fm^{-1}

According to [19], *Q* is also called the electric displacement *'D'* in the material. When the dielectric is present the electric displacement is given by *'*$D = \varepsilon_o \varepsilon_r E$*'* [18], where *'*$\varepsilon_r$*'*

denotes the relative permittivity of the dielectric and it is given as the ratio of the *"increased capacitance to the capacitance in the absence of the dielectric"* [18]. The electric displacement is continuous throughout the insulation even if two or more different dielectrics are present, whereas *"E"* differs due to the different polarisation degrees of the different dielectric materials [19]. Now if a void (space filled with air) exists in the insulation, then the air molecules will be polarised in such a way as shown in Figure 2.3.

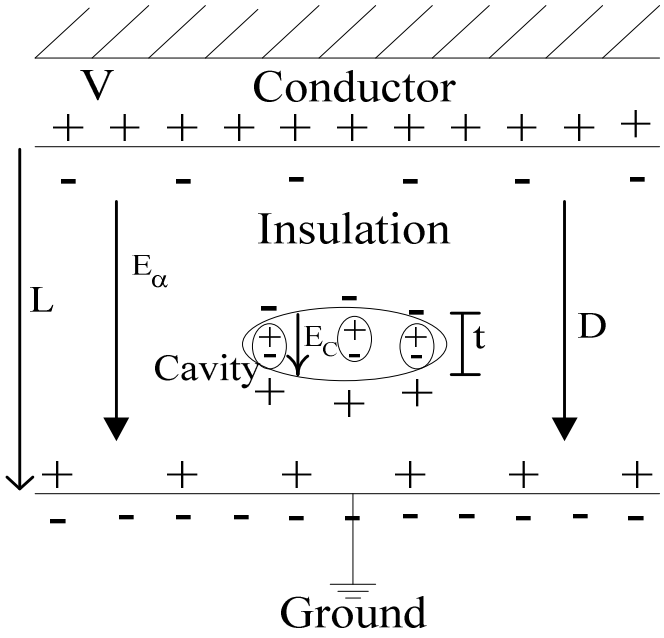

Figure 2.3: Polarization in an insulation dielectric containing a gas filled void

The diagram above shows that the air molecules will be aligned in the direction of the local electric field. The electric field *"E_c"* across the cavity is given by *"$E_c = \varepsilon_r E_a$"*. E_a is the field in the void free part of the insulation. If E_c goes over the breakdown strength field of the gas (i.e. air in this case) then partial discharges will occur provided that a *"free electron exists in order to start the ionisation process"* [20]. This can also be stated in terms of voltages, in other words partial discharge will occur if the voltage across the cavity exceeds the breakdown voltage of the gas contained in the cavity.

2.1.3 Generic Factors Affecting Partial Discharge Inception

The partial discharges that occur in cable insulation can result in the insulation failing due to damage caused around the surface of the cavity. This can produce "gaseous by-products" and cause a chemical change at the surface of the cavity. Furthermore partial discharges can lead to electrical trees, water trees and tracking. Thus, finding the parameters affecting partial discharge inception and the consequences on cables are necessary to predict the life of the cable insulation. These parameters include the following:

- Type of material Insulation (material properties)
- Type of gas in the void and in the external gap (gas properties)
- Geometry of cable insulation and conductor and their installation [21]
- Environment (internal & external temperature & pressure of the insulation & the gas) [21]
- Location of voids within the cable dielectric and surrounding airgap [21]
- Type of system (i.e. if it is an AC or a DC system)
- Loading conditions (magnitude of constant load/how often change of load occurs, transients etc.)
- Current ageing state of insulation

2.2 Gas Breakdown Processes

The discharge process depends on the ionization and de-ionization processes occurring in the cavity, or in a space outside the cable, (for example when a voltage is applied across the conductor-insulation and the ground boundary, where the cable is installed in an aircraft). Ionization and de-ionization occur due to elastic and inelastic collisions between electrons, between electrons and atoms or molecules and between atoms or molecules [16]. All cases result in electrons being liberated and these electrons are able to move under the

application of an electric field causing an electrical discharge. The types of collisions and ionization processes are explained in the next section according to [16, 19].

2.2.1 Elastic and Inelastic Collisions

When an electron is under the influence of an electric field, it gains kinetic energy. While the electron is moving, it can strike a molecule or an atom to liberate another electron/s. An elastic collision is one in which the electron barely loses any energy after bouncing from the molecule or the atom. The energy that it loses is proportional to "*m/M"* where *m* is the mass of the electron and *M* the mass of the molecule. Inelastic collisions are the main issue since the electron loses a significant amount of energy after colliding with a molecule. These collisions cause a change in the *"internal energy level of the molecule"* producing ionized molecules/atoms. In order for that electron to be able to initialize an ionization process, the energy transferred from the moving electron or molecule to another molecule, has to be equal or greater than the energy required to ionize the gaseous molecules [18]. This energy is given by [18]:

$$\Delta W = e\lambda_e E \tag{2.2}$$

ΔW = Average energy gained between collisions (Joules or J)
e = Electronic charge = $1.60217646 \times 10^{-19}$ (Coulombs or C)
λ_e = Electrons' mean free path (meters or m)
E = Electric field strength (Vm^{-1})

The mean free path *"λ_e"* is determined by three parameters for a fixed mass of gas, as for example in a cavity. These parameters are the temperature of the gas, the volume *"V_G"* it occupies and the pressure *"P"* within the void. If the temperature is fixed inside the cavity then *"P x V_G = Constant"* and λ_e is inversely proportional to *P* and directly

proportional to V_G. This also means that ΔW is also proportional to the electric field and inversely proportional to P.

Inelastic collisions might lead to the so called *Townsend avalanche*. This is the process by which an electron causes ionization of molecules after collision and the electrons freed from the molecule have enough energy to collide further with more molecules to cause further ionization. As a result more and more electrons are being released, leaving behind more positive ions. To describe the phenomenon and quantify it, a constant "α" has been defined which is called the "*Townsend's first ionization coefficient"*. This shows *"the number of electrons produced by a single electron per unit length in the direction of the electric field"* [18].

Inelastic collisions might lead to the following mechanisms associated with the release of electrons from molecules *(xy)* and atoms (*x or y)*, or recombination [16, 18]:

Ionization:

Direct: $e^- + x \rightarrow x^+ + e^- + e^-$. In this case a moving free electron causes the release of another electron from an atom after impact.

Dissociative: $e^- + xy \rightarrow x + y^+ + 2e^-$. In this case a moving free electron causes the release of another electron from a molecule after impact. The release of an electron also results in the molecule dissociating in an atom and a positively charged ion.

Photo: $e^- + x \rightarrow x^* + e^-$ and then $x^* \rightarrow x + hv$ the photon '*hv'* then causes ionization of another molecule of lower ionization energy: $y + hv \rightarrow y^* \rightarrow y^+ + e^-$ for this to happen the work function '*hf*' must be greater than $e.V_i$, where *'e'* is the charge of an electron, *'V_i'* is the *"ionization voltage"* [18], *'h'* is Plank's constant and *'f'* the frequency of the photon.

Thermal: High kinetic energy of electrons acquired from high temperatures can enhance collisions and cause ionization [18].

Excitation:

Direct: $e^- + x \rightarrow x^* \rightarrow e^- + x + hv$

Dissociative: $e^- + xy \rightarrow x^* \rightarrow e^- + x + y^*$

Photo: $hv + xy \rightarrow xy^*$

It has to be mentioned that the in the case of *'Excitation'*, the processes do not result in electrons being liberated. Instead, the extra energy is absorbed by the atoms /molecules to form metastable atoms x^* or metastable molecules xy^*.

Attachment / Recombination:

Direct: $e^- + xy \rightarrow xy^-$

Dissociative: $e^- + xy \rightarrow x^- + y$

Radiative: $e^- + x \rightarrow x^* \rightarrow x + hf$

Three body: $e^- + x^+ + y^- \rightarrow x + y$

Ion to Ion: $x^- + y^+ \rightarrow xy$

2.2.2 Derivation of Paschen's Law Equation

Having mentioned the processes of electron or ion recombination, another coefficient has been defined in literature which is called the electron attachment coefficient *'η'*. Using this coefficient and *"Townsend's first ionization coefficient"* [18], the number of the free electrons remaining can be calculated. This determines the magnitude of electrical discharges that might occur in the cable insulation when a voltage is applied in the presence of a cavity, or air in the presence of cable to ground boundaries. Using these two coefficients, the current resulting after simultaneous ionization and recombination can be expressed as follows according to [18]:

$$I = I_o \left\{ \frac{\alpha}{\alpha - \eta} e^{(\alpha-\eta)d} - \frac{\eta}{\alpha - \eta} \right\} \tag{2.3}$$

I = Current after the ionization and de-ionization processes are initiated (A)

I_o = Initial current before any ionization or de-ionization occurs (A)

d = Length in the airgap in which the ionizations take place (m)

α =Townsends first ionization coefficient

η = Electron attachment coefficient

Despite the mechanisms that occur within the airgap, mechanisms exist which provide more electrons or ions in the airgap. These include the *"photoelectric and positive ion action"* [18].The phenomenon of photoelectric emission from a metal surface is the cause for the former, whereas positive ion bombardment is for the latter [16]. To account for these secondary electrons being generated, the secondary ionization coefficient *'γ'* is introduced in theory. Equation 2.3 [16], is adjusted to account for γ:

$$I = I_o \left(\frac{\frac{\alpha}{\alpha - \eta} e^{(\alpha-\eta)d} - \frac{\eta}{\alpha - \eta}}{1 - \left(\frac{\gamma\alpha}{(\alpha - \eta)} \right) \left[\exp(ad) - 1 \right]} \right) \tag{2.4}$$

The above equation considers the fact that all processes are happening i.e. attaching of electrons and detaching. In non-attaching gases the term *'η'* is equal to zero and the equation becomes [16]:

$$I = I_o \left(\frac{\exp(ad)}{1 - \gamma \left[\exp(ad) - 1 \right]} \right) \tag{2.5}$$

From these equations the criterion from gaseous breakdown is found in theory by assuming that the electrons multiply to infinity. (Note: The equations that follow are taken from [16]). This can be analyzed by equating the denominator of the above equations for attaching and non-attaching gases to zero i.e.:

a. Attaching Gases :

$$1-\left(\frac{\gamma\alpha}{(\alpha-\eta)}\right)\left[\exp(ad)-1\right]=0 \tag{2.6}$$

b. Non-Attaching gases:

$$1-\gamma\left[\exp(ad)-1\right]=0 \tag{2.7}$$

d = distance between the cavity or airgap (m)

All the coefficients α, η and γ depend on the applied voltage *'V'* or electric field *'E'* and the gas number density *'N'* [16]. Thus it is implied that all these coefficients are affected by the volume *'V_G'*, the pressure *'P'* and the uniformity of the interfaces between the metal conductors and the insulation. η and γ are enhanced from the fact that ion bombardment and positive ion action is increased when the metal surfaces are not smooth [16]. V_G and P affect N which in turn affect α and η. The roughness of the metal surfaces affects E which also affects α, η and γ.

From the breakdown criterion we are lead to 'Paschen's Law' which states that the breakdown voltage is contingent on the product of *'N x d'* or *'P x d'*. *'N'* stands for the number density of molecules (m^{-3}) and this is related to gas pressure at 300 K by $2.415x10^{20}xP$ *(Pa). 'P'* stands for the pressure and *'d'* for the distance of the gap (gap length) [16]. Starting from equation 2.8 [16] for the ionization coefficient, the expression for the breakdown voltage can be derived:

$$\frac{\alpha}{N} = F \exp\left(-\frac{GN}{E}\right) \tag{2.8}$$

'α/N' is a function of the breakdown voltage *'V_{Brk}'*, the gap distance *'d'* and the number density of molecules *'N'* which is specific for a different gas. The constants *'G'* and *'F'* are given in literature and for air they are as follows: '*G = 11335x10*^{22} Vm^2' and '*F = 378.9x10*^{22} m^2'. The secondary ionization coefficient *'γ'* is also a function of V_{Brk}, *d* and *a*. Furthermore by substituting equation 2.7 for *α*, into equation 2.8, we can form an expression for the breakdown voltage across the airgap [16]:

Using equation 2.7:

$$1-\gamma\left[\exp(ad)-1\right]=0$$

$$\Rightarrow \gamma\left(e^{ad}-1\right)=1$$

$$\Rightarrow e^{ad_s}=\frac{1}{\gamma}+1$$

$$\Rightarrow ad_s=\ln\left(1+\frac{1}{\gamma}\right) \tag{2.9}$$

Substitute the expression for *α* (Equation 2.8), which is: $\alpha = NF\exp\left(-\frac{GN}{E}\right)$ into equation 2.9 to get:

$$NF\exp\left(-\frac{GN}{E}\right)\times d_s=\ln\left(1+\frac{1}{\gamma}\right)$$

Replace *E* by V_{brk}/d_s:

$$\Rightarrow \exp\left(-\frac{GNd_s}{V_{brk}}\right)=\frac{\ln\left(1+\frac{1}{\gamma}\right)}{NFd_s}$$

Take the *'natural logarithm'* of both sides to remove the exponential from the equation:

$$\Rightarrow -\frac{GNd_s}{V_{brk}} = \ln\left[\ln\left(1+\frac{1}{\gamma}\right)\right] - \ln\left(NFd_s\right)$$

$$\Rightarrow \frac{GNd_s}{V_{brk}} = \ln\left(NFd_s\right) - \ln\left[\ln\left(1+\frac{1}{\gamma}\right)\right]$$

$$\Rightarrow V_{brk} = \frac{GNd_s}{\ln\left(NFd_s\right) - \ln\left[\ln\left(1+\frac{1}{\gamma}\right)\right]}$$

$$\Rightarrow V_{brk} = \frac{GNd_s}{\ln\left[\frac{NFd_s}{\ln\left(1+\frac{1}{\gamma}\right)}\right]} \tag{2.10}$$

The Paschen's Law equation can be found in [12]. The value of *N* should be investigated since in literature according to [16], its relation to gas pressure is dependent on temperature. The value for $N = 2.415x10^{20} x\ P$, where *'P'* stands for pressure, is at 300 K (27 ^{o}C). Using the above formula, Paschen's Law can be drawn on graph as it will be shown on section 2.2.4.1. The value of γ, as mentioned before, depends on the type of gas, the material of the cable conductor and the ground as well as the insulation. The value has to be chosen carefully for each case for an aerospace environment [22].

2.2.3 Effect of Frequency on Air and Polymeric Insulation Breakdown

As it has been stated previously, an electrical discharge is actually the breakdown of the gas contained in a cavity inside the insulation, or near the insulation-metal interface,

or the ground-air interface. These types of electrical discharges are called internal partial discharges and external respectively. Aerospace cables consist of polymeric insulation and any form of discharge can cause serious damage to the insulation. This is because when ions or electrons collide with the surface of a polymer, they can alter the polymer's contact surface chemically. Internal discharges will cause the formation of electrical trees and externally cause tracking of the insulation [19]. After a gas discharges, the voltage across the airgap is reduced and this gives time for the ions or electrons to recombine. In a uniform field the breakdown of air follows the *"Townsend electron avalanche mechanism"*. This mechanism follows Paschen's curve as described by equation 2.10.

Gas breakdown (electrical discharge), occurs at much lower voltages than the breakdown of solid polymeric insulation, which according to [19] the insulation has a dielectric strength in the region of 3 MVm^{-1}. This is because the mobility in solids is much less due to the higher density of molecules. Because the molecules are much closer to each other, the collisions between them are much more frequent and the energy is transmitted very quickly from one atom to the other, not allowing the charges to gain high energies very quickly as it is the case of gases. For solids the mobility is much lower because the electrons in the solid lattices are trapped, resulting in a much lower electron drift velocity [22]:

$$W_e = \mu_e E \tag{2.11}$$

W_e = Drift velocity
μ_e = Mobility (also noted as 'b')
E = Applied electric field

Breakdown of solids is not examined here. However, one of the objectives of this thesis is to compute optimal voltage levels to be used in aircrafts based on the determination of the partial discharge inception voltage (PDIV). Thus, it has to be illustrated that the breakdown of air occurs at lower voltages than the breakdown of solid polymeric insulation. As an example, breakdown tests have been carried for a range of

frequencies (50 Hz – 1 kHz), for an unscreened aerospace cable having an AWG 18 conductor, insulated with 0.3 mm of PTFE. Results are shown in Figure 2.4.

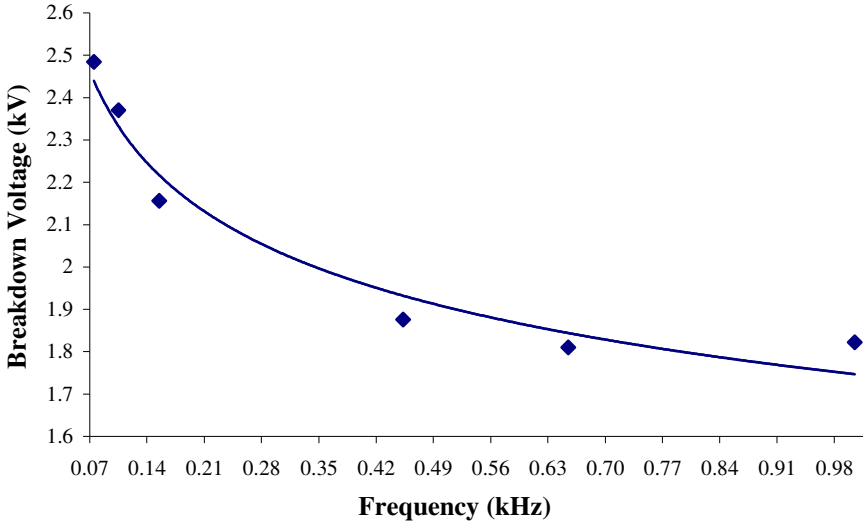

Figure 2.4: Variation of the breakdown voltage with increasing frequency from 50 Hz to 1 kHz at 100 kPa. The cable tested had an AWG 18 conductor, insulated with 0.3mm of PTFE insulation

The tests were not carried out at different temperatures since based on [16], the temperature limit of PTFE for this cable is approximately 200 ^{o}C. The PDIV for this cable was measured to be 600 V at 100 kPa, a value well below the breakdown voltage results shown in figure 2.4. Details regarding the testing procedures are described in chapter 5.

2.2.4 Calculation of Safe Operating Voltage in a Uniform Field

Partial discharges occur in a cable insulation material when the electric field in a void within the material (internal PD), is greater than the breakdown electric field of the gas contained in the void. PD can also occur externally along the surface of the dielectric due to contamination and surface irregularities, or even in the airgap between unscreened insulated cables and between the cables and ground. In the case of aircraft this might happen in cable bundles [12].

This thesis focuses on alternate and direct current PD occurring in the airgap between the cable insulation and the ground, between cables and within a void in the insulation in

order to calculate the safe operating voltage (SOV) for a cable system. The locations of these discharges are shown below:

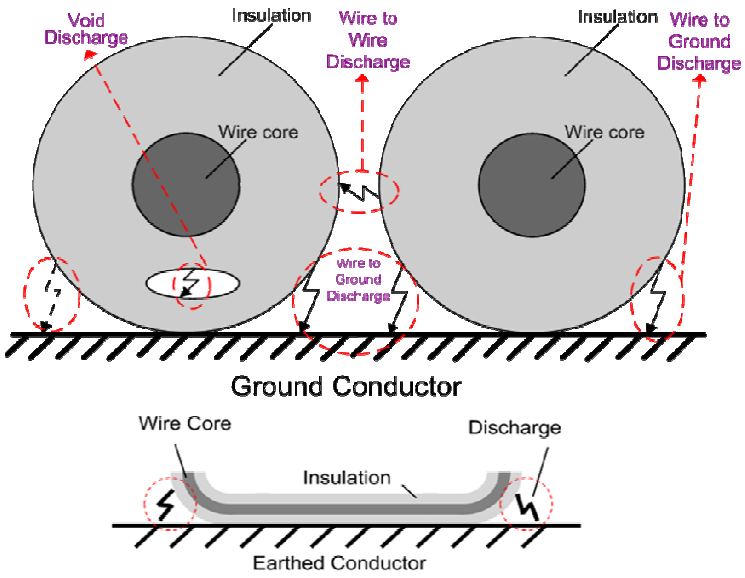

Figure 2.5: Locations of PD taken into consideration in the calculation of SOV

The derivation of the uniform equations used to calculate the partial discharge inception voltage in the case of cable to ground and cable to cable discharges is described in this section with the aid of the following figures:

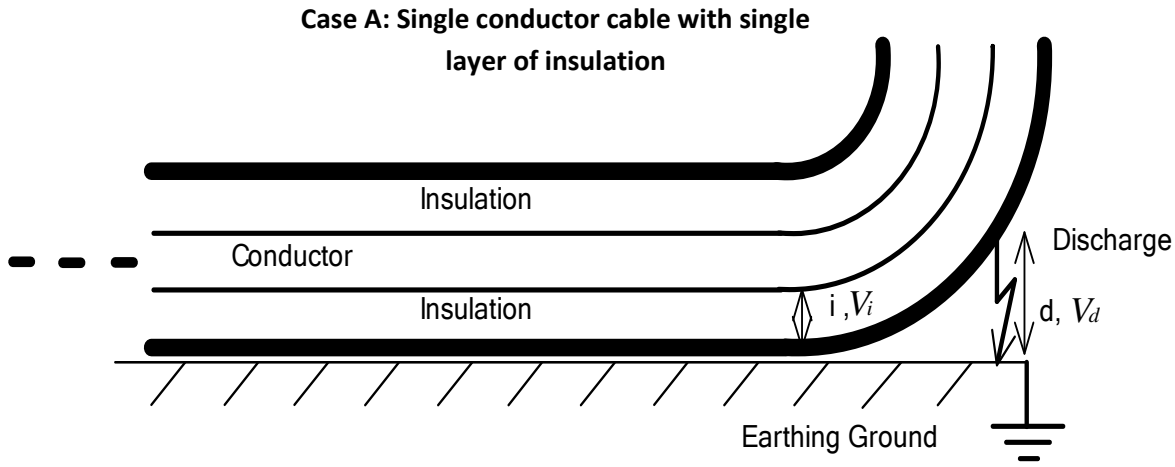

Figure 2.6: Cable to plane discharge with single insulation layer

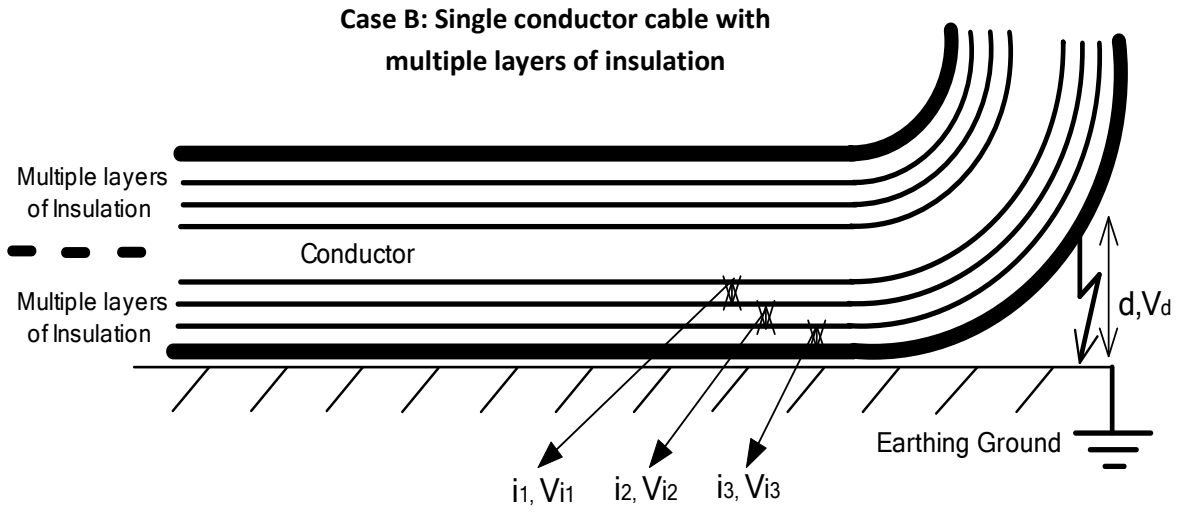

Figure 2.7: Cable to plane discharge with multiple insulation layers

The outcome of PD is to degrade the insulation material, age it and decrease its lifetime. Therefore it is clear why calculating the partial discharge inception voltage (PDIV), is of great importance. In addition, the breakdown strength of the insulation material needs to be measured using an appropriate testing procedure which gives accurate results [21]. These results are used in industry as guidelines for designing dielectric materials to be used as cable insulation and furthermore for insulation coordination.

2.2.4.1 Case A: Single conductor cable with single layer of insulation

For the following derivations, Figure 2.6 is used from the previous section. The equations that follow are derived by using Gauss Law which states that in a linear homogeneous and isotropic material, the electric field density '*D*' is equal to the free charge per unit area 'ρ_s':

$$D = \frac{Q}{A} = \rho_s$$

$$D = \varepsilon_o \varepsilon_r E_i \Rightarrow \frac{\rho_s}{\varepsilon_o \varepsilon_r}$$

$$D = \varepsilon_o E_i \Rightarrow \frac{\rho_s}{\varepsilon_o}$$

ε_o = *Permittivity of free space* = $8.85418782 \times 10^{-12}\ m^{-3}\ kg^{-1}\ s^4\ A^2$

ε_r = *Relative Permittivity of the insulation material*

ρ_s = *Free surface charge per unit area (surface charge density,* Cm^{-1})

E_i = *Electric field within the insulation material* (Vm^{-1})

To derive the formula for the voltage across the symmetrical cylindrical insulation, the electric field has to be integrated along the thickness of the insulation surrounding the conductor on which the voltage is applied:

According to Gauss Law for a cylindrical geometry:

$$V_i = \int E_i dx = \int \frac{\rho_s}{\varepsilon_o \varepsilon_r} dx = \frac{\rho_s i}{\varepsilon_o \varepsilon_r}$$

The same equation can be used to evaluate the voltage *'V_d'* across an airgap*'d'* as shown in Figure 2.6:

$$V_d = \int E_d dx = \int \frac{\rho_s}{\varepsilon_o} dx = \frac{\rho_s d}{\varepsilon_o}$$

By using the potential divider rule the fraction of the supply voltage *'$fract_{(Vd)}$'* across *'d'*, can be calculated by using Equation 2.12 which can also be found in [12]:

$$fract_{(V_d)} = \frac{V_d}{V_d + V_i} = \frac{d\varepsilon_r}{d\varepsilon_r + i} \tag{2.12}$$

This airgap breaks down according to Paschen's Law for a specific gap size, *'d'* and pressure *'P'* as shown in Figure 2.8.

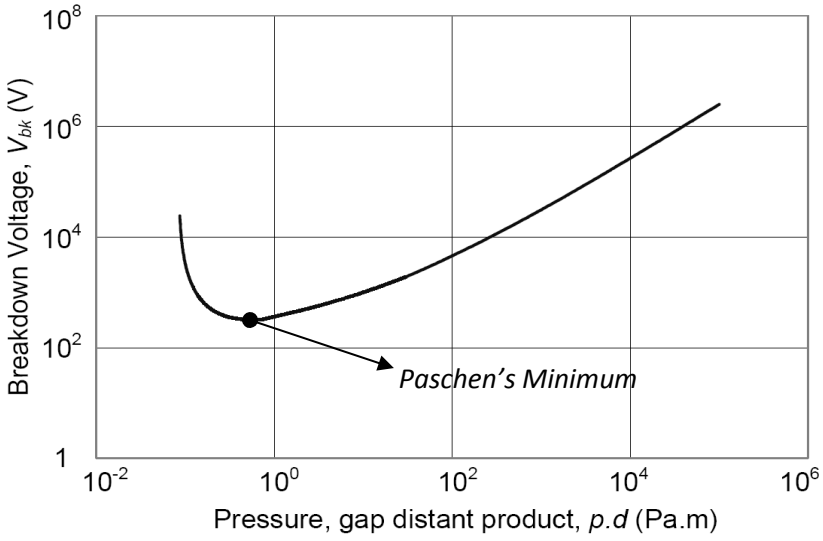

Figure 2.8: Paschen's Law for air [12]

From the graph in figure 2.8, it can be observed that a minimum point exists below which no breakdown occurs. This occurs due to physical mechanisms related to the mean free path *'λ_e'* according to the relationship [16]:

$$\lambda_e = \frac{1}{P} = \frac{1}{NQ_m} \tag{2.13}$$

Q_m = Momentum transfer cross section (m^2)
N = Number density of molecules (m^{-3})

The decrease in pressure decreases N provided that Q_m, which is the *"momentum transfer cross section"*, remains constant. If the number of molecules per unit volume is less, not only that would imply *"less frequent collisions"*, but also that each particle has more space (mean free path 'λ_e') available for it to accelerate and gain the necessary transfer momentum.

The shape of Paschen's Law curve can be explained by either assuming a fixed gap distance *'d'* or a fixed pressure *'P'*. Assuming a fixed d, moving to the left of Paschen's minimum, P decreases and the mean free path 'λ_e' increases approaching the physical gap

length. This not only implies that there are fewer molecules contained in the gap with less frequent collisions, but also that electrons, atoms or molecules are more likely to breech the gap without colliding with other molecules or atoms. Thus a bigger voltage is required to increase the kinetic energy possessed by particles and furthermore to increase the frequency of collisions and cause ionization. If a fixed *P* is assumed, going to the left of Paschen's minimum, *d* decreases approaching the mean free path 'λ_e'. This also implies that fewer molecules are contained in the gap for the pressure to be kept constant. Electrons, atoms or molecules are more likely to breech the gap without colliding with other molecules or atoms and thus a bigger voltage is also required to cause ionization.

Going to the right of Paschen's minimum, and assuming a fixed *d*, *P* increases. Effectively more molecules are contained in the gap and λ_e decreases. Collisions are much more frequent but again there is no room for molecules or atoms to accelerate to gain the necessary transfer momentum. Thus the breakdown voltage increases. If *P* is fixed, going to the right of the minimum, *d* increases. Again this implies that the number of molecules increases for the pressure to be constant. In this case, the breakdown voltage increases in order to maintain the breakdown electric field strength.

2.2.4.2 Case B: Single conductor cable with multiple insulation layers

For cables with multiple insulation layers, the same procedure is followed as in the case of a single insulation layer to derive the fraction of the supply voltage across the airgap. The only difference is the additional voltage drop across each insulation layer. The insulation thickness of each layer is marked as i_1, i_2 and i_3 and their relative permittivity respectively is ε_{r_1}, ε_{r_2} and ε_{r_3}:

According to Gauss Law for a cylindrical geometry:

$$V_{i_1} = \int E_{i_1} dx = \int \frac{\rho_s}{\varepsilon_o \varepsilon_{r_1}} dx = \frac{\rho_s i_1}{\varepsilon_o \varepsilon_{r_1}}$$

Since the same equations are valid if more insulation layers are present, expressions can be obtained for the voltage across each layer:

$$V_{i_2} = \int E_{i_2} dx = \int \frac{\rho_s}{\varepsilon_o \varepsilon_{r_2}} dx = \frac{\rho_s i_2}{\varepsilon_o \varepsilon_{r_2}}$$

$$V_{i_3} = \int E_{i_3} dx = \int \frac{\rho_s}{\varepsilon_o \varepsilon_{r_3}} dx = \frac{\rho_s i_3}{\varepsilon_o \varepsilon_{r_3}}$$

$$V_d = \int E_d dx = \int \frac{\rho_s}{\varepsilon_o} dx = \frac{\rho_s d}{\varepsilon_o}$$

Again by using the potential divider rule the fraction of the supply voltage *'fract$_{(Vd)}$'* across *'d'*, can be calculated by using Equation 2.14:

$$\Rightarrow fract_{(V_d)} = \frac{V_d}{V_d + V_{i_1} + V_{i_2} + V_{i_3}} = \frac{\frac{\rho_s d}{\varepsilon_o}}{\frac{\rho_s d}{\varepsilon_o} + \frac{\rho_s i_1}{\varepsilon_o \varepsilon_{r_1}} + \frac{\rho_s i_2}{\varepsilon_o \varepsilon_{r_2}} + \frac{\rho_s i_3}{\varepsilon_o \varepsilon_{r_3}}}$$

$$= \frac{d}{d + \frac{i_1}{\varepsilon_{r_1}} + \frac{i_2}{\varepsilon_{r_2}} + \frac{i_3}{\varepsilon_{r_3}}}$$

$$= \frac{d\varepsilon_{r_1}\varepsilon_{r_2}\varepsilon_{r_3}}{d\varepsilon_{r_1}\varepsilon_{r_2}\varepsilon_{r_3} + i_1\varepsilon_{r_2}\varepsilon_{r_3} + i_2\varepsilon_{r_1}\varepsilon_{r_3} + i_3\varepsilon_{r_1}\varepsilon_{r_2}} \quad (2.14)$$

The new voltage across the airgap is calculated with Equation 2.14. For different cavity thicknesses *"d"* and pressures *"P"*, the breakdown voltage *"V_{Brk}"* of the air inside the cavity can be found using Paschen's Law. Thus the following equation can be written:

$$fract_{(V_d)} \times V_{Inception} = V_{Brk} \quad (2.15)$$

"$V_{Inception}$" is the supply voltage which is required to ignite partial discharges, by triggering the breakdown of air particles. After calculating "$fract_{(Vd)}$" for a certain i and P, equation 2.15 can be used to calculate a range of partial discharge inception voltages (PDIVs) for a range of d. Furthermore the lowest PDIV can be chosen to determine the safe operating voltage (SOV) for the aerospace cable.

These calculations do not consider the effect of space charge which might accumulate due to the multiple interfaces as it is discussed later on in section 2.2.8. Space charge accumulation is not significant when an AC voltage is applied from a medium to a high frequency (50Hz up to several kHz). Thus the above derivations can be assumed to be valid. On the contrary, when performing calculations under a DC voltage, the space charge effect has to be assessed [23]. Another parameter which has to be taken into consideration when a DC voltage is applied is the insulation resistivity, as it will be discussed later on. It has to be noted at this point that the SAE standard AS50881 [11] makes no distinction between DC and AC voltage ratings that are used for aerospace cables.

2.2.5 Effect of Frequency and Temperature on the Electrical Properties of Air

According to [24], the permittivity of dry air is approximately 1 and this value remains constant up to radio frequencies. The effect of frequency and temperature on the electrical properties of dry and moist air has not been investigated in this thesis. However, the effect of temperature on the breakdown voltage of air (V_{Brk}) has been examined. Based on Paschen's Law, V_{Brk} depends on the pressure distance product "$p.d$". Pressure is dependent on the density of air particles within a gap. At elevated temperatures the density of air is reduced and the mean free path "λ_e" that an electron/ molecule have to travel before colliding with another electron/ molecule, is increased. Effectively a rise in temperature causes a reduction in pressure and furthermore a reduction in V_{Brk} for a fixed gap distance, until Paschen's minimum is reached. (It has to be noted here that this statement does not hold true in the case of a fixed volume like for example in a closed

void). If the temperature is increased further, the mean free path would be expected to become very large and more energy would be required to cause molecules to collide and liberate electrons and thus V_{Brk} would increase following Paschen's curve. However, after a certain temperature (θ > 1000 K), thermal ionization takes place and Paschen's Law is no longer valid [12, 22]. For temperatures up to 473 K (200 ^{o}C), Equation 2.16 [12] can be used to adjust the pressure if the temperature is increased.

$$P_{NEW} = \frac{293 \times P_{OLD}}{273 + \theta_A}(Pa) \tag{2.16}$$

P_{NEW} = *adjusted pressure (Pa)*
P_{OLD} = *initial pressure (Pa)*
θ_A = *ambient temperature (^{o}C)*

Frequency can also affect V_{Brk}. However frequency effects are not significant in the frequency range of interest which is from 50Hz up to 1 kHz, at which aircraft electrical systems operate. It is stated in [12], that there is a critical frequency at which V_{Brk} starts decreasing. This critical frequency is smaller at atmospheric pressure than at lower pressures at higher altitudes and it depends on the mobility of the ions in the air *'b'*, the peak electric field *'E_0'* and the air gap distance *'d'*, between a high voltage and a low voltage electrode. *b* depends on the mean free path *'λ_e'*, which increases if the pressure is reduced. The following equation, as taken from [12], can be used to calculate the critical frequency *'f_{crit}'*:

$$f_{crit} = \frac{bE_0}{\pi d} \tag{2.17}$$

The mobility *'b'* is given by the following equation in [12],

$$b = \frac{q\lambda_e}{mc} \tag{2.18}$$

q = Charge of the positive ion ($1.6x10^{-19}$ C)

λ_e = Mean free path (m)

m = Mass of the ion (kg)

c = Mean thermal velocity (ms^{-1})

By examining the above equation it can be realised that a decrease in pressure will cause an increase in the mean free path *'λ_e'* (according to Equation 2.13) and thus an increase in the mobility of ions *'b'* in the air and thus cause an increase in the critical frequency *'f_{crit}'*. As discussed previously, the temperature also affects λ_e and thus the mobility of the ions. An increase in temperature will increase λ and b and consequently will increase f_{crit}. More information and references on the subject of critical frequency can be found in [12]. In this thesis the effect of frequency is neglected since it is insignificant for the operational frequency range which is taken into consideration. However when rating the insulation in power electronic converters, which may be operating at switching frequencies of 10 kHz and greater, the above formulae should be used appropriately.

2.2.6 Application of Calculations in the Aerospace Environment

As discussed in the previous section pressure, airgap distance and the type and thickness the insulation material, govern the PDIV calculation. According to [12] the temperature and pressure in the aerospace environment vary according to altitude as shown on the following graph:

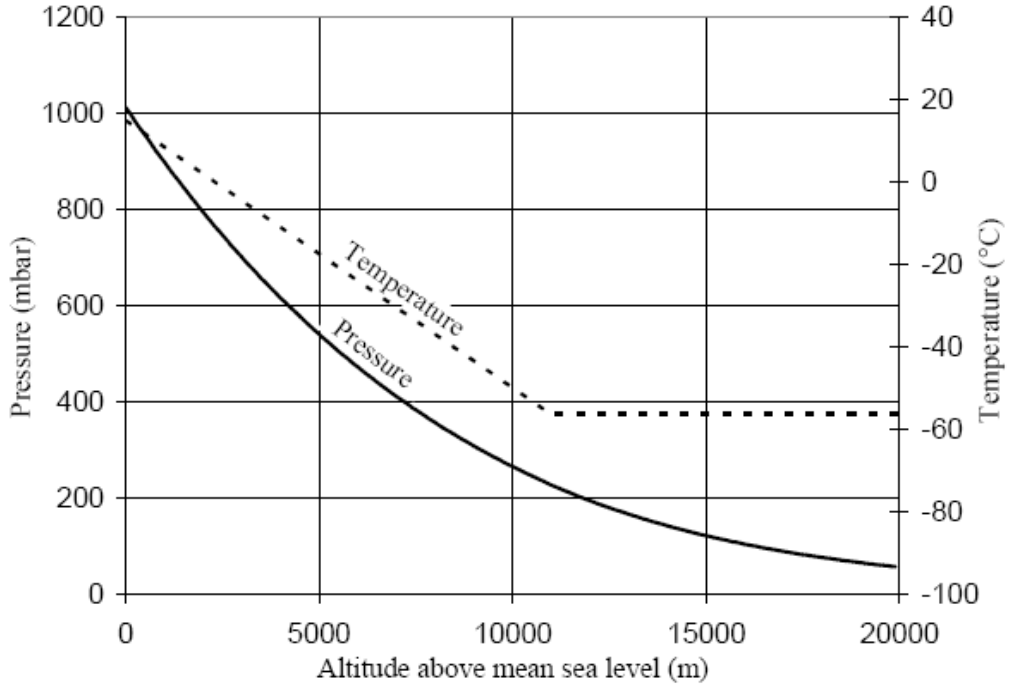

Figure 2.9: Variation of temperature and air pressure with increase in altitude [12].

As observed from Figure 2.9, the air pressure and temperature fall with an increase in altitude. This does not mean that cables supplying electrical energy will be exposed to such temperatures or pressures. This depends on the location at which they will be installed. For example, the cables could be installed within the aircraft cabin, where the temperature and pressure are regulated by the aircraft system to be approximately 25^{o}C and 100 kPa respectively. Otherwise the cables could be exposed to the outside atmosphere, if for instance they are installed along the aircraft wing or around the aircraft engines. At these sites the temperature could vary at 40,000 feet (around 12.192 km), from about -55.6 ^{o}C (along the wing) to 200^{o}C close to the engines in the nacelle [12]. The ambient pressure would be 18.8 kPa at this altitude. Figure 2.10 shows how the calculated PDIV is affected by the ambient pressure *'P'* and temperature *'T'*. Note that the results shown below are based on the calculation procedure described in Section 2.2.4.1 and 2.2.5. This procedure is described in detail in Chapter 3. The results are for a cable consisting of a single layer of PTFE insulation with a relative permittivity *'ε_r = 2.1'*.

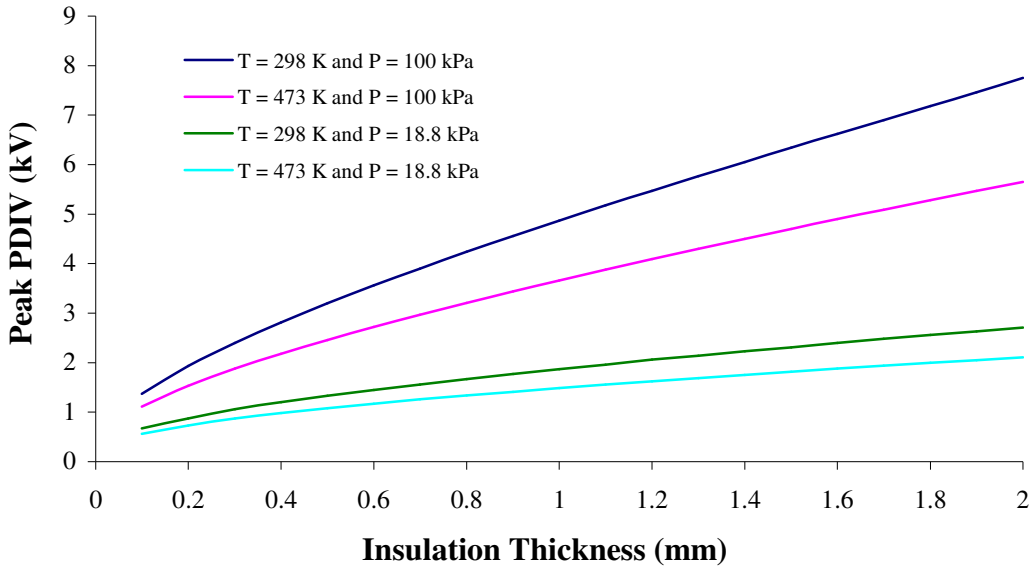

Figure 2.10: Variation of the peak PDIV with increasing cable insulation thickness, at temperatures of 298 K and 473 K and at pressures of 100 kPa and 18.8 kPa

In conclusion, the parameters affecting the PDIV in air have been stated. These parameters are the pressure and the temperature of the air as well as the airgap distance, the type of insulation material and its thickness. The sections that follow describe the dependence of the material properties on frequency and temperature.

2.2.7 Effect of Frequency and Temperature on a Material's Electrical Properties

The relative permittivity is defined as a measure to which a material concentrates electric flux. It is the ratio of the static relative permittivity 'ε_s' to the permittivity of free space 'ε_0', in other words the ratio of the electrical energy stored in a dielectric when an electric field is applied, to the energy stored if in the place of the dielectric there was a vacuum. The amount of electrical energy stored is dependent on the degree of polarization of the dielectric. Thus ε_r is determined by the degree of polarization. In non polar polymers the relative permittivity is low whereas in polar polymers is relatively large [19]. Take for example a non polar polymer PTFE, which is used as cable insulation in aircraft cabling systems having an $\varepsilon_r = 2.1$. Mica on the other hand, a ceramic raw material, is a

polar dielectric having an ε_r = 7 [25]. The relative permittivity depends on the following parameters:

- Frequency
- Temperature
- Density (for non-polar polymers ε_r increases linearly with increase in density)

As the frequency increases, polarization tends to decrease since it consists of four mechanisms, each of which takes place at different frequencies, depending whether or not this happens at the atomic level or the molecular level. The four polarisation mechanisms are the electronic, the molecular, the orientational and the interfacial polarisation [18, 19]. As the frequency increases some of these mechanisms are relatively slower and cannot keep up and as a result the relative permittivity decreases.

At low frequencies temperature can affect the degree of polarization by disorientating the dipoles formed when the dielectric is placed in an electric field. This can also increase or decrease the relative permittivity. The degree to which the dipoles disorientate depends on the type of material and the bonding between molecules and atoms [19].

As far as density is concerned, the higher the density the higher the relative permittivity. This is reasonable since if more molecules are present in a certain volume, it means that more dipoles can be formed with the application of an electric field [19].

In this thesis, PTFE (a non polar material), has been used for analysis and based on [16], its relative permittivity remains constant up to a temperature of 200^{o}C and throughout the range of operating frequencies seen in aircraft power systems (400 Hz-1 kHz). It is important though to illustrate the difference in the PDIV between two cables consisting of the same insulation thickness but of different materials and thus having a different relative permittivity. Figure 2.11 shows this difference in PDIV. It has to be noted that the results shown in the figure below were obtained by using the calculation procedure described in the previous Section 2.2.4.1, for a single unscreened cable lying on a ground plane. In this

case the PDIV is based on PD occurring between the outer cable insulation surface and the grounded plane.

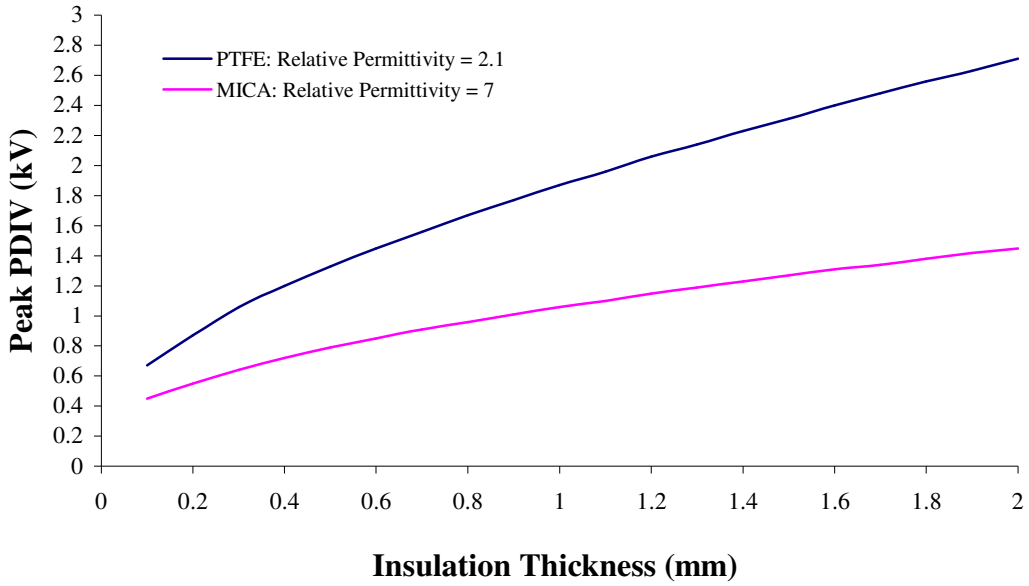

Figure 2.11: Peak PDIV for a range of insulation thicknesses, for cable consisting of PTFE insulation (ε_r= 2.1) and Mica (ε_r= 2.1), at an ambient pressure and temperature of 18.8 kPa and 25^{o}C respectively

If the relative permittivity changes in a space in the insulation, the capacitance of that local space will either increase or decrease, enhancing or reducing respectively the local electric field. A higher electric field through the insulation would cause a higher percentage voltage across that region. For example it has been mentioned that if the electric field across the healthy part of the insulation is E_a, then the electric field across an existing cavity in the insulation will be $\varepsilon_r E_a$. Thus the higher the relative permittivity the greater will be the electric field across the gap and the PDIV will consequently be smaller.

2.2.8 Effect of Space Charge on the Electric Field Distribution

Space charges can be electrons and protons and/or negative and positive ions that are trapped inside a dielectric. Electrons or protons are generated when high electric fields are applied on the cable conductor, in which case the charges are injected from the conductor into the insulation and become trapped inside. Positive or negative ions result from

molecular dissociation [26]. Space charge can also accumulate inside the insulation *"by charge separation from ionic impurities within the material"* [26]. According to Gorur G. Raju in [16] the space charge is created due to the "large difference in the mobility of electrons and positive ions" and this gives rise to an "electric field in-homogeneity". Another incident that can cause space charge accumulation is a temperature difference across the insulation and also if the insulation consists of multiple layers and multiple interfaces.

Equation 2.15 for $fract_{(Vd)}$, does not take into account the effect of "space charges". Space charges either reduce or enhance the local electric field in different areas within the insulation [23]. The space charges can be (according to R.N Hampton), of a long term or a short term type. Long term refers to a slow space charge decay after the applied voltage has been turned off and this way affecting the *"material's strength and enhancing ageing"* [23]. For 'short term' as the name suggests, the space charge decays fast when the voltage is switched off. In either two situations the space charge accumulation is contingent on the magnitude of the electric field, the type of material, number of layers, impurity percentage and the current state of the insulation, i.e. how long was it used and under what electrical and environmental conditions.

Three conditions can lead to space charge build up. The first is that electric field and or temperature across the insulation is equal or greater to the "space charge accumulation threshold". A significant temperature gradient affects the conductivity *'σ'* of the insulation and the permittivity *'ε'*. This induces space charge, either due to the temperature difference which causes alteration in the value of σ and ε in different areas in the insulation, or the existence of multiple layer insulation which again results in different σ and ε values for each layer. These effects cause the *"Maxwell-Wagner-Sillars (MWS) polarisation*", which only applies if the electric field is not high enough to cause charge injection from the electrodes [27]. The effect of space charges under alternating current (AC) conditions is insignificant because space charge does not have enough time to accumulate. However under direct current (DC) conditions the effect becomes considerable.

2.2.9 Interfacial Effects of Layer Components in Cable Insulation on the Electric Field Distribution

The existence of interfaces in a cable introduces problems regarding the enhancement of *"electrical, mechanical and thermal stresses of the insulation"* [27]. According to [27] the interfaces can be the cause of initiating partial discharges due to non-smooth contact of one interface with the other. This stands true when the cable is both under an AC or a DC voltage. *"When the cable is under DC voltage, the partial discharge activity is a second order problem because of smaller repetition rates than in the case of AC voltage"*[27]. Despite the smaller repetition rate under DC, space charge can accumulate "in the insulation bulk particularly if multiple interfaces exist". The area of interfacial contact attracts space charges more than usual if materials of low mobility are present for example in polymers. It is of great importance the effect that the presence of multiple interfaces has on polymeric insulation layers in a cable, when a DC or an AC electric field is applied. Since space charges can vary the electric field distribution quite a lot from its normal geometrical form, they speed up the decay and the breakdown of the insulation [27].

Based on [27] if the cable has two insulation layers, the non uniform electric fields in insulation layer 1 and 2 respectively, including the effect of surface free charge density at the interface, is given below by the first term in equation 2.19. The second term is added to account for the effect of space charge gathered in the bulk [27]:

$$E_{(1,2)}(r) = \frac{\varepsilon_{2,1} V}{\varepsilon_{1,2} \ln\left(\frac{r_2}{r_i}\right) + \varepsilon_{2,1} \ln\left(\frac{r_i}{r_1}\right)} + \frac{1}{r}\int_{r_i}^{r} \frac{p(r)}{\varepsilon(r)} r dr \qquad (2.19)$$

$E_{(1,2)}$ = Electric field in Insulation layer 1 and 2 respectively (Vm^{-1})
$\varepsilon_{1,2}$ = Relative permittivity in insulation layer 1 and 2 respectively
V_S = Supply Voltage (V)
$r_{1,2}$ = Radius of insulation 1 and 2 respectively (m)

p(r) = Space charge density (Cm^{-3})

ε(r) = Relative permittivity as a function of the radius in the insulation layers

This "general" equation is derived by [27], taking into account the geometrical Laplacian and Poison's field related with the surface charge density at the interface. For more information on the derivation of the equation look at [27]. It has to be noted that in this dissertation the space charge and the interfacial effects are not included in the safe operating voltage assessment, but they are mentioned here to point out the necessity of further research on this subject.

2.2.10 Discussion on the Relative Effect of Supply Frequency and Temperature on Gas and Solid Insulation

Partial discharges can occur internally within a cavity in a dielectric or externally, as described in Section 2.2.4, between the insulation and the ground when the cable is installed for example in an aircraft. The breakdown voltage of the gas *"V_{Brk}"* in the gap determines the inception voltage at which partial discharges will initiate. Thus, if the voltage across the airgap is equal or greater to V_{Brk}, then partial discharges will be generated. As discussed, the voltage across the gap is a fraction of the supply voltage and can be calculated approximately using the potential divider rule as used in circuit analysis. The diagram for analyzing partial discharges is shown below in Figure 2.12.

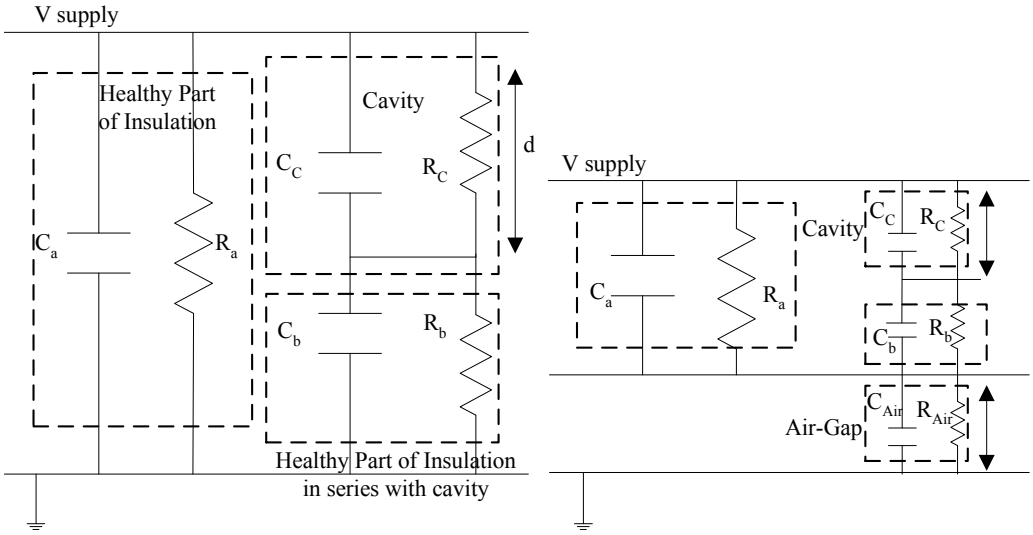

a). Circuit for Void discharge

b). Circuit for Void and Air-gap discharge

Figure 2.12: Circuitry used for analysing PD under an AC and a DC voltage.

From Figure 2.12 it is obvious that relative changes in the impedance values of the part of the circuit representing the cavity in series with the healthy part of the insulation, will result in changes in the voltage across the void. Furthermore this might result in changes in the inception voltage. This also stands in the case of an external airgap. The concerning impedances are determined by the capacitance and the resistivity of each part. Thus, the inception voltage depends on the fraction of the voltage across the gap and the breakdown voltage of air.

The question is: 'Does a change in frequency and /or the temperature trigger a change in the resistance or the capacitance of the system? If so, under what processes they cause this change'. Does it alter the electrical properties (relative permittivity *'ε_r"* and the dissipation factor *'tan (δ)'*) of the dielectric and/or of the air in the external or internal gap? Does the increase in the system temperature result in changes in the resistivity *'p'*, ε_r and *tan(δ)*? The frequency and temperature response of these parameters must therefore be investigated to obtain a full understanding.

Even though the impedance of the insulation decreases with frequency, the impedance of the gas in the gap, for example air, also decreases with the same proportion. Thus the fraction of the voltage across the gap remains unaltered and no change in the

PDIV is expected. This statement holds, provided that the breakdown voltage of the air based on Paschen's law remains unaltered and if the electrical parameters of insulation and gases in the gaps remain unchanged.

Under AC conditions the resistive part of the circuits in Figure 2.12 is infinite and the voltage across the insulation and the airgap and the cavity within the insulation, is determined by the capacitive reactance. There will be point at very low frequencies where the capacitive reactance will be comparable with the resistance part and thus both circuit elements will affect the voltage distribution.

The main concern is a change in ε_r and *tan(δ)* with increase in frequency and temperature. As mentioned in Section 2.3.4, for PTFE and other Polyethylene dielectrics these electrical properties remain fairly constant up to frequencies of several kilohertz and temperatures up to 200 $^{\circ}$C. For PTFE, *tan(δ)* is approximately 0.0001 and ε_r = 2.1. On the other hand according to [12], at about 10 kHz the relative permittivity *"ε_r"* of Polyvinyl Chloride (PVC) insulation decreases slightly. Furthermore for this type of dielectric, the capacitance of the healthy part of the insulation in series with the cavity decreases and the capacitive reactance increases. As a result the voltage across the insulation increases whilst the fraction of the voltage across the external airgap or internal cavity decreases. If the PD inception voltage was "X" Volts before ε_r decreased due to the frequency increase, the applied voltage on the conductor can be increased further, since the maximum voltage across the gap is now less than before. It has to be mentioned that in this situation, a higher inception voltage was achieved due to the increase in frequency affecting the relative permittivity of the solid insulation rather than the permittivity of the air.

The relative permittivity of PTFE remains constant since it is a non–polar polymer and thus at low frequencies the inception voltages will not be affected. According to [16], *tan(δ)* is found to vary from 10 x 10^{-5} to 8 x 10^{-5} as the frequency increased from 100 Hz to 1 kHz at 1 atmosphere (100 kPa), while the temperature was kept constant. A further increase in frequency from 1 kHz to 30 kHz caused *tan(δ)* to increase to an approximate value of 25 x 10^{-5}. From this information it is obvious that frequency does not affect ε and *tan(δ)* directly within the frequency range of interest. However the indirect effect of the increasing frequency (i.e. increase in dielectric losses and therefore the dielectric's

temperature) on these parameters requires further investigation. Since for PTFE insulation, which is used in this thesis report as a basis for insulation voltage rating and current rating analysis, the effect of frequency on PD within the range of interest (50 Hz up to 1 kHz) is insignificant, the effect of temperature remains to be examined. The power dissipated in the dielectric per unit length '$W_{dielectric}$' if the cable is unloaded is given by [18]:

$$W_{dielectric} = V_s^2 2\pi f C \tan(\delta) \left(Wm^{-1}\right) \tag{2.20}$$

V_S = *Supply voltage (kV)*
f = Frequency of supply (Hz)
C = Capacitance of insulation (F)
tan(δ) = Dissipation factor

If the cable is loaded then the power losses per unit length 'W_C' produced due to the current *'I'* flowing through the cable conductor having a resistance per metre *'R_C',* is given by *'$W_C = I^2R_C$'*. Thus the total power dissipated in the dielectric is the sum of all losses *'$W_{dielectric} + W_C$'*. From equation 2.20, it can be observed that by increasing the frequency will cause the energy dissipated in the dielectric *'$W_{dielectric}$'* to increase. This will cause an increase in the insulation temperature which in turn might lead to further alterations in the resistivity of the insulation and/or of the airgap. For PTFE, *tan(δ)* is approximately 0.0001. If this value remains constant and the capacitance is relatively small (in the order of Pico farads), the dielectric losses are also very small for supply voltages up to 600 V. This is the PD inception voltage for the type of cable being examined at 11.6 kPa. Even if the frequency rises from 50 Hz to 1 kHz, the increase in the losses will be minute.

To illustrate the effect of frequency on the temperature rise of the insulation, a screened PTFE insulated cable is used here as an example. A 500 mm length of screened cable was tested having a capacitance of approximately 535 pF. It has to be noted however that in the case of unscreened cables, the capacitance depends on the cable installation method. The inception voltage of this cable was found to be 600 V using a method which

will be described in Chapter 5. At a supply frequency of 1 kHz the dielectric losses are calculated to be 0.121 mW, based on equation 2.20. Knowing that the thermal resistivity *(p_T)* of PTFE is 5 Km/W, the thermal resistance of the insulation can be calculated using the formula [28]:

$$T_R = \frac{p_T}{2\pi} \ln\left(\frac{r_2}{r_1}\right) (Km/W) \tag{2.21}$$

T_R = Thermal resistance (Km/W)
p_T =Thermal resistivity (Km/W)
r_1, r_2 = Internal and external cable radius respectively (m)

Thus if *'T_R'* is 0.174 Km/W, the temperature increase (*$\Delta\theta = W.T_R$*) is almost 0 K and the electrical parameters of the insulation are not affected, unless the increase in frequency causes an increase in *tan(δ)* orders of magnitude. Even if the resistivity changes at higher temperatures when the cable is loaded, the resistive part of the circuit still remains infinite compared to the capacitive part and unless the electrical permittivity *'ε_r'* changes (and thus the capacitance) because of the heat, then the fraction of the voltage remains the same as well.

Under DC conditions the capacitive part of the impedance relative to the resistive, is infinite and the fraction of the voltage across the gap is determined mainly by the resistance of the insulation and the air in the gap. The higher the resistivity, the higher the electric field will be in that region. Therefore an increase in insulation temperature will decrease the resistivity of the insulation relatively to the resistivity of air in the gap. Furthermore the local electric field through the healthy part of the insulation decreases. This might result in a smaller inception voltage (PDIV), because the voltage across the airgap will be higher.

What is certain is that the increase in frequency will increase the repetition rate of partial discharges which will follow the frequency of the supply voltage (discharges occurring every half a cycle). At very low frequencies this might not be the case depending

on the material used. Furthermore the time constant 'τ' of the charging voltage across the cavity or airgap, relative to the positive and the negative rising time of the system voltage, will determine the repetition rate.

2.3 Test Methods for Detecting Partial Discharges

Partial discharge (PD) measurements are made by *"integrating the discharge current at the leads of the test object"* [29]. Different quantities are measured when performing the test depending on the type of the supply voltage, that is whether it is a DC or an AC voltage. Since partial discharge occurrence is a random process, a lot of data has to be recorded to achieve accurate results. Currently for the detection of PD, whether an AC or a DC voltage is applied on the testing object, the circuits used are according to the "IEC60270" standard. The smallest discharge frequency that can be observed depends on the resolution of the analogue to digital converter of the PD detector used. The maximum recording time depends on the memory size of the detector. Test circuits for both AC and DC are shown in section 2.3.3.

Methods for testing PD include electrical and non-electrical methods. Non electrical methods involve acoustic, visual or optical and chemical detection. These will not be described here. This section will focus on the description of electrical methods only.

2.3.1 Electrical Methods for Detecting Partial Discharge

Three electrical methods currently exist for PD detection. All methods make use of an *"RCL type pulse detection circuit with different sensitivities"* [29]. An RCL circuit consists of a resistance, a capacitance and an inductance connected in parallel. In the past RC types were also used but the RCL type gives a greater sensitivity and is less vulnerable to noise [29]. The three methods for partial discharge detection are:

- Testing capacitance connected in series with the RCL impedance and both connected in parallel with a *"corona free blocking capacitor"*.
- Testing capacitance connected in parallel with the blocking capacitor which is in series with the RCL impedance.
- Two identical branches: Each branch consisting of a testing capacitance with the RCL impedance. Furthermore both branches can be placed in parallel with the blocking capacitor. This is also known as the balanced circuit.

The purpose of using the last configuration is where PD tests require the elimination/balancing of outside interference. However, the most common arrangement used is the second one. In [29], it is mentioned that when high frequency PD is investigated, an RC type is used in place of the RCL circuit. Despite the fact that a different type (RC instead of RCL) is used, the circuit configurations adopted are the same as the ones described above. All PD testing circuit configurations are shown in BS EN 60270 [30].

2.3.2 Characteristics of Partial Discharges

A partial discharge is a localised current pulse and according to [30] it has duration of less than 1 microsecond. This current pulse is reflected as a voltage pulse in the monitoring system which displays the discharge. The duration of the pulse differs if the partial discharge is the outcome of a *Townsend breakdown*, or a *Streamer breakdown*. Another form of partial discharge can occur which is called a *"Pulse-Less discharge"* [20]. The figures below show a partial discharge (current pulse) as obtained from [20], in the case of a *Townsend* and a *Streamer* mechanism respectively:

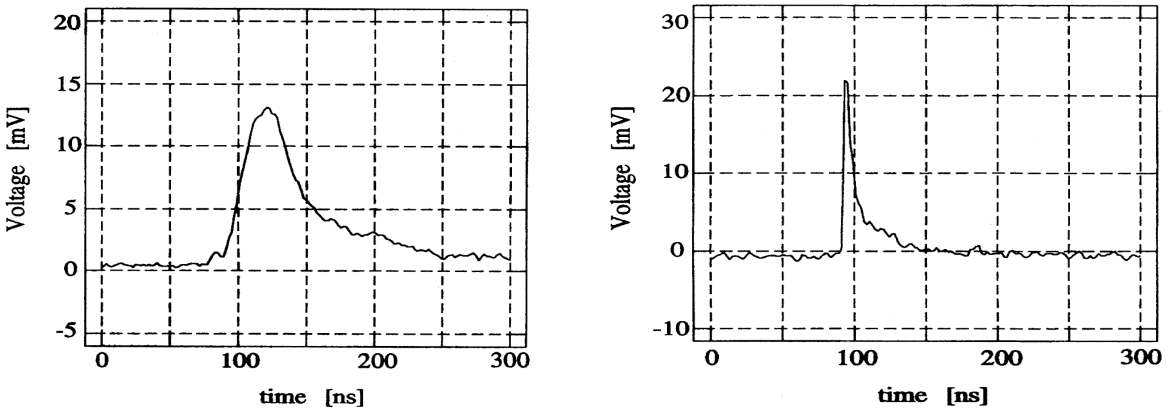

a). b).

Figure 2.13: Typical voltage pulse resulting from a) *Townsend breakdown* mechanism and b). *Streamer breakdown*, at the output of the PD detector [20]

2.3.3 Partial Discharge Detection Circuit

Just to explain the partial discharge measuring method, the 2nd standard testing circuit is used as shown in the following figure:

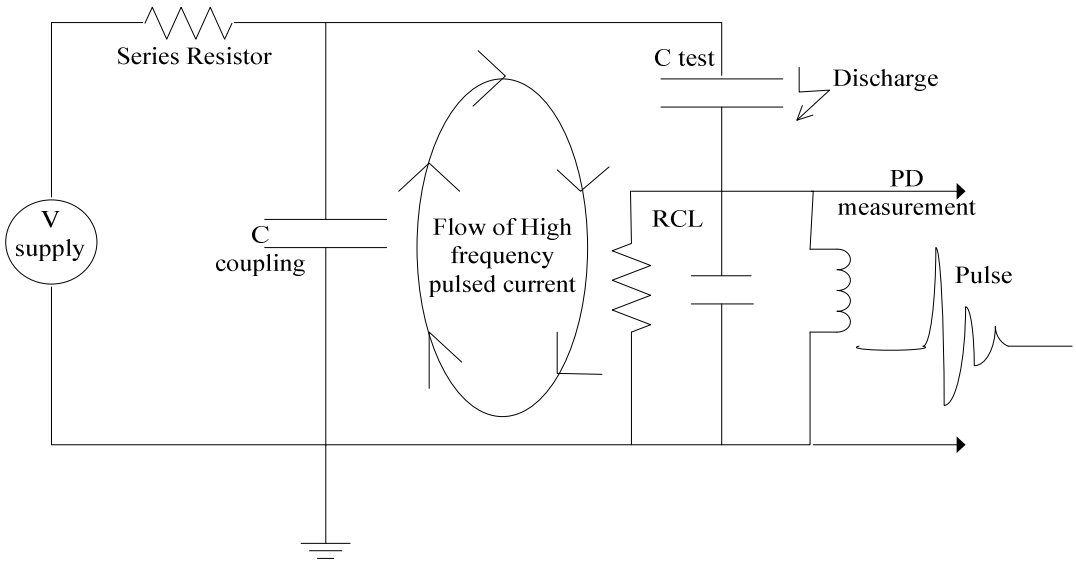

Figure 2.14: Circuit diagram describing the method of partial discharge measurement

Before starting the experiment the PD detector has to be calibrated so that the monitoring system can measure the amplitude of PD properly. When a new testing capacitance is connected to the circuit, the system requires calibration because the testing capacitance

itself affects the circuit characteristics. The calibration method involves the injection of charge (short duration current pulse) of known magnitude on the testing capacitance. This way the monitoring system can appoint a certain voltage for that discharge pulse, if the same magnitude appears through the testing capacitance when a high voltage is applied. Further information on how the test is performed will be described later on.

2.3.3.1 Partial discharge tests under an AC voltage:

When the applied voltage is sinusoidal, then the quantities that are measured are the discharge magnitude, the instantaneous voltage applied 'V_{inst}' across the testing object and the phase angle at which the discharge occurs. According to [31] the data obtained are used to plot a histogram of discharge magnitude 'q' against phase angle 'φ'. With this data the different types and causes of PD can be deduced because each type results in a different discharge magnitude to phase relationship [31]. The dielectric circuit used to analyse AC PD is shown below in Figure 2.15.

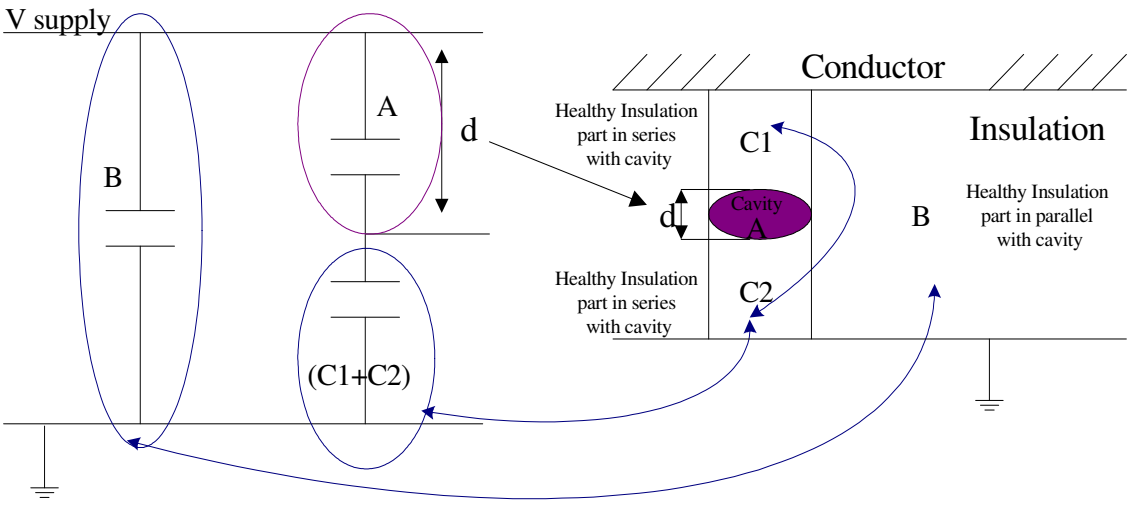

Figure 2.15: Circuit used to analyse partial discharges under an AC voltage

2.3.3.2 Partial discharge tests under a DC voltage:

Under DC the basic quantities that are measured are the discharge magnitude 'q', the time 't' at which the discharge occurs and the instantaneous voltage 'V_{inst}' across the test object

[31]. In addition to the time of discharge occurrence, the time difference between discharges can also be recorded [20] and finally the frequency of discharges [32]. Again by generating graphs of PD magnitude against time of occurrence, the type of defect in the testing object can be observed. For example different types of defect can be separated if the discharges occur on the surface of the testing object, or if a cavity is present etc. All the quantities measured can also be used to plot distribution and density functions. These give a clear indication of the different types of PD effects that are present. PD under a DC voltage can also be presented in the following ways according to [20]:

- On a "Probability Density Histogram" where the probability density of discharges *"h (q)"* in 1/pC is plotted against discharge magnitude *"q"* in pC.
- A plot of discharge magnitude *"q"* in pC and/or the discharge repetition rate *"f_{PD}"* in 1/min, against the supply test voltage in kilo-Volts (kV).
- Average magnitude of the successor/predecessor discharge "$\overline{q_{suc/pre}}$" in pC against discharge magnitude *"q"* in pC.
- Average time "$\overline{\Delta t_{suc/pre}}$" in seconds to the successor/predecessor discharge against discharge magnitude *"q"* in pC.
- Cumulative discharge repetition rate in 1/min against PD magnitude *"q"* in pC.

The dielectric circuit used to analyse DC PD is shown below in figure 2.16. As opposed to the AC case the circuit includes the resistances of the healthy part of the insulation, the resistance of the void and the resistance of the insulation part in series with the void.

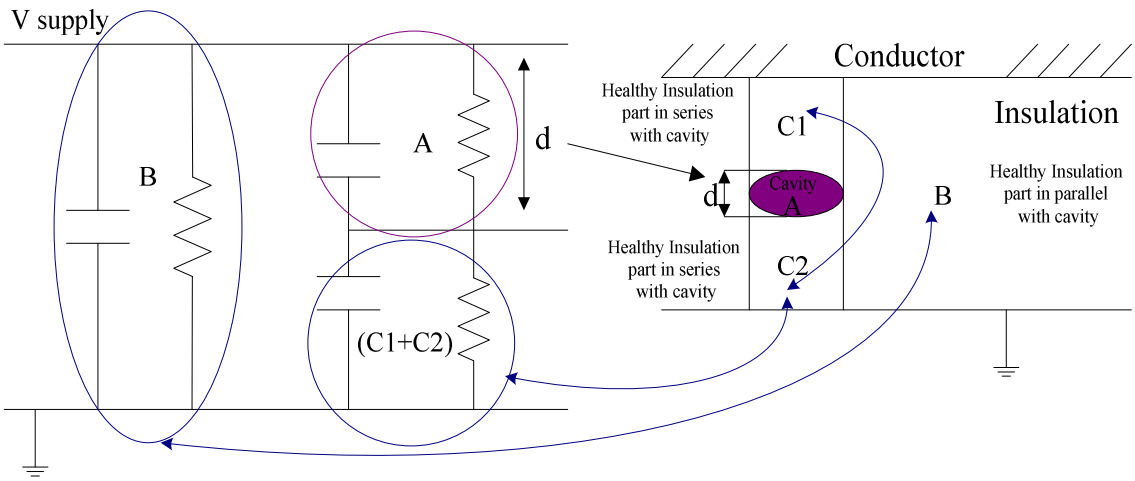

Figure 2.16: Circuit used to analyse partial discharges under a DC voltage

2.3.4 Information on Partial Discharge Tests for an Aerospace Cable Sample

Any type of cable must undergo PD tests, as well as "flashover, arc-tracking and multi-stress ageing" tests [33]. For aerospace applications, the cable must be tested in an environment similar to the actual one when the aircraft is in flight. Ideally the cable should be placed in a low pressure chamber, where the temperature inside the chamber can be varied according to the position of the cables placed in the aircraft. For example a high surrounding temperature should be used if the cable is installed near the aircraft's engines in the nacelle or near other heat sources.

- Based on recent information received from the department of Electrical Systems – EDYNE of AIRBUS France, the sensitivity of the PD detector should be "5 pC or less".

- A minimum length of the cable sample must be used for testing so that its capacitance allows detection by the PD detector. *"The minimum length should not be smaller than 850 mm"* [59]. The ends of the cable are subject to partial

discharges. These end effects can be avoided by following a standard procedure. This might involve, for example, placing the two ends in insulating oil.

- The supply voltage should be raised at a rate of 50 V/s if the extinction voltage specified by the manufacturer is up to 3 kV. If it is greater than this value, then it should be raised at 100 V/s. However in the ASTM D 149 standard the rate of rise is specified as 500 V/s [33] if the cable insulation is tested for breakdown. The length of the test specimen used was about 12 inches long, that is about 30.5 cm. As far as repetition rates are concerned, it has to be noted that in DC conditions the PD inception voltage is considered according to [20], only when the discharge repetition rate is greater than 1 discharge per minute.

2.4 Significance of Partial Discharges in Measuring SOV

PD tests are the most appropriate tests used to assess the quality and lifetime of cable. These tests are done to investigate the dielectric capability of a cable, specifically the existence of air filled voids in the dielectric insulation along the cable [34]. These tests can also be done to investigate external partial discharges like the cases described in section 1.3.1. In this case the airgap between the insulation and the ground is of great significance. These scenarios occur in places where the cable is installed and where the ends of a cable are bending to be connected to a voltage bus where the power is further distributed to the loads all around the aircraft. By considering the different types of discharges, the inception voltage at which each discharge type is initiated can be determined. The discharge having the lowest partial discharge inception voltage (PDIV) is the determining type of discharge and the corresponding PDIV could be used to further determine a safe operating voltage (SOV) for a cable system.

2.5 AC and DC Electric Fields

As it was described in the section 2.3.1, Paschen's Law can be used to determine SOV. Paschen's Law gives the relationship between the breakdown voltage of air and the pressure-distance product. Thus if the operating voltage is an AC voltage, the fraction of the voltage across the gap, (being a function of the relative permittivity, the insulation thickness of the cable and the airgap size), can be determined. The equation of the fraction of the voltage across the gap has been derived based on a linear electric field distribution assuming an AC supply voltage. If however the supply voltage is a DC voltage, then the equation is not valid. The equation has to be derived based on an electric field which depends on the resistivity of the materials instead of the relative permittivity. Therefore investigating the differences between AC and DC electric field distributions is vital, if a DC SOV calculation is to be developed either assuming a uniform or a non uniform electric field distribution.

When an alternating current passes through a cable, the electric field changes continuously whereas in the case of direct current the electric field is constant. Using this fact, the differences between AC and DC electric fields can be deduced and explained.

The electric field distribution in a cable for example depends on the conductivity, the permittivity, the geometry of the insulation, the applied voltage and the space charge density [30]. Considering the geometry and the applied voltage to be constant, under AC conditions the permittivity governs the distribution and the nature of the electric field. The electric field will concentrate in the region of lower permittivity. Under steady state DC, the electric field is dependent mostly on the conductivity and the space charge density and thus it will concentrate in the region of lower conductivity [35].

According to [33], space charge accumulation greatly affects the electric field. The breakdown voltage of an aerospace cable was tested under DC and variable frequency AC voltages at different temperatures. The results showed that under DC conditions the breakdown voltages were lower than in AC. The reason given for this phenomenon was long term space charge accumulation. These space charges were lowering the local electric field within the insulation because the dipoles' orientations, within the polymeric

insulation, were aligned in the opposite direction to the field. Space charge of this polarity is called homo-charge. However the space charge being accumulated could create dipoles aligned to the direction of the field. This type of space charge is called hetero-charge and would result in lower breakdown voltages.

When the testing specimen is under an AC electric field the resistive part of the insulation is relatively infinite to the capacitive one. In steady state DC conditions the capacitances act as an open circuit and the resistive part of the dielectric, in other words the conductivity governs the electric field distribution. Any external parameters such as temperature and temperature gradient can alter the conductivity of the insulation. For example when a screened cable is under loading conditions, the insulation will be less hot near the sheath and thus the conductivity will be lower, resulting in a higher electric field near the sheath rather than near the conductor [36]. Because of this change in the electric field distribution in a DC cable, PD will stop in certain areas in the cable insulation and will ignite in others. This fact is also confirmed by R.N. Hampton in [23], where it is stated that the electric field inversion from the conductor to the insulation shield occurs in all materials and that the degree of inversion is dependent upon the materials used as dielectric insulation.

PD repetition is explained in AC with the fact that the voltage varies sinusoidally with a certain frequency whereas in DC the repetition occurs because of the "finite resistivity of the insulation". This allows the recharging of the cavity's capacitance up to the original breakdown voltage level of the cavity. Since in the DC case PD repetition rate depends on the time constant *'τ'* of the charging cavity (which is large due to the high insulation resistance), resulting repetition rates are smaller. This also implies that the repetition rate is dependent on the conductivity of the insulation and therefore its resistance *'R_b'*. This resistance can change "degrees of magnitude if the temperature is increased from 20 ^{0}C to 60 ^{0}C and 90 ^{0}C", resulting in a similar change of τ [20]:

$$\tau = \frac{R_b R_C \left(C_b + C_c\right)}{R_b + R_c} \tag{2.22}$$

R_b = *Resistance of the insulation in series with the cavity (Ω)*

R_C = *Surface Resistance of the cavity (Ω)*

C_b = *Capacitance in series with the cavity (F)*

C_C = *Capacitance of the cavity (F)*

The repetition rates at DC and AC are only equal if 'dV/dt = V/τ' [20]. The parameters in equation 2.22 are shown in the circuit in figure 2.17:

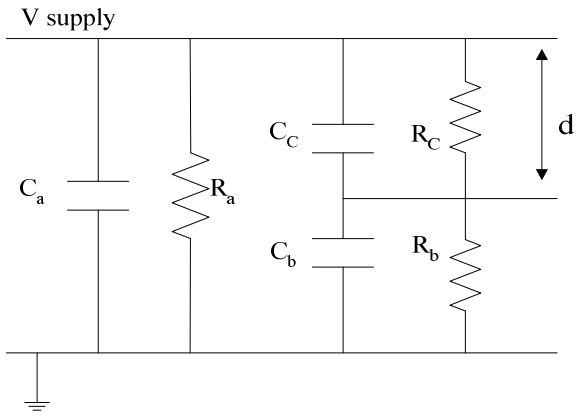

Figure 2.17: Circuit diagram for analysing DC partials discharges [16, 29].

PD magnitudes at DC voltage are also smaller due to the fact that the overvoltage 'ΔV' that appears across the cavity/void is smaller under DC than under AC conditions. This is due to the fact that the time it takes for the voltage to rise above the minimum breakdown voltage is much less than the average statistical time lag *'t_L'* (the time it takes for a PD initiating electron to appear – see Figure 2.18):

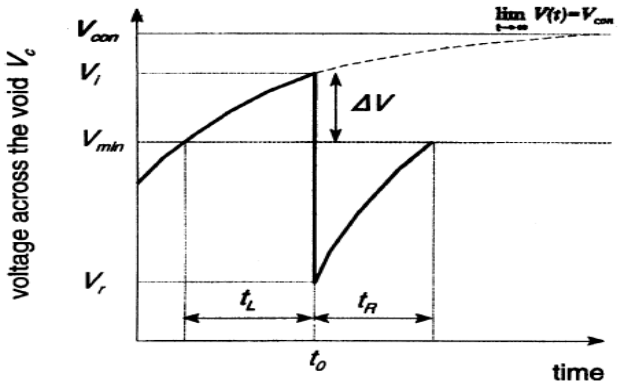

Figure 2.18: Voltage across cavity in a solid dielectric taken from [20]

V_{min} = *Minimum breakdown voltage (kV)*

t_R = *Recovery time (ms)*

V_r = *Residual voltage across the cavity after a discharge (kV)*

V_I = *Voltage across the cavity at which PD is initiated (kV)*

V_{con} = *Maximum voltage that would be seen across the void if no PD occurred (kV)*

At the stage where the voltage might be switched on or off, increased stepwise or even if a polarity reversal occurs, the PD magnitudes will increase since the field resembles the AC case where the voltage changes very fast with time (i.e. *'dV/dt'* is high).

AC PD *"leads to material erosion and electrical treeing"* [37] which in turn leads to insulation breakdown. As far as DC PD is concerned, this does not cause breakdown directly, but only helps to recognize the vulnerable areas in the dielectric insulation which might be the cause of electrical breakdown [37].

2.5.1 Differences in the Calculation of the Electric Field

Calculation of electric field differs in AC and DC conditions because in the latter case the variation of the temperature and the electric field affects the value of conductivity. In addition long term charges accumulate at interfaces distorting the electric field. These charges can enhance the local field as hetero-charge or reduce it as homo-charge. The relative permittivity *'ε_r'* and the dissipation factor *'tan(δ)'* is also subject to change with a variation on temperature but the question is how significant are these effects when a DC voltage is present.

Direct current electric fields can be time dependent if you look at different conditions such as switching on or off the High Voltage DC (HVDC) supply, sudden drop of electronic loads etc [31]. Under AC conditions, the electric field is given by equation 2.21 for a screened cable and it depends on the geometry (cylindrical radius of insulation *'r'*, radius of conductor and insulation) and the voltage *'V'* applied on the conductor of the cable [35].

$$E(r) = \frac{V}{r \ln\left(\frac{R_o}{R_i}\right)} \tag{2.21}$$

R_o = *External radius of insulation (m)*

R_i = *Internal radius of insulation (m)*

r = *Radius of the point of interest in the insulation (m)*

Under DC "steady state conditions", the electric field *'E(r)'* is given by equation 2.22 [35]:

$$E(r) = V \frac{r^{k-1} \exp(-\gamma_E E)}{\int_{R_i}^{R_o} r^{k-1} \exp(-\gamma_E E)\, dr} \tag{2.22}$$

Where *k* can be calculated using the following formula [35]:

$$k = \frac{\alpha \Delta\theta}{\ln\left(\frac{R_o}{R_i}\right)} \tag{2.23}$$

E(r) depends also on the conductivity *'σ'* (reciprocal of resistivity *'p'*) and this varies according to the electric field *'E'* and the temperature *'θ'* [36]:

$$\rho = \rho_o e^{-a_T \theta} e^{-\gamma_E E} \tag{2.24}$$

p_o= *Resistivity of Insulation when Temperature coefficient = 0 (Ωm)*

γ_E = *Field dependency coefficient*

α_T = *Temperature dependency coefficient*

From equation 2.22 we can see that if $k = 0$ (i.e. no temperature drop from the conductor to the insulation) and $\gamma_E = 0$ (i.e. the field dependency is zero), the equation is simplified to equation 2.21 where the insulation behaves capacitively. According to Jeroense and Morshuis [35], equation 2.22 is simplified if we neglect the field dependency of the stress distribution. This is a good approximation if relatively low stresses and temperature drops are involved and equation 2.25 is obtained if $\gamma_E = 0$ [35]:

$$E(r) = V\frac{r^{k-1}}{\int_{R_i}^{R_o} r^{k-1}dr} = V\frac{k}{R_o\left[1-\left(\frac{R_i}{R_o}\right)^k\right]}\left(\frac{r}{R_o}\right)^{k-1} \tag{2.25}$$

According to R. N. Hampton in [23], the value of k is given by [23]:

$$\kappa = \frac{\left(\alpha W/2\pi\lambda\right)+\left(\beta V/r_2 - r_1\right)}{\left(\beta V/r_2 - r_1\right)+1} \tag{2.26}$$

This is in agreement with the findings of C.K Eoll in [36] where the symbol 'γ_E' in his paper represents the term '$\beta V / (r_2\text{-}r_1)$'. However in [23], equation 2.25 is derived excluding the effect of stress dependence 'β' which is denoted as 'γ_E' in [36]. Equation 2.22 includes the effect of stress dependency. Equation 2.25 and the equation given by R.N. Hampton is exactly the same but the latter includes stress dependency in the evaluation for k above.

When a load is applied (i.e. connected to the cable) the temperature changes along the cable and thus the electric field distribution. The cable might be subject to load changes, supply changes, polarity reversals or the load might be switched on and off. All these changes on the cable, affect the electric field distribution and thus the maximum voltage capability of the cable insulation. The reason why in AC conditions the electric field distribution does not depend on the conductivity is because the voltage changes in a relatively short amount of time. This time is much smaller than "the time constant of the

insulation which is determined by the permittivity and the conductivity of the insulation" [35].

The above equations do not include the effect of power losses due to the leakage current being produced in the dielectric. Up to several kilo-Volts, these losses are so small that can be neglected. This is a statement which requires further examination. If the opposite is true however, [36, 38] provide equations to account for leakage current losses.

2.5.2 Similarities

The cavity thickness and the pulse width relation observed in a DC PD are also observed in the AC PD case. This relationship shows that the discharge pulse width increases with cavity thickness whereas the pulse height decreases [20]. Partial discharge repetition rates are the same for DC and AC when *'$V/\tau = dV/dt$'*. PD Magnitudes are comparable only at very small frequencies where *dV/dt* is very small. The electric fields are calculated using the same equation only when the DC voltage is changing either due to changing loads, switched on/off etc.

2.6 Summary

In Chapter 2, a literature review has been carried out on PD and the effect of this phenomenon on aircraft cables. The locations where PD is most likely to occur have been illustrated and the recommended voltage selection process to avoid these discharges in an aircraft environment, has been described. The calculations take into consideration the effect of temperature on the breakdown voltage of air, which is related to the pressure distance product according to Paschen's law.

The factors influencing the cable insulation properties and the properties of air have been explained. Furthermore a discussion has been carried out on the effects of temperature and frequency on the air electrical properties relatively to the cable insulation electrical properties.

The chapter also provides information gathered from literature on the existing electrical methods used to measure and analyse PD under both AC and DC voltage conditions. The relevant standards for testing an aerospace cable are also given together with the testing procedure. Finally, gathering information from literature, a comparison has been carried out on the calculation of the electric field when the cables are operated under AC and DC conditions.

The chapters that follow compare the safe operating voltage (SOV) of certain AC and DC cable systems. In both cases, (AC and DC), the SOV is calculated based on the partial discharge inception voltage (PDIV) and by using the same methodology, assuming that the electric field distribution is determined by the relative permittivity of the dielectric materials, the dielectric thickness and the airgap distance. Furthermore PD tests are carried out under AC and DC conditions to evaluate the differences and the similarities in PDIVs, PD repetition rates and PD magnitudes.

Chapter 3

Cable System Optimisation

In this chapter, two methodologies are developed and explained in order to evaluate the maximum power that can be transferred though a certain cable system, considering restrictions on system weight and/or volume. The cable system might operate under AC or DC voltages and for illustration purposes a cable duct system is used for modelling and analysis.

3.1 Introduction

Installing a certain cabling system requires knowledge of the space available to accommodate the needs of the electrical system. Once this volume is evaluated, then the cables have to be placed in that volume in a configuration so as to achieve a maximum power rating. For example if a one-circuit three phase AC electrical system is used, this would require four cables coming out of a generator (three phases + neutral). The three phase cables would have to be spaced as far apart to account for thermal and partial discharge issues and in an order so that there is a minimum impedance unbalance and thus minimum current flowing through the neutral. In an aircraft system the overall cable weight would also have to be spread equally over the whole plane for stability issues etc. This chapter examines a certain cable system to be used in an aircraft, the best way to fit these cables in a duct, taking into consideration the volume, the weight, the maximum transmission voltage and current in each cable. The cable systems analysed include a one-circuit three phase AC with no neutral, one-circuit three phase AC with neutral, a two-circuit grounded DC system (two cables positive & two cables negative), a two-circuit

floating DC ((two cables positive & two cables negative), a three-circuit floating DC and a two-circuit three phase AC with a neutral. Schematics with details for each system configuration are shown in the next section of this chapter in Figure 3.2. It has to be clarified here that the floating DC systems have the positive cable floating between zero and maximum positive voltage, whereas the negative cable floating between zero and negative maximum voltage.

3.2 Development of Calculation Techniques for Limited Available Space

For all the cable systems described in Section 3.1, the method described in Chapter 2 for determining the partial discharge inception voltage (PDIV), was used to determine the safe operating voltage (SOV) in an aircraft environment, based on the insulation thickness of the cables in the duct, the airgap size and the type of insulation material. The analysis is based on the use of uniform electric field calculation models and the use of Paschen's Law, which relates the breakdown voltage of air to the pressure-airgap distance product. The flow chart shown below gives an introductory illustration of the methodology adopted.

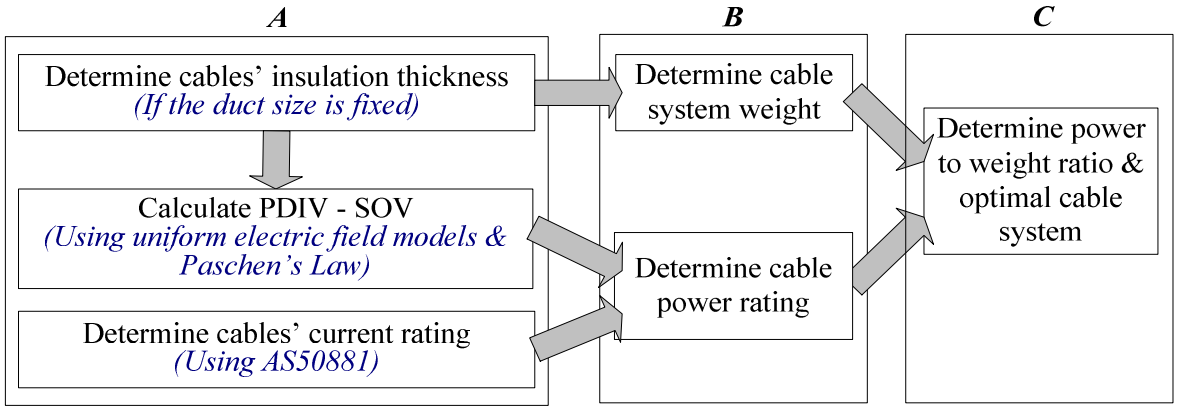

Figure 3.1: Flow chart: Introductory illustration of the cable system optimisation methodology

The procedure shown in Figure 3.1 was carried out for all cable systems described. The optimal cable system would be the one satisfying the electrical power transfer requirements and also offering the largest power to weight ratio. The analysis begins in the next section by explaining how the maximum insulation thickness was computed.

3.2.1 Maximum Cable Size Calculation for a Fixed Duct Size

Analysis has been carried out for each cable system placed in a duct as shown below in Figure 3.2. Furthermore equations have been developed for each case for calculating the maximum cable size if the duct diameter is known. Similarly if the cable diameter is known, the minimum duct size can be computed.

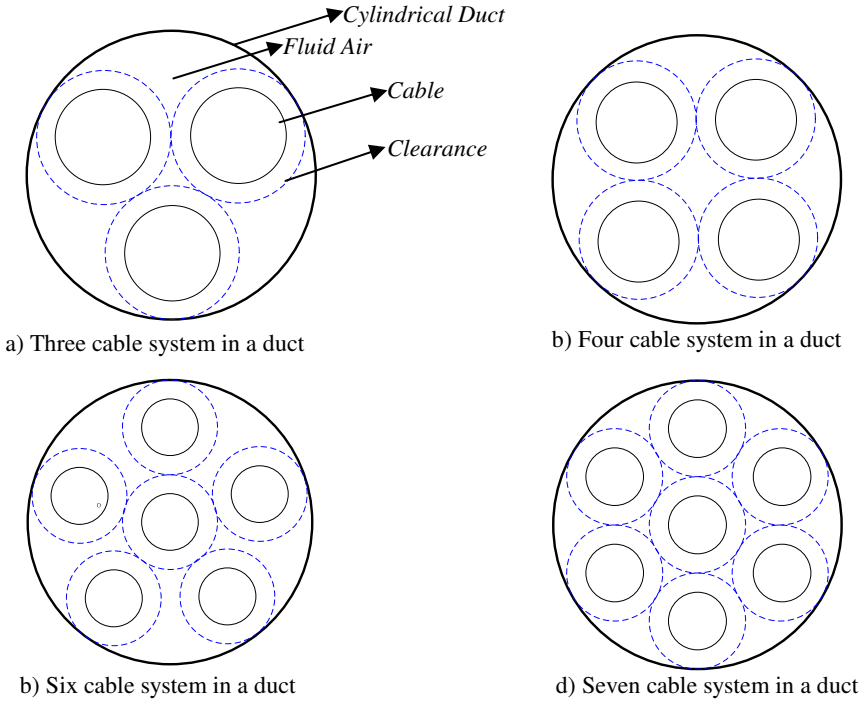

Figure 3.2: Cable systems in a duct. Dotted lines indicate the clearance between cable to cable and cable to duct.

The three-cable in a duct system represents a three phase AC system with no neutral. The four cable system represents a three phase AC system with neutral or a two-circuit grounded DC (2 cables positive and 2 cables negative), or a two-circuit floating DC

system where the conductors are allowed to float. The six cable system can be a two-circuit, three-phase AC with no neutral or a three-circuit floating DC system. The seven cable system represents a two-circuit, three phase AC with neutral. For each system, equations 3.1-3.4 have been derived to calculate the maximum cable size when the duct diameter is known. (Note: The derivations are shown in Appendix C-1). Given a certain AWG size of conductor, the insulation thickness can be calculated after computing the maximum cable size. The insulation thickness will be used to find the maximum possible safe operating voltage based on Paschen's Law (at specific ambient temperature and pressure), so that partial discharges are avoided.

- *Three Cable System:*

$$r_C = \frac{r_{Duct} - \left(1/\sqrt{3}\right) \times d_{WW} - d_{WG}}{\left(2/\sqrt{3} + 1\right)} \tag{3.1}$$

- *Four Cable System:*

$$r_C = \frac{r_{Duct} - \left(1/\sqrt{2}\right) \times d_{WW} - d_{WG}}{\left(\sqrt{2} + 1\right)} \tag{3.2}$$

- *Six Cable System:*

$$r_C = \frac{r_{Duct} - d_{WW} - d_{WG}}{3} \tag{3.3}$$

- *Seven Cable System:*

$$r_C = \frac{r_{Duct} - d_{WW} - d_{WG}}{3} \tag{3.4}$$

r_C = *Cable radius (m)*

r_{Duct} = *Duct radius (m)*

d_{WW} = *Clearance/Shortest distance between two cables in duct (m)*

r_{WG} = *Clearance/ Shortest distance between cables and duct (m)*

For all cable systems a fixed duct size was set to illustrate the calculation procedure. To begin with, a duct with a diameter of 30 mm was used having a clearance of d_{WG} = 2 mm, between cable and duct and a clearance of d_{WW} = 4 mm between cable to cable, to allow the cables to be pulled through. The cable clearances, were approximately chosen according to [39, 40], which state that the inner diameter of the duct should be 25% larger than the maximum diameter of the cable bundle. This means that in order to have a 30 mm duct diameter, the cable bundle should have a maximum diameter of 22.5 mm. By using the above equations the maximum cable sizes were calculated. AWG conductor sizes from 4/0 down to 22 were listed. Knowing the maximum cable size and conductor size, the insulation thickness was calculated. Take for example the three cable system having a conductor size of 2/0 which has a radius of 4.63 mm. If the radius of the duct is 15 mm then by using equation 3.1, r_{cable} = 4.96 mm. Thus the insulation thickness is equal to 4.96 mm – 4.63 mm = 0.33 mm. This value of r_{cable} is for d_{WG} = 2 mm and d_{WW} = 4 mm. The cable bundle radius can be calculated when r_{cable} = 4.96 mm, by assuming that there are no clearances between the cables and the duct. Considering this value of r_{cable}, the resulting cable bundle diameter is approximately 22 mm. This result satisfies the regulations for the maximum cable bundle size that can be installed in a conduit of specific diameter, since for a 30 mm diameter duct, the cable bundle diameter should be 22.5 mm. For the rest of the cable systems for which the number of cables in the duct is greater than three, the cable bundle radius is less taking into consideration the same clearances. It can be argued here that the duct used could have a smaller size and thus saving in volume. However for reasons of comparison and for calculation simplicity, the same clearance values are used. Table 3.1 gives the insulation thickness results for all cable systems using equations 3.1-3.4, taking into account the clearances mentioned and the 30 mm duct.

TABLE 3.1
CABLE GAUGE SIZES AND CORRESPONDING
INSULATION THICKNESS FOR ALL CABLE SYSTEMS

Cable Size	Conductor Diameter	Max Insulation Thickness (3 cables)	Max Insulation Thickness (4 cables)	Max Insulation Thickness (6 cables)	Max Insulation Thickness (7 cables)
AWG	(mm)	(mm)	(mm)	(mm)	(mm)
2/0	9.260	0.330	-	-	-
1/0	8.250	0.840	0.090	-	-
1	7.350	1.290	0.540	-	-
2	6.540	1.690	0.940	-	-
4	5.190	2.370	1.620	0.405	0.405
6	4.110	2.910	2.160	0.945	0.945
8	3.260	3.330	2.580	1.370	1.37
10	2.590	3.670	2.920	1.705	1.705
12	2.050	3.940	3.190	1.975	1.975
14	1.630	4.170	3.400	2.185	2.185
16	1.290	4.320	3.570	2.355	2.355
18	1.020	4.450	3.700	2.490	2.49
20	0.810	4.560	3.810	2.594	2.594
22	0.640	4.640	3.890	2.678	2.678

It has to be mentioned here that in cases where more than three cables are considered, the larger AWG conductor sizes (2-2/0) cannot fit into the 30 mm duct. These cases are marked on table 3.1 with a dash symbol. In addition, by using the values listed in the above table the safe operating voltage for each insulation thickness can be calculated. This is illustrated the next section.

3.2.2 Safe Operating Voltage (SOV) Calculation

The Safe Operating Voltage (SOV) is determined by calculating the RMS partial discharge inception voltage (PDIV). In practice the partial discharge extinction voltage (PDEV) should be used as the SOV, to eliminate the probability of PD initiation. Based on experience and on literature [11, 41, 42], PDEV can be about 20% less than the PDIV under AC conditions, but this value tends to vary. The PDEV cannot be calculated and thus the PDIV is used in this analysis to compute cable system voltages.

As described in Chapter 2 - Section 2.2.4, the SOV can be calculated using uniform electric field approximation models and Paschen's Law. This work has also been carried out by M.C Halleck [43] which states that a uniform electric field approximation can be used as long as the radius of conductor curvature is greater than 0.79 mm. If the radius of curvature is smaller, then the PDIV estimation will be overestimated *"to a maximum of 10%, to 20% for square edged electrodes"* [43]. However the overestimation is also dependent on the thickness of the insulation and this will be shown later on. In this analysis, the types of partial discharges that are examined were shown in Section 2.2.4 in Figure 2.5. The figure is again shown below.

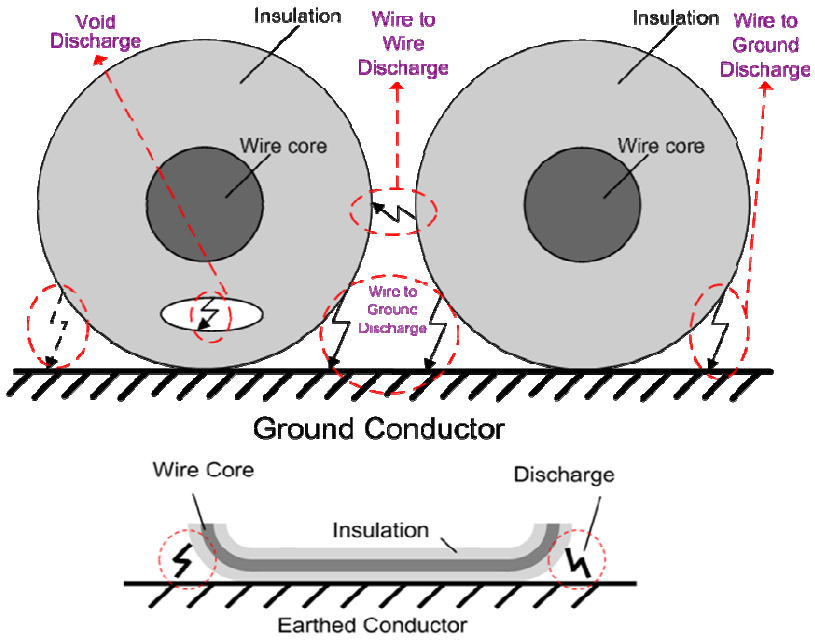

Figure 3.3: Locations of PD taken into consideration in the calculation of SOV

The description of the *SOV* determination begins by explaining how the cable to ground, cable to cable and the void discharge inception voltages are calculated. For each discharge type the safe operating voltage is symbolised as SOV_{CG}, SOV_{CC} and SOV_V respectively. Once the inception voltages for each discharge type are evaluated, the lowest one is chosen to represent the *SOV* of the cable system.

3.2.2.1 Cable to ground airgap discharges

Figure 3.4 shown below, illustrates how a uniform field calculation can be used for the three cable system, to obtain an approximate expression for the fraction of the voltage across the air gap *'fract$_{(Vd)}$'*, between each cable and the grounded duct. *fract$_{(Vd)}$* , is a function of the cable insulation thickness, the relative permittivity of the insulation material and the cable to ground airgap distance.

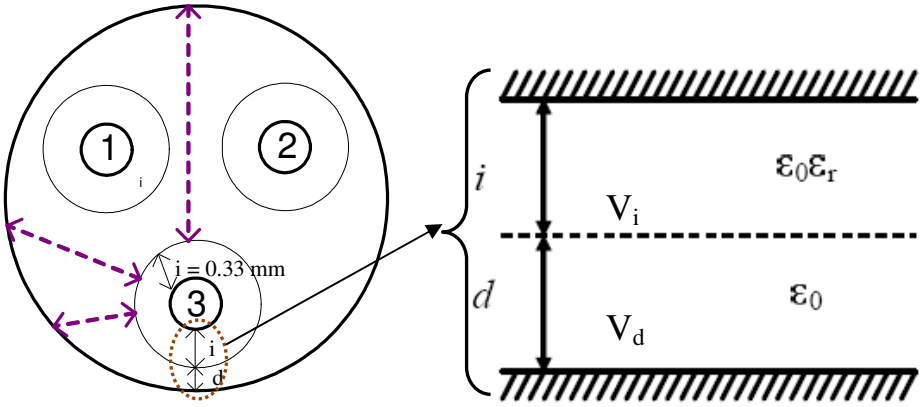

Figure 3.4: Three cable system: Cable to ground discharge "Diagram showing the simplification of the electric field calculation by using a uniform model"

A uniform field approximation is applied since the air gap distances are quite small. In addition it is also assumed that the other conductors do not have an impact on the electric field in the gap and thus Paschen's Law can be applied to solve the problem. It has to be noted that results are conservative since for small conductor sizes the electric field concentrates around the conductor-insulation boundary. The purple dotted arrows illustrate that a partial discharge or breakdown of the airgap could happen anywhere between the high voltage conductor and the enclosing duct. Thus the air gap distance *'d'* varies and it would be very difficult to predict at which value of *d* breakdown would occur. Thus in this procedure, discharge inception voltages are calculated for a possible range of *d* and the lowest one is picked as the safe operating voltage (SOV_{CG}) [12]. Looking at equation 3.5, the fraction of voltage across the air gap *'fract$_{(Vd)}$'* is calculated by:

$$fract_{(V_d)} = \frac{V_d}{V_d + V_i} = \frac{\varepsilon_r}{\varepsilon_r + \frac{i}{d}}$$

$$\Rightarrow fract_{(V_d)} = \frac{\varepsilon_r}{\varepsilon_r + \frac{(R-r)}{(T-R)}} \tag{3.5}$$

$fract_{(Vd)}$ = Fraction of the voltage across the airgap

V_d = Voltage across airgap (V)

V_i = Voltage across insulation (V)

i =Insulation thickness (mm)

d =Shortest airgap distance between cable and duct (mm)

ε_r =Relative permittivity of insulation

T = Duct radius (mm)

R = Cable radius (mm)

T - R =d_{WG} = Cable to ground airgap distance (mm)

r = Conductor radius (mm)

After *$fract_{(Vd)}$* is evaluated, Equation 3.6 can be used to find the discharge inception voltage *'$V_{inception}$'* at which partial discharges ignite, provided that the breakdown voltage of the air is known. The breakdown voltage *'V_{brk}'* of the air between the insulation and the duct is obtained from Paschen's Law, shown in Figure 3.5 for a specific pressure, temperature and airgap distance:

$$V_{Inception} = SOV_{CG} = \frac{V_{Brk}}{fract_{(V_d)}} \tag{3.6}$$

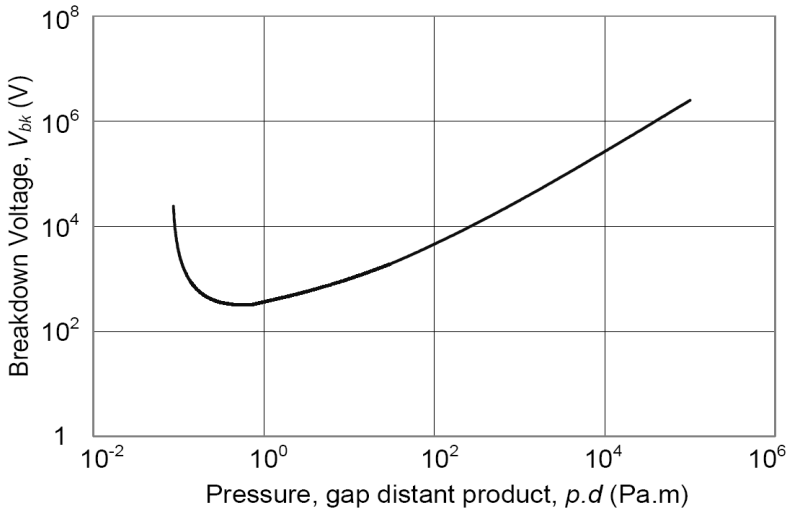

Figure 3.5: Paschen's Law for air [12]

For a constant pressure of 11.6 kPa which is the approximate pressure at an altitude of 50,000 feet and an ambient temperature of 343 K [12], the airgap distance is varied from 10 µm to 2 cm. $fract_{(Vd)}$ is calculated for all cases and then plotted on the same graph as Paschen's Law for the same *p.d* product. By dividing the points of $fract_{(Vd)}$ from the corresponding points on the V_{Brk} or Paschen's Law curve, the inception voltage ($V_{inception}$ or PDIV) curve is computed. From this curve the minimum point is chosen as the Safe Operating Voltage (SOV).

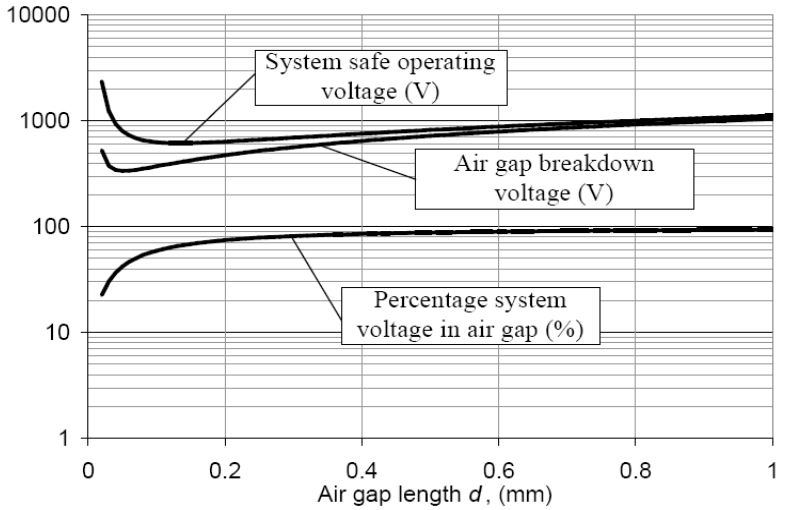

Figure 3.6: Plotting $fract_{(Vd)}$ as a percentage on Paschen's Law curve to obtain the $V_{inception}$ curve [12]

3.2.2.2 Cable to cable airgap discharges

The above calculations only include the case of a cable to ground discharge and this is not the only type of discharge that could take place. A discharge might occur between two cables (cable to cable airgap discharge), or even within a void in the insulation. The former case is shown diagrammatically in Figure 3.7:

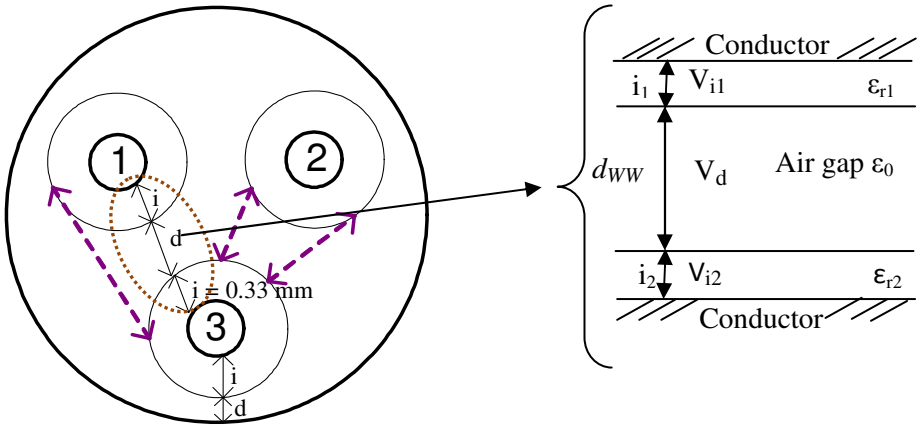

Figure 3.7: Three cable system: Cable to cable discharge "diagram showing the simplified electric field calculation by using a uniform field model"

In the cable to cable case, by integrating the electric field across the insulation thicknesses and the air gap distance, equation 3.8 is derived as shown in Chapter 2, Section 2.2.4.2.

$$fract_{(V_d)} = \frac{d\varepsilon_{r_1}\varepsilon_{r_2}}{d_{WW}\varepsilon_{r_1}\varepsilon_{r_2} + i_1\varepsilon_{r_2} + i_2\varepsilon_{r_1}} \tag{3.8}$$

d = Clearance/Shortest air gap distance between two cables in the duct (mm)

ε_{r1}, ε_{r2} = relative permittivity of insulation for cable 1 and cable 2 respectively

i_1, i_2 = Insulation thicknesses of cable 1 and cable 2 respectively (mm)

If the insulation of the two cables is of the same type, for example PTFE with a relative permittivity of 2.1, then $\varepsilon_{r1} = \varepsilon_{r2}$. If the insulation thicknesses are also equal, then $i_1 = i_2$. Based on these assumptions Equation 3.8 can be adjusted as follows:

$$fract_{(V_d)} = \frac{d_{WW}\varepsilon_{r_1}}{d_{WW}\varepsilon_{r_1} + 2i_1} = \frac{\varepsilon_{r_1}}{\varepsilon_{r_1} + 2\dfrac{R-r}{d_{WW}}} \tag{3.9}$$

This result shows that in the uniform field calculation case, the equation used to calculate $fract_{(Vd)}$ for the cable to ground case, can also be used for a cable to cable case. However for the latter, the insulation thickness used is twice as much: "2.i =2.(R-r)" (look at equation 3.9). Following the calculation of $fract_{(Vd)}$, the same procedure has been carried out to compute SOV_{CC}.

3.2.2.3 Void discharges in the insulation

When considering cable to ground discharges, the SOV which is calculated using a uniform electric field model, is always smaller in magnitude than the SOV which would be calculated if a coaxial electric field model was used. This is because a coaxial field model, as it will be analysed later on, results in a higher electric field at the surface of the cable conductor within the insulation, than within the airgaps [44]. Thus the 'cable to ground' SOV resulting from uniform field calculations is conservative and lies on the 'safe side', even though this also depends on the conductor size [43]. On the other hand, by using the uniform field model for a void discharge, SOV results would be greatly overestimated.

A discussion will follow in Section 3.5.2 as to why a non uniform (coaxial), electric field model was chosen for the calculation of the SOV_V for void discharges. The aim of Section 3.2 is to show the maximum power transfer calculation methodology. Figure 3.8 shows the electric field coaxial geometry approximation.

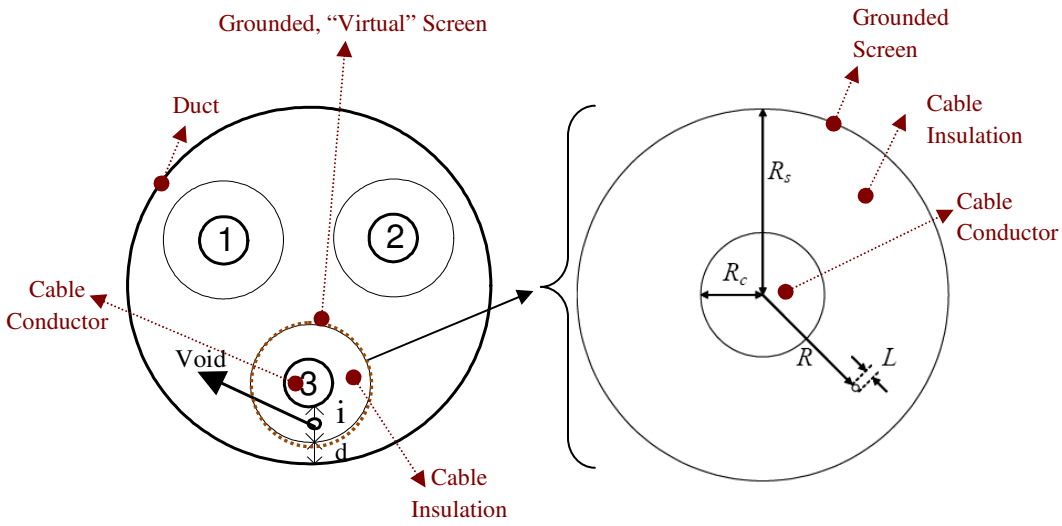

Figure 3.8: Non uniform (coaxial) model used for void discharge calculations: a). Three cable duct system & b). Coaxial cable model [45]

Using the above model as shown in Figure 3.8b, Malik [45] has derived an equation to calculate the partial discharge inception voltage. This equation is shown below and it makes the assumption that a screen covers the cable insulation. This might not always be the case however this assumption does provide conservative results since it considers a high concentration of the electric field within the insulation, especially at the conductor insulation boundary [45].

$$V_C = \frac{E_V R_{pos}}{K} \ln\left[\left(\frac{R_S}{R_C}\right)\left(1+\frac{L}{R_{pos}}\right)^{K-1}\right] \tag{3.11}$$

L stands for the void's size/length. S is the insulation thickness, R_S the cable radius, R_C the conductor radius, R_{pos} the position radius of the void from the conductor centre to the outer insulation surface, K the field enhancement factor and E_V the electric field in the void.

The PDIV can be calculated by replacing E_V in the above equation with the breakdown electric field of air 'E_{Brk}' as defined by Paschen's Law. Thus the discharge

inception voltage of a cable through void discharge depends on the size and shape of the void, its location on an axis along the electric field line, the relative permittivity of the insulation material and the air pressure in the void. The worst situation for voids formation is when they are created near the conductor surface where the electric field is the strongest, especially if the conductor is very small. In addition the void is assumed to have a flat disc shape. For this type of void, the electric field in the void will be enhanced by a factor equal to the relative permittivity of the bulk insulation. In addition the size of the void used in the calculations which will follow, is assumed to be 80 μm. According to [12, 45], the larger the void size the smaller will be the discharge inception voltage. Hence a void of 80 μm will result in a lower SOV_V, to be on the safe side. A very detailed explanation on the factors affecting a void discharge is given in [12].

3.2.2.4 Safe Operating Voltage (SOV)

Sections 3.2.2.1-3.2.2.3, provide the equations that are used to calculate the safe operating voltages for cable to ground (CG), for cable to cable (CC) and for (CV) void discharges. After calculating the inception voltages for the three types of discharges (SOV_{CG}, SOV_{CC} and SOV_V), for a specific conductor size and insulation thickness, the lowest one is chosen as the *SOV* of the cable system. As an example consider a conductor with a radius of 0.322mm and an insulation thickness of 4.64mm. The results for SOV_{CG}, SOV_{CC} and SOV_{CV} are 2.3 kV, 2.0 kV and 4.5 kV respectively. The lowest is the cable to cable discharge inception voltage (SOV_{CC}). The actual cable to cable RMS SOV_{CC} is 3.5 kV and this voltage rating represents the maximum phase to phase voltage rating that can be applied across two cables. Thus the phase to phase voltage has to be divided by √3 to obtain the maximum single phase voltage rating, which is found to be 2.0 kV.

Furthermore, for all insulation thicknesses as listed in table 3.1, the SOV was calculated based on a pressure of 11.6 kPa at an altitude of 50,000 feet and an ambient temperature of 343 K. Figure 3.9 shows all the SOV results for all cable systems that have been examined.

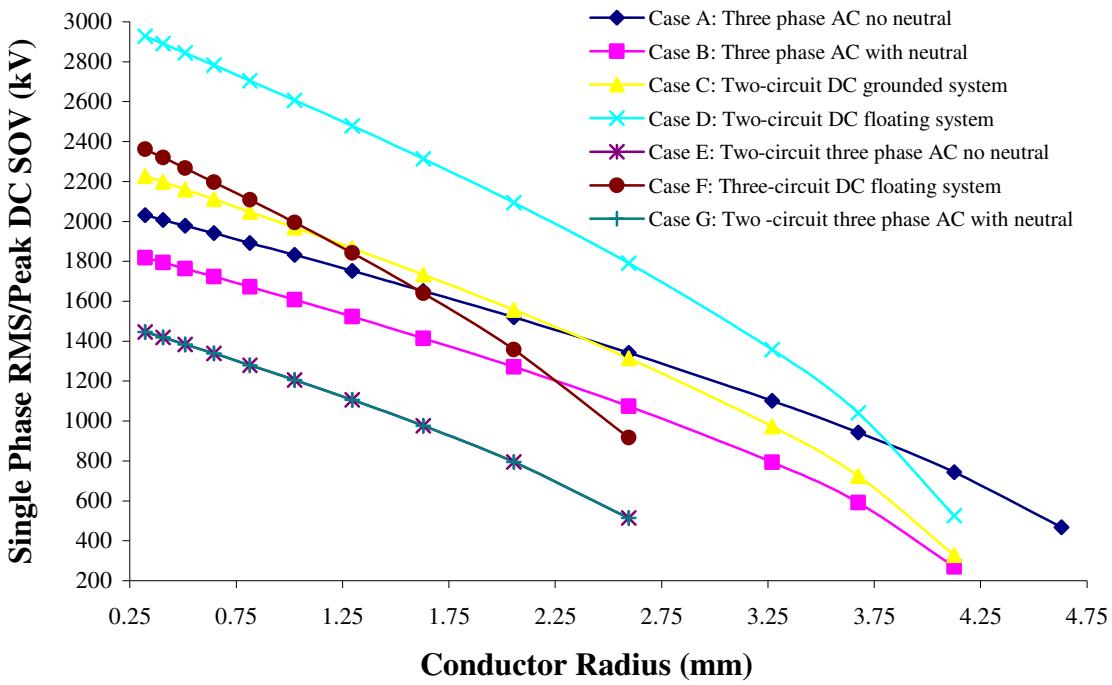

Figure 3.9: Variation of the single phase RMS/Peak DC voltage rating (SOV) with increase in conductor size for a fixed duct diameter of 30mm

All cable systems show a decrease in the voltage rating with increase in conductor diameter. This is explained by the fact that a larger conductor size implies less insulation thickness for a fixed cable size. The bigger the number of cables in the duct, the smaller is the maximum cable size. Thus, for the same AWG conductor size, the insulation thickness is smaller resulting in smaller voltage ratings.

For all cable system cases, either AC with and without neutral or grounded DC, the simulations determined that the mode of discharge with the lowest inception voltage was discharge in the air gap between two cables, in other words discharge caused by the phase to phase voltage. While the insulation between two cables is twice as thick as that between a single cable and the ground, the safe operating voltage does not double. For most systems in which the electric field can be considered uniform, the safe operating voltage appears to be roughly proportional to the square root of the insulation thickness. The double insulation thickness therefore only improves the voltage capability between two cables by a factor of around 1.4 in comparison to the voltage capability of a single cable. However,

in an AC system the voltage between two phases will be 1.7 times that of the phase to ground value, while for a grounded DC system the voltage between two cables will be double that between a cable and the ground.

The DC floating case exhibits higher voltage ratings, since the limiting discharge type is the cable to ground discharge. To obtain a better understanding look at table 3.2. The table shows the SOV results for the two DC cases and for each conductor size, considering cable to ground and cable to cable discharges.

TABLE 3.2
CABLE GAUGE SIZES AND CORRESPONDING
SOV FOR THE FOUR-CABLE DC SYSTEMS: "USED FOR COMPARISON"

AWG	DC floating System: Cable to Ground (V)	DC floating System: Cable to Cable (V)	DC Grounded System: Cable to Ground (V)	DC Grounded System: Cable to Cable (V)
1/0	525.7	657.6	525.7	657.6/2 = 328.8
1	1039.5	1449.8	1039.5	1449.8/2 = 724.9
2	1357.1	1945.1	1357.1	1945.1/2 = 972.55
4	1791.2	2629.1	1791.2	2629.1/2 = 1314.55
6	2093.7	3112.6	2093.7	3112.6/2 = 1556.3
8	2314.0	3465.5	2314.0	3465.5/2 = 1732.75
10	2478.0	3731.0	2478.0	3731.0/2 = 1865.5
12	2606.4	3938.5	2606.4	3938.5/2 = 1969.25
14	2704.7	4096.1	2704.7	4096.1/2 = 2048.05
16	2783.3	4221.9	2783.3	4221.9/2 = 2110.95
18	2844.2	4320.2	2844.2	4320.2/2 = 2160.1
20	2890.6	4395.0	2890.6	4395.0/2 = 2197.5
22	2928.0	4455.3	2928.0	4455.3/2 = 2227.65

The cable to ground discharge voltages are exactly the same for both cases since the insulation thickness is identical in both cable systems. For the same reason the cable to cable discharge voltages are the same. However in the DC grounded system, this cable to cable voltage has to be divided by 2 in order to find how much the voltage across the cable to ground should be. This voltage is lower than the cable to ground discharge inception voltage calculated initially and it is thus taken to be the Safe Operating Voltage (SOV). In the DC floating system, it is possible for one cable to be raised up to maximum system voltage. In other words if the voltage across two cables is 657.6 V, as shown in the first row of table 3.2 in the second column, this voltage can suddenly appear across the cable

and the ground. This would be the worst situation since the cable to cable voltage would appear across a single insulation layer (cable to ground). If the cable to ground capability is 525.7 Volts for an AWG 1/0 size conductor, then a value of 657.6 would be improper to use. Thus the cable to ground voltage is chosen as the SOV.

3.2.3 Maximum Operating Current Calculation

As mentioned in the introduction the temperature and altitude do not only affect the voltage rating but also affect the current rating. For example take an AWG 8 cable conductor size operating at 150°C. If it is assumed that the ambient temperature can be 20°C or 100°C, following the current calculation procedure and data provided in AS50881, the current rating is found to be 115 Amps and 90 Amps respectively. Note that these values are calculated based on the case of a single copper cable in free air. Furthermore it is required to derate these values if they are installed in bundles and consider the effect of higher altitudes.

The current rating for each conductor size is obtained from AS50881 [11]. The standard contains three figures for calculating the current up to an operating supply frequency of 800Hz. The first figure is used for finding the current depending on the temperature difference (conductor temperature rating minus the ambient). The other two give the derating factor if the cables are placed in a bundle and the correction factor for the altitude. The current rating is simply calculated by multiplying the data from the three figures together. Take for example an AWG cable conductor size of 2/0 which corresponds to a diameter of 9.26 mm. The current value depending on the temperature difference is 367 A. If we take the three cable system data in column three from table 3.1 (case A: three phase AC with no neutral), the derating factor for three cables in a bundle is 0.7375 and the correction factor to account for the altitude is 0.7917 [11]. Thus, the current rating = 367 x 0.7375 x 0.7917 = 214.28 A. Similarly for the four cable system (case B: three phase AC with neutral), the derating factors are the same since the neutral would carry no current if the system is balanced. For the DC cases, the altitude correction factor remains the same as expected, whilst the derating factor for cables in a bundle is reduced to 0.6667 because

current flows in all four cables. Thus for the DC cases: the current rating = 367 x 0.6667 x 0.7917 = 193.70 A'. The corresponding derating factor for six and seven cables in the duct is 0.5775. Considering supply frequencies greater than 800 Hz, the current ratings have to be derated further since skin and proximity effects become significant. It has to be noted that the standard does not provide information for frequencies exceeding 800 Hz.

3.2.4 Maximum Power Transfer Calculation for a Fixed Duct Size

Using the results for the SOV and safe operating current (SOI), the maximum power transfer is calculated for each cable system and for a range of AWG conductor sizes. Furthermore the weight of each system is computed as well as the power to weight ratio. This is done because in aircraft the cable system weight is of vital importance for fuel saving. These calculations form the basis for an overall cable system optimisation methodology. The optimisation methodology is shown on the next page in detail, in Figure 3.10.

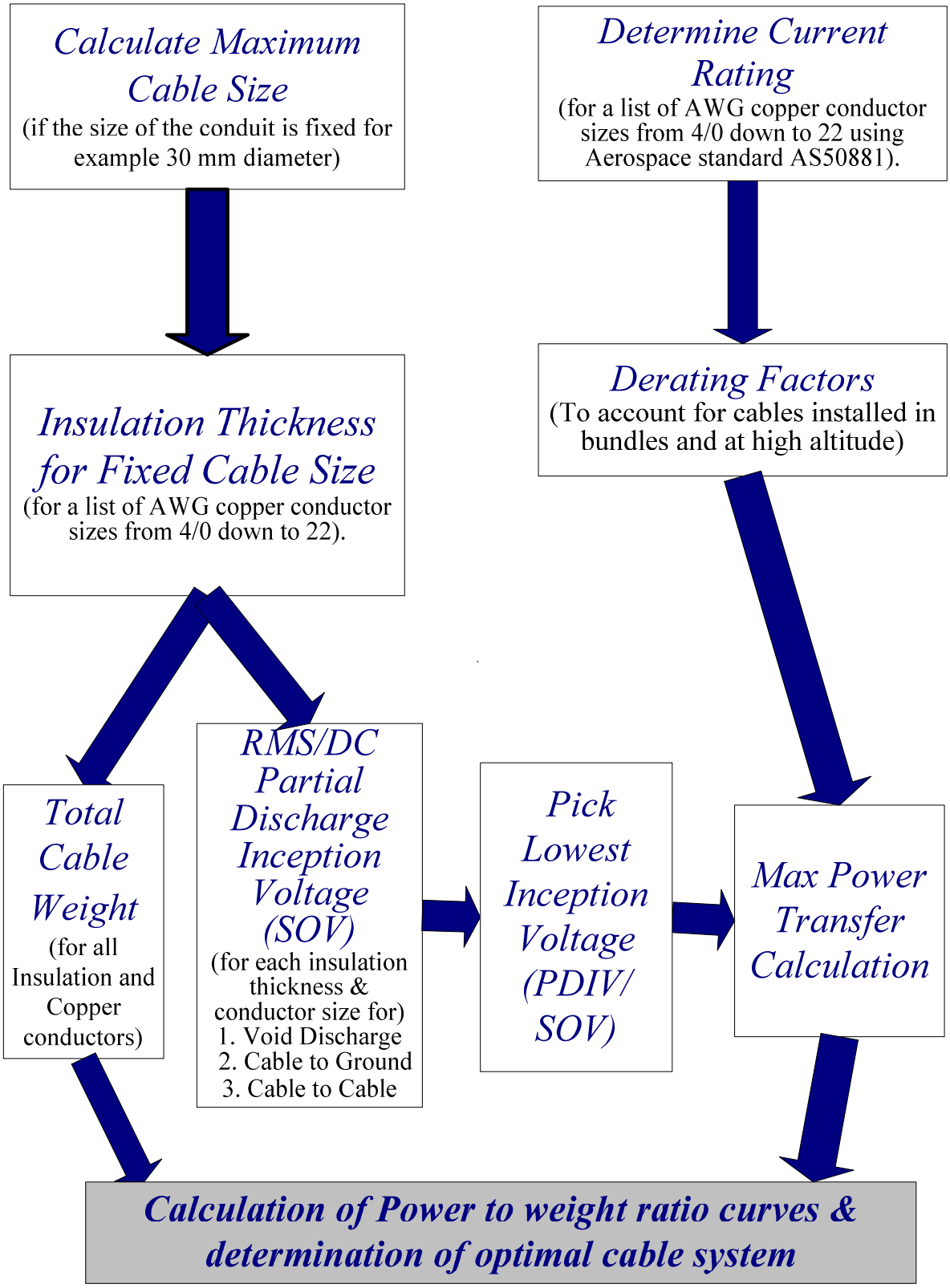

Figure 3.10: Flow chart: Detailed illustration of the cable system optimisation methodology

3.2.4.1 Maximum power transfer

The methodology illustrated in figure 3.10 has been adopted to determine the maximum power transfer for each cable system. Results for all the cable systems including insulation thicknesses and current ratings are shown in Table 3.3, for a duct having a diameter of 30 mm, and the cables consisting of PTFE insulation and copper conductors.

TABLE 3.3
CABLE GAUGE SIZES AND CORRESPONDING CURRENT RATING
AND MAXIMUM INSULATION THICKNESS FOR ALL CABLE SYSTEMS

Cable Gauge	Conductor Diameter / mm	One Circuit AC System with No Neutral : SOI	Two Circuit DC Systems: SOI	Two Circuit AC System with no neutral ,Three Circuit DC Floating System and Two Circuit AC System with neutral: SOI	Max Insulation Thickness (3 cables)	Max Insulation Thickness (4 cables)	Max Insulation Thickness (6 cables)	Max Insulation Thickness (7 cables)
AWG	(mm)	(A)	(A)	(A)	(mm)	(mm)	(mm)	(mm)
2/0	9.260	214.280	193.700	167.795	0.330	-	-	-
1/0	8.250	182.170	164.670	142.649	0.840	0.090	-	-
1	7.350	160.570	145.150	125.732	1.290	0.540	-	-
2	6.540	137.210	124.030	107.444	1.690	0.940	-	-
4	5.190	99.260	89.730	77.725	2.370	1.620	0.405	0.405
6	4.110	72.980	65.980	57.151	2.910	2.160	0.945	0.945
8	3.260	53.720	48.560	42.063	3.330	2.580	1.370	1.37
10	2.590	36.200	32.720	28.347	3.670	2.920	1.705	1.705
12	2.050	27.440	24.810	21.489	3.940	3.190	1.975	1.975
14	1.630	20.440	18.470	16.002	4.170	3.400	2.185	2.185
16	1.290	15.180	13.720	11.887	4.320	3.570	2.355	2.355
18	1.020	12.850	11.610	10.059	4.450	3.700	2.490	2.49
20	0.810	9.810	8.870	7.681	4.560	3.810	2.594	2.594
22	0.640	7.420	6.700	5.807	4.640	3.890	2.678	2.678

For all insulation thicknesses, a safe operating voltage (single phase RMS for AC systems and Peak DC), was computed for the whole range of AWG sizes listed on Table 3.3 and for all cable systems. The maximum power transfer for each case was simply calculated: $P_{MAX} = 3 \; x \; SOV_{RMS} \; x \; SOI_{RMS}$, for the three phase systems and $P_{MAX} = SOV_{DC} \; x \; SOI_{DC}$ for the DC systems. If the number of circuits in the duct were two or three, then these mathematical expressions were multiplied by two or three respectively. Figure 3.11 shows the total RMS/DC power rating as a function of the single phase RMS/peak DC voltage rating for cases A – G.

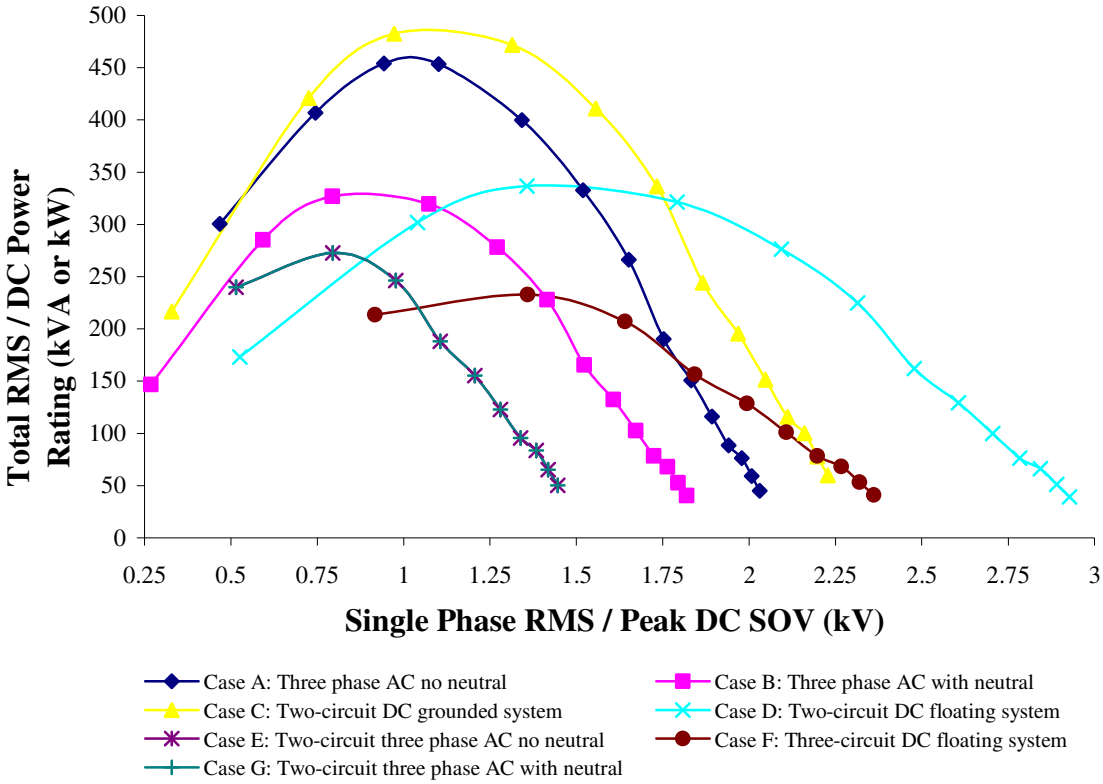

Figure 3.11: Variation of power rating with increase in the single phase RMS /peak DC voltage rating (SOV), for a fixed duct diameter of 30mm

Examining this in more detail, 'Case A' results show that the maximum power transfer occurs for the AWG 2 (3.27 mm) cable with a current rating of 137.2 A. The 1.69mm of insulation is capable of withstanding a voltage of 1.1 kV. This gives the power transfer capability of approximately 453 kVA.

Moving to the smallest conductor cable, AWG 22 gives a current carrying capability of 7.42 A. The insulation thickness in this case is 4.64 mm, a *factor of 2.75* greater than the AWG 2 cable. The voltage rating in this case is about *2.03 kV*. This is greater by factor of only *1.85* compared to the AWG 2 case. These results show that the increase in voltage rating is not linear with the increase of the insulation thickness. I.e. doubling the insulation thickness will not cause doubling of the voltage capability of the system. The low current rating of this cable gives rise to the low power transfer capability.

Another thing to observe is the lower power transfer capability of the systems having six and seven cables in the duct. If more cables are installed in the duct, the space available to be filled with insulation will be less. Furthermore the insulation thickness will be less and the voltage ratings will be smaller. Thus, the combination of smaller voltage ratings and a smaller cable bundle derating factor, results in smaller power transfers. In terms of maximum power transfer, the grounded DC system is the best having a maximum power rating of about 475 kVA.

3.2.4.2 Power to weight ratio

As weight is an important factor for aircraft, the power to weight ratio must also be considered. After the computation of maximum power transfer for each cable system with different AWG cable sizes and insulation thicknesses, the cable weight '*W*' was evaluated in kilograms per metre, based on the density of copper and the insulation (PTFE for example) which is 8920 $kg.m^{-3}$ and 1200 $kg.m^{-3}$ respectively. Since the cross sectional area of the conductor and the insulation is known, the weight per unit length was evaluated.

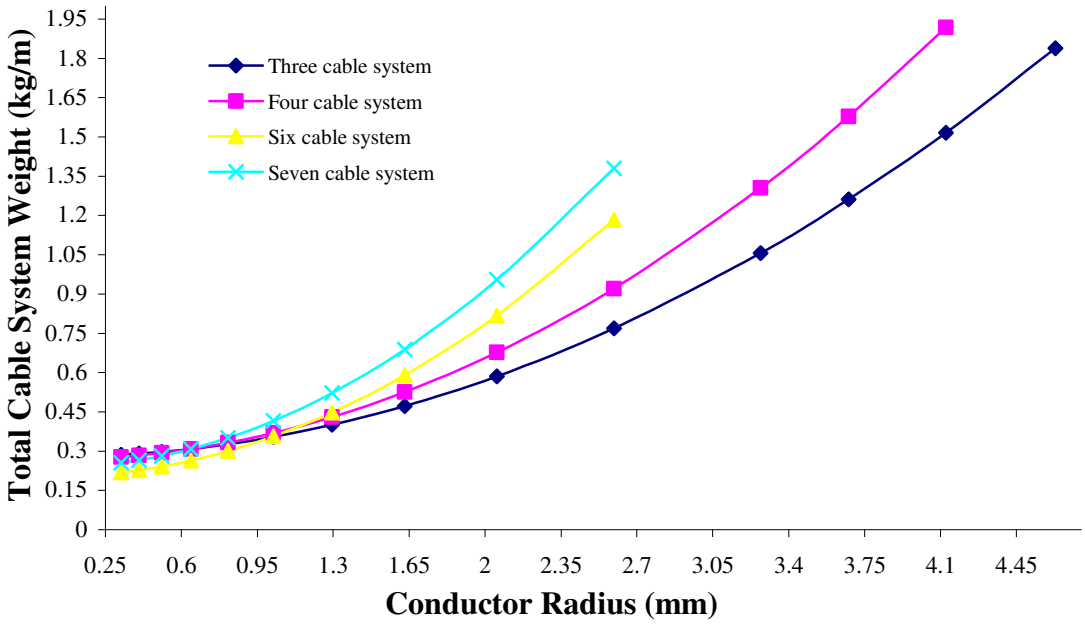

Figure 3.12: Variation of total cable system weight excluding the duct weight with increase in conductor size for a fixed duct diameter of 30mm

For the cable duct systems consisting of six and seven cables, conductor sizes greater than 2.6 mm (i.e. below AWG 4), are not feasible since the size of the duct and the clearances taken into consideration do not allow it. For all cable duct systems consisting of conductors having a radius bigger than 1 mm, the bigger the number of cables in the duct, the heavier the cable system will be. However for very small conductor radii, the *six and the seven cable systems* show similar weights with the *Three and the Four cable systems*, since the amount of copper and insulation in the systems is also similar.

Following the computation of the cable systems' weight, the power to weight ratio was calculated for each case. This was done in order to distinguish which system can provide an optimal solution, suggesting suitable voltage levels to be used for more electric aircrafts. As shown in Figure 3.13, the maximum power to weight ratio occurs in the region of 1.4 kV to 1.8 kV for cases A, B and C, i.e. at a voltage slightly higher than that of maximum power transfer. For case D it occurs approximately at a voltage of 2.3 kV. Although the shift from operating in the 0.8-1.0kV to the 1.4-1.8kV range for cases A, B and C and from 1.45kV to 2.3kV for case D decreases the maximum power throughout, this is more than compensated by the reduction in cable weight leading to an increase in power to weight ratio. Above this operating range the power to weight ratio drops steeply due to a lessened effect of weight saving associated with these higher voltages.

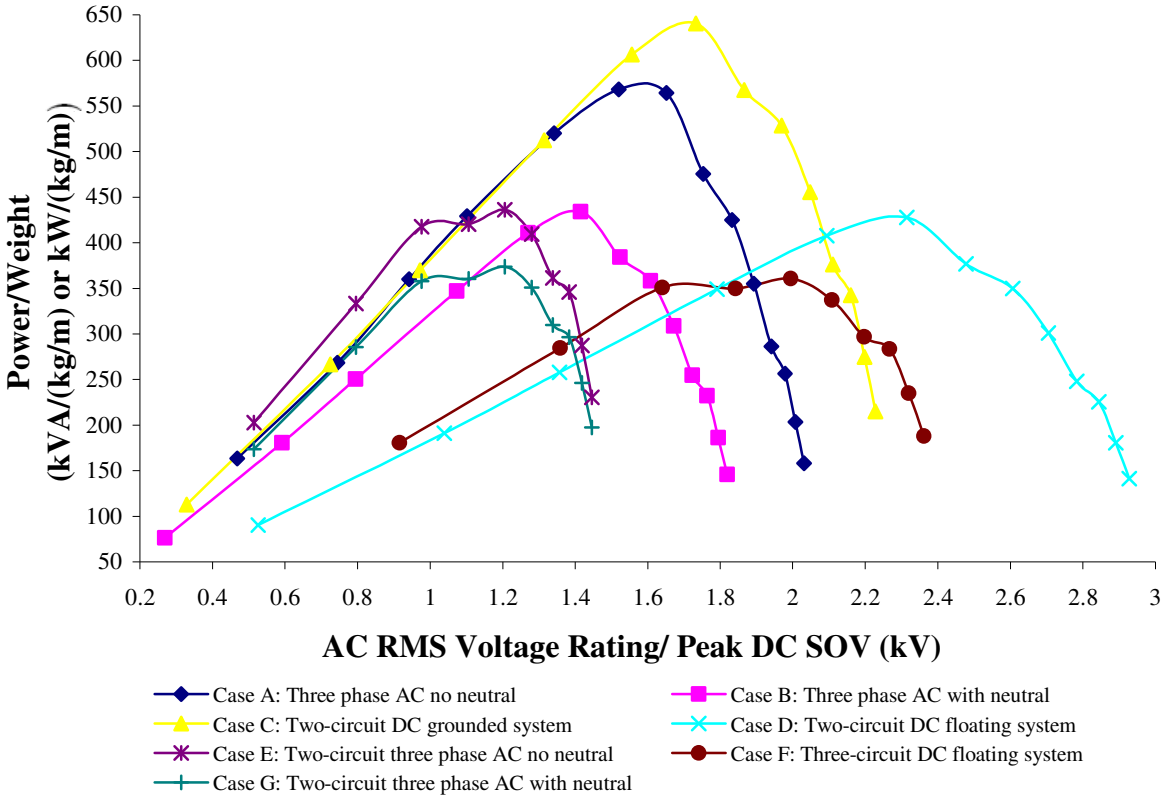

Figure 3.13: Variation of power to weight ratio per unit length, with increase in cable voltage rating (SOV) for a fixed duct diameter of 30mm

Comparing the cases A-G in Figure 3.13, the system offering the highest power to weight ratio is the grounded DC system (Case C). The use of a DC system where the insulation is maximally utilized gives good power transfer efficiencies. In contrast, the AC system power transfer is determined by the RMS voltage rating, this being a factor of $\sqrt{2}$ lower than the maximum operating voltage. The use of a DC system where the conductors are allowed to float, is not optimal as one conductor has to be rated for the entire system voltage even if it will not always operate at this value.

For the AC systems, Case A is the most efficient. This is because the duct consists of only three cables and can therefore accommodate larger insulation thicknesses in comparison to Case B. It follows that higher voltages levels are possible by using the system in Case A. However, the analysis does not include the weight of any neutral conductor in the analysis, something that would definitely be required on the new

generation of composite aircraft. The results presented may therefore be slightly optimistic. The analysis has also not examined other aspects of the power system such as generators, power electronics and loads. It is likely that any such power to weight optimization would be best carried out at system level in the future, but this work is a first step in moving to that full analysis.

3.2.5 Maximum Power Transfer Calculation for a Varying Duct Size

The next step in this optimization procedure was to examine the possibility of using larger duct diameters. This would enable larger cable insulation thicknesses to be calculated based on the optimal cable size equations. Furthermore larger ducts imply higher voltage ratings.

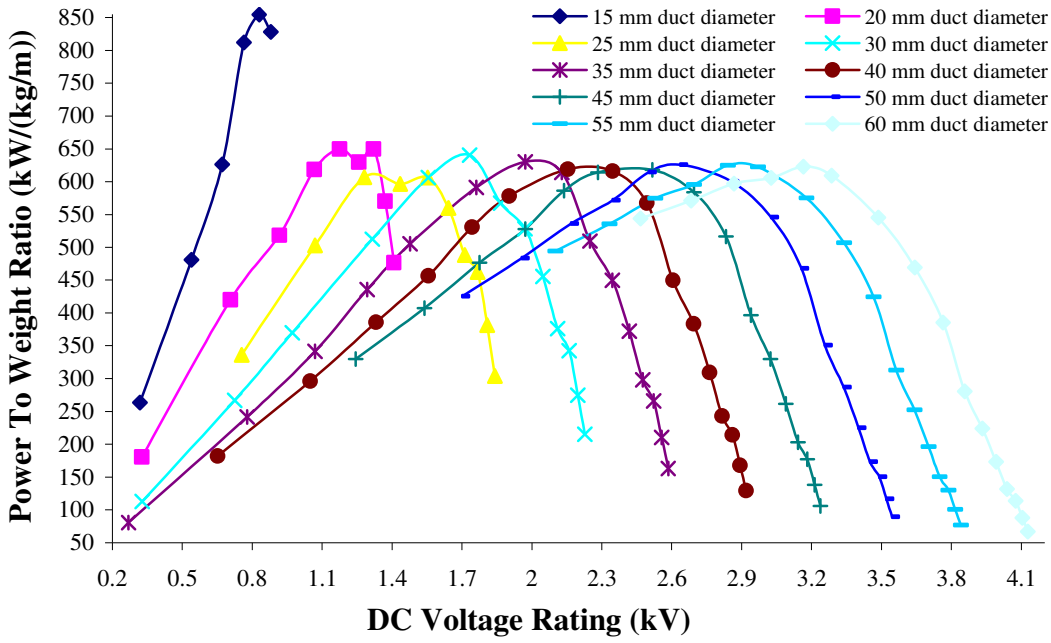

Figure 3.14: Variation of the power to weight ratio per unit length with increase in the DC voltage rating (SOV), for the two-circuit DC grounded cable system, for different duct diameters

One important observation from the figure above is the fact that for duct diameters larger than 20 mm the maximum power to weight ratio point is almost constant with the shift at higher operating voltage levels. This is because even though the maximum power transfers due to thicker insulation and thus higher voltage ratings increase, the insulation weight also increases significantly. As a result the weight of the cable system increases in such a way, compensating for the increase in power transfer.

The 15 mm duct cable system has a much higher maximum power to weight ratio due to the very low weight of the system. Unfortunately the maximum power transfer as it is shown in Figure 3.15 would not be enough to satisfy the needs of the more electric aircraft.

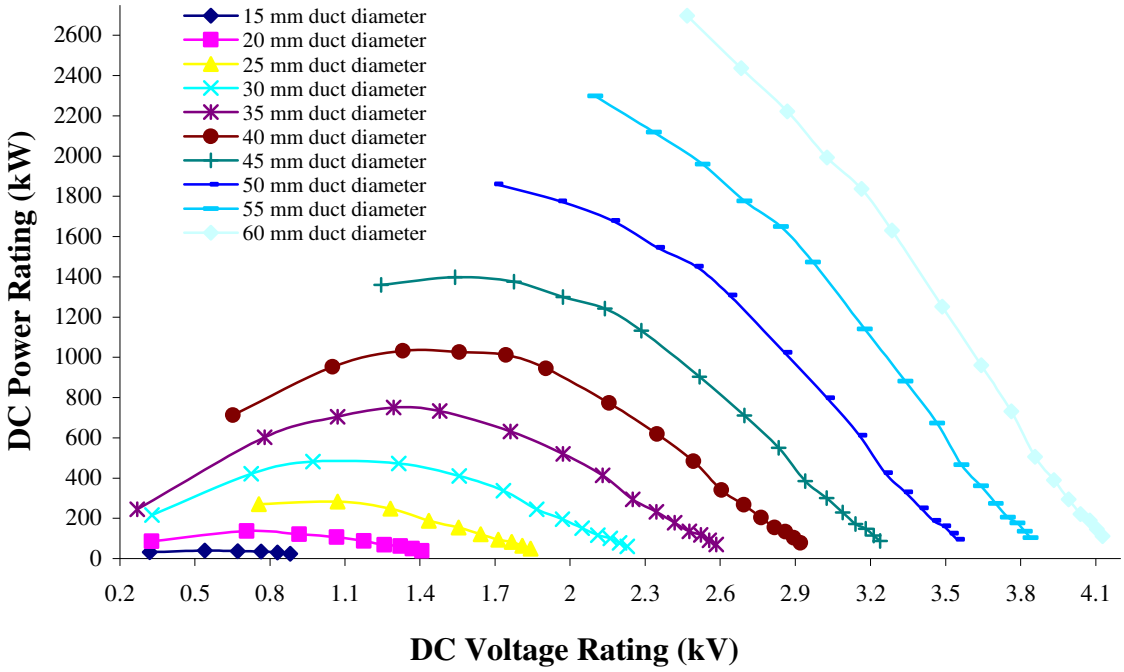

Figure 3.15: Variation of DC power rating with increase in DC cable voltage rating (SOV), for the two-circuit DC grounded cable system, for different duct diameters

The DC cable system in a 30 mm duct would be satisfactory in the case of the more electric aircraft, if it was to carry for example a power of 250 kVA from the generator to the main distribution feeder/bus-bars (this is the approximate output power of one of the generators on the Boeing 787 aircraft [6]). By looking at the 30 mm duct curve, 250 kVA

can be supplied in two cases; if the operating supply voltage is approximately 400 V or 1.8 kV. The former case involves a relatively large conductor size and small insulation thickness whereas the latter case involves a small conductor and a thick insulation. . According to Figure 3.14, 1.8 kV provides a higher power to weight ratio and thus it would be preferred.

3.3 Using Multiple Smaller Cable Duct Systems

As it was shown previously in Figure 3.14, the 15 mm duct cable system offers a much higher power to weight ratio but the amount of power that can be transferred cannot satisfy the high power demands of the more electric aircraft (look at Figure 3.15). However if multiple small cable duct systems are used instead of one big cable duct system, in some cases the same power could be delivered with less impact on the overall system weight. The only obvious disadvantage in this case will be the negative impact on system volume. For example if a power demand of approximately 250 kVA is required and a DC grounded system is considered, using ***seven*** 15 mm duct systems of AWG 18 size conductors, results in less system weight and thus in a higher power to weight ratio, compared to ***one*** 30 mm duct system consisting of AWG 10 size conductors. Figure 3.16 below illustrates this replacement; however note that the diagrams are not to scale.

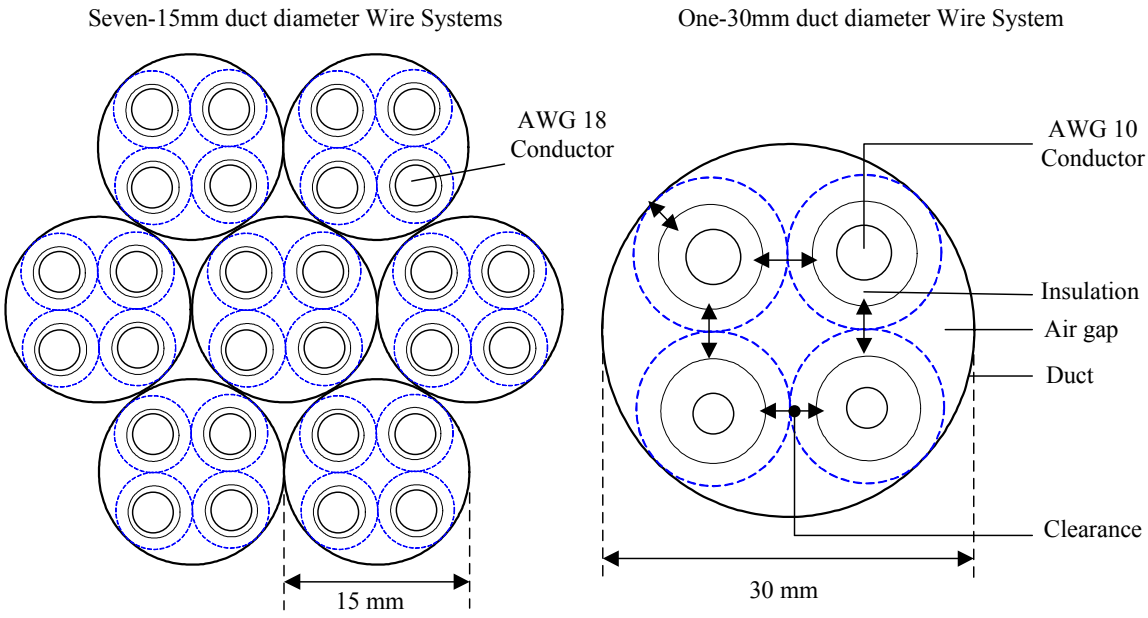

Figure 3.16: Replacement of ***one*** 30 mm duct system having AWG 10 size conductors, with ***seven*** 15 mm duct systems having AWG 18 size conductors

3.3.1 Maximum Power Transfer for Multiple Smaller Cable Systems

The replacement of a 30 mm diameter duct with multiple 15 mm diameter ducts for the four cable DC grounded system was carried out. For example, a 30 mm duct system consisting of four AWG 22 size conductors was replaced by a certain number of 15 mm duct systems consisting of four AWG 22 sized conductors. The same replacement procedure was carried out with the 30 mm duct system still having the same four AWG 22 conductors and the 15 mm duct systems having four AWG 20 conductors. The replacement was repeated with 15 mm duct systems with AWG 18, then AWG 16, AWG 14 and AWG 12 conductors. These are the conductor sizes that can fit into the 15 mm diameter duct, considering the insulation thickness required for each voltage level. In addition the same procedure was carried out for the 30 mm duct system consisting of AWG 20 conductors, then AWG 18 and so on, up to AWG 1/0. The procedure is illustrated in Figure 3.17.

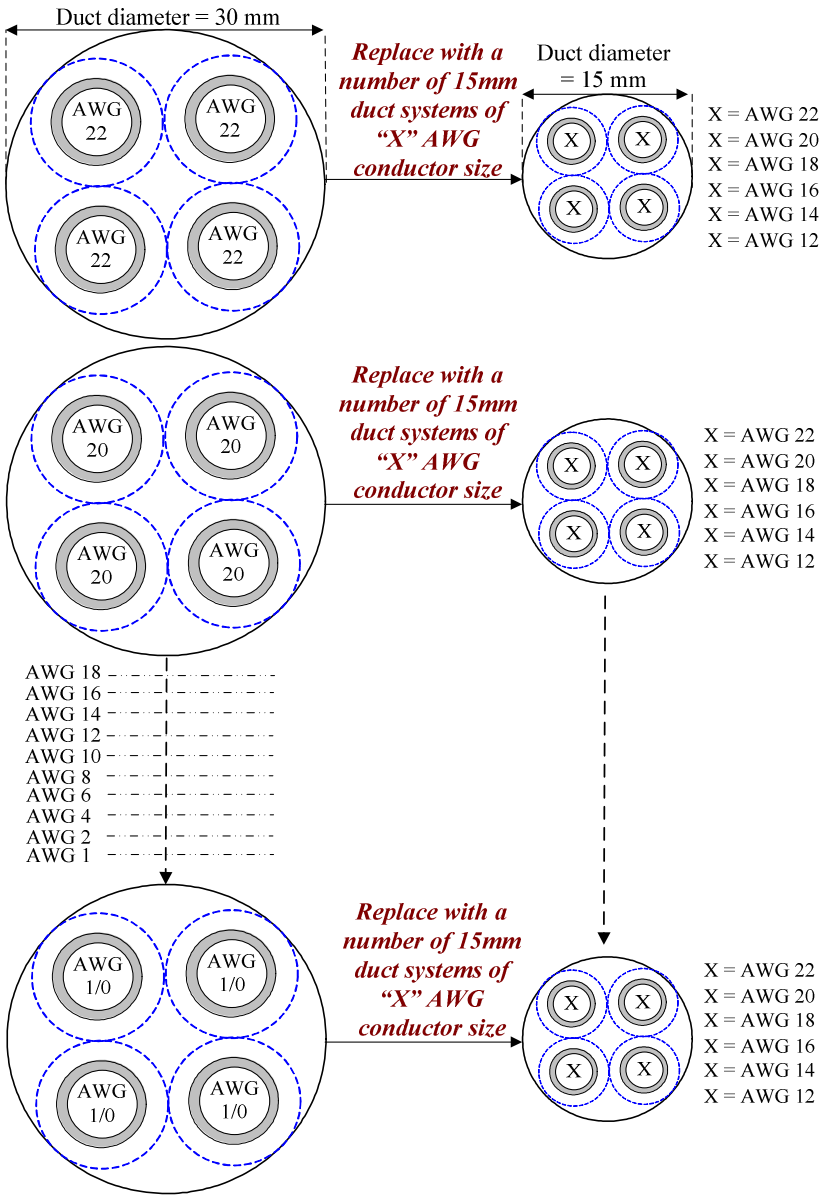

Figure 3.17: Illustration of the procedure carried out to replace the **one** 30 mm diameter duct system with **multiple** smaller systems having a 15 mm diameter duct

DC power transfer results and corresponding system weights are shown in figure 3.18. The purple points on the graph which are connected with a line, represent the DC power transfer results for the 30 mm duct consisting of AWG 22 conductors, AWG 20 and so on up to AWG 1/0 (Look also at Figure 3.17). The six different coloured points, that are on the same y-axis line with the corresponding 30 mm duct points, are the DC power transfer results of the 15 mm ducts that have been used for replacement having conductors sizes

AWG 22, AWG 20, AWG 18, AWG 16, AWG 14 and AWG 12 (look also at figure 3.17). These points are circled on figure 3.18.

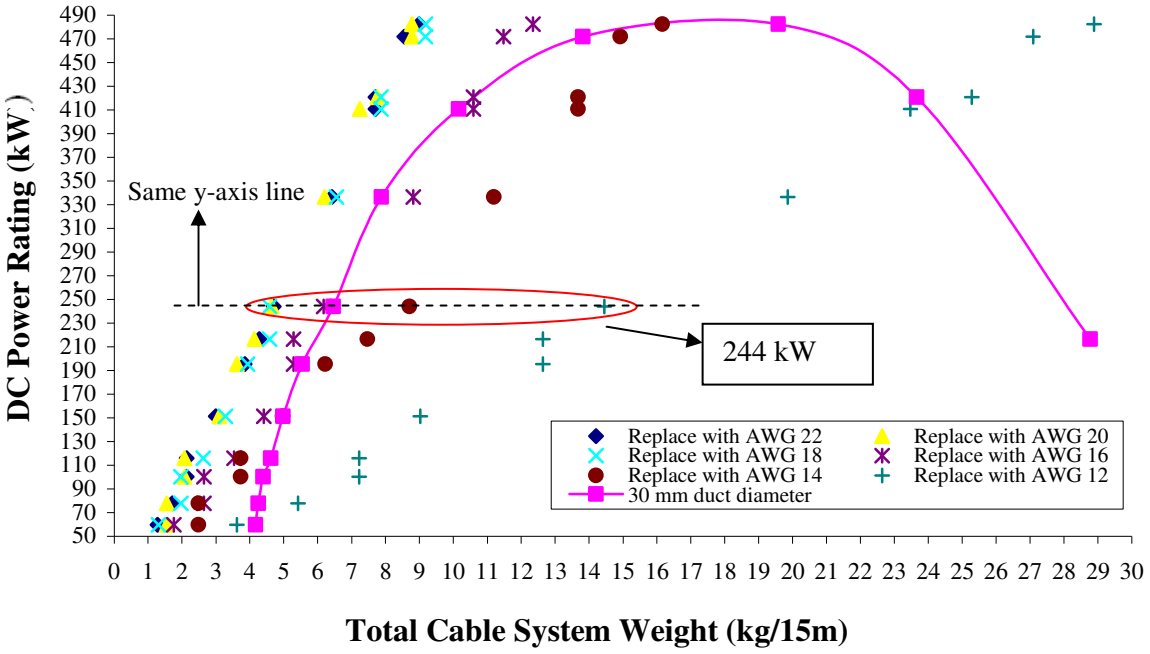

Figure 3.18: Variation of DC power rating with cable system weight, for 15 mm and 30 mm duct cable systems. Values of weight are for a cabling system having a length of 15 m

Looking at figure 3.18, if a power transfer of 244 kW (≈ 250 kW) is required, one cable system of 30 mm duct diameter with AWG 10 size conductors can be used or multiple cable systems having a duct diameter of 15 mm. All 15 mm duct systems offer a better weight solution with the exception of the 15 mm duct system consisting of AWG 12 and AWG 14 size conductors. The savings in weight by using ***seven*** 15 mm duct systems consisting of AWG 18 sized conductors would be about 1.75 kg (6.46 kg – 4.71 kg). That is about a weight saving of 27% for a 15 m cable run. It has to be noted that the thermal effect if ***multiple*** systems are used was not taken into account. It is assumed that the multiple duct systems are kept apart with spacers so that each one does not obstruct heat dissipation. Another important observation that can be made using the above graph is that for higher powers of about 470 kW there is possible weight saving of 38%. This is the case if the 30 mm duct consisting of AWG 4 sized conductors is replaced by ***twenty*** 15 mm duct systems with AWG 22 conductors. Once again is worth mentioning the obvious

disadvantage of using ***multiple*** smaller systems which is the fact that they occupy more space. To obtain the data shown in figure 3.18 above, the following calculation procedure was implemented:

- Obtain 'P_factor (P_f)', i.e. how many 15 mm duct systems of certain AWG conductor size are required to achieve the same power as **one** 30 mm duct system for conductor sizes of AWG 1/0 down to AWG 22 (P_factors are not whole numbers, thus it is necessary to round them up to the next whole number i.e. 3.21 → 4. This results in a decrease in current utilisation of conductors in the 15 mm duct system)
- Multiply the weight of one 15 mm duct system by P_f to obtain the total weight of the 15 mm duct systems used to replace the **one** 30 mm duct system.

In order to understand why there is a decrease in the total system weight by using smaller multiple duct sizes, it is necessary to observe the change in the total system cross sectional surface area of the different duct systems. The 30 mm duct system consisting of four AWG 10 sized conductors is used in Figure 3.19 as an example.

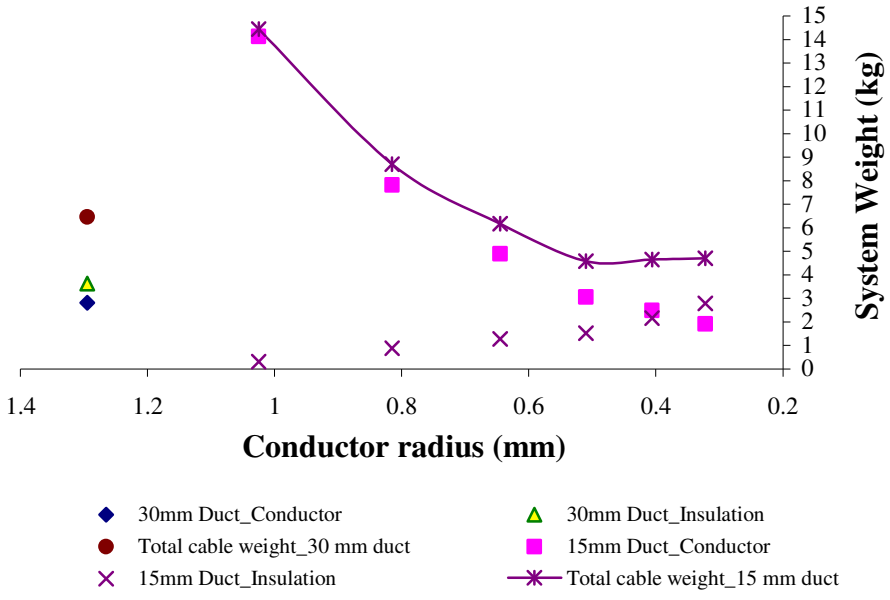

a).

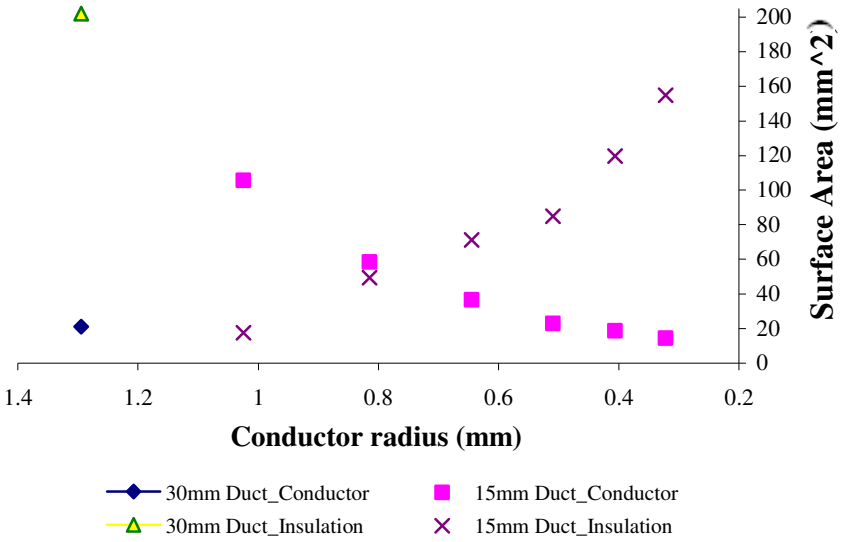

b).

Figure 3.19: Variation of insulation and conductor system weight and CSA of cable systems, having a duct diameter of 15 mm and 30 mm. Values of weight are for a 15 m long cable run

By decreasing the conductor radius and thus the conductors' cross sectional area (CSA) in the fixed size duct with constant clearance between cables and duct, there is more space available for adding more insulation based on Equations 3.1-3.4.The increase in the insulation surface area due to the increase in the insulation thickness is shown in figure 3.19b, together with the decrease in the surface area of the conductor. The insulation and conductor cross sectional areas (CSA) for the 15 mm duct systems is the sum of all 15 mm duct systems used to achieve a power demand of 244 kW. To compare the 15 mm ***multiple*** systems and the ***one*** 30 mm duct system, the CSA of the insulation and the conductor in the 30 mm duct are shown as well. The graph on Figure 3.19a shows the weights of the insulation and the conductors separately. For each conductor radius adding the insulation and conductor weights results in the total cable system weight. The summation of some points having the same conductor radius give larger weight values than the 30 mm duct system's total weight and some give less.

Table 3.4 below, shows the number of 15 mm duct systems required to satisfy the power transfer ratings *'P'* of the 30 mm duct system consisting of four cables (2 +ve DC and 2 –ve DC), together with the current utilisation *'I_U'* of each system.

TABLE 3.4

NUMBER OF 15 MM DUCT SYSTEMS REQUIRED TO REPLACE ONE 30 MM DUCT SYSTEM AND CURRENT UTILIZATION OF CABLES

30 mm duct system		15 mm duct systems											
		AWG 22		AWG 20		AWG 18		AWG 16		AWG 14		AWG 12	
AWG	DC P (kVA)	P_f	I_U (%)	P_f	I_U (%)	P_f	I_U (%)	P_f	I_U (%)	P_f	I_U (%)	P_f	I_U (%)
1/0	**217**	**10**	**91.7**	**8**	**92.0**	**7**	**87.2**	**6**	**97.9**	**6**	**90.6**	**7**	**97.5**
1	421	18	99	15	95.3	12	98.9	12	95.2	11	96.0	14	94.7
2	483	21	97.3	17	96.4	14	97.1	14	93.5	13	93.2	16	95.0
4	472	20	99.9	17	94.3	14	95.0	13	98.5	12	98.7	15	99.1
6	411	18	96.6	14	99.6	12	96.5	12	92.9	11	93.7	13	99.6
8	337	15	95	12	95.3	10	94.9	10	91.3	9	93.8	11	96.4
10	244	11	94	9	92.2	7	98.3	7	94.7	7	87.5	8	96.2
12	195	9	91.9	7	94.8	6	91.8	6	88.4	5	98.1	7	88.0
14	151	7	91.5	6	85.7	5	85.3	5	82.1	4	95.0	5	95.4
16	116	5	98.1	4	98.4	4	81.6	4	78.6	3	96.9	4	91.3
18	100	5	84.9	4	85.2	3	94.3	3	90.7	3	83.9	4	79.1
20	78	4	82.5	3	88.2	3	73.2	3	70.5	2	97.8	3	81.9
22	60	3	84.3	3	67.6	2	84.2	2	81.0	2	75.0	2	94.1

For instance the first row on the above table shows that for ***one*** 30 mm duct system, consisting of four AWG 1/0 size conductors transmitting at DC can provide a power transfer of 217 kVA. This power can also be transferred by ***ten*** 15 mm duct systems consisting of AGW 22 size conductors with a current utilisation 'I_U' of 91.7 %. Alternatively, this power demand could also be achieved by ***eight*** 15 mm duct systems consisting of AWG 20 size conductor with an I_U of 92 % and so on.

Another issue arises by replacing ***one*** 30 mm duct diameter system with ***multiple*** 15 mm duct systems. The reason for achieving higher power transfers by using multiple systems is the fact that more conductors are used and thus more current can be supplied to the load point for the same voltage. However this gives rise to termination practicality issues. At load equipment points, the equipment current capability should be higher than in the case if one - 30 mm duct system was to be used.

Another possibility could be replacing a 30 mm duct system consisting of certain conductor size with other 30 mm duct systems of different conductor sizes and thus insulation thicknesses.

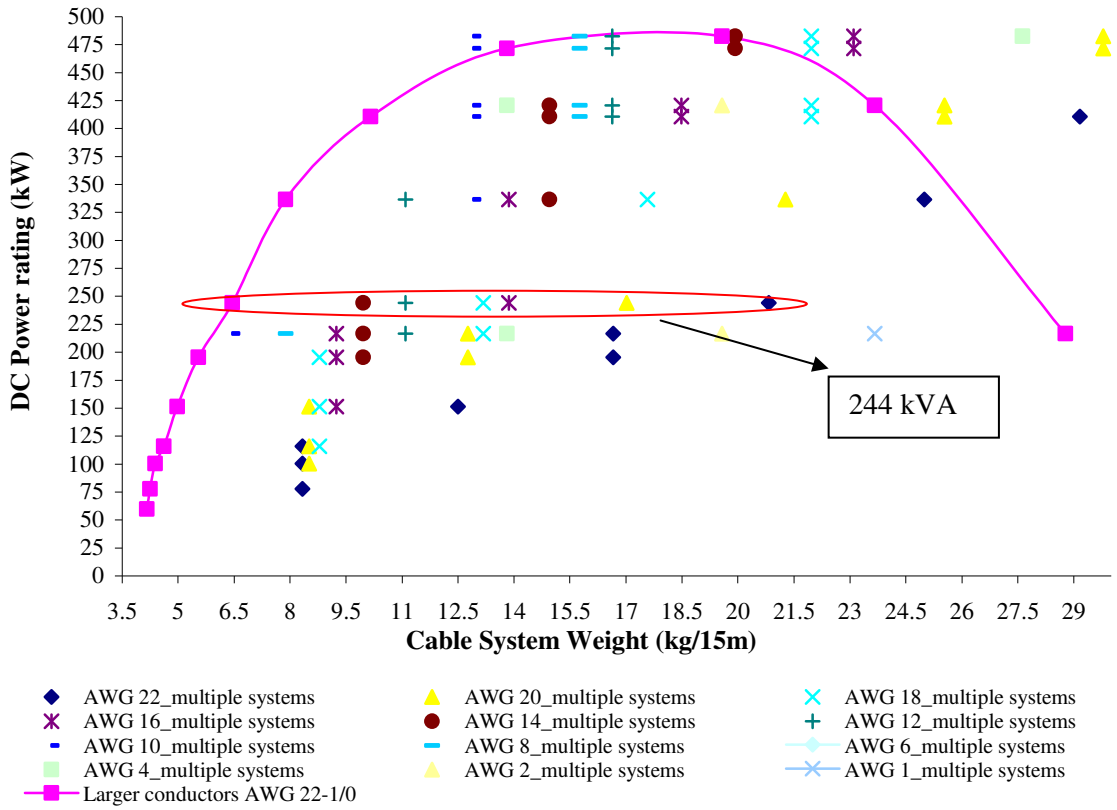

Figure 3.20: Variation of DC power rating with cable system weight for 30 mm cable systems: Replacing large AWG conductor sizes with smaller sizes: AWG 22 down to AWG 1. Cabling system is 15 m long

Figures 3.18 and 3.20 can be used to choose the best DC system in terms of higher power to weight ratios. The question to be answered here is: 'Which system can achieve a specific power demand and at the same time provide the lightest system?' Initially ***one*** 30 mm duct system consisting of AWG 10 size conductors, is used to transfer a power of 244 kW (≈ 250 kW). 'Would it better to replace this system with multiple smaller duct size systems (i.e. multiple 15 mm duct systems), or with multiple systems of the same duct size (i.e. 30 mm duct systems with smaller size conductors)?' According to Figure 3.20, ***one*** 30 mm duct system with AWG 10 size conductors, is the best option since it offers the lightest

system at 6.5kg/15m. According to figure 3.18, replacing the 30 mm duct system with AWG 10 size conductors, with ***seven*** 15 mm duct systems consisting of AWG 18 size conductors, or ***nine*** consisting of AWG 20, or ***eleven*** consisting of AWG 22, or ***seven*** consisting of AWG 16, also result in a decrease in system weight. The weights of these 15 mm duct systems respectively are as follows: 4.59 kg/15m, 4.65 kg/15m, 4.71 kg/15m and 6.17 kg/15m. It is obvious that using multiple 15 mm duct systems instead of ***one*** 30 mm duct system will offer a better weight solution with the exception of the 15 mm duct systems having conductor sizes of AWG 14 and AWG 12. For these cases the ***one*** 30 mm duct system with AWG 10 conductors would be preferred. Table 3.5A and 3.5B, show the number P_f, of 30 mm duct systems required to achieve the same power as ***one*** 30 mm duct system, consisting of larger AWG conductor sizes and also the current utilisation *'I_U'* of cable systems.

TABLE 3.5 A

NUMBER OF 30 MM DUCT SYSTEMS REQUIRED TO REPLACE ONE 30 MM DUCT SYSTEM OF BIGGER AWG SIZED CONDUCTORS AND CURRENT UTILIZATION OF THE CABLES

30 mm duct system		Multiple 30 mm duct systems											
		AWG 22		AWG 20		AWG 18		AWG 16		AWG 14		AWG 12	
AWG	RMS P (kVA)	P_f	I_U (%)	P_f	I_U (%)	P_f	I_U (%)	P_f	I_U (%)	P_f	I_U (%)	P_f	I_U (%)
1/0	217	4	90.7	3	92.6	3	72.0	2	93.5	2	71.6	2	55.4
1	421	8	88.1	6	90.0	5	83.9	4	90.8	3	92.7	3	71.8
2	483	9	89.8	7	88.4	5	96.2	5	83.3	4	79.7	3	82.3
4	472	8	98.7	7	86.5	5	94.0	5	81.4	4	77.9	3	80.5
6	411	7	98.2	6	87.8	5	81.9	4	88.6	3	90.5	3	70.1
8	337	6	93.9	5	86.4	4	83.9	3	96.8	3	74.1	2	86.1
10	244	5	81.8	4	78.3	3	81.1	3	70.2	2	80.7	2	62.5
12	195	4	81.8	3	83.6	2	97.4	2	84.3	2	64.6	1	100
14	151	3	84.5	2	97.1	2	75.4	2	65.3	1	100	1	77.4
16	116	2	97.0	2	74.3	2	57.7	1	100	1	76.6	1	59.3
18	100	2	84.0	2	64.4	1	100	1	86.6	1	66.3	1	51.3
20	78	2	65.2	1	100	1	77.7	1	67.3	1	51.5	1	39.9

TABLE 3.5 B

30 mm duct system		Multiple 30 mm duct systems											
		AWG 10		AWG 8		AWG 6		AWG 4		AWG 2		AWG 1	
AWG	RMS P (kVA)	P_f	I_U (%)	P_f	I_U (%)	P_f	I_U (%)	P_f	I_U (%)	P_f	I_U (%)	P_f	I_U (%)
1/0	217	1	88.7	1	64.4	1	52.7	1	45.9	1	44.9	1	51.5
1	421	2	86.2	2	62.5	2	51.2	1	89.2	1	87.2	1	100
2	483	2	98.8	2	71.7	2	58.7	2	51.1	1	100	2	57.3
4	472	2	96.6	2	70.1	2	57.4	1	100	1	97.8	2	56.1
6	411	2	84.1	2	61.0	1	100	1	87.1	1	85.1	1	97.6
8	337	2	68.9	1	100	1	81.9	1	71.3	1	69.7	1	80.0
10	244	1	100	1	72.6	1	59.5	1	51.8	1	50.6	1	58.0
12	195	1	80.0	1	58.1	1	47.6	1	41.4	1	40.5	1	46.4
14	151	1	62.0	1	45.0	1	36.8	1	32.1	1	31.4	1	36.0
16	116	1	47.5	1	34.4	1	28.2	1	24.6	1	24.0	1	27.5
18	100	1	41.1	1	29.8	1	24.4	1	21.3	1	20.8	1	23.8
20	78	1	31.9	1	23.2	1	19.0	1	16.5	1	16.2	1	18.5

3.3.2 Power System Impedance, Losses and Voltage Drop

As mentioned in the introduction another way to decrease the weight of the aircraft could be increasing the frequency of the operating system. This is because for transformers an increase in frequency will result in less iron required to accommodate the needed magnetic flux. However increasing the currently used operating frequencies will have a negative impact on the weight of generators and motors and in addition it will cause an increase in the impedance of the system [7]. If the power factor is already low according to the electrical system design, an increase in frequency will result in reactive voltage drops becoming a limitation rather than resistive [7, 13].

Further work is required for AC systems in order to obtain impedance values for the cable duct systems being examined, to evaluate the power losses of each system. At aircraft electrical frequencies capacitive losses might also affect the dielectric strength of cable insulation.

3.3.3 DC System Power Losses and Voltage Drop Evaluation

For DC cable systems, the losses are due to the resistance of the cables which depends on the conductor material, its length and its cross sectional area. Assuming that the cables coming out of the generators producing 250 kVA from the aircraft wings are 15 metres long, voltage drops and power losses can be calculated. The figures below show the results for different combinations of 15 mm duct systems used to replace one 30 mm duct system, as described in the previous section, for a four cable grounded DC system installed in a duct.

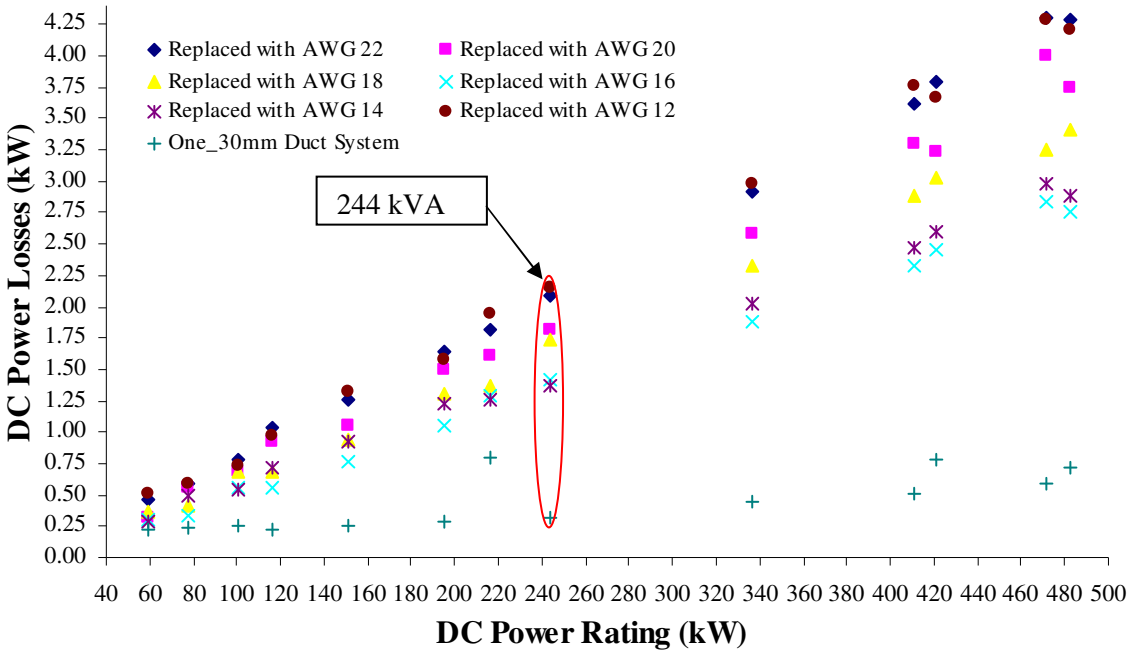

Figure 3.21: DC power losses at different power demands: Comparison of 15 mm duct systems used to replace ***one*** 30 mm duct system. Cables are 15 m long

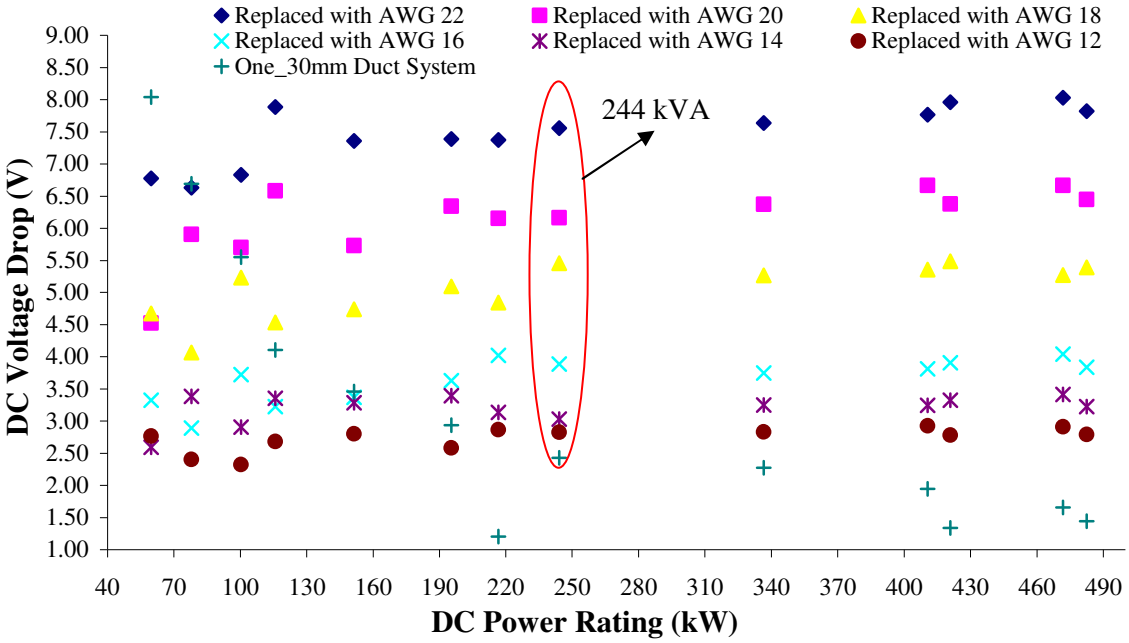

Figure 3.22: DC voltage drop at different power demands: Comparison of 30 mm duct systems consisting of small conductors, used to replace ***one*** 30 mm duct system having larger conductors. Cables are 15 m long

Even though it has been shown previously that by using ***multiple*** 15 mm duct systems instead of ***one*** 30 mm duct system there is a reduction in cable system weight, the power losses as well as the voltage drop increase by using multiple systems for a power demand of 244 kVA.

Concluding, in order to decide on whether multiple smaller cable duct systems can be used to replace one bigger cable system, all the above factors have to be further investigated (note: if the savings in aircraft fuel resulting from the relative decrease in system weight are greater than the extra power required due to the power losses, then it could be the case that multiple smaller cable systems replacing one bigger system would be advantageous. Of course there are other issues that arise as well with bigger voltage drops concerning power system stability and quality and the tolerances of aircraft power system equipment).

3.4 Development of Calculation Techniques for a Fixed Power Demand

3.4.1 Cable Duct Size Optimisation: Methodology

In the previous section a methodology was described on how to calculate the safe operating voltages (SOV) if the duct diameter is fixed. Thus after calculating SOV and the current ratings for specific AWG sized conductors, maximum power transfer was calculated. This procedure can be carried out if the duct size is known and the electrical transmission or distribution system needs to be improved in terms of higher power transfer. This way the appropriate cables to be installed can be chosen to achieve a higher power transfer.

In this section a reverse methodology is adopted. That is if the power demand is known, the voltages required to achieve that power transfer, can be computed for each conductor size carrying a certain amount of current. Furthermore the insulation thicknesses necessary to avoid PD can be calculated and by using Equations 3.1 to 3.4 for finding the maximum cable size, the maximum duct size can be determined. This method could be adopted when the aircraft electrical loads are well defined and an optimal distribution system is to be developed. Figure 3.23 shown on the next page, illustrates the reverse optimisation methodology.

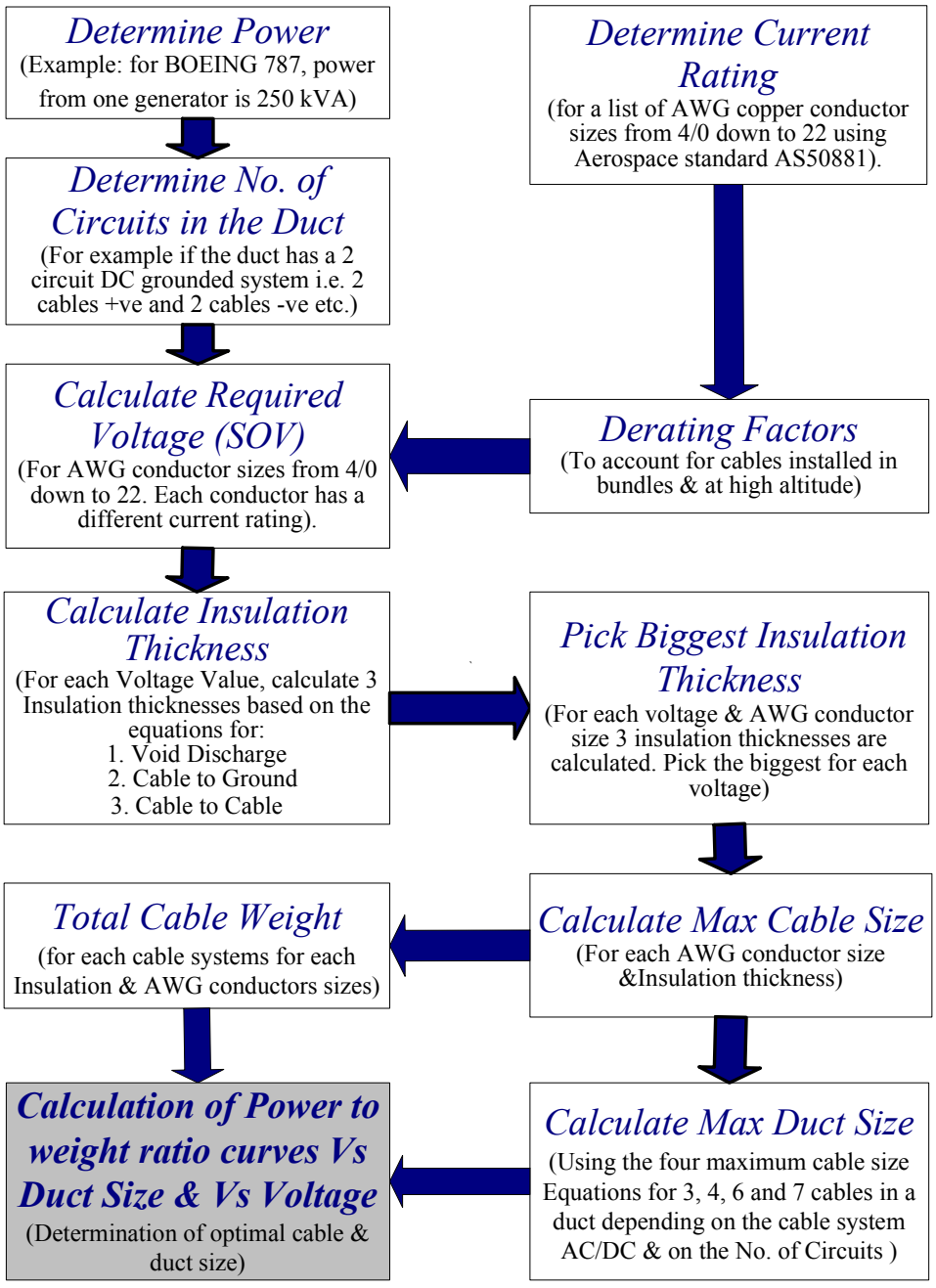

Figure 3.23: Flow chart: Detailed illustration of the cable duct size optimisation methodology

3.4.2 Determining the Optimal Cable Duct Size

The electrical system of the more electric aircraft (MEA), is more likely to consist of 2 engines, each having 2 generators and each producing 250 kVA [6]. If a fixed power of

250 kVA is considered in the calculations, the resulting power to weight ratio curves for all the cable systems under examination are shown below in Figure 3.24.

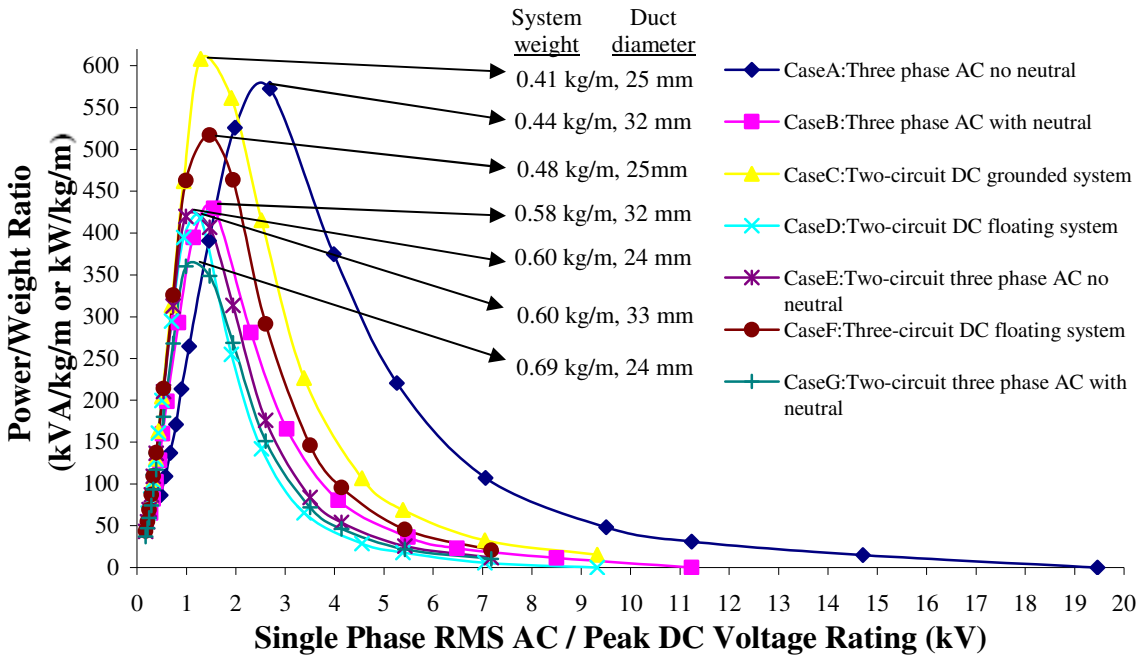

Figure 3.24: Power to weight ratio curves Vs voltage rating for all systems under examination, for a power demand of 250 kVA

Looking at Figure 3.24, one cable duct system at a time, it can be observed that as the current rating decreases with decreasing conductor size, the higher the voltage required to achieve 250 kVA. The higher the voltage, the thicker the insulation has to be to avoid PD. The decrease in conductor size and thus conductor weight, dominates the increase in insulation weight resulting in a decrease in the overall cable system weight and thus an increase in the power to weight ratio. Once a certain maximum point is reached, a further increase in the voltage level will result in an even thicker and heavier insulation, causing the power to weight ratio to drop. This is because after the maximum point, the increase in the insulation weight, dominates the conductor weight decrease.

Cases B and G can be used to explain the difference in the power to weight ratio results, if the duct contains a larger number of cables. If the two systems consist of conductors of the same AWG size, the system with a smaller number of cables (Case B)

will have its conductors operating at a higher current rating. This is due to the larger derating factor for cables in a bundle (derating factor = 0.738, as determined using the method stated in AS50881 [11]). On the other hand in Case G, the bundle derating factor is 0.578 and the current rating for each conductor is smaller by a factor of 1.277 (=0.738/*0.578*), whilst the number of conductors carrying current is *twice* the number of conductors in Case B. Thus the total current that can be transferred in Case G, is actually larger by a factor of *1.566 (=2 x 1/1.277)*. The voltage required by each cable to achieve 250 kVA will be: "(V_r *x 1.566)/6*", whereas the voltage required in case B will be "V_r*/3*". Thus the voltage required in Case G is less and the maximum power to weight ratio for Case G will occur at lower voltages than in Case B for the same conductor size.

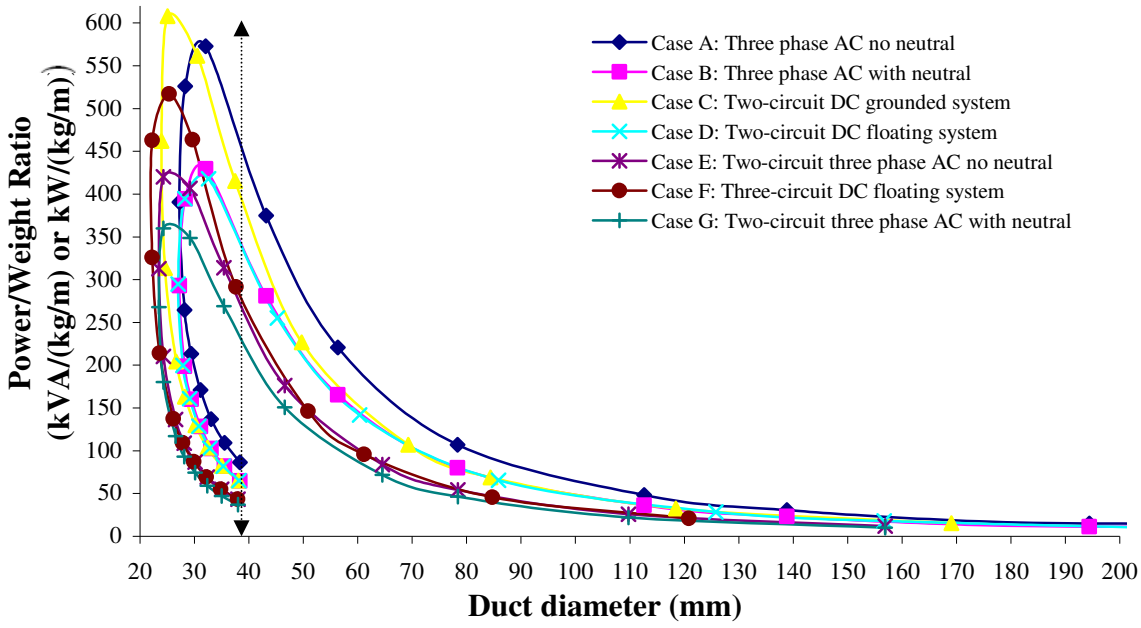

Figure 3.25: Power to weight ratio Vs duct size for all systems under examination

In Figure 3.24 as well as in Figure 3.25, it is important to notice that maximum power to weight ratios occur at duct diameters within the range of about 25-32 mm. As a matter of fact the DC case, which was previously proven in Section 2.3.1 to be the best solution for a 250 kVA power demand, occurs when the duct has a diameter of about 30 mm. This was the fixed duct value used in Section 3.2 to illustrate the calculation

procedure for achieving a maximum power transfer, with a minimum impact on system weight.

At the left of the dotted line shown in Figure 3.25, for the same duct diameter a low and high power to weight ratio point exists. The high point signifies a big insulation thickness and a small conductor radius whereas the low point stands for a small insulation thickness and a big conductor radius. On the right side of the dotted line, the increase in the insulation weight dominates and even though the conductor size decreases further, the ratio drops.

3.5 Discussion of Accuracy of Calculation Techniques

The subsections that follow give a discussion for the selection of the electric field models (uniform & non uniform) that have been used to evaluate SOV, based on cable to ground airgap discharges, cable to cable airgap discharges and insulation void discharges. For airgap discharges, a uniform field model was used whereas for insulation void discharges, a non uniform (coaxial) model was used. Furthermore the limitations of these models are stated. Finite element analysis (FEA) is also carried out to support the arguments that will follow.

3.5.1 Cable to Ground and Cable to Cable Airgap Discharges

In order to aid the understanding of the discussion that is carried out in this section, Figure 3.3 from section 3.2.2 is shown again to illustrate the three types of discharges that were examined.

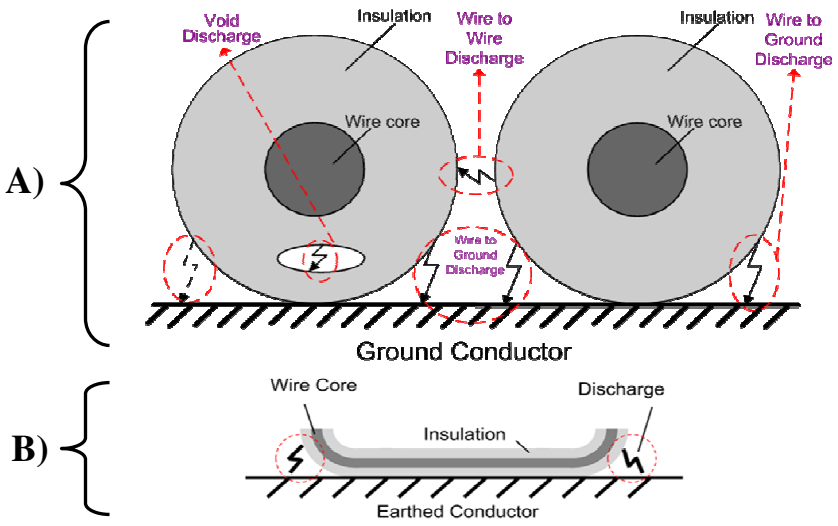

Figure 3.26: Locations of PD taken into consideration in the calculation of SOV

For the wire/cable to ground discharges and cable to cable discharges shown in figure 3.26**A,** the radius of curvature of the conductor is equal to the radius of the conductor. Thus according to the information given by M.C Halleck [43], there will be an overestimation in the cable to ground PDIV when calculated using a uniform electric field model, for conductor sizes of AWG 16 up to AWG 22. The corresponding conductor sizes in mm are 0.65 mm and 0.32 mm respectively. For cable to ground discharges as in figure 3.26**B** the radius of curvature is assumed to be greater than 0.79 mm and the PDIV calculated values are valid. This assumption can be made, since the cable installation engineer can decide the bending radius of the cable before connecting it to the main power distribution board. In addition it has to be noted that PDIV calculations for cable to ground discharges in Figure 3.26**A**, give exactly the same results as in the case of figure 3.26**B,** since the calculations are carried out for a range of airgap distances as it was described previously.

Another important factor that can disturb the uniformity of the electric field is the ratio of the insulation thickness to the conductor radius or in other terms, the cable radius to the conductor radius. This factor is also discussed briefly by M.C Halleck [43]. However, even if the electric field becomes more and more non uniform by increasing the insulation thickness whilst keeping the conductor size fixed, SOV results become even

more conservative. Figure 3.27 shows the plot of the fractional voltages '$fract_{(Vd)}$' ,using uniform and non uniform (coaxial) Equations 3.12 and 3.13 respectively, against the ratio of cable radius to conductor radius *'R/r'* having a constant airgap size *'d_{WG}'* of 2 mm. This value of d_{WG} is the smallest airgap distance in the cable duct system being analysed and it is the region in the airgap where the electric field is the highest.

- *Uniform Field:*

$$fract_{(V_d)} = \frac{\varepsilon_r}{\varepsilon_r + \frac{(R-r)}{(T-R)}} \tag{3.12}$$

- *Non Uniform Field:*

$$fract_{(V_d)} = \frac{\varepsilon_r}{\varepsilon_r + \frac{\ln\left(\frac{R}{r}\right)}{\ln\left(\frac{T}{R}\right)}} \tag{3.13}$$

fract(Vd) = fraction of the voltage across the airgap

T = Duct radius (mm)

R = Cable radius (mm)

r = Conductor radius (mm)

(R-r) = i =Insulation thickness (mm)

(T-R) = d_{WG} =shortest airgap distance between cable and duct (mm)

ε_r = relative permittivity of insulation

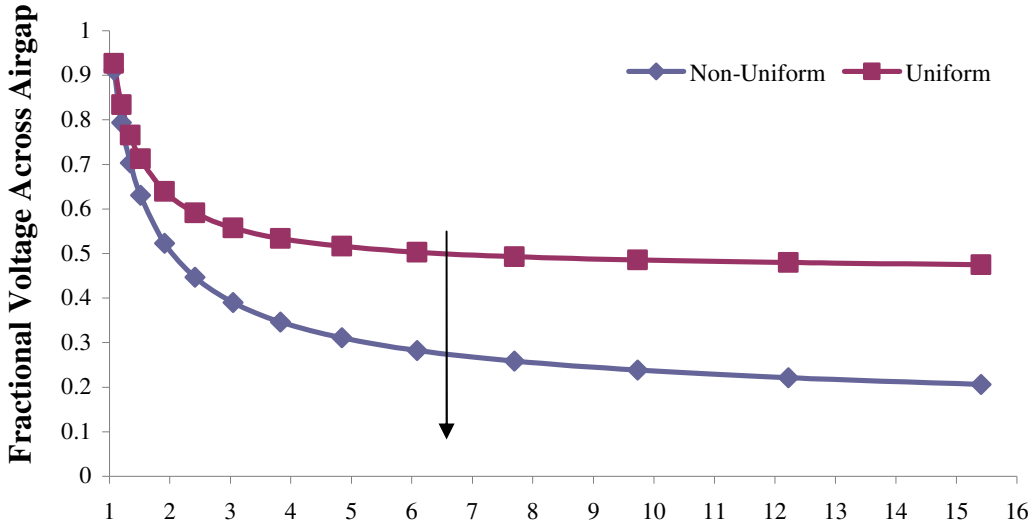

Figure 3.27: Graph of fractional voltage across airgap against ratio of cable to conductor radius for the uniform and non uniform field cases

For airgap distances larger than 2 mm the difference between the two curves increases. Even though as the airgap distance decreases and the uniform curve moves closer to the non uniform curve in the direction of the arrow shown in figure 3.27, the uniform case continues to provide more conservative results even up to an airgap of 0.1 mm. Assuming that Paschen's Law is valid for all airgap sizes being considered, the fractional voltage across the airgap '$fract_{(Vd)}$' is higher in the uniform than in the non uniform case scenario. Comparing the two cases, the electric field and thus the voltage across the airgap between the insulation and the ground that causes breakdown (V_{Brk}), is identical in both situations. Thus, the uniform model which results in bigger $fract_{(Vd)}$ values for the range of d over which SOV is calculated, will always provide more conservative results according to the equation:

$$V_{Inception} = SOV = \frac{V_{Brk}}{fract_{(V_d)}} \tag{3.14}$$

3.5.2 Void Discharges in the Insulation

In the case where SOV was calculated considering a void discharge within the insulation, a non uniform (coaxial) electric field model was used. This is because the uniform electric field model (parallel plate capacitor) greatly underestimates the electric field within the insulation where voids are located and the resulting SOV_V is greatly overestimated. In order to illustrate the above argument, Figure 3.28 is used to compare the electric field distribution results for the cable system in a duct, using a non uniform and a uniform electric field model. For both uniform and non uniform models two curves are plotted. One curve accounts for the case of having a small conductor and big insulation, whilst the other curve accounts for a big conductor and a small insulation.

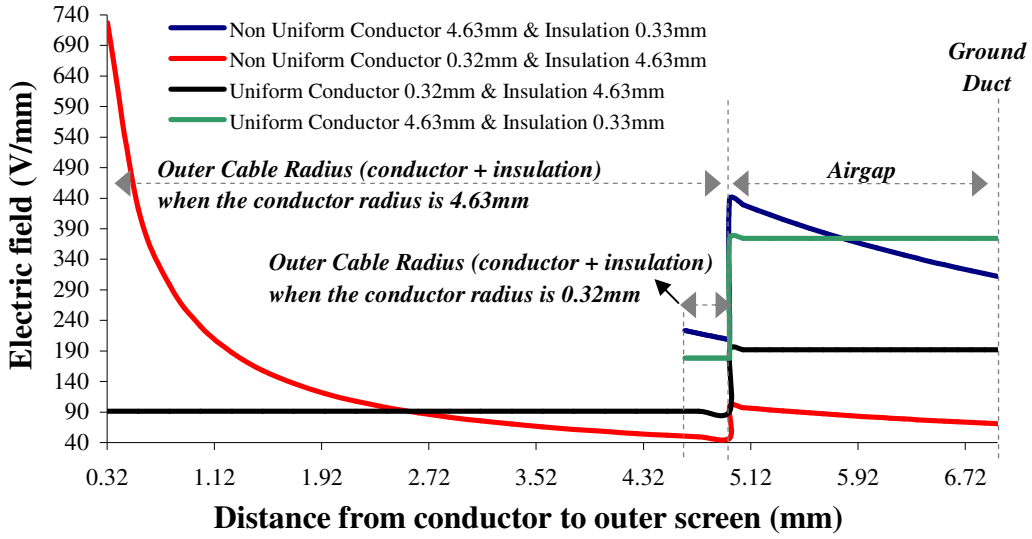

Figure 3.28: Electric field plot from the conductor to the inner surface of the duct for a small conductor size and a large insulation thickness and vice versa

In Figure 3.28 it is shown that in the uniform model case the electric field is constant throughout the insulation. The electric field is also constant across the airgap, but the magnitude is greater due to the lower permittivity of the air compared to the insulation [44]. Observe the high electric field near the conductor surface in the non uniform case. The uniform model greatly underestimates the electric field and thus the non uniform

calculations as in equation 3.11, should be used to account for the worst case, in which the calculated safe operating voltage (SOV_V) would be the smallest.

Concluding from figure 3.28, the uniform equation underestimates the electric field in the insulation and near conductor but overestimates the field in the airgap especially when the conductor is very small and the insulation is big. When the conductor is big and insulation small, more or less the voltage (integration of the electric field across the air gap distance), is the same using the non uniform and the uniform models. It has to be noted that when using the uniform model for void discharge calculations, the position of the void is not important since the electric field is constant throughout the insulation. In addition, these equation models also assume that the cable is screened, which in fact lead to more conservative results than in the case of unscreened cables in a duct, having a certain airgap between the outer cable insulation and the grounded duct.

3.5.3 FEA Electric Field Simulations and Analysis

3.5.3.1 Electric field distribution in the airgap between cable and duct

In order to evaluate the deviation of the results produced by the above equations and the real situation, a finite element analysis software tool (FEA) called '*Opera: Vector Fields'* was used to model the 3 phase cable system in a duct. Thus a comparison has been carried out between the electric field distribution predicted by the uniform and the non uniform electric field models and FEA.

Figures 3.29 and 3.30 show the results obtained in Opera for the voltage across the 2 mm air gap for Case 1 *'small insulation & big conductor'* and Case 2 *'big insulation and small conductor'* respectively. A voltage of 800 volts was used as a boundary condition for phase conductor A, 290 Volts for phase conductor B and -1100 Volts for phase conductor C. These random voltage values, based on a three phase system model, were used to investigate if the electric field along the shortest airgap distance from any of the conductors to the ground is affected by the other phase conductors and consequently whether the

uniform and non uniform single cable models can be used to compute safe operating voltages.

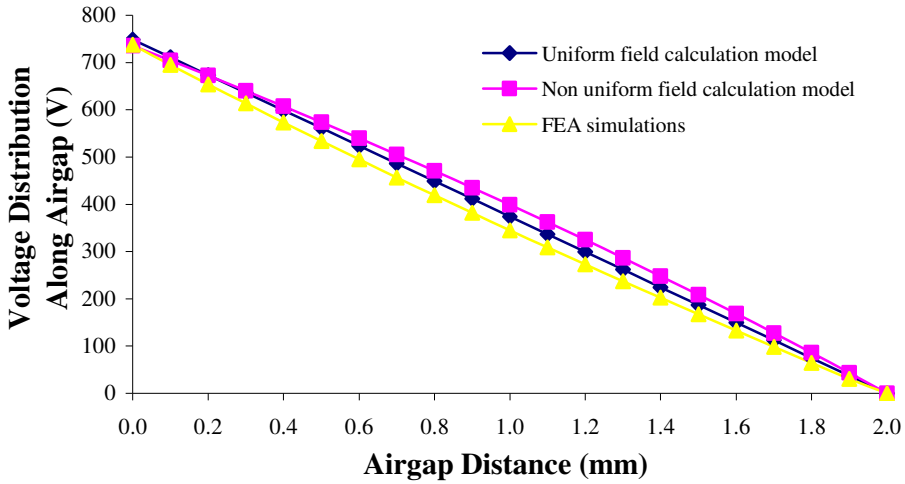

Figure 3.29: Three phase AC system: Cable to grounded duct: Voltage distribution along the 2mm airgap when the conductor radius is 4.63mm and the insulation thickness is 0.33mm

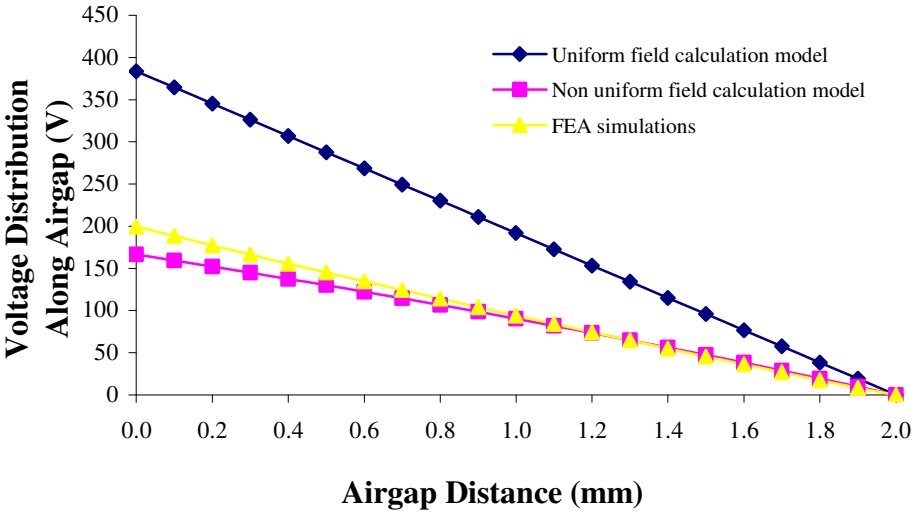

Figure 3.30: Three phase AC system: Cable to grounded duct - Voltage distribution along the 2mm airgap when the conductor radius is 0.322mm and the insulation thickness is 4.64mm

From figure 3.29, it can be deduced that the uniform field model agrees with FEA when the conductor is big and the insulation is small. On the contrary, when the insulation thickness is big and the conductor size is small (Figure 3.30), it greatly overestimates the

electric field in the airgap. Nevertheless the uniform model can be used for SOV_{CG} calculations since it provides conservative results.

3.5.3.2 Electric field distribution in the airgap between cables

Looking at the cable to cable case, only the uniform model is used and compared with FEA. This is because the modelling of discharges between cables is rather a formidable task due to the geometric complexity. Figures 3.31 and 3.32 refer to Case 1 *'small Insulation & big conductor'* and Case 2 *'big insulation and small conductor'* respectively.

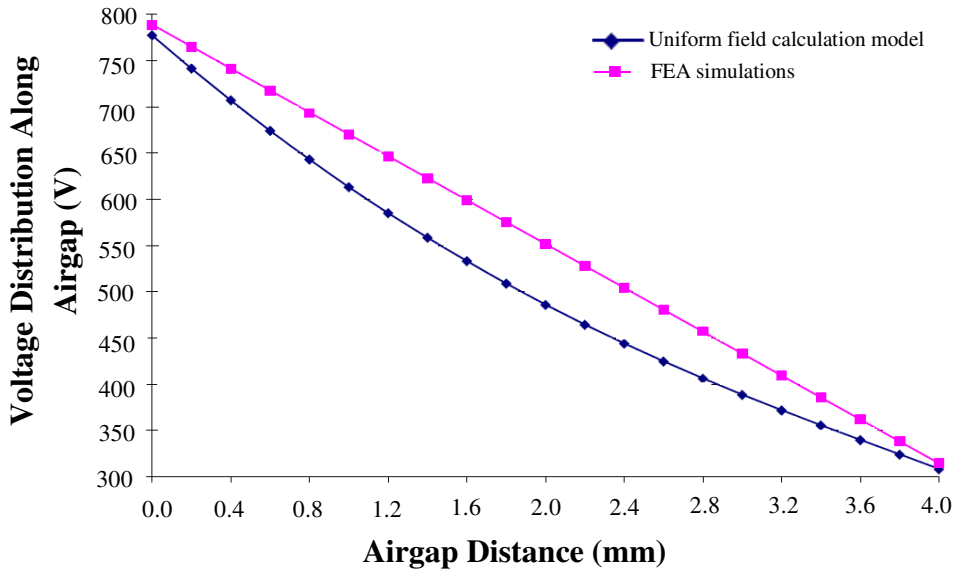

Figure 3.31: Three phase AC system: Cable to cable: Voltage distribution along the 4mm airgap when the conductor radius is 4.63mm and the insulation thickness is 0.33mm.

The voltage across the two cables is approximately the same when comparing the FEA and the uniform models. However the distribution of the voltage across the airgap differs because the electric field is slightly distorted by the other phase conductor and the grounded duct surrounding the cable system. In the situation where the thickness of the insulation is big and the conductor is small (look at Figures 3.32 and 3.33 shown below), the electric field distortion is not intensified but a higher electric field is concentrated

within the insulation especially near the conductor. It follows that the voltage drop across the insulation will be much bigger than across the airgap. This implies that the uniform model once again provides very conservative results.

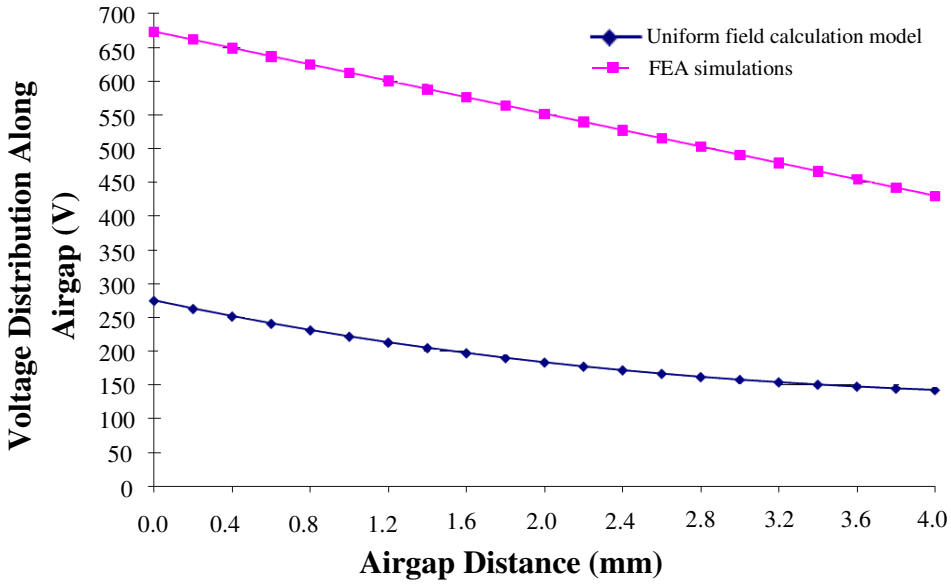

Figure 3.32: Three phase AC system: Cable to cable: Voltage distribution along the 4mm airgap when the conductor radius is 0.32mm and the insulation thickness is 4.64mm

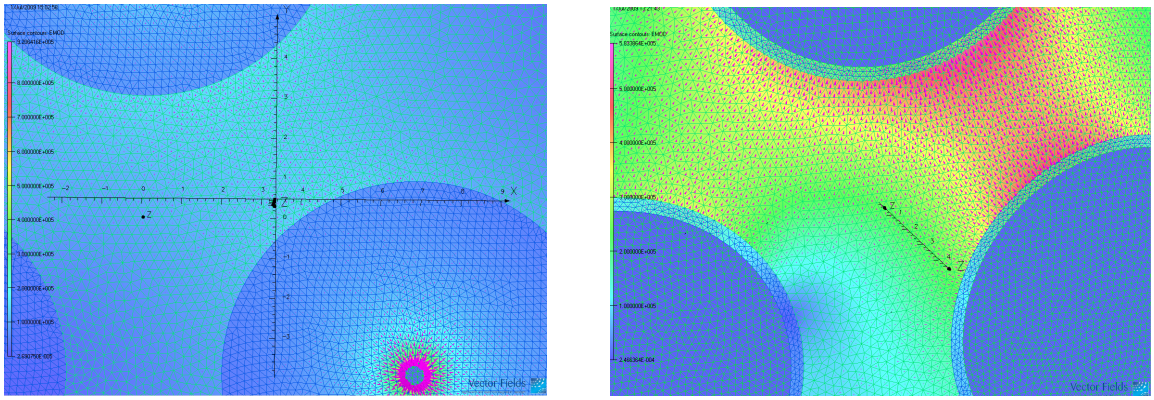

a). Conductor radius is 0.33mm & insulation thickness is 4.64mm.

b). Conductor radius is 4.64mm & insulation thickness is 0.33mm.

Figure 3.33: FEA models of a three phase system in duct: Electric field concentration across the insulation and the airgap between phases.

Concluding from the FEA analysis and the comparison of the uniform and the non uniform electric field models, the equations used in the cable system optimisation in Section 3.2.2.1-3.2.2.4 are satisfactory. For the cable to ground and the cable to cable SOV calculations, the uniform electric field model is used, since it predicts a high electric field in the airgap. Thus SOV_{CG} and SOV_{CC} results are conservative. In the case of a void discharge, the non uniform electric field model is used, since it predicts a high electric field near the conductor-insulation interface. This is the worst void location since the electric field is at its peak.

It has to be noted that FEA was not used to perform the cable system optimisation, because building FEA cable system models for every possible case that has been examined using simple equations, would be a rather formidable task.

3.6 Calculations and AS50881 Results Comparison

AS50881 [11] includes a figure providing the RMS *"corona start voltage*" for different insulation thicknesses and number of insulation layers. This RMS corona start voltage is taken to be the safe operating voltage. It is also stated as RMS partial discharge inception voltage or as RMS PDIV. However the RMS PDIV values in AS50881 are not used in the analysis that has been carried out, because there is no reference on the discharge types, (cable to ground airgap discharges, cable to cable airgap discharges and internal void discharges – look at Section 2.2.4, Figure 2.5), that have been taken into consideration for the determination of these values. In addition, the voltage Vs equivalent insulation thicknesses curves that are provided include only information for ambient temperatures of -50^{o}C and 200 ^{o}C. The ambient temperature chosen for this analysis was 70^{o}C. This value is used in a calculation example given in AS50881, for computing the current rating of a certain cable in a bundle.

Safe operating currents ratings (SOI) for specific AWG sizes are also provided in the AS50881 standard. These current rating values were used, since all the factors that can affect the current rating are clearly stated. Current derating factors are included to account for the temperature difference between conductor operating temperature and ambient

temperature, the number of cables in bundles, the conductor percentage loading and the altitude at which the cables operate. One important factor that has not been accounted for in the standard is the effect of the insulation thickness on the current rating. This factor is dealt with in this section. Furthermore, from SOV and SOI, the maximum power transfer was determined.

3.6.1 Insulation Thickness Effect on SOI: FEA Analysis

The current ratings given by AS50881 are based on the temperature difference between a bare conductor and air and as described these values have to be derated considering the altitude, whether the cables are to be installed in bundles and the percentage loading of the cables. It is not mentioned in the standard whether these ratings include the effect of increasing insulation. In computing current ratings for power cables, the insulation thickness is a determining factor. A thicker insulation results in a bigger thermal resistance between the conductor and the air and therefore this would obstruct heat dissipation and would cause the temperature of the conductor to rise above its limits. Thus the maximum power transfer and thus the maximum steady state current flowing in the conductor, has to be reduced to avoid overheating the cable above specified limits.

Finite element analysis (FEA) was used to model a three phase AC system installed in a duct of fixed diameter, to determine the effect of increasing cable insulation whilst decreasing the conductor radius on the current rating. The software used is called *'Opera: Vector Fields'*. It has to be noted that three duct sizes are examined having a diameter of 30 mm, 45 mm and 60 mm. The cable radius is fixed at 4.96 mm according to the Equation 3.1 used in Section 3.2.1, to calculate the maximum cable size for a 30 mm diameter duct. Thus, a duct with a diameter bigger than 30 mm implies a bigger airgap between the cables and the surrounding duct. Current rating results are shown below in Figure 3.34.

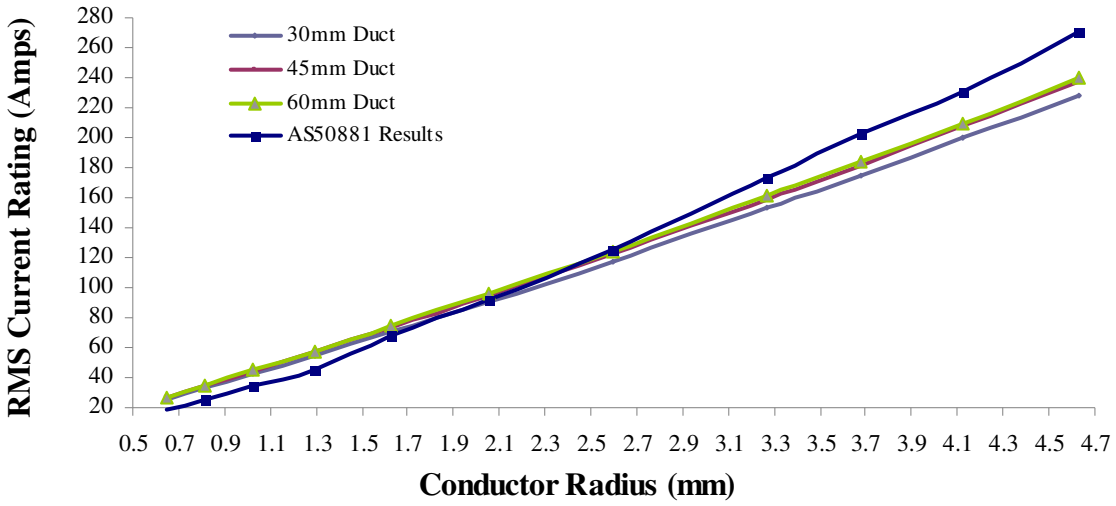

Figure 3.34: FEA simulation, effect of increasing insulation thickness (i.e. smaller conductor size), on the current rating of cables in duct

According to the simulation results there is no significant difference in the current ratings for different duct diameters. This is due to the fact that the thermal resistance of the air in the gap surrounding the cables dominates the thermal resistance of the cable insulation. However as expected, by increasing the conductor size and thus decreasing the insulation thickness, the current ratings increase for all duct sizes. There is however a difference when compared with the AS50881 current rating values. The Standard underestimates the current rating when the conductor is very small up to a conductor radius of about 1.7 mm. The maximum percentage difference from a conductor size of 0.65 mm up to 1.7 mm is approximately 24%. At a radius of 2.7 mm up to 4.7mm, there is an overestimation of the rating with a maximum percentage difference of approximately 18%. This difference might be due to the fact that AS50881 takes into account convection heat transfer effects in determining the current ratings. On the other hand the FEA simulations that have been carried out do not take these effects into account.

As it has been mentioned previously in Section 3.2.1, for cables installed in a duct, the cable bundle radius should be 25% less than the duct radius. For three cables installed in a duct and for the clearances taken into consideration, the cable bundle radius was approximately 22 mm and thus satisfying this requirement. For more cables installed in the duct the cable radius is even smaller and the cross sectional area of the air relatively to the

total cross sectional area occupied by the cables is even bigger. As a result the thermal resistance of the air will also dominate the thermal resistance of the insulation. Therefore any changes in the thickness of the cable insulation, for the range of AWG sizes that were used in the analysis, will have no effect on the current rating. It must also be emphasized that the more the number of cables in the duct, the less the space available to be filled with insulation. Compared to the effect on the current rating that the maximum insulation thickness has in the three cable case, the insulation effect will be less by having more cables in the duct.

Although the insulation thickness effect has been examined for a fixed duct size of 30 mm, further work has to be carried out when bigger ducts are considered, like in section 3.2.5. For bigger ducts the maximum cable size is bigger for the same clearances and more space is available for insulation. Thus it might be the case that the thermal resistance of the insulation dominates the thermal resistance of the air. Therefore an increase in the insulation thickness might affect the current ratings significantly.

3.6.2 Insulation Thickness Effect on SOV

A key point in this analysis is the assumption that the electric field is uniform. This will only be the case if the ratio of the outer cable radius to the conductor radius is sufficient so that a uniform field occurs. Work by Halleck [43] concluded that for cables with a conductor radius of less than 0.79mm, electric fields could be non-uniform [43]. In most cases, both the radius of the conductor and the relative thickness of the insulation should be considered. To adjust the approach presented for non uniform electric fields, an alternative method must replace the equation used for the calculation of the percentage of system voltage across the air gap ($fract_{(Vd)}$). One option is the use of a model describing the electric field based on a coaxial system, or finite element analysis. Both methods (uniform and non-uniform models describing the electric field), have been used to compare calculated safe voltage ratings against those found in AS50881 [11]. In this standard, the safe operating voltage is based on likelihood of partial discharge between the “outside of an unshielded cable covering and any grounded structural elements over which the cable

passes, or between the insulation and a braided shield". It includes a graph of partial discharge inception voltages (PDIVs) against equivalent cable insulation thicknesses for a range of altitudes. For each altitude it provides PDIVs for an ambient temperature of 200 ^{o}C and -50 ^{o}C.

In the graph shown below in Figure 3.35, which compares AS50881 PDIV results and the calculation results, the environmental conditions that were taken into consideration were an ambient temperature of 200^{o}C and an atmospheric pressure of 18.75 kPa (i.e. at an altitude of 40,000 feet). The calculations carried out using the non-uniform approximation models, were performed using a large fixed sized conductor whilst increasing the insulation thickness and also for a small conductor.

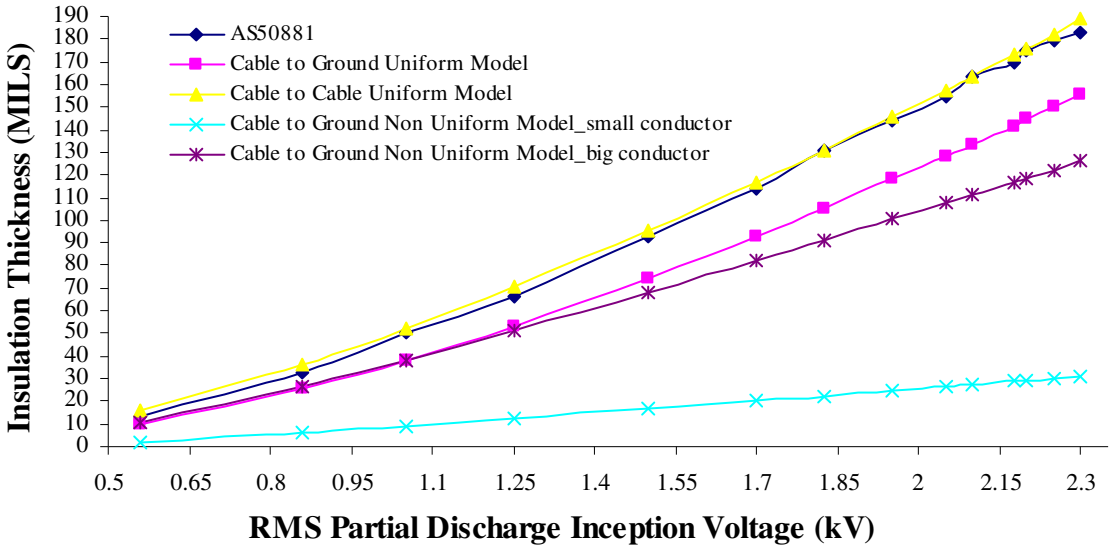

Figure 3.35: Comparison of AS50881 PDIV results and calculated PDIV results: Graph of insulation thickness against the RMS PDIV

It is obvious that the standard has considered the fact that the worst case discharge scenario is the cable to cable case as it was described earlier. However if the non uniform cable to ground discharge model is used, the results prove that the uniform field model and thus the AS50881 results are quite conservative. The only case that the non uniform field model might give similar results is when the conductor radius is bigger than 4.63 mm. As shown in figure 3.35, if the conductor size is small the amount of insulation required with the increase in voltage is very small compared with the other cases.

3.7 Summary

For Chapter 3, two techniques (***A*** and ***B***) have been developed to optimise certain cable systems installed in a duct. Technique ***A***, has considered a fixed duct size to model a situation in which the space available for a cable system is limited. Furthermore specific equations were derived to calculate the maximum cable size for a list of AWG conductor sizes, taking into account a clearance between cables and between cables and the duct. In addition, maximum power transfers and power to weight ratios were computed based on the partial discharge inception voltage of different types of PD. This was done by using theoretical equation model approximations found from literature. These equations made use of the famous *Paschen's Law,* which relates the breakdown voltage of air and the pressure-distance product.

From the results obtained by using technique ***A***, it was observed that cable systems installed in smaller duct sizes had larger power to weight ratios, even though their maximum power transfer capability was much lower than cable systems installed in bigger ducts. Thus, the possibility of replacing one big duct system with multiple smaller ones was also examined. Results showed that even though weight savings could be achieved by making these replacements, the power losses and the voltage drops were significantly affected in the negative sense.

In technique ***B***, a reverse methodology has been adopted by considering a fixed power demand to determine the optimal cable duct size. Furthermore, a discussion was carried out, regarding the accuracy of the results obtained by using the uniform and the non-uniform electric field models, to calculate partial discharge inception voltages (PDIVs).

Finally, two comparisons were carried out. The current ratings, calculated according to the Wiring Aerospace Vehicle Standard (AS50881), were compared with the current ratings obtained by performing finite element analysis (FEA) simulations. This was done to examine the impact of using thicker insulation, on the current ratings of different AWG conductor sizes. In addition, the calculated PDIV results were compared with the data provided by AS50881.

Chapter 3 is new work, as it proposes two methodologies for optimising high voltage cable systems to be used in the More Electric Aircraft (MEA). This expands on the work carried out by Nelms [12] and Halleck [43], in which calculation techniques had been developed for calculating the safe operating voltage of an aircraft cable system, taking into consideration environmental conditions at altitude. Chapter 3 extends the work carried out in [12], in which the author performs optimisation on a cable system installed in a fixed sized duct.

In this thesis the possibility of bigger sized ducts has been examined and it has been found that maximum power to weight ratios of different cable systems do not increase if the diameter of the duct increases. Even though larger cables can be used in bigger ducts and thus more power can be transferred, the increase in weight counterbalances this increase and the power to weight ratio remains approximately the same.

In addition, a 'more practical methodology' has been developed for optimising a certain cable system. This methodology starts from a fixed power (where the aircraft power loads are known), to determine the cable duct system (AC / DC and how many cables should be installed in the duct) and results in less system weight. The method engineers currently use for cable selection is based on choosing by experience, a cable with the capability to satisfy the current and voltage requirements of the aircraft electrical system. The new methods developed in Chapter 3 can be used by engineers to select exactly the cable they need, the cable system (AC/DC), the number of cables to use and in parallel figuring out how much space the cable system will occupy.

The conclusion from the work done in Chapter 3 is that a DC cable system is the best choice for transferring power due to its higher power to weight ratio for a specific power demand. However, the calculations for DC systems use the same approach as an AC system, in which the safe operating voltage depends on cable insulation thickness, the insulation relative permittivity and the airgap size. The same approach has been carried out since there is no distinction between AC and DC cables in the 'Wiring Aerospace Vehicle Standard' (AS50881) [11]. However, this is certainly not applicable for DC since the safe operating voltage for this case depends on the insulation resistivity and not the relative permittivity. Further research has to look at this aspect.

After examining the possibility of using multiple smaller cable systems installed in a duct instead of one large system, it was also concluded that even though significant savings in weight can be achieved, losses and voltage drops increase. Design engineers can use these results to quantify the increase in losses and voltage drops, to help them select the appropriate methods to transfer power around the aircraft.

Chapter 4

PCB Technology Vs Round Cables

This chapter examines the possibility of replacing cabling harness with printed circuit board (PCB) technology. An initial assessment has been carried out to determine whether more power can be delivered via insulated flat solid conductors as in a PCB, instead of using round cables. The reason why there is a need to investigate this aspect, is because using new PCB technology can offer several advantages in contrast to a cabling harness. The advantages will be discussed in this chapter together with any drawbacks and limitations in maximum power transfer via PCBs.

4.1 Introduction

Flat conductor cabling technology (FCC) has been developed in the early 1970s by NASA for satellite and spacecraft applications [46]. FCCs have also been used in BOEING 747 for a 90 kVA, 120 V and 250 A three phase system, operating at 400 Hz, transferring power from the Auxiliary Power Unit (APU) to the main distribution feeder [47]. Main drivers for the usage of FCCs were the reduction in system weight, the space saving achieved due to the flat geometry of the cables (more compact), the reduction in testing and installation times (cost saving) and the higher power transfer capability. These advantages will be discussed later on in more detail. Figure 4.1a and 4.1b show the FCCs used by NASA and the BOEING 747 respectively.

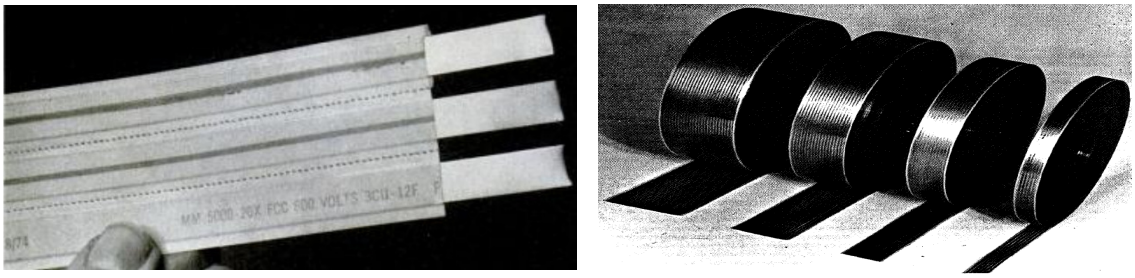

a). FCC used by NASA

b). FCCs used in BOEING 747

Figure 4.1: Flat conductor cabling technology (FCC) used by NASA for spacecraft applications [46] and by BOEING 747 for transferring power from the APU [47]

With the advancement of flexible PCB technology it is possible to use flat conductors as in flexible PCBs, to replace simple FCCs and round cable harnesses currently used in electrical systems for transportation as for example in aircraft. Examples of flexible PCB harnesses are shown in figure 4.2.

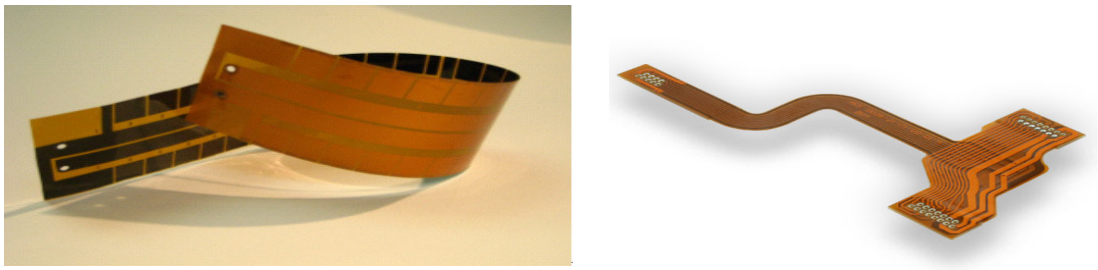

Figure 4.2: Flexible PCB harnesses

Flat conductor cables are referred to in literature as FCCs [47] or FFCs [48]. The geometry of FCCs/FFCs and flexible PCB systems is quite similar and one could argue on whether there is an actual difference between two systems. Even though for modelling and analysis (as it is carried out in this thesis) the two systems are considered to be identical, there is a difference in the manufacturing procedure. The early methods used for fabricating FCCs are listed in [47]. These methods are quite similar to the methods used for flexible PCB fabrication. Even though this is also confirmed in [48], an important difference is also stated. In flexible PCBs, the copper trace is chemically etched to produce a specific pattern and thus the copper trace can be designed to have many geometric shapes

and to follow different routes. As a result complex packaging issues can be dealt with very easily.

Flexible PCBs are more compact and robust and are easier to handle than FFCs/FCCs during installation and maintenance. As a result, labour times can be reduced even further (saving cost). PCB technology can transform the conventional systems of transmitting power and electronic signals to a more computer like architecture, performing a variety of functions such as electronic sensing, condition monitoring and protection of the whole aircraft system.

Even though it is more expensive to build a PCB harness than a cabling harness, the overall cost of using PCBs is less [49]. As mentioned before, this is due to the fact that it takes a much longer time to install a cable harness and the testing procedure is much more difficult, thus requiring more hours of labour. As a consequence of using a PCB rather than a cabling harness, maintenance and repair times can be reduced significantly since there will be a reduction in the number of parts making up the electrical harness. The next section discusses the issues associated with the design of PCBs.

4.1.1 Issues Associated With the Design of PCBs

As discussed, PCB technology could replace a cabling harness since it can offer a reduction in maintenance and installation costs. Furthermore it would be even more beneficial if the PCB system could offer a bigger power to weight ratio than a round cable system. The aim of this chapter is to examine this possibility.

Extensive research has already been carried out in literature for the current carrying capacities of the flat PCB conductors, as mentioned in [50, 51]. The standards IPC 2221A, 2222A and 2223B [52-54], provide current rating data and design considerations for different trace geometries and insulation thicknesses. However, there is little information in literature concerning partial discharges within PCBs and partial discharge inception voltages (PDIVs).

4.1.1.1 Partial discharges (PD) and surface flashover

As explained in chapter 3, PDIVs can be used to determine the voltage rating of a cable system. It has to be noted again in this section that the determination of the voltage rating of any cable system can be based on PDIV, only if no other failure mechanisms occur at lower voltages. An excellent discussion on the failure mechanisms concerning aircraft cables can be found in [4]. Based on [4], all forms of arcing are considered to be the main mechanisms of insulation degradation and cable system failure. Thus the investigation of PDIVs which are much lower than the voltages leading to arcs can provide a safe operating voltage (SOV). On the contrary, according to [55] one of the most critical failure mechanisms for PCBs is surface flashover.

Dunbar [5], classifies the phenomenon of surface flashover within the range of 50-250 V. The voltages within this range are below the minimum breakdown voltage in air (Paschen's minimum – 327 V). It is therefore implied that determining the voltage rating based on PDIVs is not a suitable method. However it is also stated that flashover can be avoided by taking certain precautions. These will be described later on. In addition the conductor trace spacing for a given voltage as determined in [52], is based on the work carried out by Dr. Charles Jennings of Sandia National Laboratories in 1976. This work was focused on "dielectric breakdown, current carrying capacity and insulation resistance" on a specific material called FR-5 [55]. It is therefore reasonable to question the data found in [52] and to seek for a suitable method to determine PCB voltage ratings and conductor spacing.

Flashover is defined by Dunbar [5] as "a disruptive discharge around or over the surface of a solid or a liquid". It follows that a surface flashover in PCBs occurs along the surface of solid insulation, between two trace conductors having a significant voltage across them. The shortest distance at which surface flashover can occur along the surface of the insulation, is called the creepage distance, whilst the shortest distance where flashover can occur in the airgap between the conductor traces is called the "clearance distance". These distances are illustrated in Figures 4.3a and 4.3b. Surface flashover can be

dealt with, by completely covering the trace conductors with insulating coatings. Figure 4.3c shows how flashover can be avoided by applying insulation all around the traces.

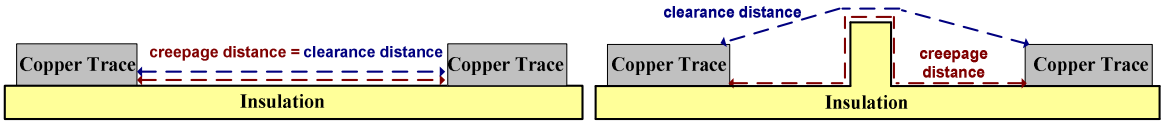

a). PCB Case A: creepage distance = clearance distance

b). PCB Case B: creepage distance ≠ clearance

c). PCB copper traces fully covered in insulation to avoid surface flashover

Figure 4.3: Illustration of creepage and clearance and methods used to elongate these distances, to avoid different kinds of flashover [5].

In the case where the PCB copper traces are fully encapsulated by insulation as in Figure 4.3c, surface flashover can still occur if there is a high electric field along the insulation surface between the traces. However in this case, the electric field along the creepage distance line can be significantly reduced depending on the insulation material and the level of contamination along the insulation surface. By placing the PCB system shown in Figure 4.3c in a grounded rectangular duct, the electric field along the surface can be reduced even further. Figures 4.4a and 4.4b show how the electric field distribution changes by adding the duct. More details on the factors affecting surface flashover can be found in [5].

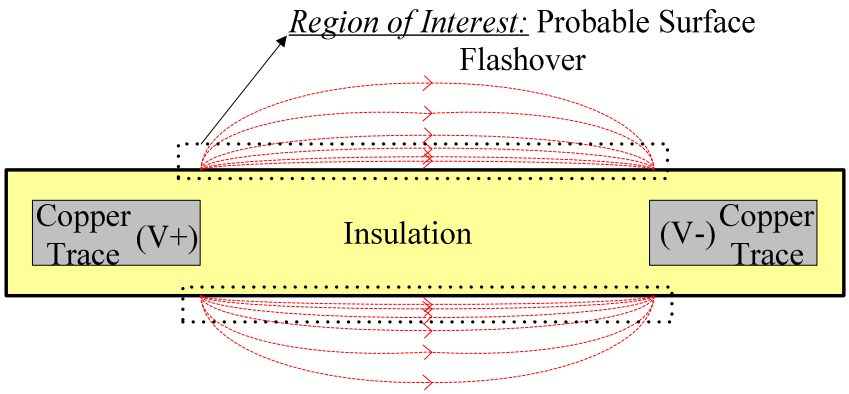

a). Electric field distribution in a two conductor trace PCB embedded in insulation

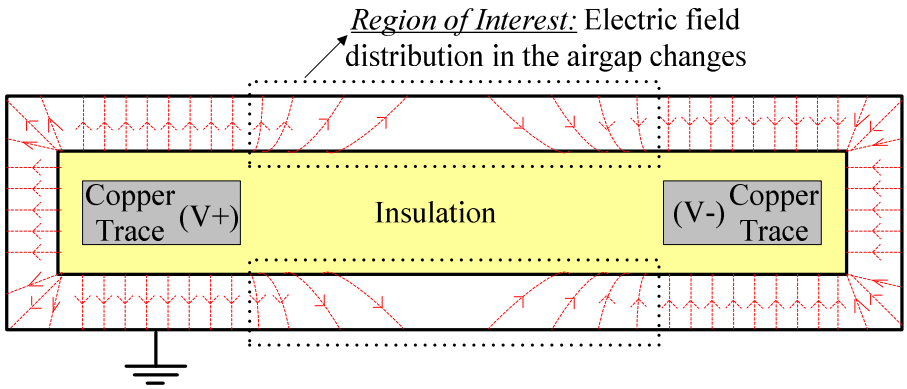

b). Electric field distribution in a two-conductor trace PCB, embedded in insulation and placed in a grounded rectangular duct

Figure 4.4: Illustration of the electric filed distribution for a). An insulated two-conductor trace PCB and b). An insulated two-conductor trace PCB, placed in a grounded rectangular duct [5].

It is obvious from Figures 4.4a and 4.4b that the electric field lines change direction eliminating the probability of surface flashover. It will be shown later on that the electric field distribution is also affected by the insulation thickness between the traces.

From this point onwards, a similar PCB model is used for analysis as in Figure 4.4b and the report is focused on the different types of PD that can occur in voids in the insulation and in the airgaps between the outer surface of the insulation and the grounded duct.

4.1.1.2 Discussion of PD occurring in a PCB

The PCB model that has been investigated in this report was designed in the FEA software *'Opera: Vector Fields'*. The PCB consists of three rectangular copper traces fully covered with a homogeneous PTFE insulation, uniformly distributed around the traces and placed in a grounded rectangular duct. It is assumed that the most critical mechanism for insulation deterioration is the breakdown of air in voids in the insulation, or the breakdown of air between the outer insulation surface and the grounded duct. The breakdown of air in voids in the insulation is referred to as void discharges and the breakdown of air in the airgap is referred to as PCB to ground discharges. The PCB model together with the partial discharges occurring at different locations is shown in Figure 4.5.

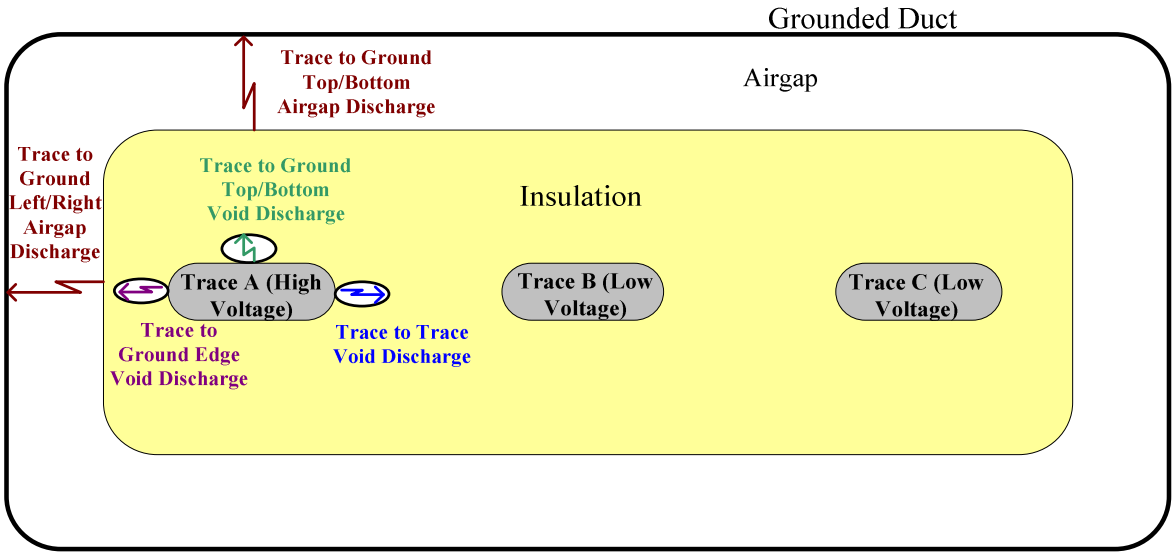

Figure 4.5: PCB model used for analysis and different locations where PD can occur

If the outside surface of PCB is plated with a grounded conductor, theoretically the only type of discharge that should be considered is the void discharge, since no airgap exists between the outer insulation surface and the surrounding ground. It was concluded in Chapter 3 that for a void size of 80 μm, discharges occur at higher voltages. This would also be an advantage for screened cables. What needs to be examined though is the electric field enhancement at the trace edges and the electric field non-uniformity caused by the PCB geometry. The different types of PD are explained in detail in the next section.

In addition, the void discharge between conductor traces in the PCB has to be taken into consideration if the traces are at a different potential. Take for an example a three phase distribution system. At all times there will be a potential difference between the traces. On the contrary if a four cable grounded DC system was to be considered (as in Chapter 3), the PCB could be designed so that there is no potential difference between the traces along their route. However, this method would actually complicate the design of the connectors at generation and termination points. Figure 4.6 illustrates this possibility.

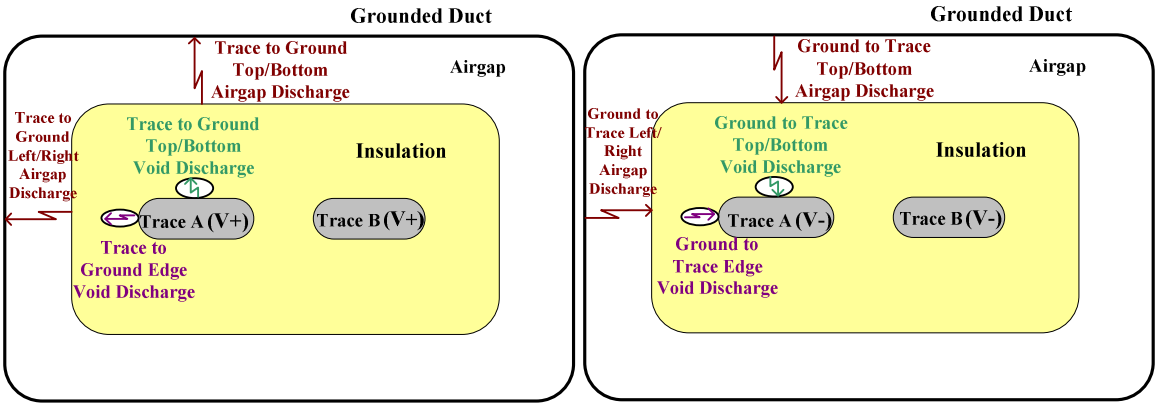

Figure 4.6: Possible PCB model consisting of a four cable grounded DC system

In a three phase AC system, trace separation by introducing a ground around each trace individually is not possible, because the current induced on the ground/neutral conductors would cause them to heat up. This would cause severe damage to the insulation and the system will fail catastrophically. Another issue resulting from the PCB three phase AC model chosen for PD analysis is the geometric unbalance between phases, which in turn results in a significant current flowing through the neutral or grounding conductor. This would cause the neutral/ground conductors to heat up. Furthermore the insulation temperature would rise above limits, causing a reduction in the lifetime of the insulation or even cause premature breakdown. This issue could be solved by transposing the conductor traces along their route, as it is done in ground power systems [56].

4.1.1.3 Objective: Comparing a PCB and a round cable system

The surface area perpendicular to the direction of heat transfer of a thin rectangular conductor would be bigger than a round one. This could imply higher current ratings for the same cross sectional area of copper conductors. Higher current ratings are a result of the increased surface area over which heat is dissipated. The question that this chapter will answer is whether this current rating increase is significant, taking into consideration the insulation thickness and the copper trace to trace proximity. The idea is to compare three insulated round conductors installed in a duct, (as in the case of a three phase system which

was described in the optimisation calculations previously), with three flat conductors in a PCB having the same insulation and conductor cross sectional area and thus the same weight. If the voltage rating remains more or less the same as in the case of insulated round conductors and the current rating increases, it might be the case that higher power to weight ratios could be achieved.

4.1.2 Round Cable to PCB System Transformation

To compare a three phase system comprising of three insulated round conductors placed in a duct, with a three phase system of three flat conductors as in a PCB, the procedure which will be described in this chapter was carried out, making the following assumptions:

- Same cross sectional area of metal conductor and insulation was used to transform the three phase duct system to a three phase PCB system.
- Since the cables in the duct had a 2mm gap between the cables and the grounded duct, a maximum gap of 2mm was also included between the PCB's outer insulation and a rectangular grounded duct.

The transformation of the single circuit three phase duct system to the PCB system is clearly illustrated in figure 4.7. It has to be mentioned, that the assumption of an airgap existing between the outside insulation surface of the PCB and the rectangular duct, as shown in figure 4.7, is not realistic. No information has been found in literature about the encasing of PCBs in a grounded structure. However it is mentioned in [57] that internal laminations are used for grounding the PCB. Copper and carbon fibre are some of the most commonly used materials for PCB grounding purposes. Thus a more practical PCB model to be used for analysis would be to consider a PCB system encased in a grounded structure with no airgaps. Nevertheless, the duct has been introduced into the analysis with the 2 mm airgap, to explore the calculated partial discharge inception voltages (PDIVs) based on Paschen's Law, at different locations in a PCB module.

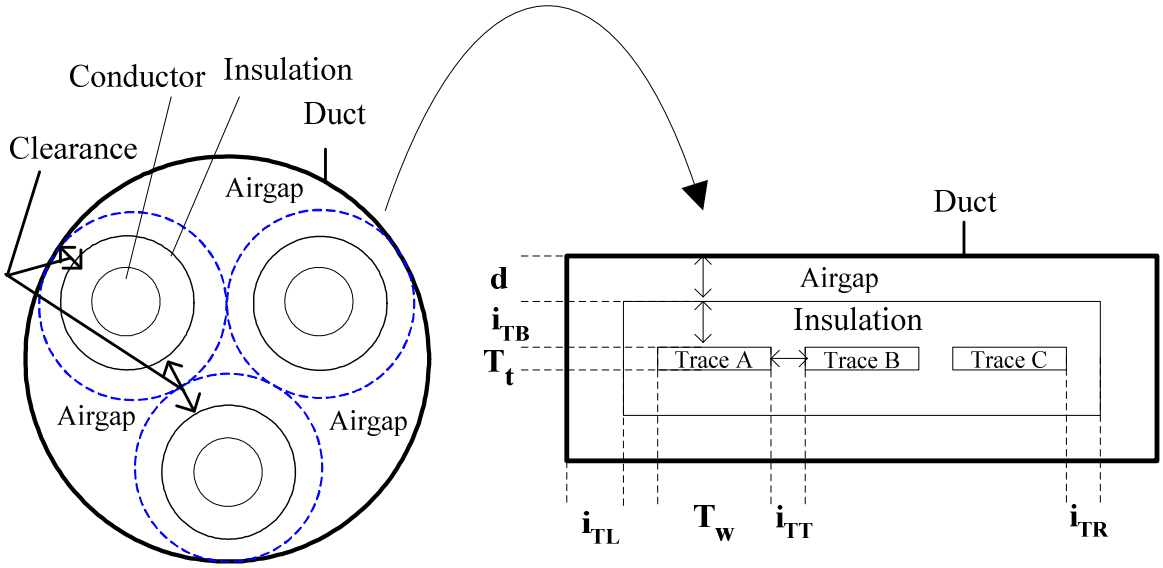

Figure 4.7: Three-phase insulated round conductor duct system to PCB system transformation

Using the same cross sectional area of conductor and insulation, the rectangular dimensions T_w (trace width) and T_t (trace thickness), were varied in order to evaluate the effect of increasing the area perpendicular to the direction of heat flow, on the current rating. Note that by changing T_w or T_t for the same conductor size, the insulation thickness between trace and ground i_{TB} and trace to trace i_{TT}, change as well. The variation of the current and the voltage ratings with changes in T_w, T_t, i_{TB} and i_{TT} will be shown later on.

As it can be observed from figure 4.7, the analysis of the PCB system is more complex than the round cable duct system. This is due to the physical dimensions of the conductor traces and the insulation thicknesses that can be varied. The next section of this chapter describes the methodology and the calculation techniques that have been adopted, to analyse the more complex PCB system.

4.2 Development of Calculation Techniques for Different PCB Geometries

To deal with the geometric complexity of the PCB model, Equation 4.1 has been developed as part of this work and it contains all the dimensional parameters shown above in Figure 4.7, in order to analyse the PCB system. The equation has been used for calculating the insulation thickness i_{TB}. The assumptions that have been made to derive Equation 4.1 to be used in this thesis are that i_{TT} is a function of i_{TB} having the following relationship: $i_{TT} = \lambda i_{TB}$ and also that $i_{TB} = i_{TL} = i_{TR}$. (Note: The derivation of equation 4.1 is shown in Appendix C-2).

$$i^2_{TB} + \frac{1}{2}\left(T_t + \frac{3T_W}{1+\lambda}\right) i_{TB} - \frac{1}{4}\left(\frac{i_A}{1+\lambda}\right) = 0 \qquad (4.1)$$

i_{TB} = Insulation thickness between trace and outer insulation – air gap boundary (mm)

i_A = Total cross sectional area of insulation as in the 3 phase round conductor duct system (mm^2)

λ = factor relating i_{TB} and i_{TT}

T_W = Trace width (mm)

T_t =Trace thickness (mm)

From the equation above it can be noticed that the geometry of the PCB can be altered by changing T_w, T_t and λ. Since the conductor size is fixed, only one of the parameters (T_w or T_t) is necessary to change. On the contrary different values of λ must be examined for each value of T_w or T_t.

4.2.1 Parameters Affecting the PCB Geometry

The value of λ was varied from 0.25 to 20 for a range of T_t. Since the area of the conductor was constant for each AWG size conductor, T_w was calculated for each value of T_t.

Equation 4.1 shown above was then used to compute i_{TB}. Figure 4.8 illustrates the effect of changing the λ factor on the PCB geometry, when T_w = 3.53mm and when T_w = 13.07mm, for a conductor size of AWG 16.

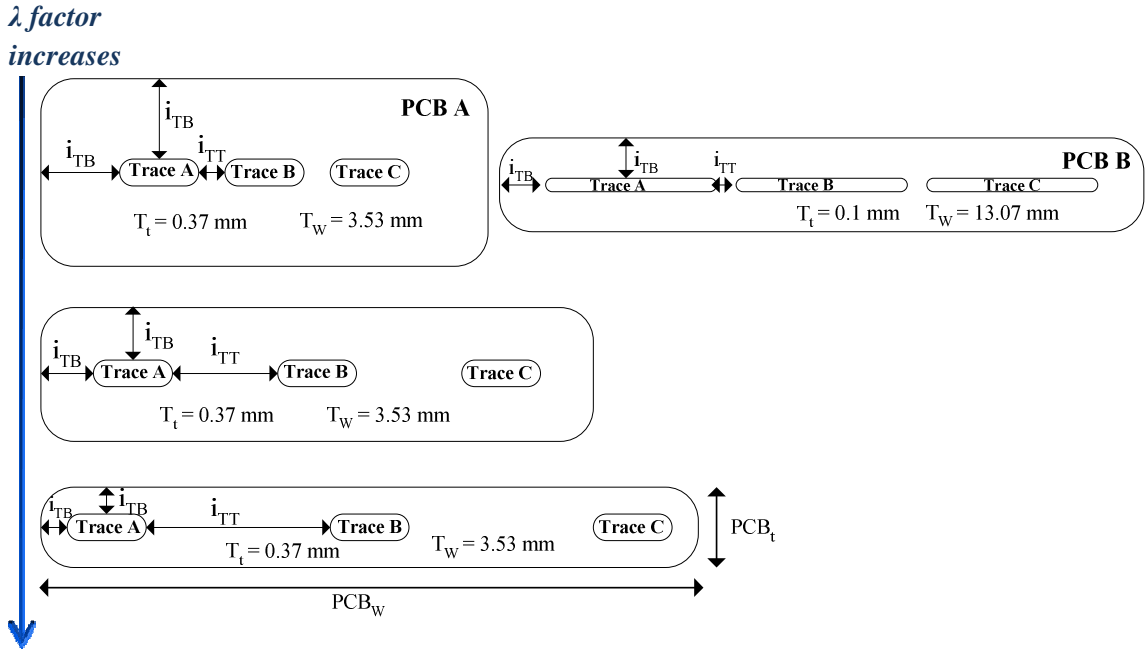

Figure 4.8: Illustration of the Effect on increasing the λ factor on the PCB geometry

Looking at figure 4.8, it can be observed that for the same trace conductor size, an increase in the λ factor causes an increase in the thickness between the traces *'i_{TT}'*, whilst causing a decrease in the insulation thickness at the top and on the sides of the trace *'i_{TB}'*. As a result the total PCB thickness *'PCB_t'* decreases, whilst the total PCB width *'PCB_W'* increases.

For a bigger conductor trace width *'T_w'*, an increase in the λ factor affects the PCB dimensions in the same way. However when comparing different conductor sizes for the same λ factor, the conductor having a bigger T_w results in an even wider and less thick PCB (compare PCB *A* and PCB *B* on figure 4.8).

Table 6 shows the data obtained initially for a conductor size of AWG 16, for λ = 0.25 and λ = 2 for different T_w. The calculations were repeated for different values of λ.

The effects of increasing the λ factor and using different conductor thickness can also be observed from table 6. By increasing the value of λ, for the same values of T_w and T_t, the conductor traces move further apart from each other (i_{TT} increases) and since the insulation cross sectional area is fixed, i_{TB} decreases. By increasing the trace thickness, for the same value of λ, the trace width *'T_w'* decreases causing both i_{TB} and i_{TT} to increase.

TABLE 4.1

CALCULATED PCB DIMENSIONS USED TO MODEL THE PCB IN 'OPERA: VECTOR FIELDS'

FOR AWG 16 AND λ =2		**FOR AWG 16 AND λ =0.25**		**INSULATION CROSS SECTIONAL AREA: I_A = 76 MM^2**	**CONDUCTOR CROSS SECTIONAL AREA C_A = 3.92 MM^2**
i_{tB} (mm)	i_{TT} (mm)	i_{tB} (mm)	i_{TT} (mm)	T_W(mm)	T_t(mm)
2.17	4.34	2.5	0.63	13.07	0.10
2.50	5.01	3.01	0.75	10.05	0.13
2.75	5.50	3.43	0.86	8.17	0.16
2.94	5.87	3.77	0.94	6.88	0.19
3.08	6.17	4.04	1.01	5.94	0.22
3.20	6.40	4.27	1.07	5.23	0.25
3.29	6.59	4.47	1.12	4.67	0.28
3.37	6.75	4.63	1.16	4.22	0.31
3.44	6.87	4.77	1.19	3.84	0.34
3.49	6.98	4.90	1.22	3.53	0.37

Furthermore all the data were used to construct models in a finite element analysis tool called *'Opera: Vector Fields'*, to determine the current ratings of the conductor traces. The same operating and ambient temperatures were used as in the cable duct models, (423 K for the trace operating temperature and 343 K for ambient), which were examined in the previous chapters. The same insulation and conductor materials were taken into consideration (copper metal having an electrical resistivity of 1.72×10^{-8} Ωm and PTFE insulation having a relative permittivity of 2.1).

4.2.2 PCB Current Rating

4.2.2.1 PCB and round cable comparison

FEA simulations were carried out initially, using PCB models of different dimensions, Table 4.1, for conductors sizes AWG 22 down to AWG 10. This was done to observe how the current rating is affected with changes in T_w, T_t and the λ factor (relationship between i_{TB} and i_{TT}) and in addition to determine whether by using a PCB, higher current ratings can be achieved. It has to be noted that the current rating is affected positively by an increase in the area perpendicular to the direction of heat dissipation, whereas it is negatively affected by the amount of insulation which provides a certain thermal resistance. The current rating results for each case are shown below in figure 4.9 for the middle trace (trace B - as shown in figures 4.7 and 4.8). Results obtained for trace B were chosen for display, since this exhibited a slightly lower current rating for the values of λ taken into consideration, due to its position, where heat flow from left and right was obstructed.

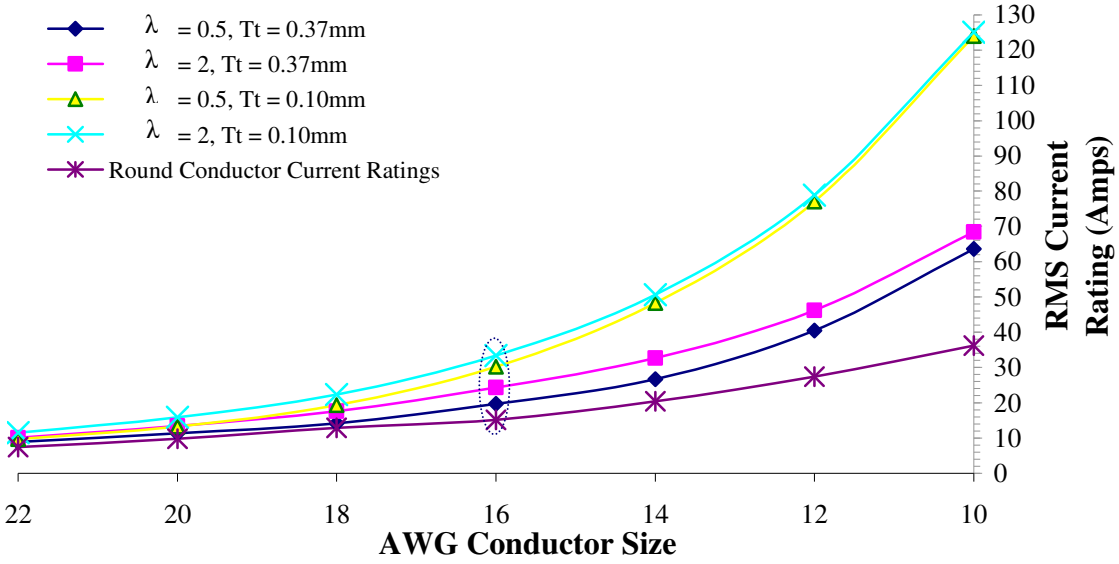

Figure 4.9: PCB current rating against AWG conductor size for different values of λ and T_t

For the smallest AWG sized conductor, the effect on the current rating of changing λ and the values of T_t that were chosen is very small. However it is shown that for larger conductor sizes, the bigger the distance between the traces and the bigger the trace width (i.e. higher λ factor and lower i_{TB} thickness), an increase in the current rating can be achieved. For example according to the AWG 16 points on figure 4.9, the current rating can be doubled from 15 Amps up to approximately 32 Amps. It has to be noted that the factor that most influences the current rating, is the change in T_t.

4.2.2.2 Current rating computation using FEA

The corresponding single phase RMS current ratings for bigger λ factors and thus a bigger range of i_{TT}, are shown in figure 4.10. The current ratings shown below have also been de-rated by a factor of 0.713, to account for the high altitude, as it was taken into account for the round conductor system based on AS50881 [11]. A trace conductor operating temperature of 423 K has been applied and an ambient duct temperature of 343 K. These boundary conditions were also used in the round cable duct system calculations. It must be mentioned that these values are typical values used in [11].

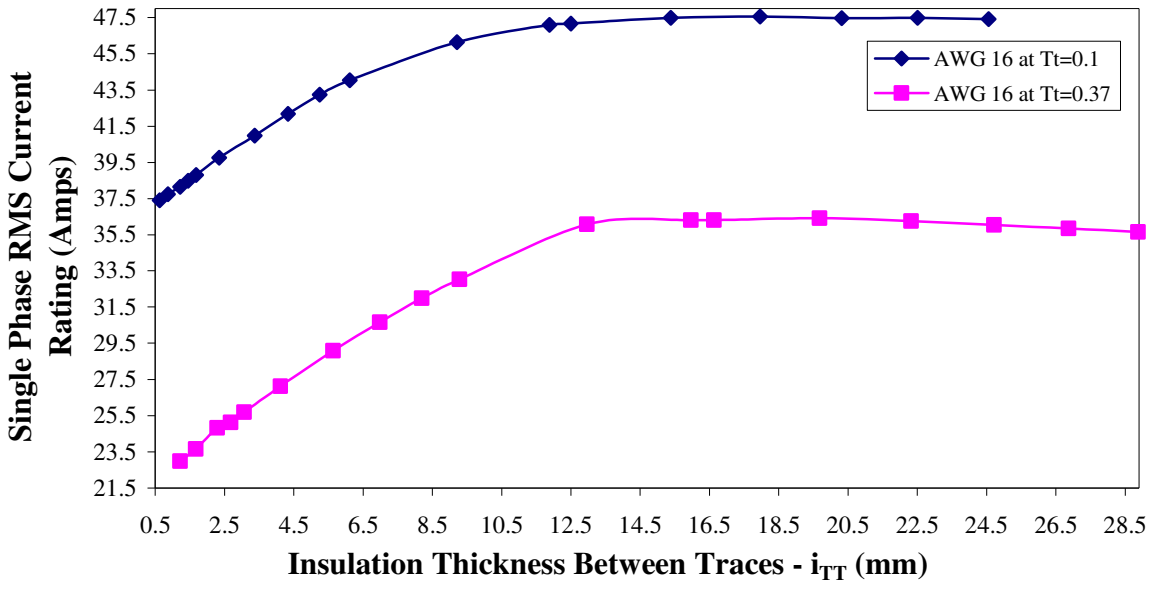

Figure 4.10: Plot of current ratings against PCB trace to trace insulation thickness for different λ factors i.e. different PCB dimensions and for T_t=0.1 mm and T_t=0.37mm. Altitude de-rating taken into account

While simulating a thermal analysis in FEA to determine the above results, it was observed that the middle trace (trace B) had a slightly lower current rating compared to the other two traces on either side (trace A and C), up to an i_{TT} value of 11 mm when T_t = 0.1 mm and up to a value of 14 mm when T_t = 0.37 mm. A further increase in i_{TT} caused the ratings of trace A and C to become smaller than the current rating of trace B. These results are shown in figure 4.11.

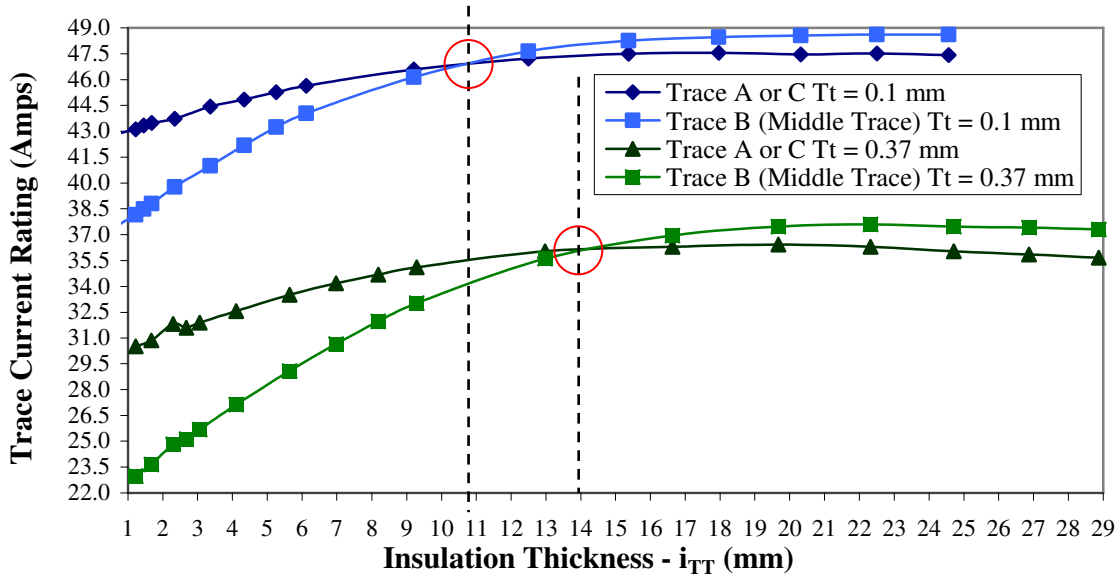

Figure 4.11: Plot of current ratings against PCB trace to trace insulation thickness for different λ factors i.e. different PCB dimensions and for T_t=0.1 mm and T_t=0.37mm. Altitude de-rating taken into account

In each case (T_t = 0.1 mm and T_t = 0.37 mm), for the specified range of i_{TT}, the smallest current rating value was chosen to calculate the power rating as it will be shown later on. FEA simulations results are also shown below in figure 4.12 to illustrate how the heat flux (heat flow per unit area), changes with an increase in the λ factor and thus an increase in i_{TT}. As the traces become further apart and i_{TB} decreases, the effective heat dissipation area (perpendicular to the direction of heat flow), increases for the middle trace much faster than for the other two traces. Note that the PCB conductor traces in figure 4.12 above, all have the same size. The diagrams are not in scale.

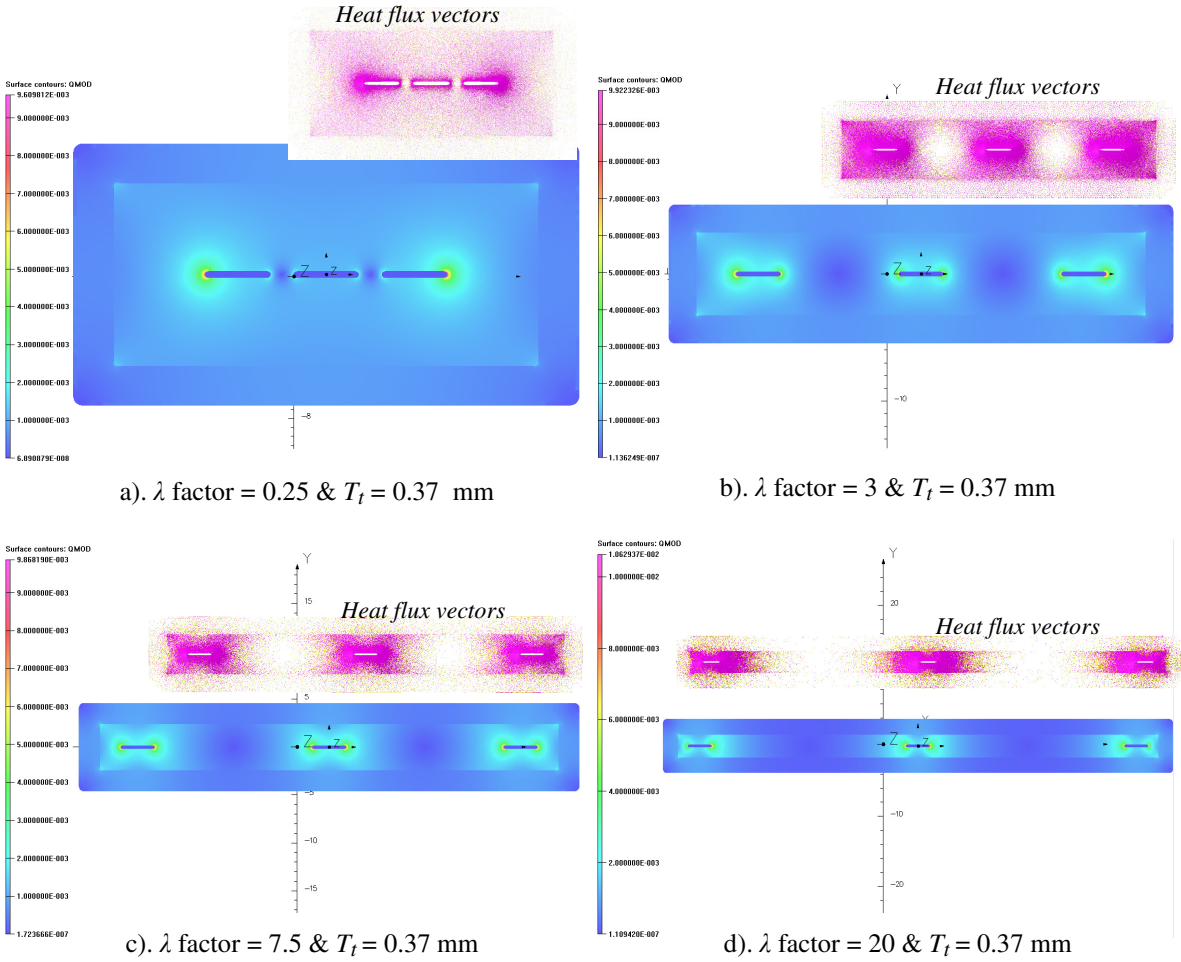

a). λ factor = 0.25 & T_t = 0.37 mm

b). λ factor = 3 & T_t = 0.37 mm

c). λ factor = 7.5 & T_t = 0.37 mm

d). λ factor = 20 & T_t = 0.37 mm

Figure 4.12: Illustration of how the heat flow changes as the λ factor and thus i_{TT} increase, using "Opera Vector Fields" FEA models for T_t = 0.37 mm.

The equation of heat conduction based on Fourier's Law states that $\Delta\theta = T_{Total} \times W$ [58]. '$\Delta\theta$' is the temperature difference between the operating temperatures of the conductor to the ambient temperature on the duct. 'T_{Total}' is the total thermal resistance which consists of the thermal resistance of the insulation plus the thermal resistance of the air. 'W' is the power being dissipated from the conductor per unit length. If $\Delta\theta$ is constant and the thermal resistance decreases due to the PCB dimensions changing (increase in the effective heat dissipation area), the power dissipation and thus the maximum allowable current through the conductor trace will increase.

Looking at the case where T_t = 0.37 mm, when i_{TT} increases from 1.22 mm to 14 mm, a change in the insulation thermal resistance causes a significant change in the total thermal resistance ($T_{R\_Insulation} + T_{R\_Air}$). However for 14 mm < i_{TT} < 29 mm, the total

thermal resistance is governed by the air thermal resistance and this remains fairly constant within this range of i_{TT}. Thus a further increase in i_{TT} will not result in an increase in the current rating.

4.2.3 PCB Voltage Optimisation

Based on Figure 4.9, taking the case of an AWG 16 sized conductor as an example, it would seem that by using a PCB with an λ factor = 2 and T_t = 0.10 mm, would result in maximum power transfer. However to determine whether this would be the case, the voltage ratings had to be computed. As it will be shown later on, an optimum insulation thickness between the PCB traces and between the traces and the surrounding duct exists, which results in a maximum voltage rating.

4.2.3.1 Determination of the most critical PD locations in the PCB model

As mentioned in Section 4.1.1.2, the voltage ratings are going to be computed taking into consideration the partial discharge inception voltages (PDIVs), for the different types of partial discharge (PD) that can occur in the PCB. These are shown below in Figure 4.13.

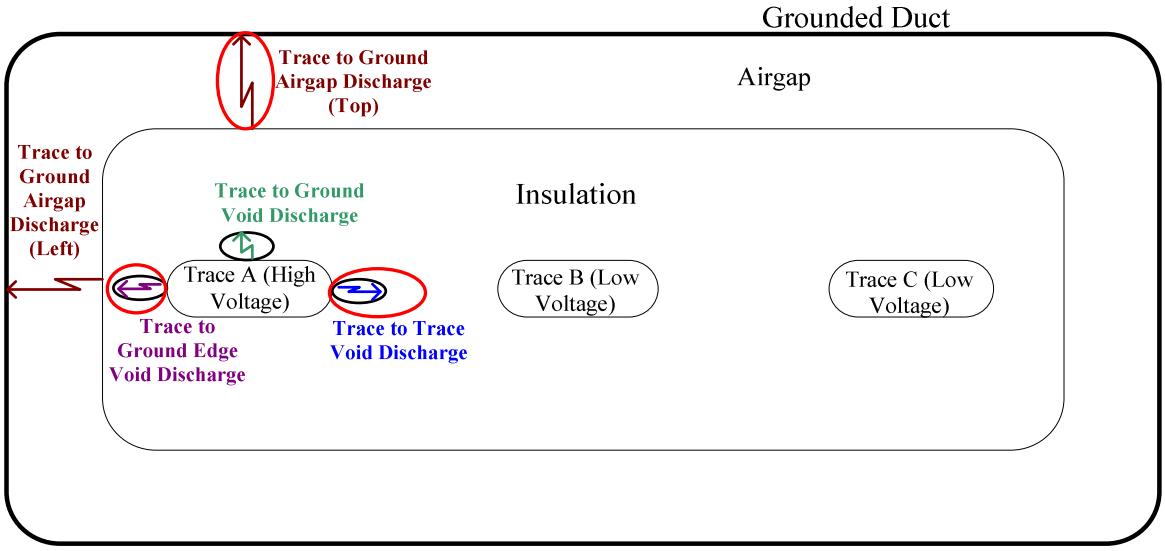

Figure 4.13: Possible types and locations of partial discharges in the PCB model

After performing initial FEA electric field simulations, it was observed that at the location where *'Trace to Ground Airgap Discharges (Top)'* could occur, a higher electric field was present than at the location where *'Trace to Ground Airgap Discharges (Left)'* could occur (look at Figure 4.13). This can be explained by the fact that the electric field concentrates at sharp points or edges. Thus at the conductor trace edges the field is the highest, resulting in a higher voltage across the insulation than across the airgap. On the other hand, the electric field through the insulation and through the airgap at the top is nearly uniform and the electric field in the airgap at the top is higher than in the insulation. This is due to the lower relative permittivity of the air. In addition, the *'Trace to Ground Void Discharge'* will always occur at higher operating voltages than the *'Trace to Ground Edge Void Discharge'*.

Thus in determining the voltage rating for the PCB trace conductors, only PD occurring in the void between traces, in the void between trace-edge and ground and in the airgap at the top of the PCB were examined. These types of discharges are abbreviated as *TTVoid*, *TGVoid* and *TGAirgap* respectively and are marked with a red circle in Figure 4.13 above. Figure 4.14 shows the electric field distribution of a PCB model to support the above statements that mention which partial discharge locations are the most critical and which are going to be examined in this chapter.

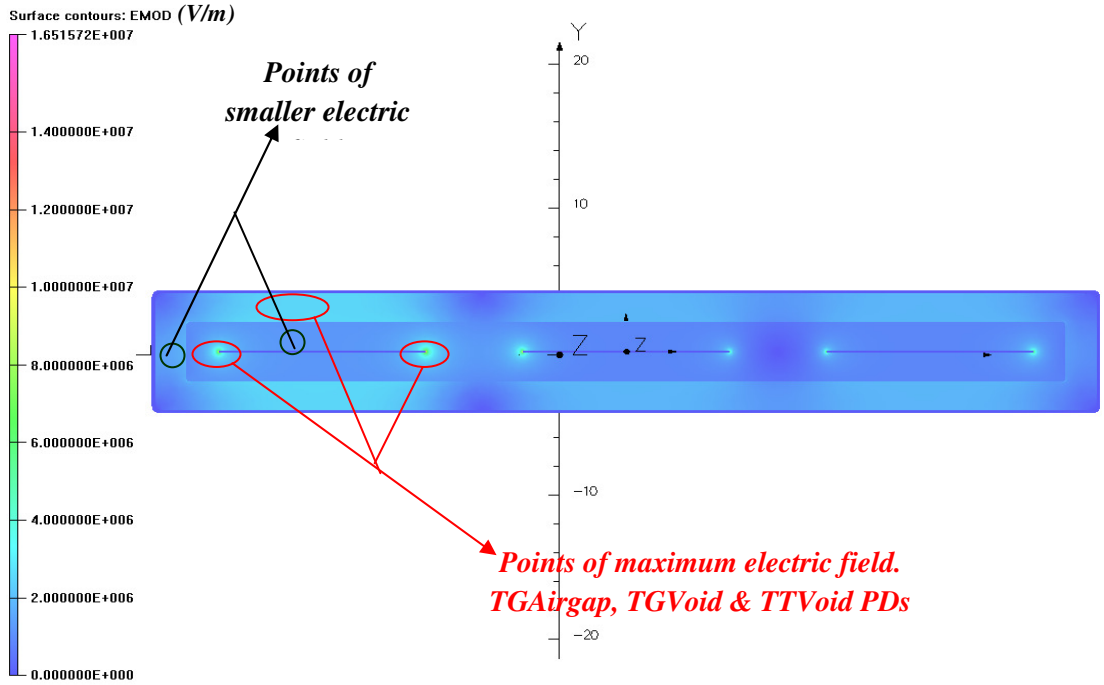

Figure 4.14: Electric field distribution in PCB model to show the most critical PD locations

However, it is important to note that PD at different locations can only be used to determine the voltage rating of a system, if the breakdown voltage of the insulation is higher than the partial discharge inception voltage (PDIV). In this PCB power rating assessment, the breakdown voltage of the PCB insulation is assumed to be much higher.

4.2.3.2 Geometric factors affecting the optimal voltage rating

Theoretically the higher the value of λ, the greater would be the inception voltage when considering a void in the insulation between traces *'TTVoid'*, since i_{TT} would also greater (look at Figure 4.15b). On the other hand i_{TB} would be smaller resulting in lower inception voltages for the trace to ground airgap discharge *'TGAirgap'* and for the trace to ground void discharge *'TGVoid'*. In any case the voltage rating would be limited by the lowest inception voltage and thus an optimum insulation thickness i_{TT} must be established and thus an optimum i_{TB}. Figure 4.15 is used to illustrate the optimisation procedure carried out in order to achieve a maximum voltage rating. If the operating system is a three phase system, then ideally the partial discharge inception voltage between traces divided by $\sqrt{3}$, *'*$Vi_{TT}/\sqrt{3}$*'*, should be equal to inception voltage between traces and ground *'*Vi_{TB}*'*. If $Vi_{TT}/\sqrt{3}$

> Vi_{TB} then a smaller λ factor should be used so that i_{TT} is decreased and i_{TB} is increased. If $Vi_{TT}/\sqrt{3} < Vi_{TB}$, then a bigger λ factor should be used to increase i_{TT} and decrease i_{TB}.

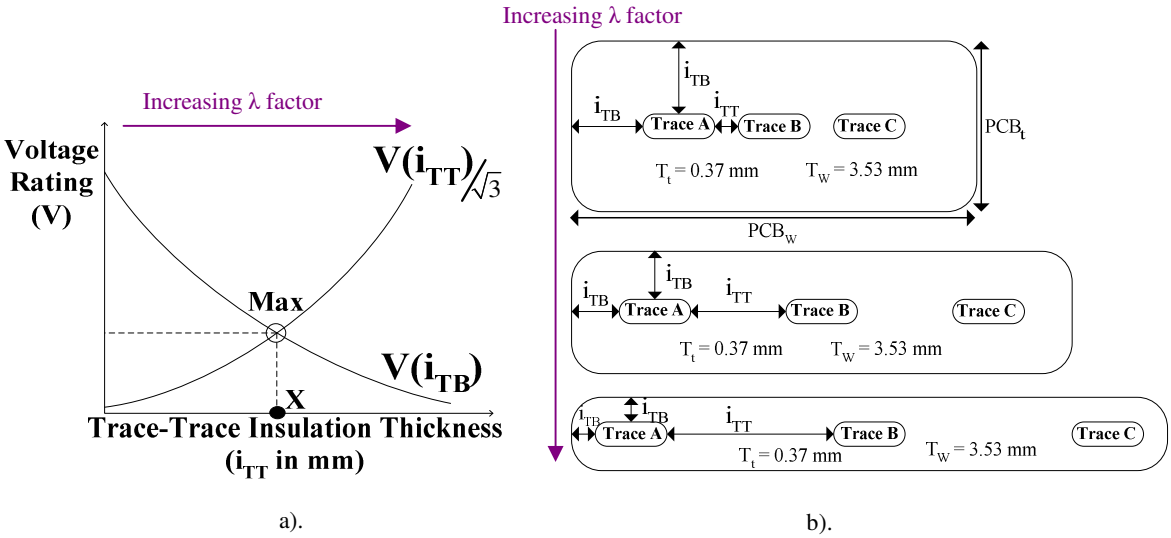

a). b).

Figure 4.15: Effect of the λ factor on the voltage rating of the PCB conductor traces

It has to be mentioned here that the graph on figure 4.15a should include one more curve, representing the inception voltage based on an insulation void discharge between the trace and the ground. This is not shown here, since the aim of this section is to point out in simple terms the fact that by changing the PCB geometric parameters, the discharge type (*TTVoid or TGAirgap or TGVoid)* that results in a lower PDIV changes as well. Looking at figure 4.15a, going from left to right up to point **X,** the lowest inception voltage is the one determined by a *TTVoid* discharge and this is used as the PCB's trace voltage rating. Beyond point **X,** the lowest inception voltage is determined by a *TGAirgap* discharge and this is the voltage that is used this time, as the trace voltage rating.

4.2.3.3 Calculation of the voltage rating using uniform field models

To begin with, uniform field approximations were used to calculate the voltage rating based on partial discharge inception voltages, by carrying out the same procedure as the cable duct system in chapter 3, based on [12]. However, to compute the void partial discharge inception voltage for each PCB model, uniform models were used instead of non

uniform ones (like the coaxial cable electric field model that was used previously). This was due to the difference in the geometry of the system. These equations are shown in Figure 4.16 together with an illustration of the direction of the electric field lines in the PCB, as it is approximated by the uniform models.

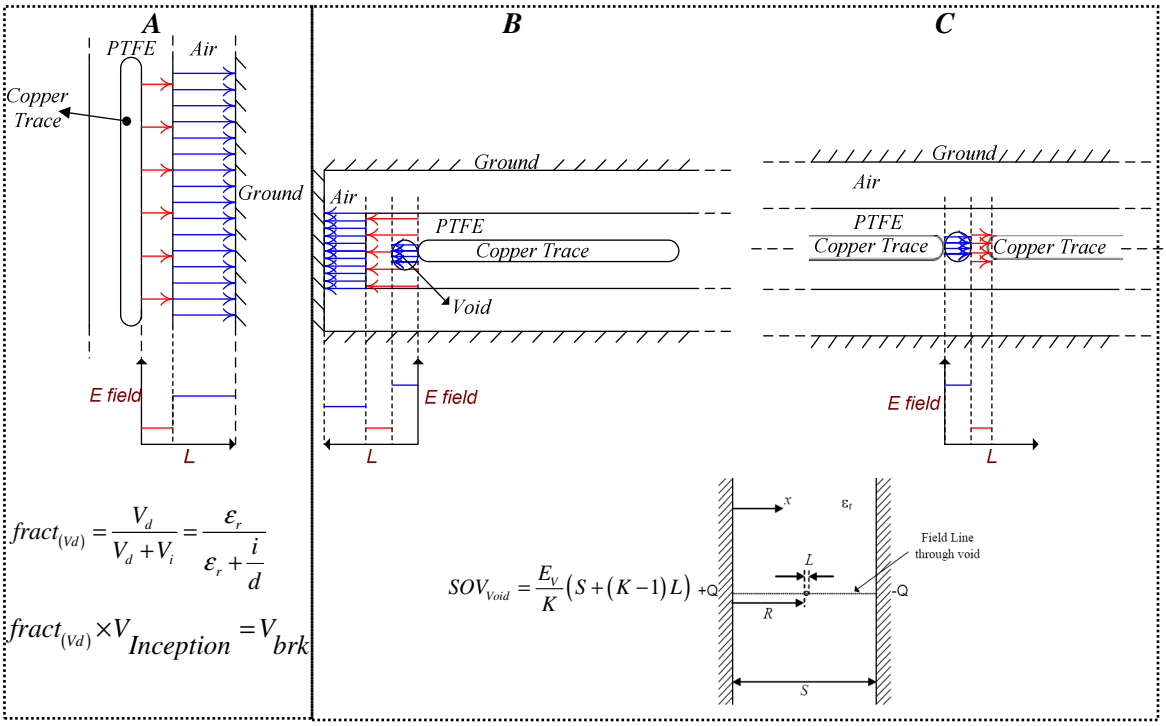

Figure 4.16: Electric field equation models used for the PCB voltage rating calculation

SOV_{Void} = Trace to trace or trace to ground void discharge inception voltage (kV)

E_V = Electric field causing breakdown as from Paschen's Law data (kV/mm)

S = Insulation thickness i_{TB} or i_{TT} (mm)

K = electric field enhancement factor (in this case K = ε_r =2.1)

L = Void size (mm) (It has to be noted that a fixed void size of 80 microns having a disc shape was used in this analysis)

Model **A,** which is shown in Figure 4.16, is used for calculating the inception voltage based on airgap discharges. The fraction of the voltage across the airgap *'$fract_{(Vd)}$'*, is obtained for every insulation thickness and for a range of airgap distances. Then, by

using Paschen's Law the discharge inception voltage is calculated by simply dividing *'fract$_{(Vd)}$'* from the air breakdown voltage *'V_{brk}'* of the airgap between the insulation and the duct. Models **B** and **C** are used for calculating the inception voltage based on void discharges occurring between traces and between the trace and the ground. The same equation is used for the two types of void discharges. However the insulation thickness used in each case, differs according to the PCB dimensions. The discharges at the three locations are abbreviated as *'TGAirgap'*, *'TGVoid'* and *'TTVoid'* as described in Section 4.2.3.1. As it is shown in Figure 4.16, the electric field in the void and in the air gap is higher than in the insulation, due to the lower electrical permittivity of the air compared to the insulation. Voltage rating results for the three types of discharge are shown in Figure 4.17, for $T_t = 0.1$ mm and $T_t = 0.37$ mm, for $0.25 \leq \lambda \leq 20$.

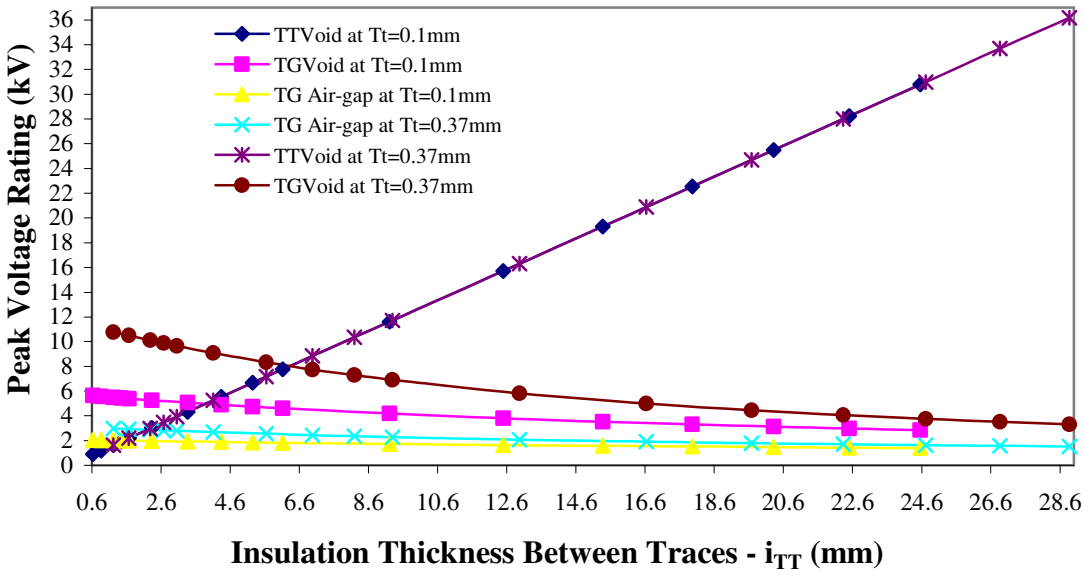

Figure 4.17: Plot of the peak single phase voltage rating, for different I_{TT}, using uniform field calculations for three types of partial discharges*: TGAirgap*, *TGVoid* and *TTVoid*

Observe how the voltage ratings are higher when the trace conductor is thicker due to the thicker insulation between traces and due to the thicker insulation between the trace and the ground. It must be noted that the peak voltage rating increases for the TTVoid case since the insulation between the traces *'i_{TT}'* increases. However for a fixed cross sectional area the increase in i_{TT} causes a decrease in the insulation thickness between the traces and the ground *'i_{TB}'*. As a result the voltage ratings for *TGVoid* and *TGAirgap* decrease.

4.2.3.4 FEA analysis: Electric field enhancement due to flat conductor geometry

After calculating the PDIV for the two types of void discharges (*TTVoid* and *TGVoid*) and for the airgap discharge (*TGAirgap*), for different λ factors and for T_t = 0.1 mm and 0.37 mm, these voltages were used as a boundary condition, each in turn on the PCB models on the conductors traces, to evaluate the electric field at the most critical points. Since the analysis carried out was for a three phase system model, the voltage on each conductor trace included a certain phase shift. Thus, it has to be clarified at this point, how the boundary conditions for all three conductors were determined for each case.

For example, once the inception voltage was calculated for a *TGAirgap* discharge, this voltage represented the peak single phase voltage (SOV_{peak}) and was set as a boundary condition for trace A on the PCB model (look at Figure 4.15). For trace B and trace C, the voltage boundary conditions were calculated based on a three phase system model. Therefore for trace B, the voltage boundary condition was calculated using *'SOV_{peak} x sin (90+120)'* and for trace C, the voltage boundary condition was calculated using *'SOV_{peak} x sin (90+240)'*. The same calculations were carried out for a *TGVoid* discharge.

The inception voltage calculated for a *TTVoid* discharge, represented the phase to phase voltage. Therefore this voltage was divided by $\sqrt{3}$ (to obtain the single phase voltage) and then entered as a boundary condition on trace A. The boundary condition on trace B was set at a voltage, so that the difference between the two traces was equal to the calculated trace to trace voltage.

FEA simulations were performed and the maximum electric field at the trace edges and in the air gap were compared with the calculated electric field giving the respective $SOV_{TGAirgap}$, SOV_{TGVoid} and SOV_{TTVoid} (which were used as boundary conditions). These calculated voltages were then adjusted accordingly using a correction factor *'CF'* (ratio of FEA simulated maximum electric field *'SMEF'*, to calculated electric field *'CEF'*). By using the uniform field equations and obtaining *CF*, it was possible to obtain an approximate trend of how *CF* varies with different PCB dimensions (different λ, T_w and T_t factors).

Figure 4.18 illustrates the points where the maximum electric field occurs in the PCB and that are used to compute *CF* for each case. The parameters for this simulation shown below are as follows: *trace size AWG 16*, T_t *= 0.10 mm,* T_W *= 13.07 mm,* λ *= 3,* i_{TB} *= 2.04 mm and* i_{TT} *= 6.12 mm.*

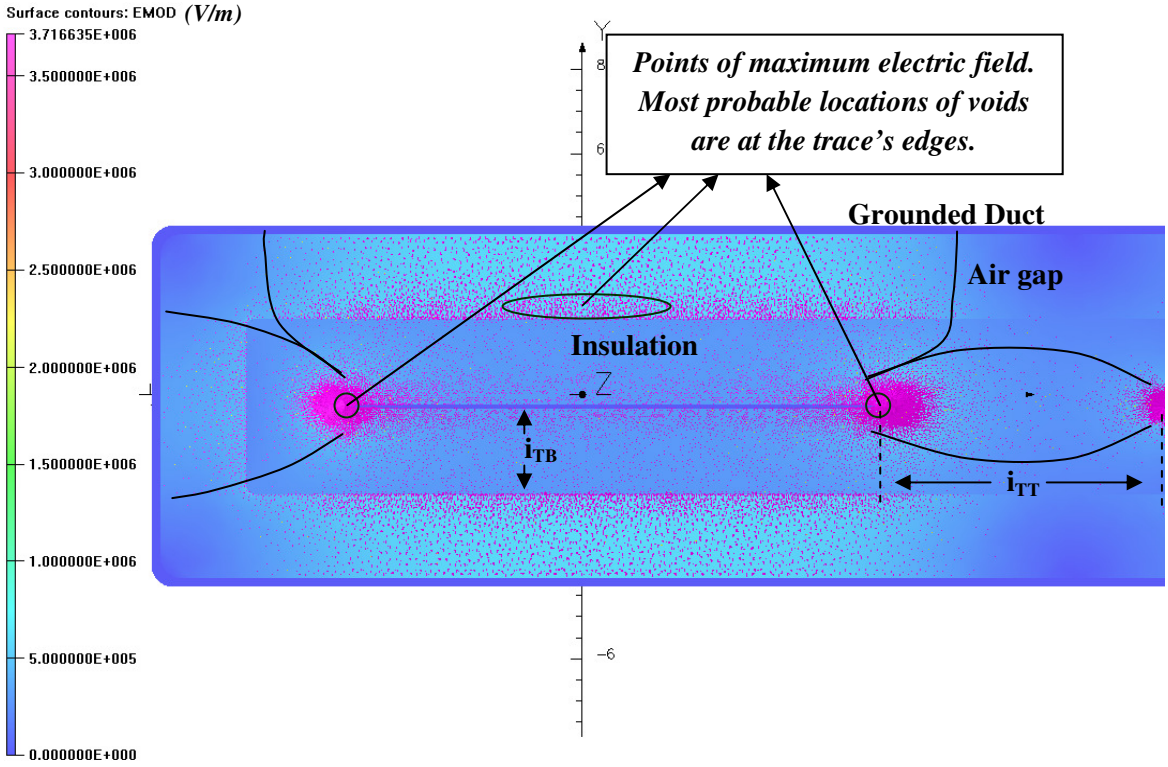

Figure 4.18: Electric field distribution with vectors in PCB to illustrate points of maximum electric stress

Figures 4.19 and 4.20 display the CF curves which were obtained using FEA for T_t = 0.1 mm and 0.37 mm for $0.25 \leq \lambda \leq 20$.

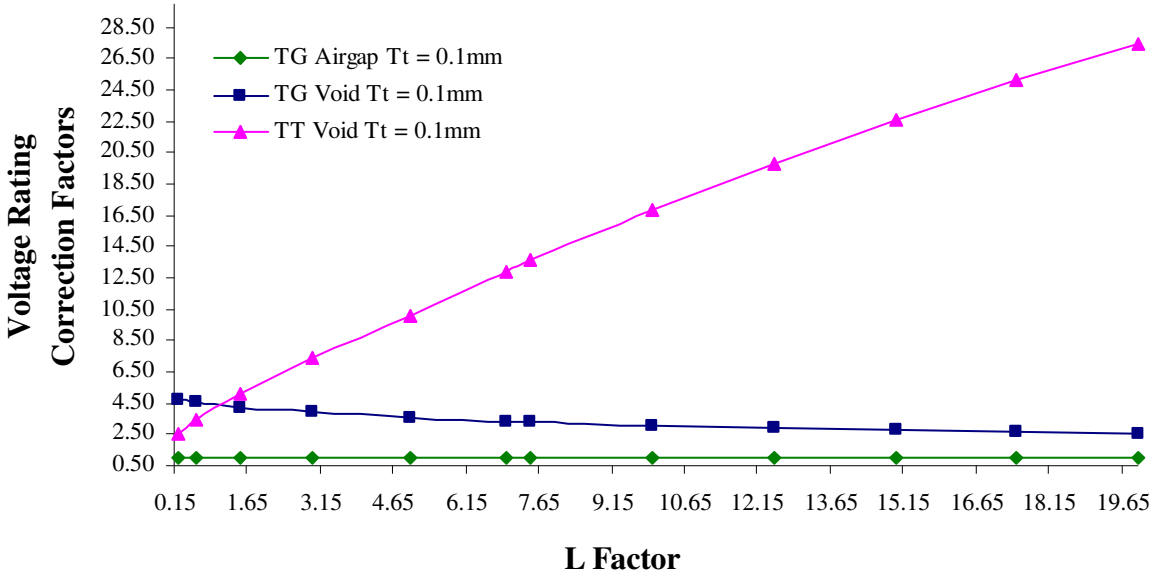

Figure 4.19: Plot of the voltage rating correction factors for more *L (=λ)* factors, for three types of partial discharges, for *TGAirgap*, *TGVoid* and *TTVoid*, when T_t = 0.1 mm.

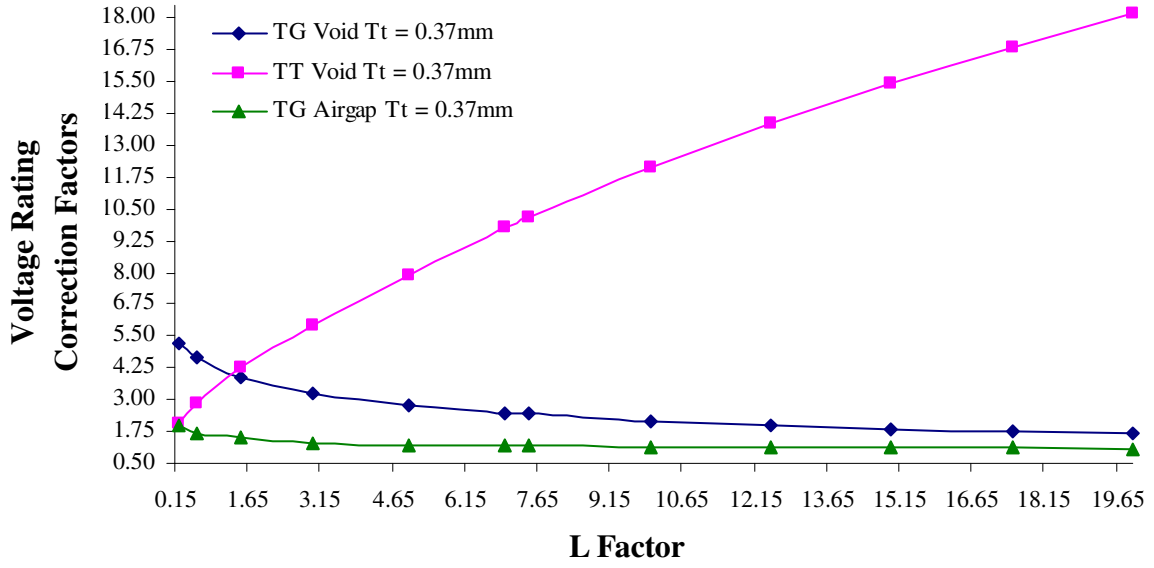

Figure 4.20: Plot of the voltage rating correction factors for more *L (=λ)* factors, for three types of partial discharges, for *TGAirgap*, *TGVoid* and *TTVoid*, when T_t = 0.37 mm.

It has to be noted that for each conductor trace and width, the edges were designed so that the edge surfaces were as smooth as possible, each having a blending radius equal to half

of the trace thickness. It is worth mentioning that up to $\lambda = 0.6$, *CF* is larger for the thicker trace for the *TGVoid* curve.

4.2.3.5 Voltage derating due to electric field enhancement

Voltage ratings are shown below in Figures 4.21 and 4.22. The correction factors '*CF*' for *TGVoid* and *TTVoid*, were divided from the voltage ratings calculated from the uniform field equations, whereas *CF* for *TGAirgap* were multiplied. This is because the calculated airgap PDIVs were providing conservative results. The green *TGAirgap* curves shown on figures 4.19 and 4.20, are actually the ratio of calculated electric field 'CEF' to the simulated electric field 'SMEF', as opposed to the other curves where *CF* = *SMEF/CEF*.

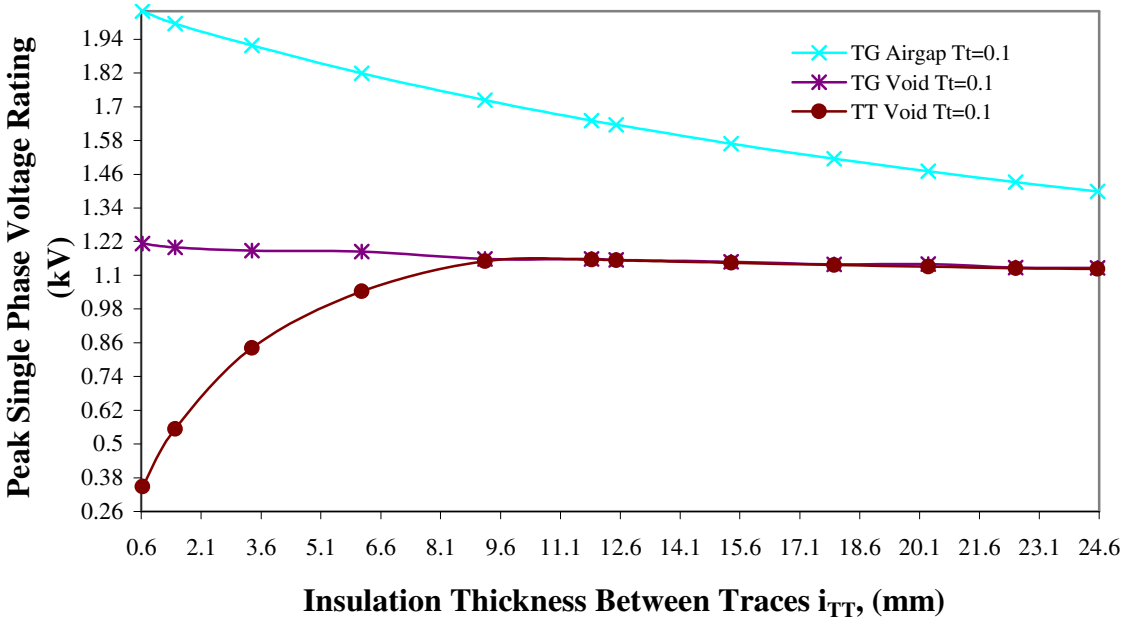

Figure 4.21: Plot of the peak single phase voltage rating for different λ factors i.e. for *TGAirgap*, *TGVoid* and *TTVoid* when $T_t = 0.1$ mm.

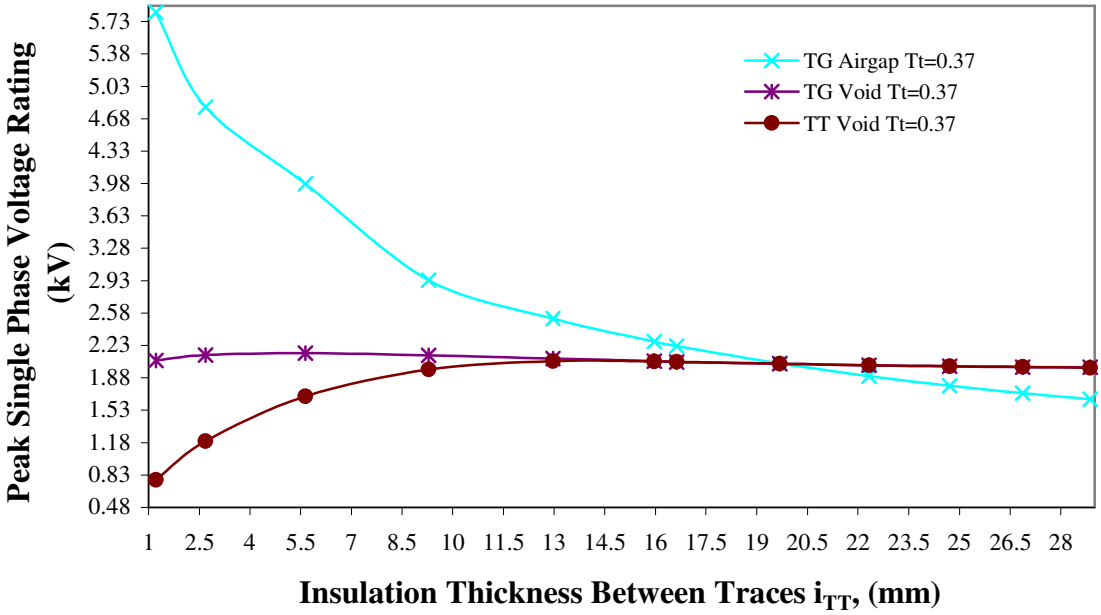

Figure 4.22: Plot of the peak single phase voltage rating for different λ factors i.e. for *TGAirgap*, *TGVoid* and *TTVoid* when T_t = 0.37 mm.

From the *TTVoid* and the *TGVoid* curves shown in Figures 4.21 and 4.22, it is obvious that the voltage ratings have a certain maximum point after which they remain fairly constant. The two curves merge when i_{TT} = 13 mm for T_t = 0.1 mm (Figure 4.21) and when i_{TT} = 9.2 mm for T_t = 0.37 mm (Figure 4.22). This can be explained by looking at the uniform field equations and the PCB geometry. The equations model the problem by looking at it in one dimension. The greater the insulation thickness, the bigger is the voltage rating based on void discharges for a fixed void size within the insulation, either at the edge or between the traces. This voltage rating is only dependent on insulation thickness, void size and shape. However the *CF* for *TTVoid*, increases faster as λ increases, causing the voltage ratings to reach a maximum. As the λ factor increases and thus i_{TT} increases, i_{TB} decreases while T_t is constant. Thus, at a certain value of λ, the distance between trace A and the duct becomes smaller than the distance between the traces. As a result the trace to trace electric field lines change direction and head for the grounded duct instead of the middle trace B (look at Figure 4.23).

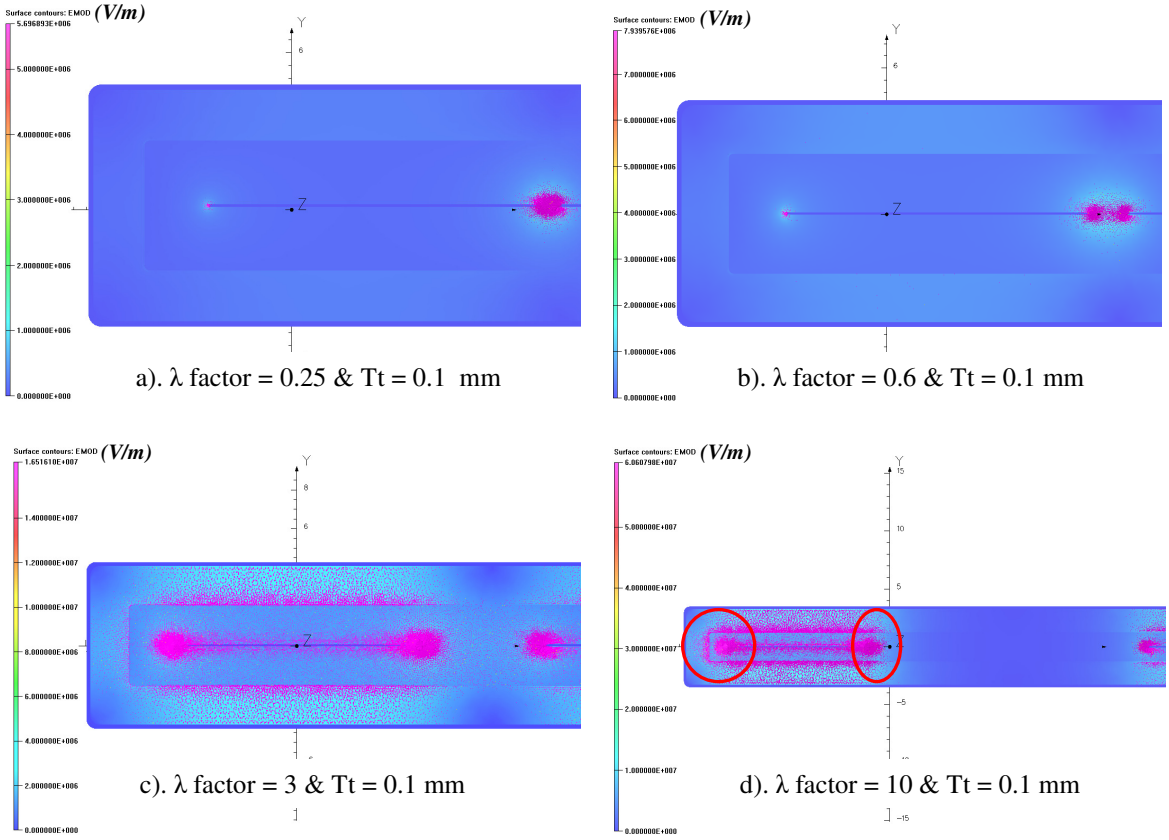

Figure 4.23: Illustration of how the electric field distribution changes as the λ factor and thus i_{TT} increase, using "Opera Vector Fields" FEA models.

It must also be mentioned that the rearrangement of the electric field lines does not only depend on the physical distances between traces and between trace and ground, but also depends on the potential difference (trace to trace and trace to the grounded duct). Looking at Figure 4.22 when T_t = 0.37 mm from a trace to trace thickness i_{TT} of 1.2 mm up to 19.7 mm, the voltage rating is limited by the trace to trace partial discharges whereas from thicknesses greater than 19.7 mm up to approximately 28.9 mm, the airgap discharges limit the voltage rating (SOV). The point where the two lines meet, *TTVoid* and *TGVoid* curves, is the optimal point as far as the voltage rating is concerned. As mentioned before, the curves meet since the electric field lines from trace to trace move towards the top and bottom of the PCB and the actual insulation thickness between the two edges and the ground is the same. The voltage across the two traces is no longer an issue, and the voltage across the two edges of trace A to the ground becomes the most critical as far as void discharges are concerned (look at Figure 4.23d above).

4.2.3.6 PCB and round cable system: Electric field comparison

Compared to the three round cable system installed in a duct, the electric field vectors in the air gap at the top and bottom of the PCB insulation follow a uniform pattern (look at Figure 4.24). This is the reason why for the PCB case, the voltage rating calculation results are more in agreement with FEA simulation results than in the round cable case. In the round cable case, there is a high field concentration all around the cable conductor. Thus the uniform field calculation results overestimate the voltage across the gaps between cables and between cables and the surrounding duct, resulting in lower voltage ratings (i.e. more conservative results). Note that the magnitudes of the maximum electric field for the two cases shown in the figure below are not the same, because the voltage boundary conditions around the conductors are different. The aim here is to show the difference in the electric field concentration at different locations in the airgaps around the insulation.

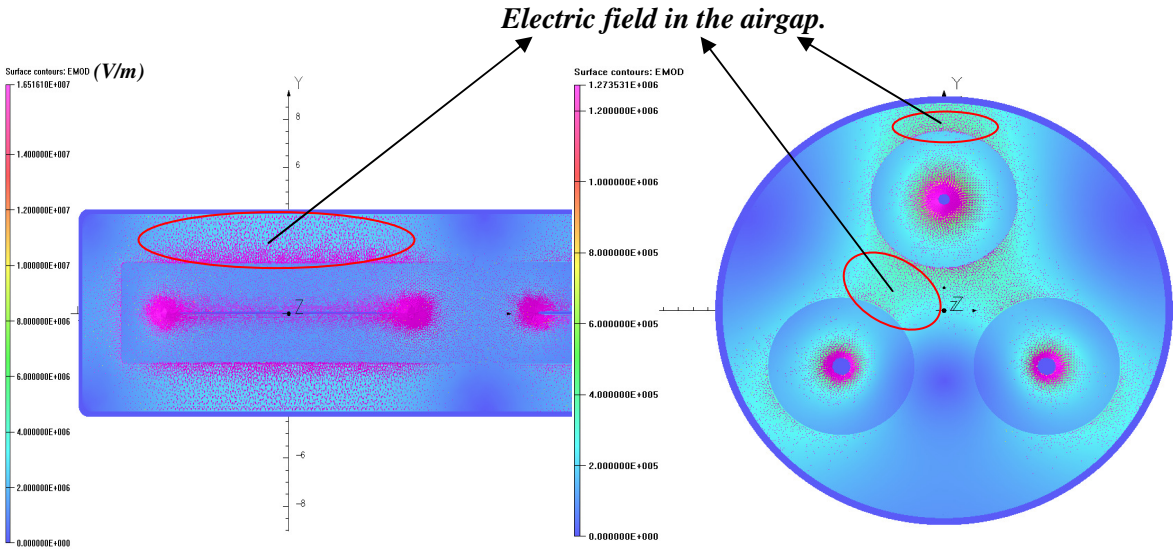

Figure 4.24: PCB and round cable duct systems: electric field comparison in the airgaps

However, as the conductor trace becomes thicker and less wide (bigger T_t and smaller T_W), the electric field becomes more and more non uniform and resembles that of a round cable (look at Figure 4.25). This phenomenon also explains why the *CF* for the *TGAirgap* case is equal to one, when the trace thickness *'T_t'* is 13.07 mm and larger than one, when T_t = 0.37 mm (look at Figures 4.19 and 4.20).

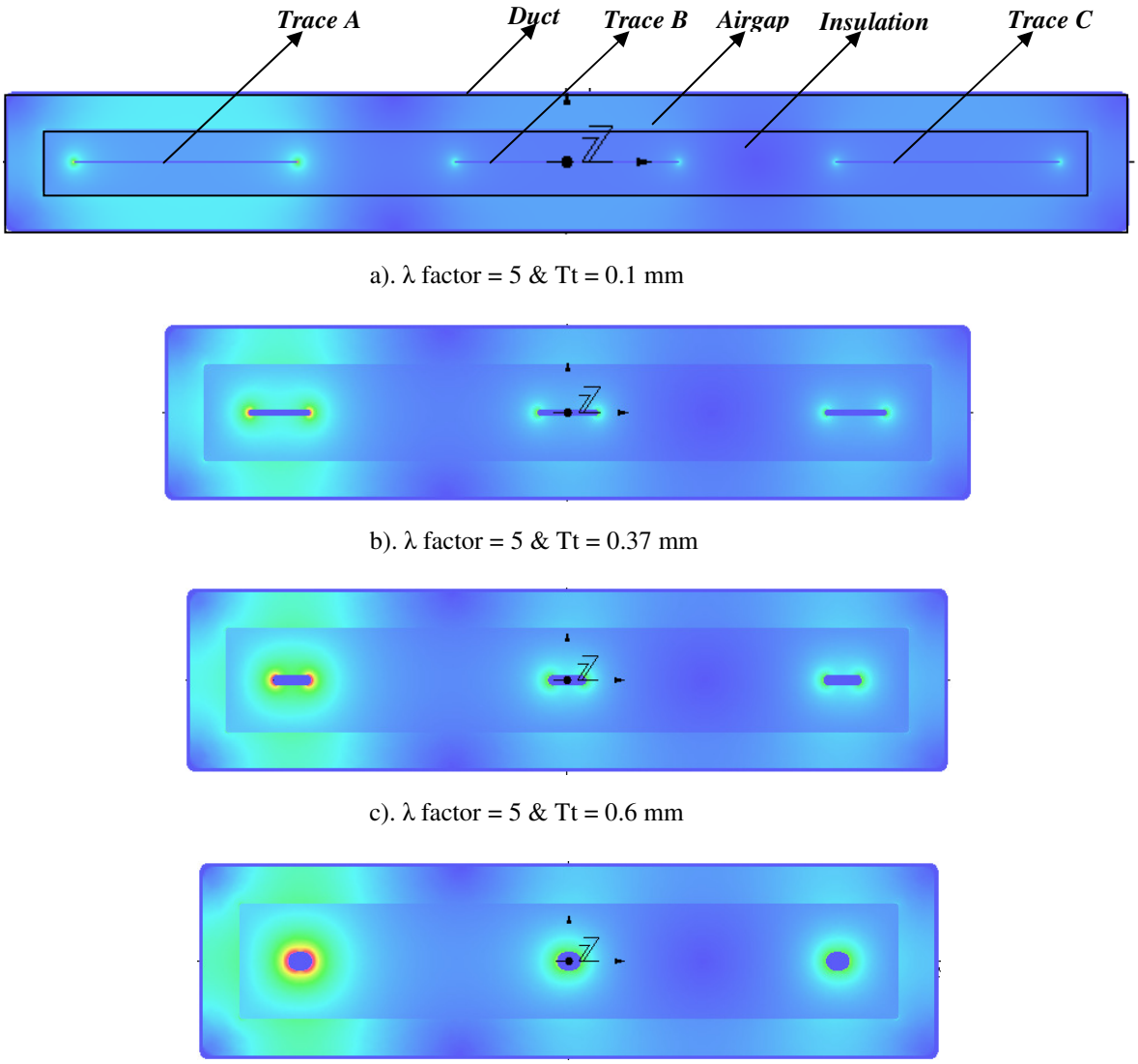

a). λ factor = 5 & Tt = 0.1 mm

b). λ factor = 5 & Tt = 0.37 mm

c). λ factor = 5 & Tt = 0.6 mm

d). λ factor = 5 & Tt = 1.0 mm

Figure 4.25: Illustration of the effect of increasing the conductor trace thickness for a fixed PCB & trace cross sectional area on the electric field distribution

4.3 Calculation of PCB Power Rating

As discussed in the previous section, finding the maximum voltage rating depends on evaluating the optimum insulation thickness between the traces and between traces and the ground. However it must be emphasized that this maximum voltage it is not necessarily the optimum voltage. The PCB optimum voltage will be the voltage that will result in

maximum power transfer. This also depends on the current rating. It might be the case that voltages lower than the maximum shown in Figure 4.15a, will result in much higher current ratings due to the PCB geometry. Figure 4.26 illustrates the PCB system optimisation which summarizes the work that has been described so far. The optimisation is based on an examination of different PCB geometries for which the voltage and the current rating is determined. For a better understanding of the methodology shown below, refer to Figures 4.27a and 4.27b.

4.3.1 Calculation Methodology

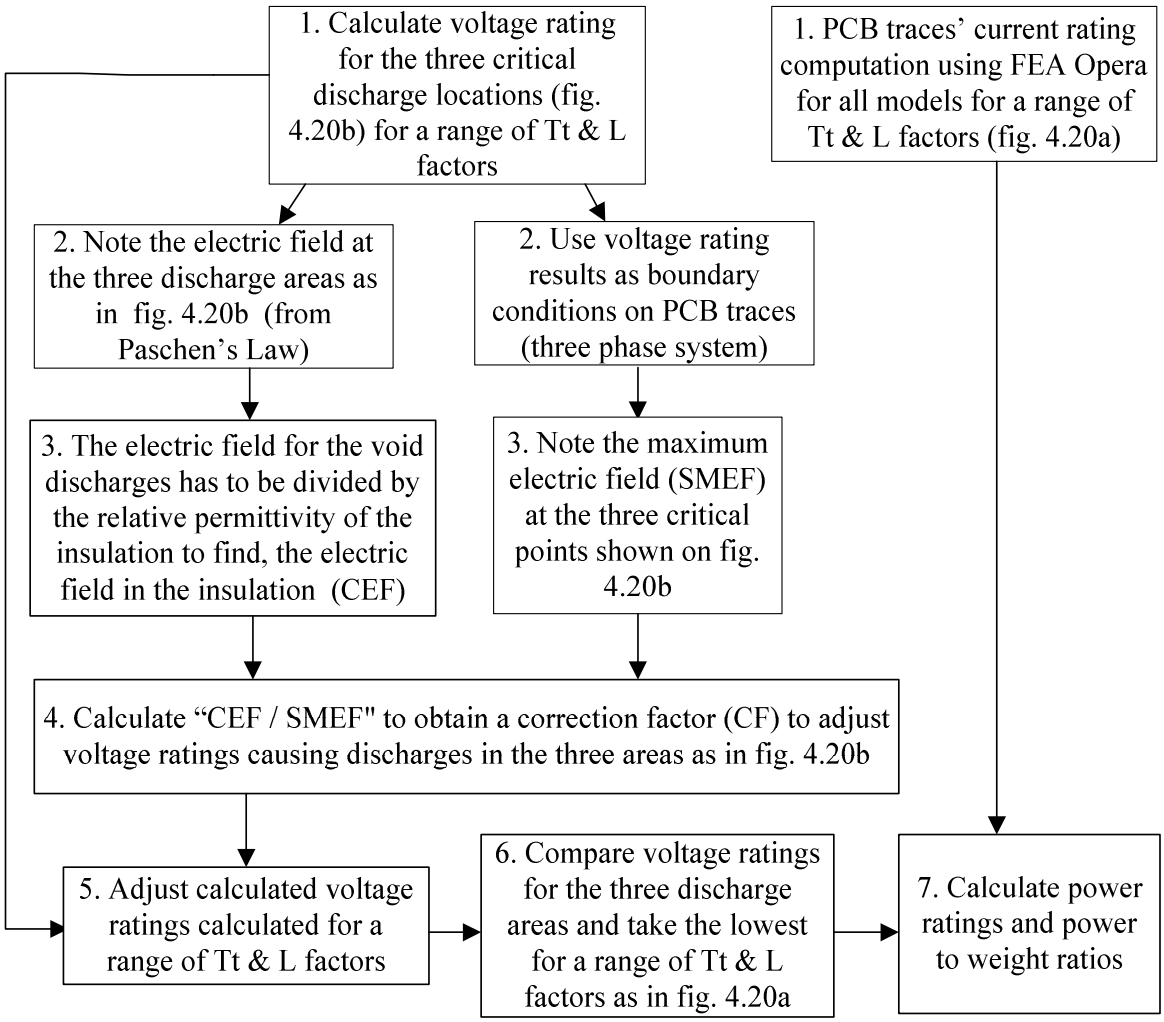

Figure 4.26: PCB maximum power transfer calculation methodology

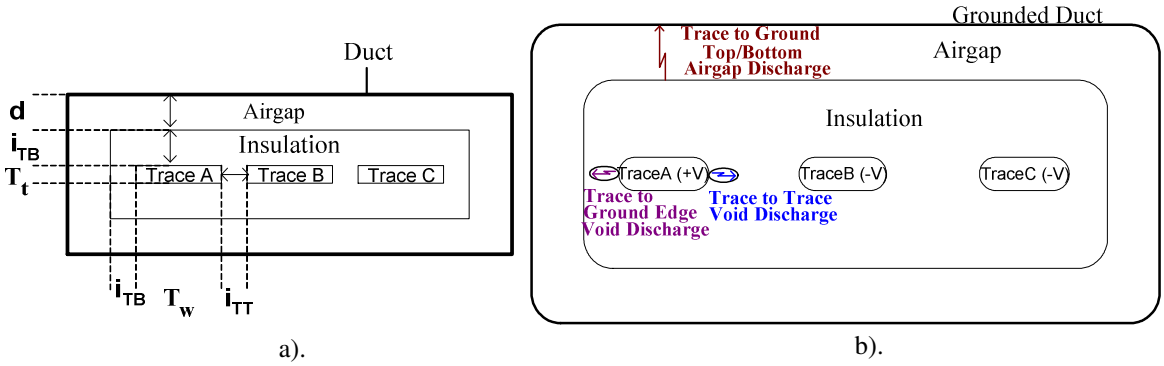

Figure 4.27: a) PCB model with dimensional parameters and b) PCB model showing the most critical PD locations

4.3.2 Max Power Transfer and Power to Weight Ratio Results

It has to be noted that in Figure 4.21, which is a plot of the voltage ratings against insulation thickness i_{TT}, the airgap discharge voltage rating curve and the other two curves do not meet. Investigating higher values of λ was not required since at an i_{TT} of approximately 12.6 mm, the voltage ratings and the current ratings reach their maximum value. Beyond this maximum point an increase in i_{TT} would only lead to a decrease in maximum power transfer and thus in the power to weight ratio.

By looking at Figures 4.28 and 4.29, a higher power rating would be achieved by not taking into account the maximum voltage rating (where curves meet, Figure 4.22), but by considering the relative current increase with respect to i_{TT}. If an i_{TT} of 15.96 mm ($L = \lambda = 7$ and $i_{TB} = 2.28$ mm) is used, the maximum three phase RMS power that can transferred is approximately 177.13 kVA (3 x 59 kVA) when the trace thickness 'T_t' = 0.37 mm.

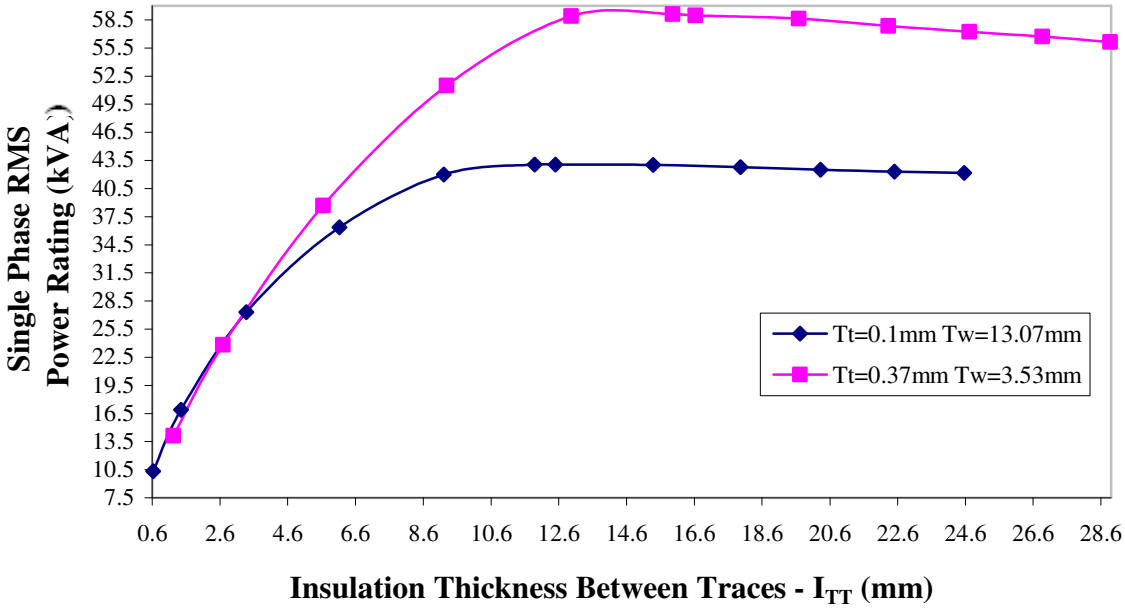

Figure 4.28: Plot of the single phase RMS power rating against PCB trace to trace insulation thickness, for $0.25 \leq \lambda \leq 20$ and for T_t=0.1 mm and T_t=0.37mm

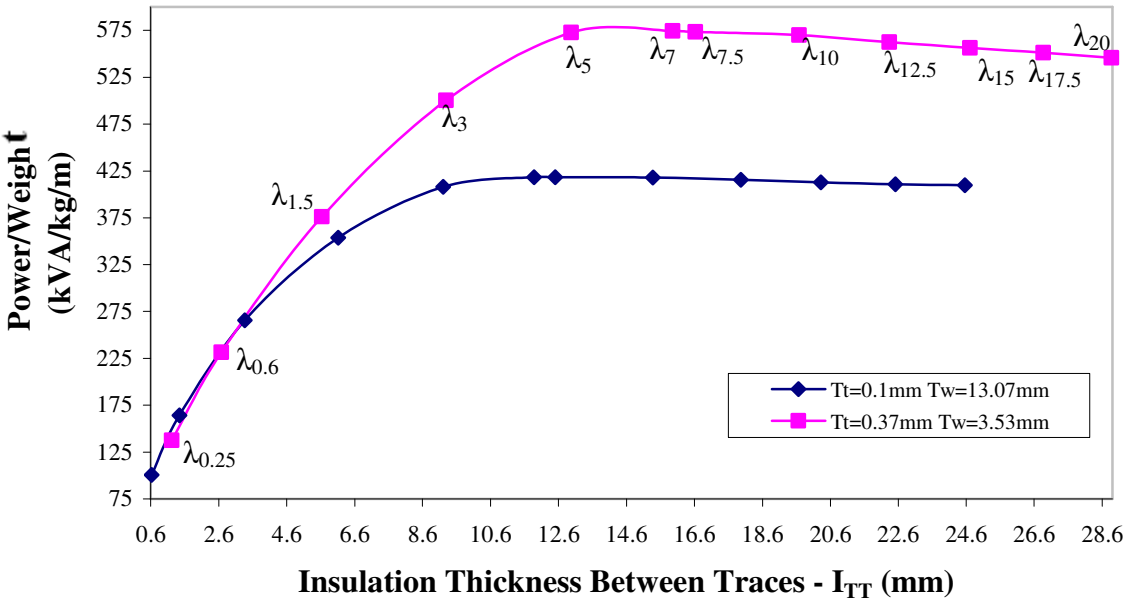

Figure 4.29: Plot of the 3-phase RMS power to weight ratio against PCB trace to trace insulation thickness for $0.25 \leq \lambda \leq 20$ and for T_t=0.1 mm and T_t=0.37mm

The maximum three phase RMS power to weight ratio that can be achieved based on the results above is 575 kVA/(kg/m). That is for a 15 m aircraft wing, the total power/weight ratio of the PCB system is 38.10 kVA/kg.

4.4 PCB and Cable Power Rating Comparison

The aim of performing the calculations and the FEA simulations in the previous section was to establish whether a PCB can replace a round conductor cable system (installed in a duct and consisting of identical conductor sizes), having the same weight. Consequently if more power can be transferred by using PCBs, then higher power to weight ratios can be achieved and thus PCBs can provide a better solution as a means of distributing power around the aircraft. In addition it might be the case that larger round conductor cable systems can also be replaced by a PCB harness consisting of smaller conductors.

4.4.1 FEA Analysis for the Round Cable System

It has been mentioned previously that the voltage rating calculations using uniform models for the round cable systems in Chapter 3, provided quite conservative results. Furthermore it might be the case that the maximum power that can be transferred through the round cable systems was underestimated. Thus before comparing the round cable and PCB systems, FEA was used in the same way as for the PCB models, to correct the voltage ratings for the three phase round cable systems having different conductor sizes.

4.4.1.1 Evaluation of most critical PD locations in the round cable model

For correcting the voltage ratings, the electric field at the three most critical locations, (on the surface of the conductors for void discharges, in the airgap for discharges between cable and ground and between cable to cable), was obtained using FEA and then compared with the calculated one. The three most critical locations where the electric field is the highest for the round cable system in the duct, are marked on Figure 4.30. In this case example, the voltage on the top conductor is 2.5 kV and the voltage on the two bottom ones is -1.25 kV based on a three phase system.

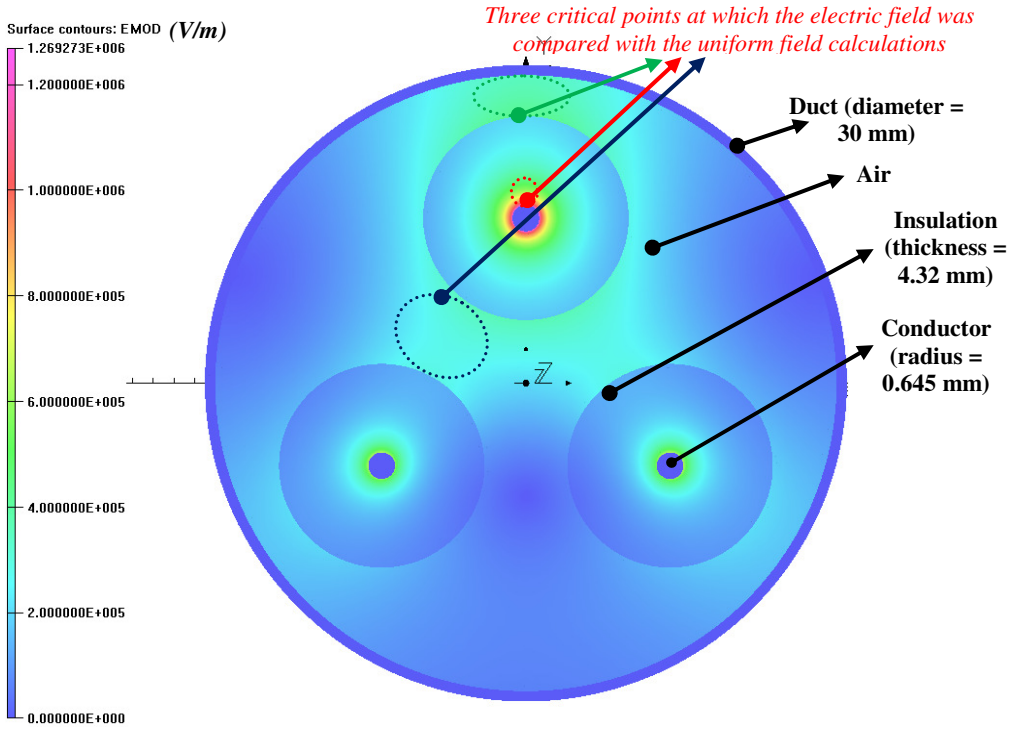

Figure 4.30: Three most critical locations of high electric field in the round cable system

In a round cable system such as the one illustrated in figure 4.30, it would be very difficult to hold the cables apart along the length of the duct. Even if spacers are used or some kind of special holders, there will be a point where the outside insulation surface of the cables will be touching each other. The worst and most realistic case in practice as far as maximum current and voltage rating capabilities are concerned would be, if the cables were touching each other and resting at the bottom of the duct. An illustration of the electric field distribution for each round cable system, is shown below in Figure 4.31 when the top conductor B is at 2.5 kV and the two bottom ones (conductor A on the left and conductor C on the right), are at -1.25 kV. These values are chosen based on a three phase system at one specific point in time. The third case (Figure 4.31c), is when conductor *A* is at 2.5 kV and the other two at -1.25 kV. If the cables are held in the middle of the duct, it does not matter which conductor has the highest voltage because of the symmetrical geometry of the balanced three phase system. Thus it does not matter which conductor is chosen for analysis. However if the cables are resting at the bottom of the duct, the electric field distribution within the insulation and the airgap is different for the top cable standing in the middle and the two bottom ones.

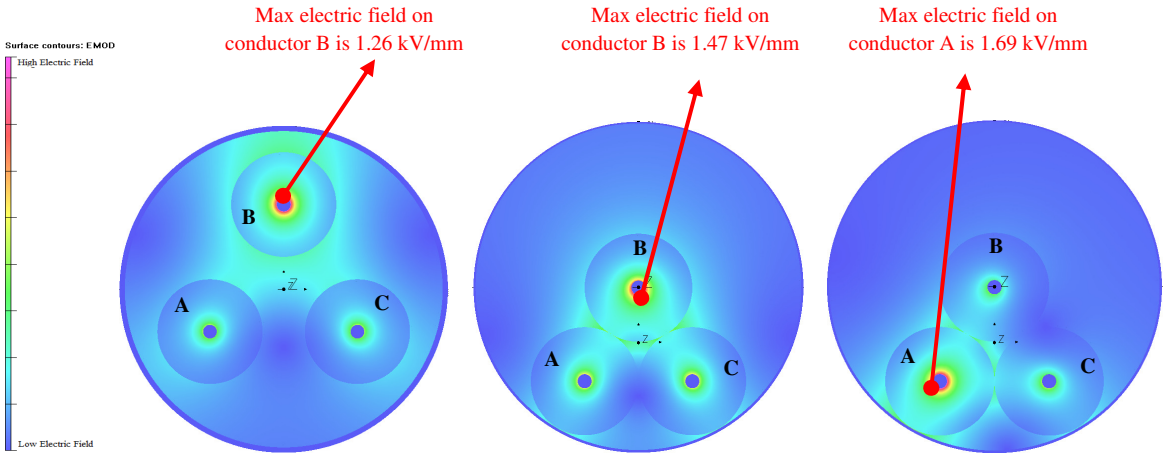

a). Round cables held in the middle of the duct

b). Round cables resting at the bottom of the duct. Top conductor is at 2.5kV

c). Round cables resting at bottom of the duct. Bottom left conductor is at 2.5kV

Figure 4.31: Three most critical locations of high electric field in the 3 phase round cable system installed in a duct

When the cables are resting at the bottom of the duct, by applying 2.5 kV on conductor B rather than on conductor A, a lower electric field is generated on the surface of the conductor and a higher electric field around the airgap where the cables are touching. On the contrary, if 2.5 kV is applied on conductor A, a higher electric field is generated on the conductor and a lower electric field where the cables are touching. As far as the electric field generated in the airgap between the cables and the duct, this is higher when 2.5 kV is applied on conductor A. Thus when considering void and cable to ground discharges, the voltage boundary conditions would be applied as in Figure 4.31c, by analysing the bottom left/right cable. For cable to cable discharges the voltage boundary conditions would be applied as in Figure 4.31b.

4.4.1.2 Adjusting round cable calculated voltage ratings

For the case in Figure 4.31a, it has been mentioned in Chapter 3 that the calculations were carried out for a range of airgap and void sizes and the safe operating voltages (SOV) were chosen to be the ones giving the smallest voltage (i.e. safest voltage). The air pressure was assumed to be 11.6 kPa (at 50,000 ft.) and the ambient temperature to be 343 K (70^{o}C). This temperature was chosen based on [11], which is used for current rating calculations.

Even though the minimum gap size from each cable was 2 mm and 4 mm between cables, the actual airgap and void size at which the SOV was computed for each type of discharge (phase to phase, phase to ground and void), are given in Table 4.2.

TABLE 4.2
CALCULATED SOV FOR THE THREE TYPES OF DISCHARGES AND THE AIR GAP AND VOID SIZES AT WHICH THESE SOV WERE COMPUTED

AWG	SOV_{CC} phase to phase (kV)	Air-gap size (mm)	SOV_{CG} phase to ground (kV)	Air-gap size (mm)	SOV_{V} void (kV)	Void size (μm)
6	3.29	1.89	2.20	1.18	4.11	80
8	3.57	1.99	2.37	1.20	4.12	80
10	3.79	2.2	2.51	1.20	3.95	80
12	3.95	2.4	2.62	1.39	3.68	80
14	4.08	2.5	2.70	1.39	3.37	80
16	4.19	2.5	2.76	1.49	3.03	80

Therefore the models were redesigned in FEA with the airgap distances as shown in Table 4.2, in order make a direct comparison of the electric field generated in FEA at the three critical locations and the calculated results. Correction factors were computed once more to correct the above voltage ratings. According to the results, the minimum airgap distance between cables at which a partial discharge will occur, is about 1.89 mm. For this distance between cables, based on Figure 4.31b (cables resting at the bottom), the electric field is significantly lower and it is difficult to predict by how much the calculation underestimates the PDIV. The same argument can be used for the electric field between cables and the grounded duct. On the other hand, for void discharges the electric field around the conductor is intensified as shown in Figure 4.31c, by approximately 34% compared to the case in Figure 4.31a.

Due to the complexity of the problem in determining whether the calculated voltage rating is underestimated or overestimated and due to time restrictions, it has been assumed

that the voltage ratings in cases shown in Figure 4.31b and 4.31c are the same as in Figure 4.31a. Further work is required to evaluate how the electric field changes in a three phase system for cables installed in a duct. It would then be possible to state whether the calculations provide conservative results or not and by how much.

4.4.2 FEA Analysis to Adjust Calculated Round Cable Current Ratings

Additionally FEA was used to determine current ratings for the conductor sizes shown in Table 4.2, when the cables are held in the middle of the duct (*Case 1*) and when they are resting at the bottom (*Case 2*). In Chapter 3, current ratings as given in AS50881 [11] were used to compute maximum power transfer ratings and power to weight ratios. An example is shown below in Figure 4.32, of how the heat flux varies in *Case 1* and *Case 2* at a conductor operating temperature of 423 K (150°C) and an ambient temperature of 343 K (70°C).

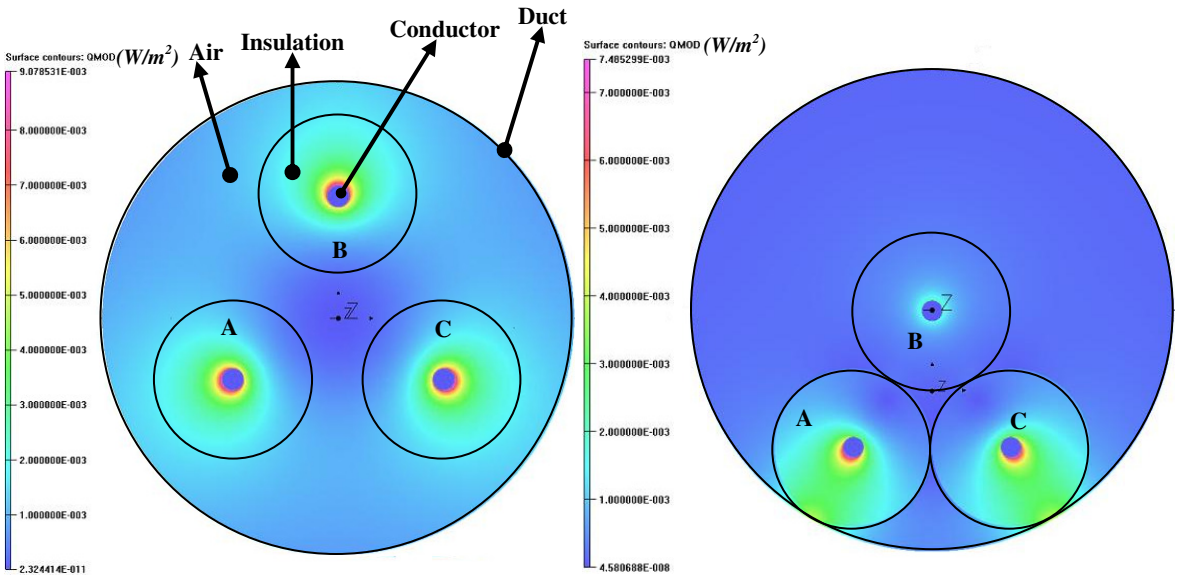

a) *Case 1* b) *Case 2*

Figure 4.32: Comparison of the electric field distribution of a three phase AC system, when cables stand in the middle of the duct with a clearance and when cables are touching and sitting at the bottom of the duct.

As it can be observed, the heat flux for cable ***B*** in *Case 2* is greatly reduced, whereas for cables ***A*** and ***C*** the flux is enhanced. Since at all times the current rating capability of the system is determined by the capability of the hottest cable, the rating is significantly lower in *Case 2*.

4.4.3 Initial Maximum Power Transfer Results

In Figure 4.33 shown below, the power ratings of a three phase PCB system with no neutral and consisting of AWG 16 conductors, is compared with a three phase round cable system in a duct, again consisting of AWG 16 conductors. Furthermore it is compared with other round cable systems consisting of AWG 14, AWG 12, AWG 10, AWG 8 and AWG 6 size conductors. On the graph in Figure 4.33, two curves were plotted for the round cable systems. The top blue curve is for *Case 1* and the lower pink curve for *Case 2*. The cases, for which the two curves are plotted, are illustrated in Figure 4.31a and 4.31b respectively for different conductor sizes.

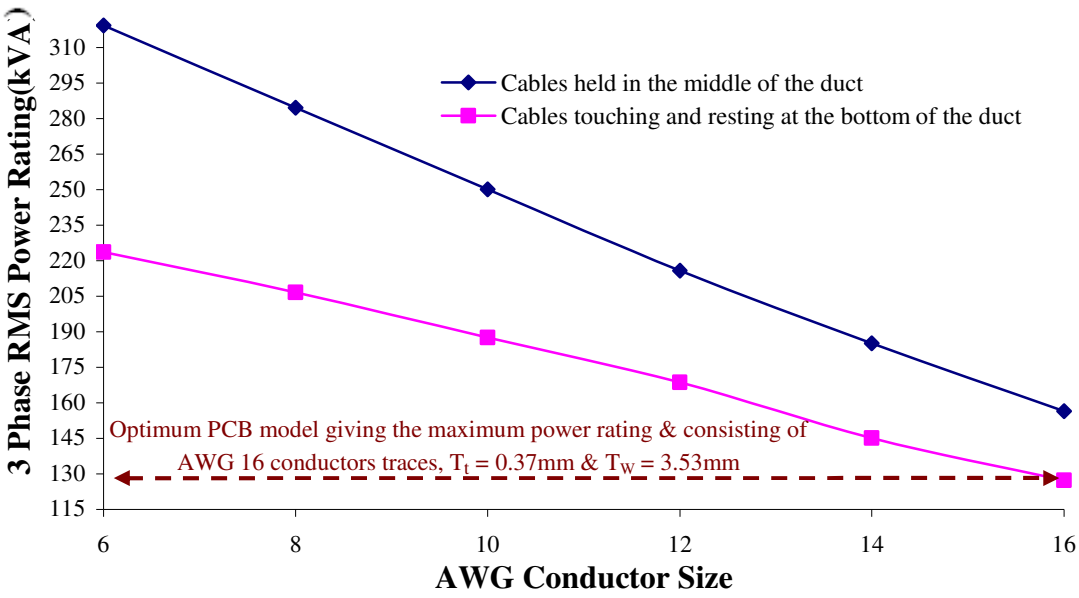

Figure 4.33: Plot of the three phase RMS power rating against AWG conductor size, for comparing PCB and round cable systems' power ratings. Results for T_t = 0.37 mm & T_W = 3.53 mm

The dotted red line in Figure 4.33 represents the PCB model having geometry as such, that results in a maximum power transfer (based on the analysis carried out in the previous section). It has to be noted that this line is just an indication to compare the round cable system power ratings for different conductor sizes. The PCB geometries that have been examined consist only of AWG 16 conductor traces.

Concluding for Figure 4.33, the PCB maximum power rating is lower than the all the round cable systems. However, after carrying out this PCB analysis, it was observed that the range of trace conductor thicknesses and widths that have been considered did not actually cover the optimum point. The range of trace thicknesses that has been examined so far, is: $0.1 \leq T_t \leq 0.37$ mm and thus the range of trace widths: $3.53 \leq T_W \leq 13.07$ mm.

4.4.4 Power Transfer Results for Thicker Conductor Traces

To check the possibility of obtaining a higher power rating by making the conductor trace thicker and thus less wide, the "λ" *factor* giving the optimum point within the range of data that has already been examined, was chosen to carry out further FEA simulations. Another PCB model was designed in FEA having a trace thickness of T_t = 1.0 mm and a trace width of T_W = 1.31 mm. Figure 4.34 illustrates the difference in the electric field distribution and the heat flux when T_t = 0.37 mm and when T_t = 1.0 mm. As an example a voltage of 2.5 kV was used as a boundary condition on trace conductor ***A*** and a voltage of -1.25 kV for conductors ***B*** and ***C***. The conductors' operating temperature was 423 K whilst the ambient temperature was 343 K.

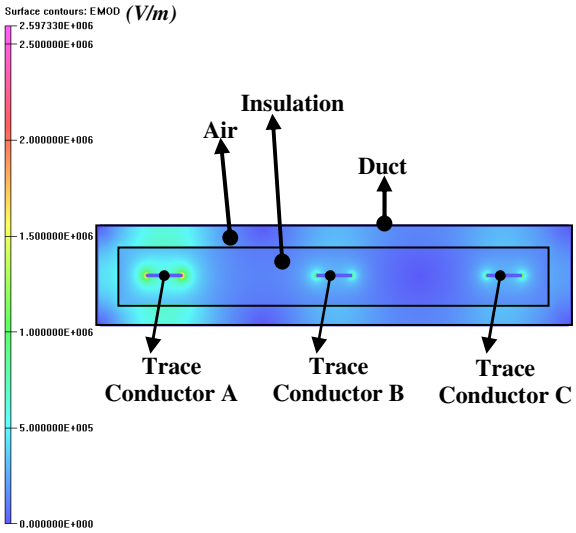

a). Electric Field for λ factor = 5 & T_t = 0.37 mm

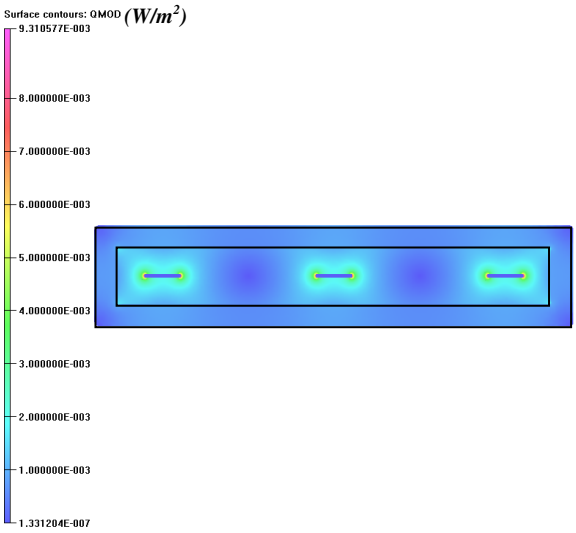

b). Heat Flux for λ factor = 5 & T_t = 0.37 mm

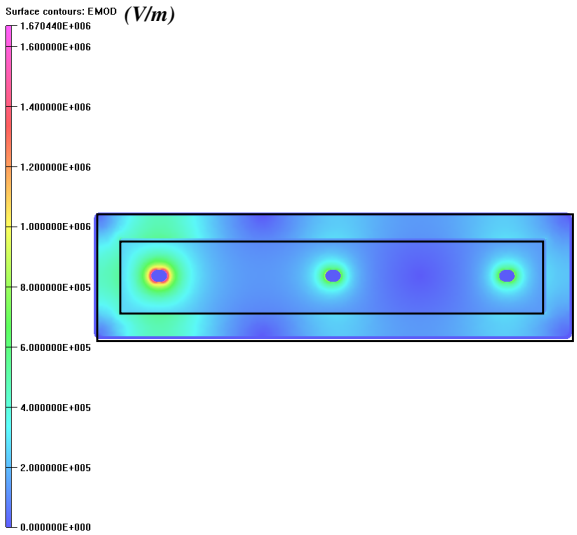

c). Electric Field for λ factor = 5 & T_t = 1.0 mm

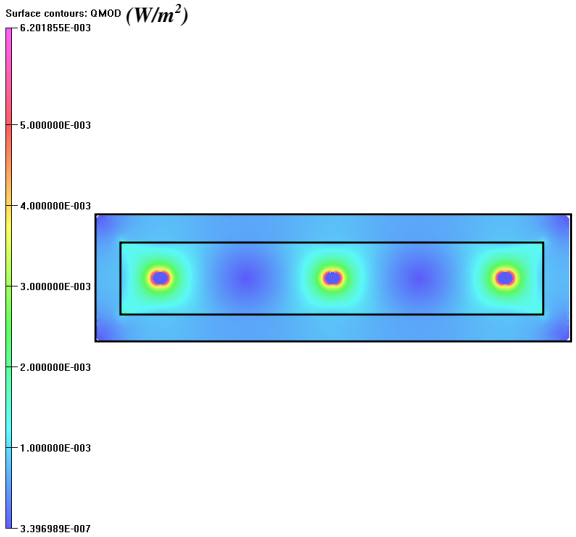

d). Heat Flux for λ factor = 5 & T_t = 1.0 mm

Figure 4.34: FEA PCB models for λ = 5. Display of the electric field distribution and the heat flux when T_t = 0.37 mm & when T_t = 1.0 mm

The maximum heat flux is bigger when the trace is less thick (T_t=0.37 mm), indicating a more efficient heat transfer and thus better current ratings for each trace. However, the electric field is greatly enhanced due to sharper edges (smaller trace edge blending radius), resulting in a lower voltage rating than the case where T_t = 1.0 mm. After carrying out the same procedure for determining the voltage and the current rating, results have shown that it is possible for the PCB system to replace the round cable system, offering higher power to weight ratios. In addition, larger conductor round cable systems

can be replaced offering a reduction in system weight. Power rating and power to weight ratio results are shown below.

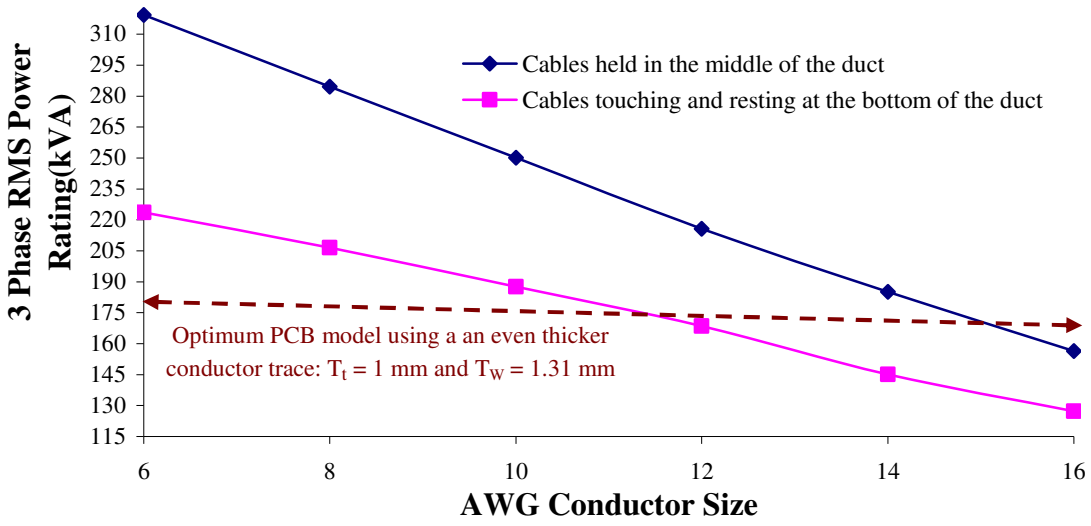

Figure 4.35: Plot of the three phase RMS power rating Vs AWG conductor size for comparing PCB and round cable systems: Results of using a thicker trace i.e. T_t = 1.0 mm & T_W = 1.31 mm

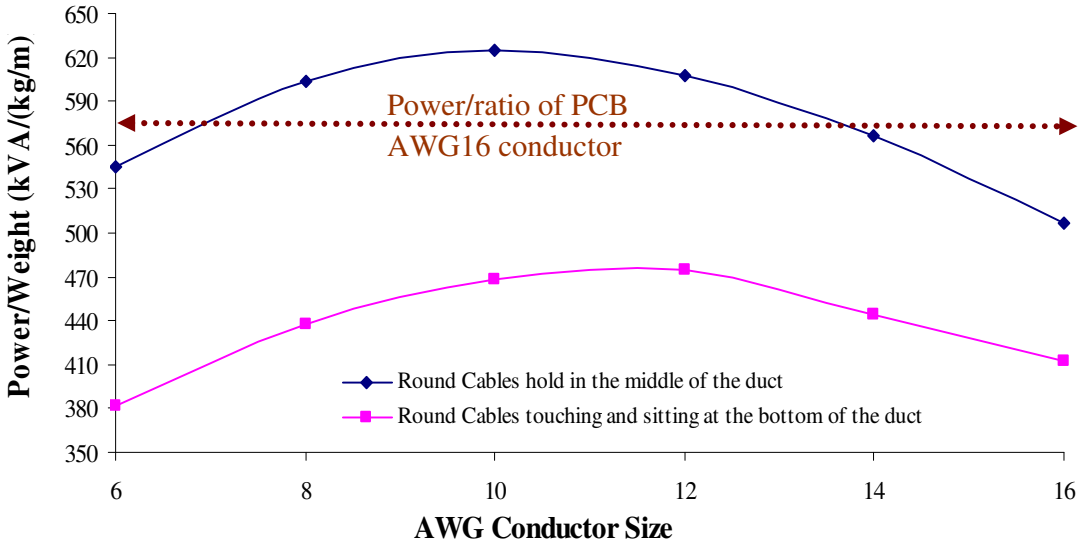

4.36: Plot of the power to weight ratio against AWG conductor size for comparing PCB and round cable systems. Results of using a thicker trace i.e. T_t = 1.0 mm & T_W = 1.31 mm

Overall by using thicker traces as in the PCB models designed in this section, it was concluded that a higher power rating can be achieved. Of course there is a limit to how

thick the conductor trace can be made, since at some point it will start taking the shape of a round conductor (due to the edges having a blending radius of half the trace thickness). Considering the above statement, the trace conductors in the PCB were replaced by round conductors of the same cross sectional area of radius 0.645 mm - AWG 16. This was done to see whether an even higher power rating could be achieved. After evaluation, results showed that the power rating was slightly less than the one shown in figure 4.36. For T_t = 1.0 mm, the 3 phase RMS power rating computed was about 177 kVA whereas for the round conductor having the same PCB geometry, the power rating was 167 kVA.

Another point to emphasize is the fact that the thicker trace conductor case (T_t=1.0mm & T_W=1.31mm), which was not initially considered in the range of trace thicknesses that had been examined, was investigated for $\lambda = 5$. More work is required to get results for $0.25 \leq \lambda \leq 20$.

4.5 Summary

Concluding for Chapter 4, a PCB harness can offer several advantages in contrast to a round cable system. Thus, an assessment of the PCB power transfer capability has been carried out. The PCB model used for analysis, consisted of one layer of copper traces along the thickness and three layers along the width, insulated with Teflon (PTFE). This simple PCB model resembled a Flat Conductor Cable (FCC) and was used to provide an insight on the considerations when designing a PCB for transferring relatively high power, rather than being used to transfer low power signals used in communications and data processing (as in computers and electrical sensors etc).

Different PCB failure mechanisms caused by the application of relatively high voltages have been discussed. Surface flashover is a failure mechanism which can occur at much lower voltages than the partial discharge inception voltage. However, if the PCB is designed in such a way as to eliminate the possibility of surface flashover, then investigation of PD at different locations in the PCB can be used to determine its voltage rating for each conductor trace.

The voltage rating determination based on PD was performed by applying the SOV calculation methodology as in Chapter 3, in combination with Finite Element Analysis (FEA). Furthermore the electric field predicted by the equation models used in Chapter 3, was compared with the FEA electric field simulation results. This was done to evaluate the electric field enhancement at the conductor trace edges within the PCB. FEA thermal modelling has also been used to determine the steady state current ratings for different PCB geometries.

Following the calculation of the power rating for different PCB geometries, the PCB model resulting in a maximum power transfer and power to weight ratio, has been compared with a round cable duct system. The cable duct system consisted of three round cables having the same conductor and insulation cross sectional area as the PCB model. This way, it was possible to determine whether replacing a round cable system with a PCB system, could offer a bigger power transfer for the same weight. The power rating and power to weight ratio for the round cable duct system, were determined in Chapter 3 using uniform electric field approximations. These approximations had resulted in an underestimation of the voltage rating. Therefore FEA was used in the same way as for the PCB models, to investigate the electric field in the insulation and in the airgaps. Since FEA was used to determine the current ratings for the PCB model, FEA was also used to determine the current ratings for the round cable system.

Finally, an assessment has been carried out regarding the effect that the configuration of the cables within the duct, has on the electric field distribution and on the current rating. When the maximum power transfer for the PCB and the round cable systems were compared, these cable configuration effects were also considered.

Overall, the work in Chapter 4 proposes a methodology for determining a safe operating voltage for an insulated flat conductor system in the form of a PCB. In addition, it shows that by using certain appropriate dimensions for the conductor traces within the PCB and a certain insulation thickness, round cable systems can be replaced by PCBs offering a bigger maximum power to weight ratio, as well as other several advantages which are described at the beginning of Chapter 4. This work illustrates the increased complexity in analysing a PCB system rather than a round cable system. The complexity

arises due to the fact that the width and the thickness of a flat conductor trace can be varied, whilst having the same cross sectional area as a round conductor. As the trace width / thickness changes, the insulation thickness between and around the traces changes, if the insulation and conductor cross sectional areas are fixed. As a result the current and the voltage capabilities of the PCB system change as well. The novelty of this piece of work is that no analysis as such has been made available in literature previously on this.

The proposed methodology can be used by engineers to analyse a PCB system with the various possible geometries using the quadratic equation which was derived (see Appendix C-2) in combination with Finite Element Analysis (FEA). The quadratic equation developed consists of parameters describing the dimensions of the conductor trace and the insulation thickness around the PCB and it allows the user to construct models in FEA with the appropriate dimensions by changing only two of the parameters of the quadratic equation.

Furthermore it must be mentioned that unlike any other work found in the literature, the PCB voltage ratings (or safe operating voltages) are based on the partial discharge inception voltage (PDIV) that can occur within a PCB or outside. For analysis it has been assumed that the breakdown voltage of the insulation is much bigger than the PDIV and also that a material such as PTFE can be used as PCB insulation. In practice, this might not be the case and further examination is required if different materials are to be incorporated into the analysis and also if the PCB consists of many layers of different insulation.

Chapter 5
AC Partial Discharge Tests

This chapter focuses on AC partial discharge tests that were performed on different unscreened aerospace cables laid in different configurations. The objectives are to determine the best method for testing an aerospace cable and to compare the partial discharge inception voltage (PDIV) for the different cable configurations. Furthermore the measured PDIV results are compared with the PDIV results obtained by using the SOV calculation methodology that was described in chapter 3. A detailed summary of the work that has been carried out can be found at the end of chapter 5.

5.1 Introduction

This section focuses on PD experimental testing. The straight PD detection circuit as well as the balanced PD detection circuit have been used as in BS EN 60270 [30], to investigate the suitability of a variety of methods for the PD testing of cables, operating under AC high voltage stresses in an aerospace environment. A number of cable samples of the same type have been tested in different configurations in an effort to replicate different aircraft cable harnesses. These configurations were compared with the currently used test configuration as found in BS EN 3475-307 [59], to check the consistency of PD results and if the discharge mechanisms involved in each configuration differ.

5.1.1 Different Types of Partial Discharge (PD)

The importance of PD in determining the safe operating voltage for aerospace cables has been discussed previously. Three types of PD commonly occur on cables and these can be

defined as cable to ground discharges, cable to cable discharges and void discharges within the cable insulation. These are illustrated again in the figure shown below.

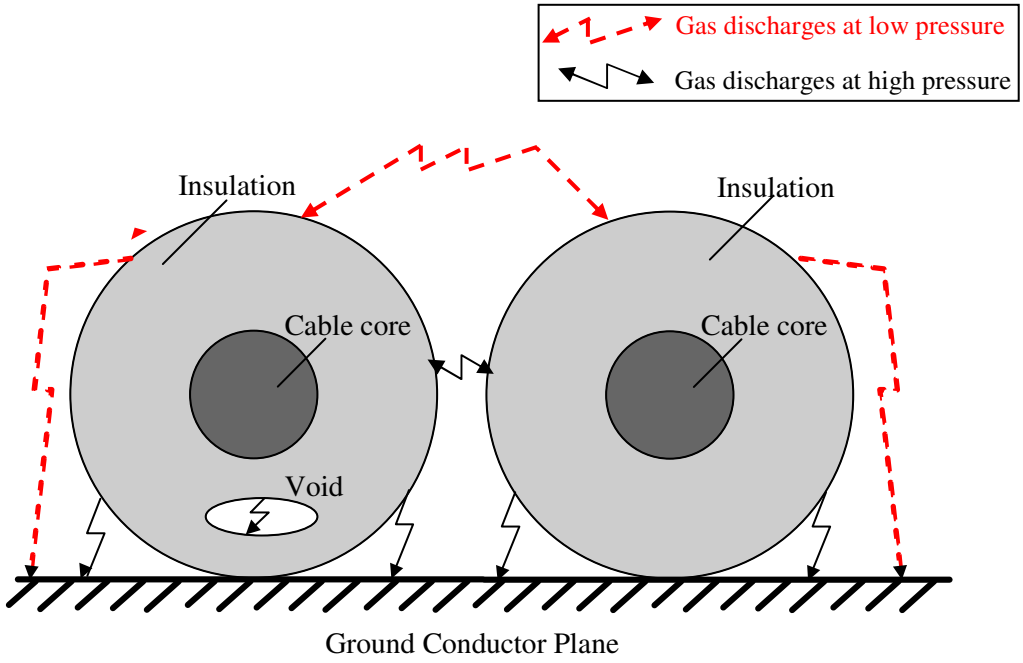

Figure 5.1: Illustration of PD locations at high and low pressures in a simple two cable system laid on a ground plane conductor

According to Dunbar [5], at relatively high pressures cable to ground discharges as shown in Figure 5.1, are more likely to occur at smaller air gaps than at low pressures. This is indicated on the figure above with red dotted lines for gas discharges occurring at low pressure and black lines for gas discharges occurring at high pressure.

Since PD must be avoided to ensure the safe operation and to prolong the life of cable insulation, appropriate tests are performed, to ensure that at relatively higher voltages which are used in the MEA, the insulation is capable of preventing PD in aircraft environments. Tests have to cover all three types of discharges as described in Figure 5.1, since the type of discharge which requires the lowest inception voltage should be the one considered in the rating of cable insulation. The partial discharge inception voltage (PDIV) for all three types of discharge varies as a function of airgap distance, insulation properties and thickness, as well as the surrounding environment (pressure and temperature) [9].

Thus, appropriate cable PD testing methods have to be devised to cover all types of discharges and to account for the worst case environment, irrespective of the cable installation configuration.

5.1.2 Methods of Configuring Cables for PD Testing

It is not certain that methods currently used for preparing cable testing samples are satisfactory in terms of simulating the actual aircraft environment and the cable harness. At the moment PD tests on aircraft cables, are being carried out in accordance with BS EN 3475-307 [59] in conjunction with BS EN 60270 [30], which describes the PD detection methods including the specifications of calibration and measuring instruments that should be used. The former standard describes methods for preparing screened and unscreened cable samples and the latter describes relevant testing procedures.

If the cable is screened, then a conductor of size AWG 20 is wrapped around the screen of one end of the cable and then earthed. High voltage is then applied on the cable conductor until the partial discharge inception voltage (PDIV) is reached. If the cable is unscreened then a braid is added tightly around the cable insulation and the same procedure is carried out as in [30] to test for PDIV. Figure 5.2 illustrates this cable testing arrangement as described in [59], including the stripping dimensions.

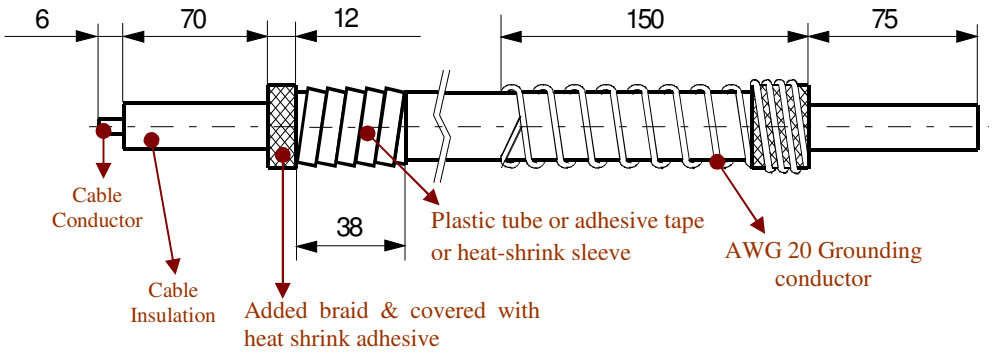

Figure 5.3: Cable testing arrangement according to BSEN 3475-307 [59]

However, if the braid used for screening is tightly wrapped around the insulation and no airgaps exist between the cable and the earthed braid, then theoretically the cable would be tested only for void discharges. In practice there will always be an airgap between the cable insulation and the screen, even though this airgap might be very small. In addition, unscreened cables will be at a certain airgap distance from an earthed/grounded surface (such as a duct, cable tray or the airframe), or from another cable. Therefore as mentioned previously the cables must be tested for all three types of discharges (cable to ground, cable to cable and void discharges).

From the discussion above, the question arises whether testing for a single cable with the addition of braid as in [59], is adequate to provide reliable results even if the cable is to be used as a single unscreened cable or in a bundle and also if this situation tests for all three types of discharges within a reasonable airgap distance range, and at different operating conditions. To examine the method of cable sample preparation for PD testing described in [59], various methods of configuring a single unscreened cable to test for cable to ground and void discharges are examined. These methods replicate possible cable installation methods within the aircraft. The cables tested might be used afterwards in a single phase AC system installed in a duct or laid on a grounded surface like a cable tray etc. In case the cables are to be operated in a three phase AC system the testing procedure is more complex according to [60].

The single unscreened cables can be tested for PD by adding braid around the unscreened cable as in [59], or simply laying the cable on a ground plane. It could also be tested by having a certain AWG size conductor grounded and wrapped around the cable insulation, or by wrapping the cable around a grounded cylinder. The last two methods would only be reasonable if the aircraft cables are installed in a similar manner. However the aim here is to show that different configurations might result in different PDIV results. The four possible cable configurations described are shown in Figure 5.3. These configurations are used in this chapter to carry out PD tests.

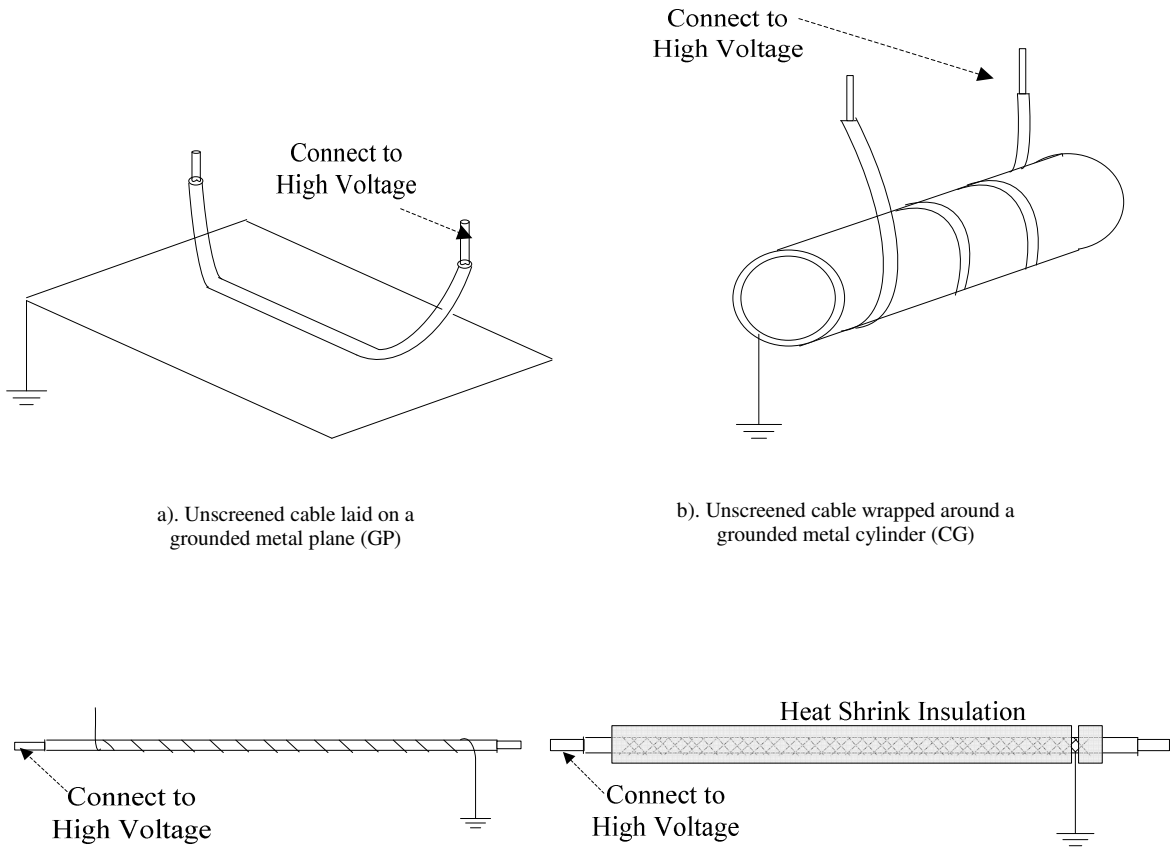

a). Unscreened cable laid on a grounded metal plane (GP)

b). Unscreened cable wrapped around a grounded metal cylinder (CG)

c). Bare cable wrapped around an unscreened cable. The cable conductor is connected to HV and the naked cable to ground (TW)

d). Unscreened cable with braid added around the insulation. Heat shrink insulation is also added to hold the braid tightly. One end of braid is connected to ground (UB)

Figure 5.3: Cable test samples laid out in different configurations for PD testing

Every cable configuration shown in Figure 5.3 will have a different electric field distribution within the airgap due to the difference in geometry along the airgap between the insulation–ground interfaces. The different cable configuration methods tested for PD are later on compared relatively to the PDIV magnitude results, as well as for the repetitiveness of the results. This is done to determine which configuration is most suitable for testing single unscreened aerospace cables at different environmental conditions (different pressures).

It must also be mentioned here that all AC PD tests have been carried out using two types of PD detectors, the ROBINSON and the LEMKE PD detectors. The former is an

analogue instrument which can only be used to detect the partial discharge inception voltage with the use of a deflection needle which deflects when PD is generated from the cable sample. The latter is a digital instrument which can also manipulate PD signals and produce graphs of PD against phase angle of the supply voltage. In addition it can analyse PD data by calculating certain statistical operators that is explained later on.

5.2 Straight PD Detection Circuit-ROBINSON

The cable samples described in the previous section were tested using the straight PD detection method based on [30]. The straight detection circuit is shown in Figure 5.4.

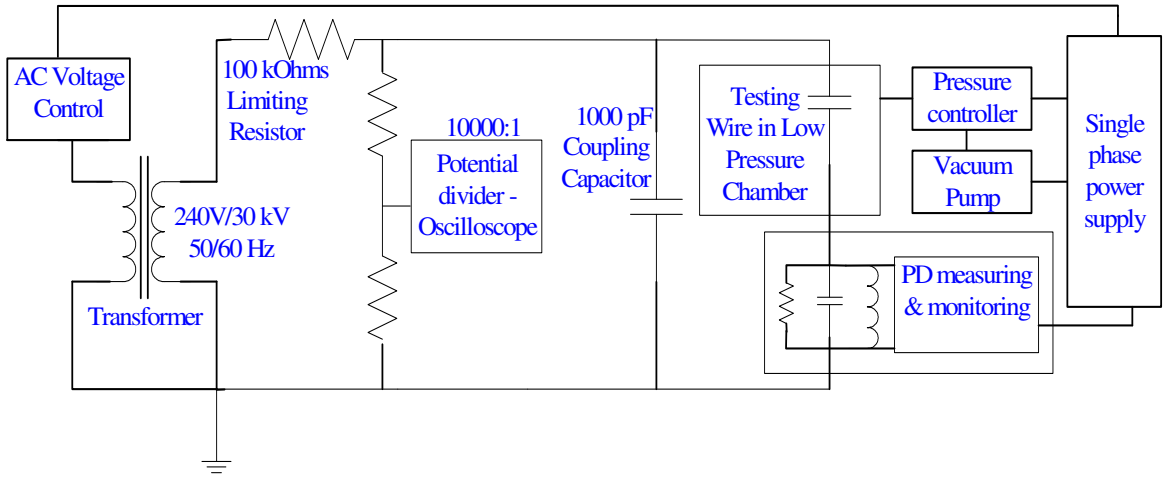

Figure 5.4: PD straight detection circuit based on [30] with the addition of a vacuum chamber and a vacuum pump controller

Tests were carried out at atmospheric pressure (≈1000 mbar or 100 kPa) and at 116 mbar or 11.6 kPa (corresponding to an aircraft altitude of 50,000 feet). According to [61], within this pressure range the change in width and in rise time of the PD output pulse, is not significant and thus requirements and specifications regarding the PD measuring instrument as in [30], are satisfactory. Thus the standard PD circuit did not require any modifications. The measuring instrument was calibrated at 50 pC. The noise levels were between 10-30 pC. The noise level was very high due to the working lab environment. According to [30], the PD measuring instrument should be able to detect a minimum of 5

pC of charge. This thesis focuses on the investigation of PDIV on different cable configurations, as far as the repetitiveness and consistency of the results is concerned and the relative magnitudes. The results were adequate to carry out an initial assessment in determining the best method of configuring unscreened cables for PD testing. Further work will make use of the balanced PD detection circuit to reduce the surrounding noise as well as testing of more cable samples of different insulation thickness and conductor size.

5.2.1 Description of Testing Procedure

The identification number of the aerospace cable that has been used for all PD tests is M22759/86-12. The cable has two insulation wraps, one of which forms the inner layer and which is made from PTFE/Polyimide/PTFE tape and one which forms the outer layer which is made from PTFE insulation. Polyimide has a relative permittivity of 3.4 and PTFE has a relative permittivity of 2.1. The total insulation thickness is 0.29 mm and the conductor has a radius of 1.04 mm.

Overall 12 samples of cable of the same type were tested (same production batch), having a length of about 500 mm. The cable samples were tested for PD in the configurations shown in figure 5.2 previously. The grounded cylinder case is abbreviated as CG, the grounded plane case as GP, the case where braid was used to screen the cable UB and finally the case where a grounded twisted bare wire was wrapped around the cable, as TW. For each cable configuration, three tests have been performed (Test A, Test B and Test C, (each test being carried out on a different cable sample). This was done to check how repetitive the PD results were for each configuration and from sample to sample. In addition, one of the cable samples was tested (Test X) in all four configurations to make sure that the difference in the results was not due to the different cables used for each test, but because of the different cable configurations.

5.2.2 Average RMS PDIV Results

For each test (Test A- Test X), 5 to 10 measurements were made for each cable sample, based on the repetitiveness and the consistency of the PDIV results. The values read on the oscilloscope were the peak to peak values of the line source voltage of which the average was taken and furthermore the RMS inception voltage was calculated. These are shown in Figure 5.5 on the next page.

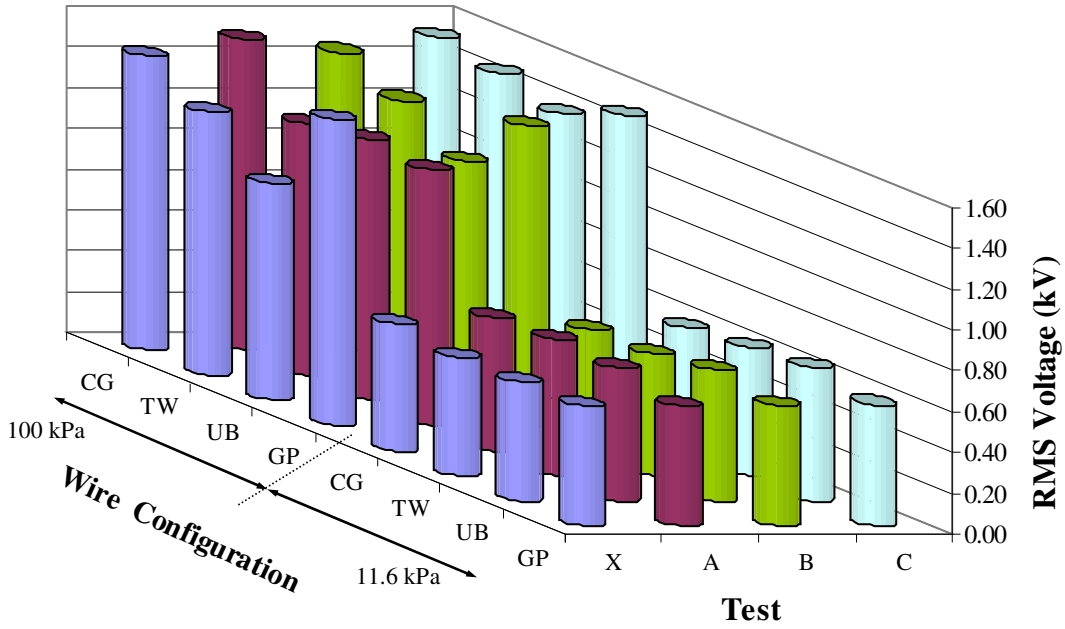

Figure 5.5: Average PDIV results for different cable configurations

From Figure 5.5 it can be observed that the average PDIV results at a pressure of 11.6 kPa (116 mbar), are more consistent than at 100 kPa (1000 mbar). For example at 100 kPa, when comparing CG and UB configurations for Test X, the maximum percentage difference between and PDIV results is approximately 26%. On the contrary when comparing the same configurations at 11.6 kPa, the percentage difference is only 7%. It was also observed during the experiments that the onset to a stable PD pattern was more

rapid at low pressure. At 100 kPa, the cable wrapped around a grounded cylinder (CG case), showed more consistency from Test X to Test C.

Each test (X and A-C), was carried out on different days and the measured atmospheric pressure (100 kPa) and temperature (20 ^{o}C) was found to vary from day to day by +/-2% and by +/-1% respectively. These slight variations cannot justify the different PDIV results obtained from Test X to Test C. Different PD initiation mechanisms might be occurring in the samples and this could be a possible explanation for the differences in the results. Another possible explanation could be that the aerospace cables tested, might have different manufacturing tolerances. However, it must be recorded that the cable samples used were of the same size, type and production batch. The difference of results from one configuration to the other is obvious at 100 kPa. In this case the atmospheric pressure and temperature was the same during the experiments, since each test was performed the same day. However more experiments are required to explain the variation in the relative PDIV magnitudes. Even though the average PDIV results show a relative pattern between the different configurations at high pressure and low pressure, a better way to compare the different methods, is to include the standard deviation of all the measurements based on the average PDIV values at 100 kPa and 11.6 kPa. These are shown below in Figures 5.6 and 5.7 respectively.

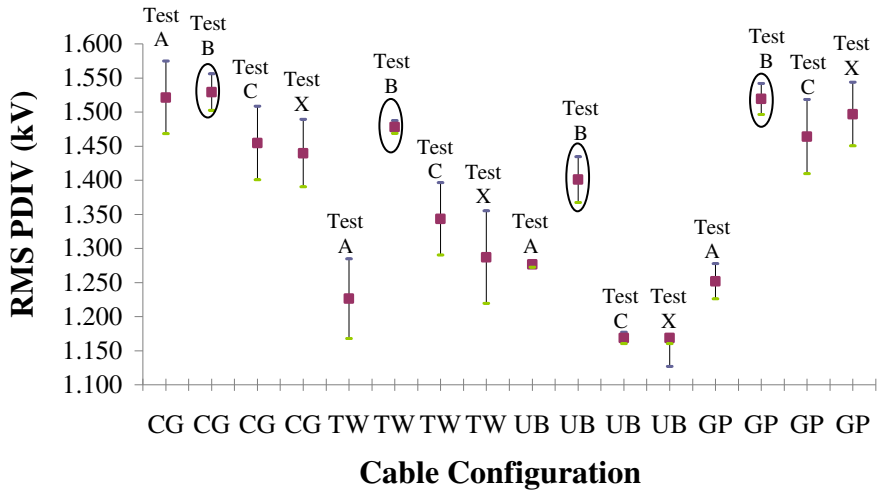

Figure 5.6: Span of PDIV measurement results at 100 kPa at different cable configurations

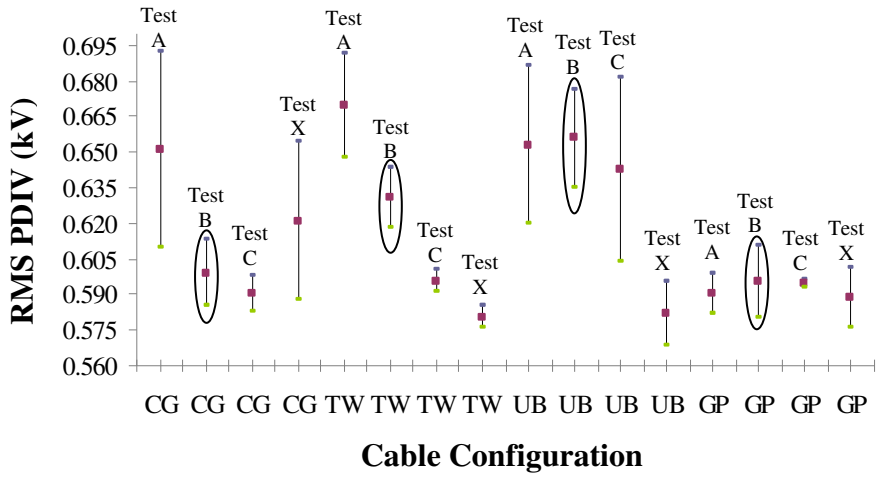

Figure 5.7: Span of PDIV measurement results at 11.6 kPa at different cable configurations

At 100 kPa the CG configuration results from the four tests (A-X), show more consistency (i.e. the average RMS PDIV measured for each test is more similar). However the relative PDIV magnitudes and their standard deviations (span of different measurements) are on average higher than the other measurement configurations. In relation to the UB case, which is based on [59], the CG configuration is more consistent. Compared to other cases the UB results have lower standard deviations for all four tests. At 11.6 kPa, the GP results demonstrate higher consistency for all tests (A-X) and also exhibit lower standard deviations. On the contrary TW shows substantial variation in the results for both high pressure and low pressure. More tests with different types of cable are required to understand the reasons behind these phenomena and to decide whether these results can be used to determine the best cable configuration in terms of consistency and accuracy.

Summarizing from the PD tests carried out, it has been shown that at both 11.6 kPa and 100 kPa the PDIV results differ for each configuration. For PD testing, the cable configuration resulting in the smallest PDIVs and having the lowest standard deviations should be used. In general, the GP cable configuration at 11.6 kPa exhibits higher consistency for all tests (A-X) and relatively lower standard deviations than all other configurations. It might be the case that using different types of cable, having different insulation materials and insulation thicknesses, will lead to a different conclusion. Thus,

further work is required to understand the PD mechanisms taking place in each configuration. If the PD mechanisms can be identified, then it will be possible to predict the behaviour of different types of cables when they are tested for PD.

5.2.3 Phase Resolved PD Magnitude Analysis

After examining the consistency of results of tests A-X and the standard deviations of each individual test, it is necessary to investigate the PD magnitude against phase angle for each configuration. These relationships can provide information on the discharge mechanisms occurring based on the insulation defects. The PD mechanisms would help in explaining the variation in the results and understanding how different sample geometries, airgap distances between cables and the ground and other electrical parameters affect the measurements. PD magnitudes against phase were plotted for Test B only, which represents the second series of tests at 100 kPa and 11.6 kPa circled on Figures 5.6 and 5.7 respectively. The plots are shown in Figures 5.8 and 5.9 for high and low pressure respectively. The data obtained was for a voltage of 10% above inception to get a more sustained PD pattern on the oscilloscope.

Results for Tests A-X are not all shown in figures 5.8 and 5.9 since they exhibited similar patterns as Test B. Test B results were chosen specifically because the number of measurements carried out was more in order to make sure that PDIV results were consistent. The fact that tests A, C and X resulted in similar PD magnitude Vs phase angle plots, shows that the same PD mechanisms are occurring for each test for the same configuration. However what needs to be further investigated, it is the difference in results between different cable configurations.

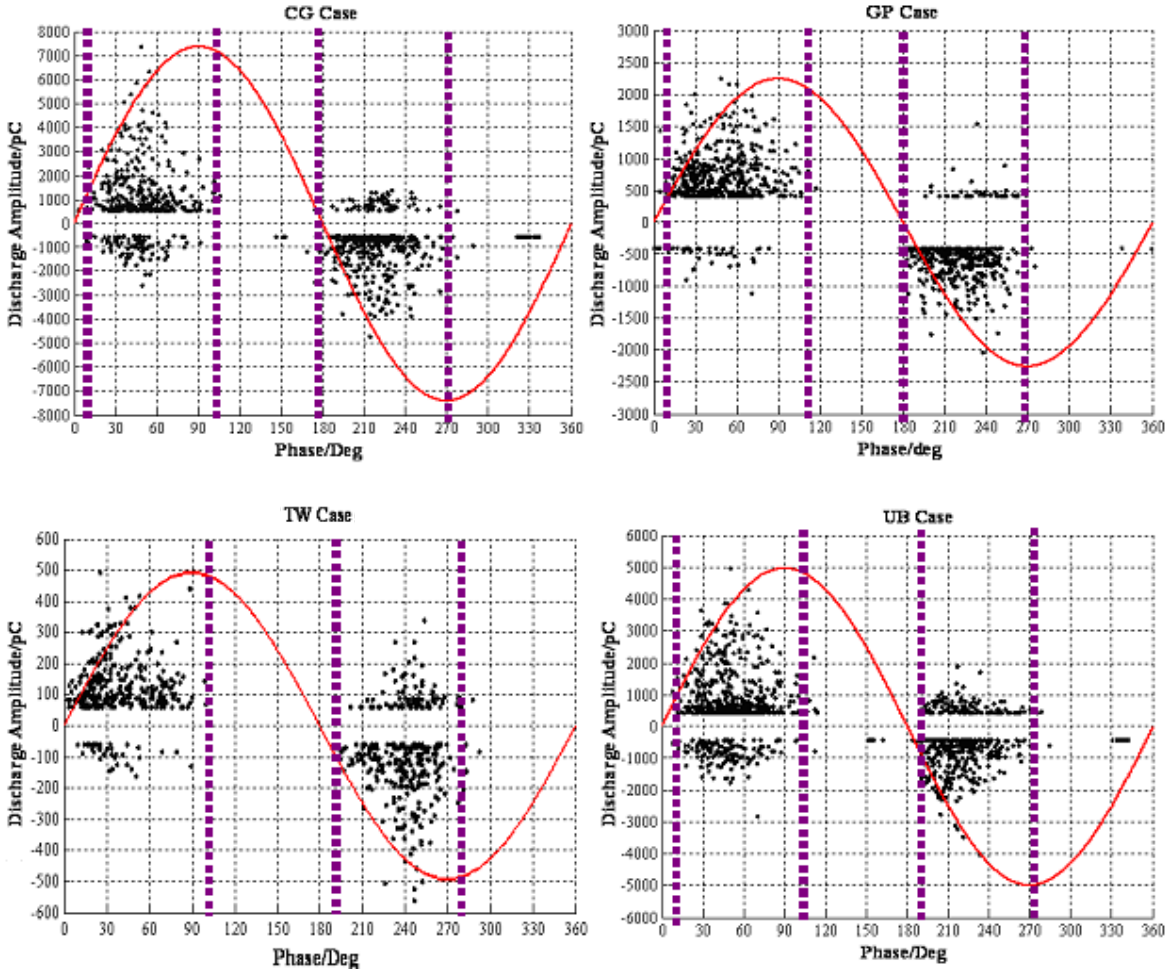

Figure 5.8: Phase resolved PD Plot for Test B results, for the four different cable configurations: CG, TW, UB and GP, at a pressure of 100 kPa

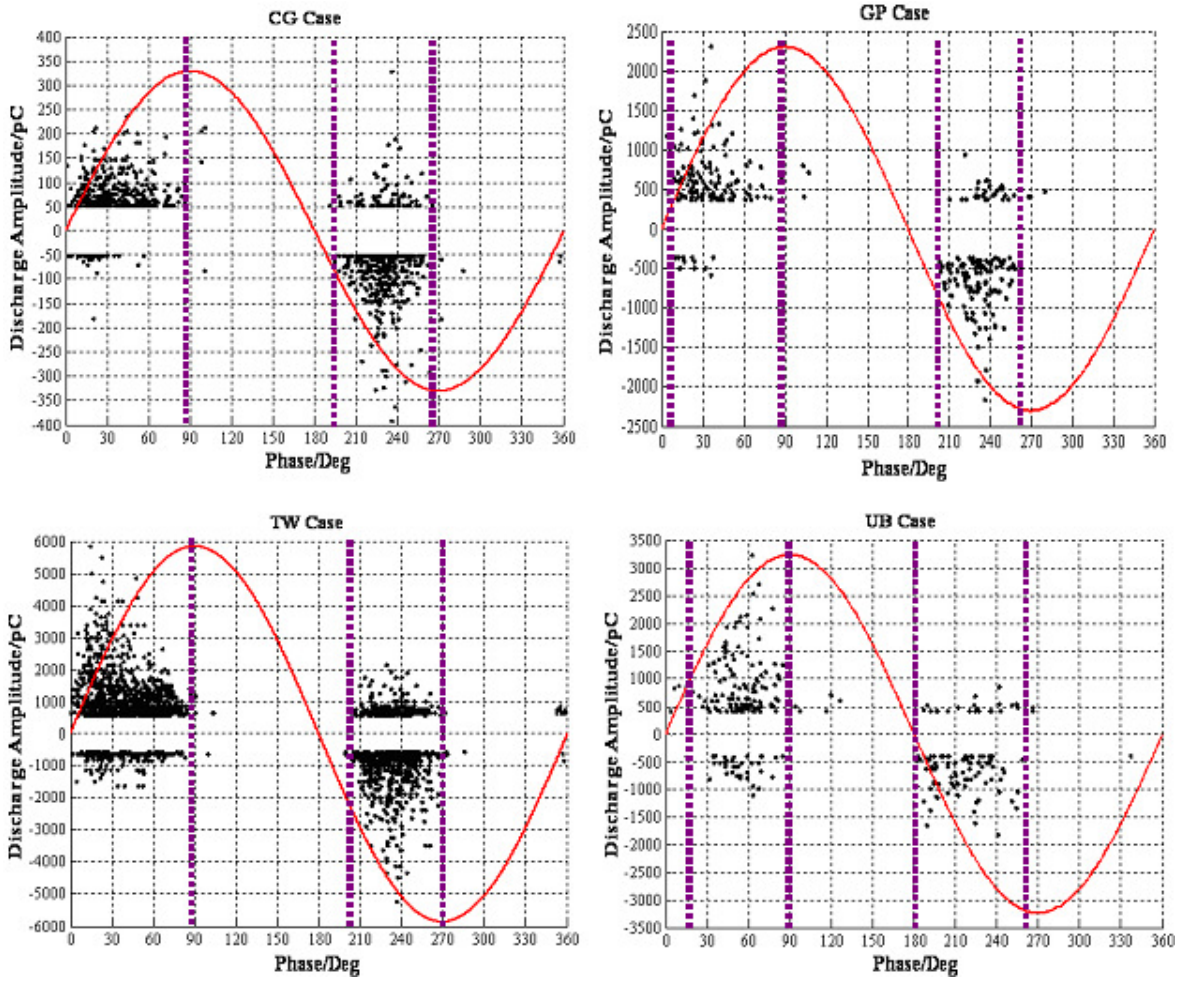

Figure 5.9: Phase resolved PD plot for Test B results, for the four different cable configurations: CG, TW, UB and GP, at a pressure of 11.6 kPa

The data shown in Figures 5.8 and 5.9 were processed using MATLAB software which was developed as in [62]. For each testing configuration the same PD test was carried out 10 to 15 times, depending on the repetitiveness of the results. Data was captured using the oscilloscope for 6 cycles (120 ms), for each PD test. For some configurations the PD magnitude was very large and the Robinson PD detector was driven to saturation. In these cases the gain from the built in Robinson amplifier had to be reduced to acquire all PD data. The reduction in gain was compensated in the MATLAB software. By stepping down the Robinson gain once, the voltage observed on the oscilloscope screen was reduced by a factor of 10. However, the noise level was reduced by a factor less than 10. In the MATLAB software the user has the option to provide some input parameters. Two of the input parameters included a gain factor and a noise threshold value. By setting

the gain factor at 10, all the data obtained from the oscilloscope including the noise, were multiplied by a factor of 10. Since the level of noise was reduced by factor of less than 10, this resulted in a higher level of noise as shown in Figures 5.8 and 5.9 (up to 500 pC). Thus the noise threshold input parameter in the MATLAB software, was set at a higher value than it actually is. As a result PD magnitudes of less than 500 pC could not be detected in some cases. The only solution, so that smaller PD magnitudes could be detected by using the analogue Robinson PD detector, would be to improve the MATLAB software by adding another function allowing the user to enter a separate threshold value for the noise. Alternatively, digital PD detectors could be used in combination with a balanced PD detection circuit. Furthermore the testing circuit could be placed in a grounded cage to eliminate the external noise entirely. As it will be described in the next section, all the AC PD tests have been repeated with a digital PD detector called 'Lemke'. In addition to this, a balanced as well as straight detection circuit have been used to compare the results obtained with the Robinson.

From the phase resolved PD plots, there seems to be a significant difference in the PD magnitude when comparing results at 100 kPa and at 11.6 kPa. This could be connected to different PD mechanisms taking place and the different partial discharge inception voltages (PDIV) results. A slight variation in the supply voltage phase at which PD concentrates was also noticed, when comparing the graphs for the different configurations at 100 kPa and 11.6 kPa. For example regarding the phase range at which PD occurs, Cases CG, GP and TW show similar patterns at 11.6 kPa whilst the UB Case differs. This difference is illustrated on Figure 5.9 with the use of dotted lines.

Overall results so far have shown a variation on the PD-phase plots but more data and analysis is required to verify these phenomena in a lower external noise environment. If the difference in these PD patterns is verified and is significant, this would imply that different airgap breakdown mechanisms are occurring in each case.

An initial assessment has been carried out on testing PDIV magnitudes for four different methods used to configure aerospace cable samples. These configurations could replicate the way cables are installed in an aircraft. It has been observed that the CG case is more consistent at high pressures (100 kPa) in terms of measurements results, for tests X to

test C than all the other methods. Nevertheless the UB case shows lower standard deviations. At low pressure (11.6 kPa) PD, the onset to a stable PD pattern was more rapid than at 100 kPa. In this situation the GP case results exhibited higher consistency as well as relatively lower standard deviations. PD magnitudes versus supply voltage phase plots, suggest that different PD mechanisms are taking place in each configuration (CG, TW, UB and GP). All results are summarised in Table 5.1. More test results are shown in the next section using the balanced circuit method to verify the above observations.

TABLE 5.1 A

SUMMARY OF OBSERVATIONS FROM AC PD TESTS AT 100 kPa

Mean PDIV(kV) for tests A-X, at 100 kPa	STDEV of PDIVs for tests A-X, at 100 kPa	Maximum PD magnitudes at 100 kPa	PD phase range and phase shift at 100 kPa
TW results in the lowest average PDIV with a value of 1.34kV. This is ≈1.5% smaller than the UB case.	CG results in the lowest STDEV with a value of +/-4.4%. UB case has a STDEV of +/-18.9%; TW has a STDEV of +/-11.1% and GP +/-12.4%.	CG, GP and UB cases exhibit PD magnitudes ≥ 2000 pC. Magnitudes for TW are significantly smaller by a factor of 10.	Considering the +ve half cycles of the PD phase plots, TW case exhibits a relative phase shift of approximately 10^{o}C. For the –ve half cycles, TW again experiences a phase shift of 10^{o}C whilst in the UB case the phase range seems to decrease by 10 ^{o}C.

TABLE 5.1 B

SUMMARY OF OBSERVATIONS FROM AC PD TESTS AT 11.6 kPa

Mean PDIV(kV) for tests A-X, at 11.6 kPa	STDEV of PDIVs for tests A-X, at 11.6 kPa	Maximum PD magnitude at 11.6 kPa	PD phase range and phase shift at 11.6 kPa
GP results in the lowest average PDIV with a value of 0.59kV. This is ≈6.3% smaller than the UB case.	GP results in the lowest STDEV with a value of +/-0.5%. UB case has a STDEV of +/-3.6%; TW has a STDEV of +/-4.1% and CG +/-4.4%.	UB and GP have PD magnitudes ≥ 2000 pC, as in the case of 100 kPa. Magnitudes for CG decrease approximately by a factor of 32 whereas for TW they increase by a factor of 10.	For +ve half cycles of the PD phase plots, the phase range for CG and TW narrows down by 5^{o}C-10^{o}C compared to the cases at 100 kPa. Likewise, GP and UB phase ranges decrease by 10 ^{o}C-20 ^{o}C. For the –ve half cycles, all configurations have a decrease in the phase range of about 15-30 ^{o}C, whilst in the UB case the phase range is the same but shifts by 10 ^{o}C.

5.3 Balanced PD Detection Circuit-Lemke

Using the balanced circuit method, as in Figure 5.10, any noise coming either from the mains supply or from other external sources can be eliminated, since noise flows through both branches of the circuit. The RLC impedance is arranged in the detection equipment in such a way, so that the interference voltages induced on the secondary coil are of opposite sign and effectively cancelling each other out.

The use of LEMKE LDS-6 allowed more data to be captured faster and obtain a much more accurate representation of the phase resolved discharge magnitude plots. This was due to the built-in PD monitoring software which could also be used to adjust the PD detect level, based on the PD magnitude signals acquired by the device.

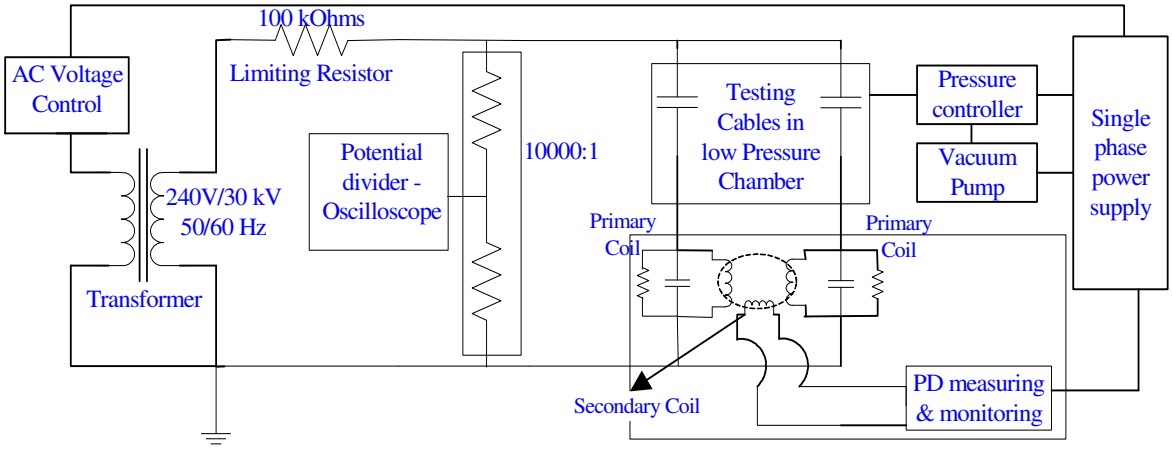

Figure 5.10: PD balanced detection circuit based on [30] with the addition of a vacuum chamber and a vacuum pump controller

Using the balanced PD detection circuit, the partial discharge inception voltage can be measured accurately as in the straight detection method. The disadvantage of this configuration is the fact that it is complex to distinguish the cable from which PD is generated from. If only positive PD pulses or only negative PD pulses were occurring in the samples, then it would be possible to separate discharges coming from the two cable specimen, since in one case the output pulse on the secondary coil would be positive and in the other case it would be negative. Unfortunately both negative and positive PD pulses could occur in both branches.

5.3.1 Average RMS PDIV Results

In Section 5.2.2, the PDIV results were plotted for each configuration for Tests A-X and the phase resolved plots for Test B in particular in Section 5.2.3 as described. This section is used to compare PDIV and PDEV results obtained using the 'Straight' and the 'Balanced' PD detection methods for the cables used in Test B for the four different cable configurations. PDIV Results and PDEV are shown in Figures 5.11 and 5.12 respectively.

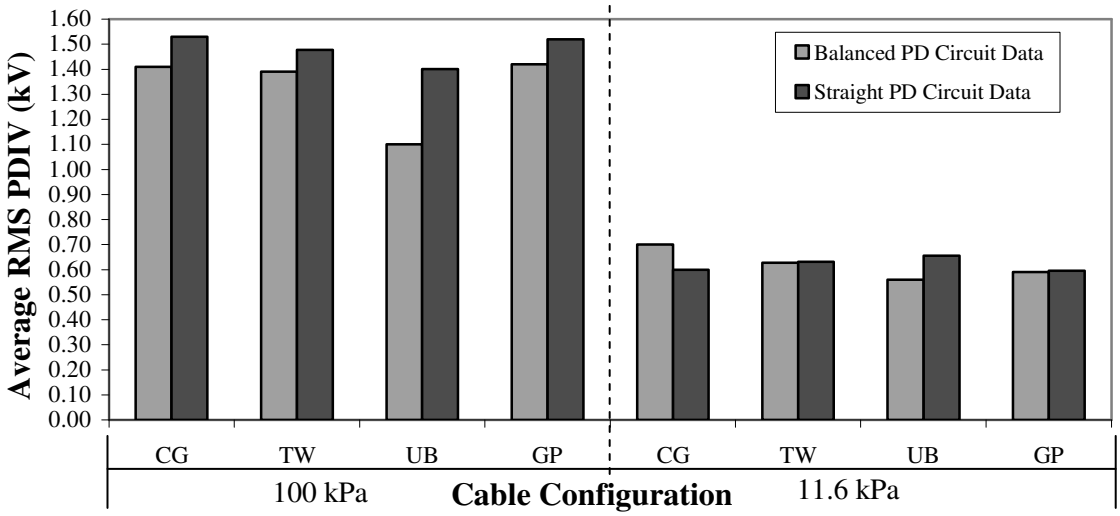

Figure 5.11: Comparison of PDIV results obtained using the "Straight" and the "Balanced" PD detection methods, at 100 kPa and at 11.6 kPa for the four different cable configurations.

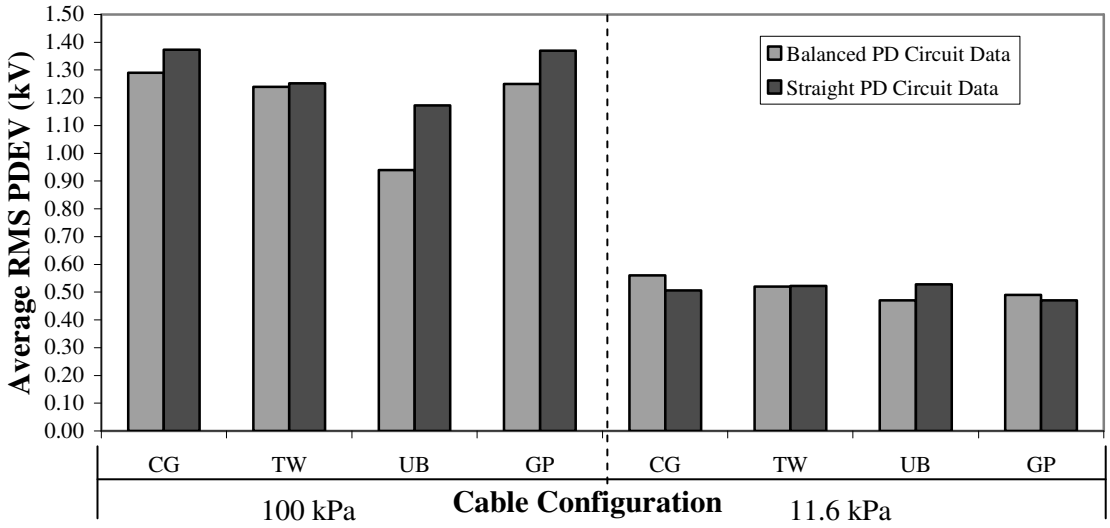

Figure 5.12: Comparison of PDEV results obtained using the "Straight" and the "Balanced" PD detection methods, at 100 kPa and at 11.6 kPa for the four different cable configurations.

From Figure 5.11, PDIV results obtained using the balanced circuit seem to be smaller in magnitude, with a maximum difference of 22% with respect to the straight PD detection method for the UB case at 100 kPa. The other cases show an average difference of approximately 9%. At 100 kPa, the difference in the results could be explained by the fact that using the LEMKE PD detection equipment provided a more accurate method of observing PD initiation. The special features of this equipment allow the user to distinguish between noise and PD, by setting a noise threshold value [63]. When using the Robinson PD detector, the needle indicator on the device used to fluctuate with external noise interference. In addition a slight increase in the voltage above inception did not result in a sustained PD. Thus, the voltage was raised even more to obtain a sustained PD pattern. This is when the needle started moving constantly at a certain rate, to make sure that the fluctuation was not due to noise but from the actual PD generated from the test samples. Using this methodology, the accuracy of the results was bound to be less and the possibility of obtaining larger inception voltages was greater. On the contrary, at 11.6 kPa a slight increase of the supply voltage above inception resulted in a more rapid PD initiation (i.e. the needle was fluctuating constantly). The PD was more sustained as it was also observed on the oscilloscope screen.

Even though the difference in PDEV results can be explained by using the same argument as the one for the PDIV results, this argument cannot be used to justify the differences between the four cable testing configurations. In both, the balanced and the straight PD detection methods, the four cable testing configurations exhibit slightly different PDIV and PDEV results. Specifically the UB configuration shows a PDIV magnitude difference of approximately 22% from all other configurations at 100 kPa. At 11.6 kPa the difference varies from 5% when comparing UB and GP, 10% when comparing UB and TW and 20% when comparing UB and CG. This difference was verified by repeating experiments using the straight detection method but this time using the LEMKE device.

5.3.2 Phase Resolved PD Magnitude Analysis

With the use of the LEMKE device more PD data was obtained and much faster. The LDS-6 software can acquire and process data automatically and at the same time produce the PD magnitude-phase resolved plots (instead of having MATLAB to produce the plots as it was done using the ROBINSON). As it can be observed from the plots in Figures 5.13 and 5.14 the PD data is much more than the data obtained by using the ROBINSON (look at Figures 5.8 and 5.9 in the previous subsection to compare). These results represent more accurate PD patterns since data was acquired for a period of 120 seconds.

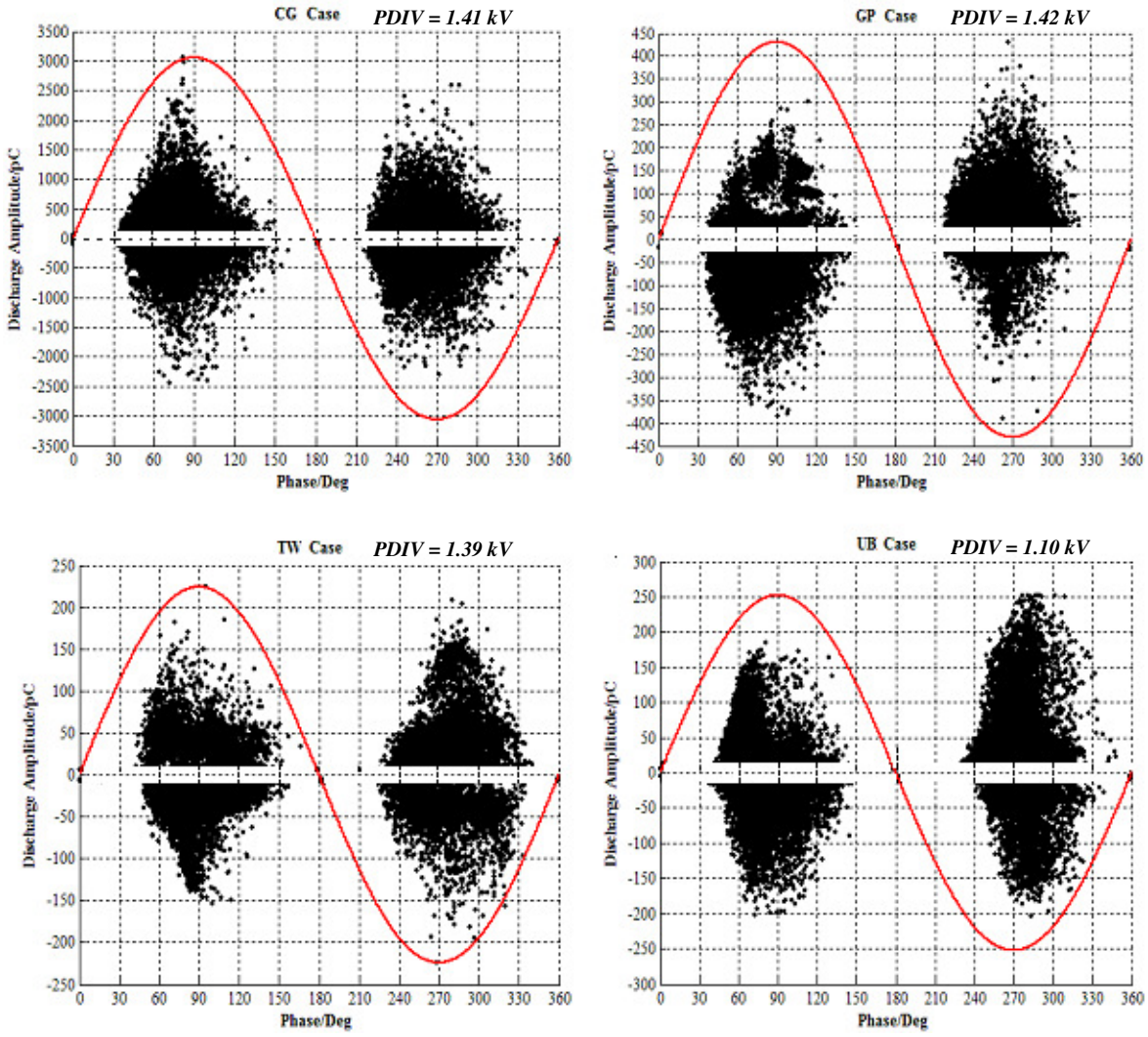

Figure 5.13: PD magnitude-phase resolved plot for the four different cable configurations: CG, TW, UB and GP, at a pressure of 100 kPa. Data obtained using a balanced PD detection circuit and the LEMKE device.

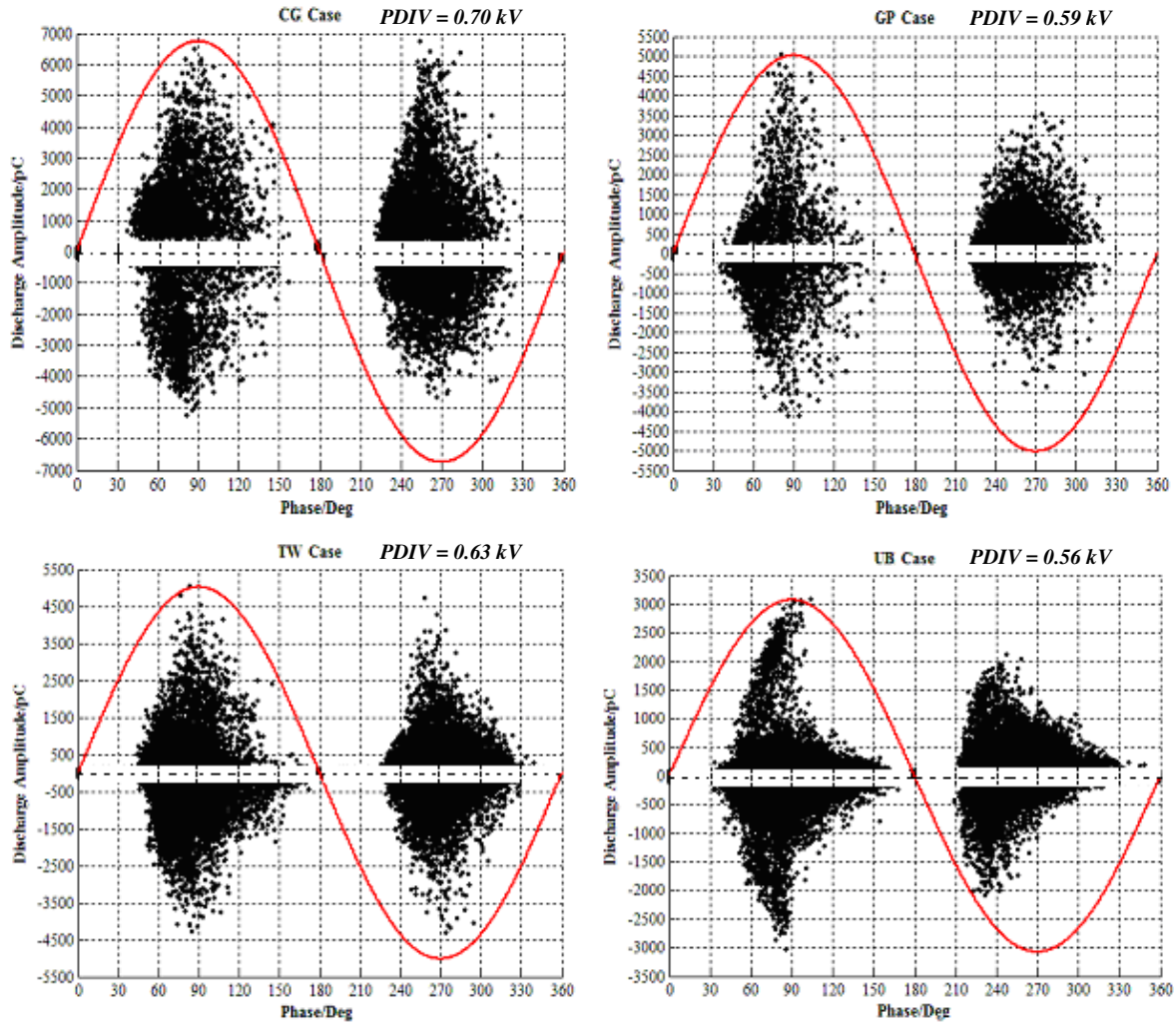

Figure 5.14: PD magnitude-phase resolved plot for the four different cable configurations: CG, TW, UB and GP, at a pressure of 11.6 kPa. Data obtained using a balanced PD detection circuit and the LEMKE device.

The PD magnitude-phase resolved plot of each cable testing configuration, displays several irregularities at 100 kPa and at 11.6 kPa. At 100 kPa the CG case exhibits a much larger PD magnitudes than the other cases. The phases at which PD occurs are very similar for the CG and the GP cases. For the TW and the UB cases there seems to be a small positive phase shift. At 11.6 kPa, PD magnitudes are much larger for all configurations. However, there is still a difference in the maximum PD magnitudes between the cable configurations. The UB case exhibits a negative phase shift as opposed to the rest of the cable configurations which exhibit a small positive phase shift.

In comparison to the graphs in Figures 5.8 and 5.9, which were plotted using MATLAB from data obtained from the ROBINSON, PD starts at a higher phase angle when the LEMKE device was used. This could be due to the fact that the PDIVs determined using the ROBINSON were 10-20% higher than the PDIV determined using the LEMKE device. Even though the actual PDIV was smaller, the voltage was raised to a value which was about 10-20% above inception. Consequently PD initiation occurred at a smaller *dV/dt* and thus at a smaller phase angle. Figure 5.15 illustrates this argument.

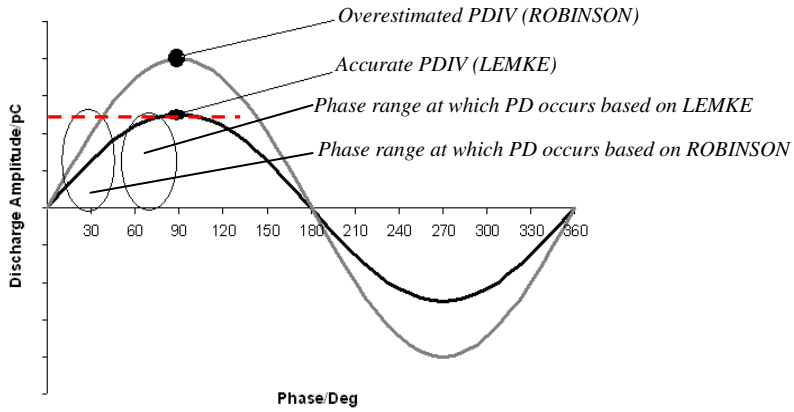

Figure 5.15: Diagram used to explain the difference in PD magnitude-phase resolved plots

A PD test on the UB cable configuration was carried out using the LEMKE PD detector to prove the above argument as shown above in Figure 5.15. In this test the voltage was raised 20% above the average PDIV, to observe how the PD magnitude-phase resolved plot would be affected. The plot is shown below in Figure 5.16.

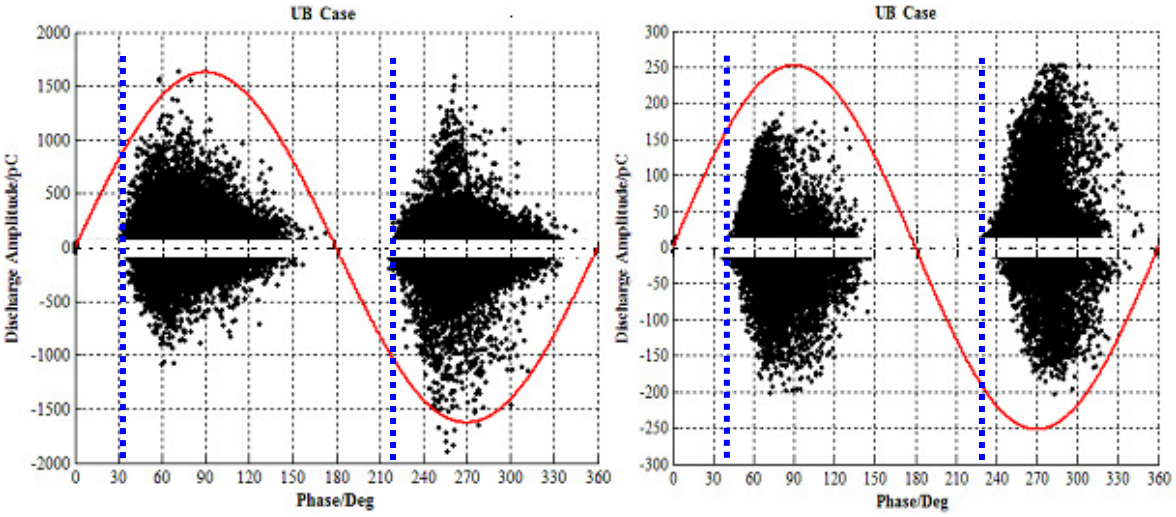

a). b).

Figure 5.16: Comparison of the PD magnitude-phase resolved plots for the UB cable configuration for: a). 10-20% above PDIV and for b). PDIV, using the LEMKE device

The first thing to notice is the difference in magnitude between the two figures. A voltage (20% above inception), causes a huge increase in the PD magnitude resembling the PD magnitudes obtained using the ROBINSON. The second thing to notice is the spreading of PD occurrence at lower and larger phase angles at both the positive and the negative half cycles. The shift of PD discharges at a lower phase is more obvious during the negative half cycle.

Another possible reason for the significant difference in phase angle, between the PD magnitude results obtained by using the straight and the balanced circuit detection methods, could be the fact that a coupling capacitor was not used in the balanced method. PD experiments were repeated using the balanced circuit detection method with the addition of a 1000 pF coupling capacitor, as the one used in the straight detection method. Results are shown in *Appendix B* for the balanced and the straight detection tests using the LEMKE detector. UB case results are shown below in Figure 5.17 to illustrate the phase shift effect with the addition of a PD free coupling capacitor connected in parallel with the testing cable samples.

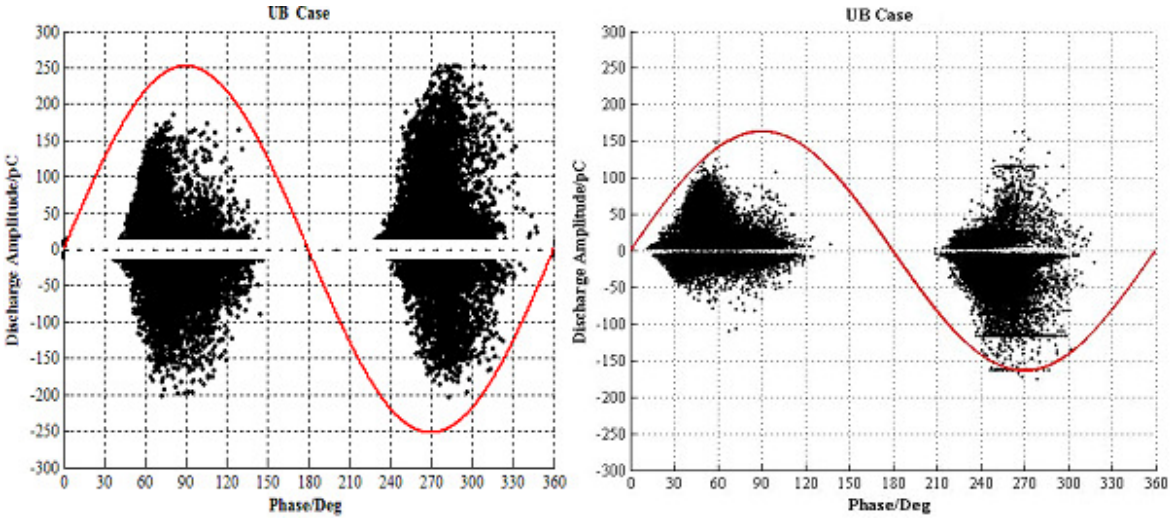

a). b).

Figure 5.17: Comparison of the PD magnitude-phase resolved plots for the UB cable configuration for: a). B/ced detection method without a coupling capacitor and for b). B/ced method with coupling capacitor

From Figures 5.16a and 5.16b a difference can be noticed not only on the phase angle but also on the PD magnitude. The difference in PD magnitudes can be attributed to the difference in inception voltages in the two cases. In Figure 5.17a the PDIV was approximately 1.25kV and in Figure 5.17b, the PDIV was approximately 1.15kV. Arguably it could be said that the PDIV might be lower in the tests in which the coupling capacitor was added to the circuit, due to PD occurring in the capacitor itself, however the whole circuit was tested for PD prior to the tests being carried out.

Concluding, results obtained in this section show that the slightest modification in the test circuit can cause a shift in the phase angle at which PD occurs and this can give misleading conclusions. Thus to compare results gathered by using the balanced and the straight detection methods, it has to be checked that the measured PDIV values are accurate in both cases and also that the testing conditions are identical. The only difference in the test circuit should be the addition of a second cable test sample in the balanced detection case.

In addition it has been shown that the different cable configurations result in different PD magnitude phase-resolved plots. This might be due to different PD

mechanisms taking place. This will be further examined in the next section with the use of certain statistical operators.

5.3.3 Analysis of AC PD Results Using Statistical Operators

After plotting the PD magnitude as a function of phase angle for each cable configuration, the next step was to carry out a comparison of these plots using PD statistical operators. These statistical operators have been established as explained in literature [64], in order to produce unique fingerprints to classify different types of PD defects. The different types of PD, (such as void discharge, surface discharge, corona discharge etc.), have been described in Chapter 2, Section 2.3. The statistical operators are defined in [64, 65] as:

- *Skewness:* A statistical operator used as symmetry or an asymmetry indicator around a mean value. For PD results, *Skewness* could show for example whether the PD data concentrate more to the left of the PD magnitude mean value, if the value of *Skewness* is negative, or more to the right of the PD magnitude mean value, if the value of *Skewness* is positive. If PD magnitude data was equally distributed around the mean, *Skewness* would be zero and the data could be represented perfectly by using a normal distribution. Figure 5.18 shown below, is used to illustrate *Skewness*. The formula to calculate this operator is defined in [64].

a). Positive *Skewness* b). Negative *Skewness*

Figure 5.18: Diagrams used to illustrate positive and negative *Skewness*

- *Kurtosis:* A statistical operator used as a sharpness indicator for the distribution of data. For a normal distribution, *Kurtosis* has a default value of 3. This number is taken into account in the formula given in [64] which is used to calculate *Kurtosis* for PD magnitude-phase resolved data. Furthermore, for a *Kurtosis* value greater than 0, the distribution is sharper than the normal distribution and if it is less than 0, the distribution is flatter. Figure 5.19 shown below, is used to illustrate *Kurtosis* [64].

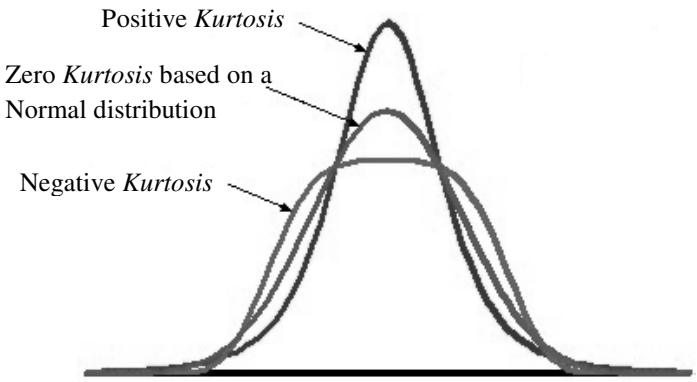

Figure 5.19: Diagram used to illustrate positive and negative "*Kurtosis"*

- *Asymmetry:* A statistical operator used as a differential indicator for the PD magnitudes, (either peak or mean pulse height), occurring in the positive and the negative half cycles of the supply voltage [66]. The formula for calculating the *Asymmetry* can also be found in [64].

- *Cross Correlation:* A statistical operator used as an asymmetry indicator for the PD discharge distribution pattern, during the positive voltage half cycle and the negative half cycle. If the two patterns are identical then the *Cross Correlation* is 1. If the two patterns are dissimilar, then the *Cross Correlation* approaches 0 [66].

Using the above statistical operators, the differences in the discharge mechanisms and the insulation defects in each cable configuration that was tested for AC PD, can be identified. Statistical operators can be calculated for the mean pulse height distribution

(mean PD magnitude in each phase window as a function of phase angle '$H_{qn}(\varphi)$'), for the maximum pulse height distribution (peak PD magnitude in each phase window as a function of phase angle '$H_{qmax}(\varphi)$') and for the pulse count distribution (PD number in each phase window as a function of phase angle '$H_n(\varphi)$'). A better description of these distributions and information on how they are calculated, can be found in [65, 67]. In Figures 5.20-5.22 which are shown below, *Skewness (Sk)*, *Kurtosis (Ku)* and *Cross Correlation (CC)*, were plotted for the four different cable configurations (*CG, GP, TW and UB*) when tested at 100 kPa and at 11.6 kPa.

It was not required to perform any calculations to produce the distributions since the data used to construct the graphs shown below in Figures 5.20-5.22, were taken from the LEMKE software. These figures can be used as a fingerprint to recognise different types of PD. Data was recorded using the LEMKE LDS-6 PD detector for positive and negative half cycles. *Sk +ve* is the *Skewness* for the positive half cycle and *Sk -ve* for the negative half cycle, (similarly for *Kurtosis* which is symbolised as *Ku +ve* and *Ku -ve*).

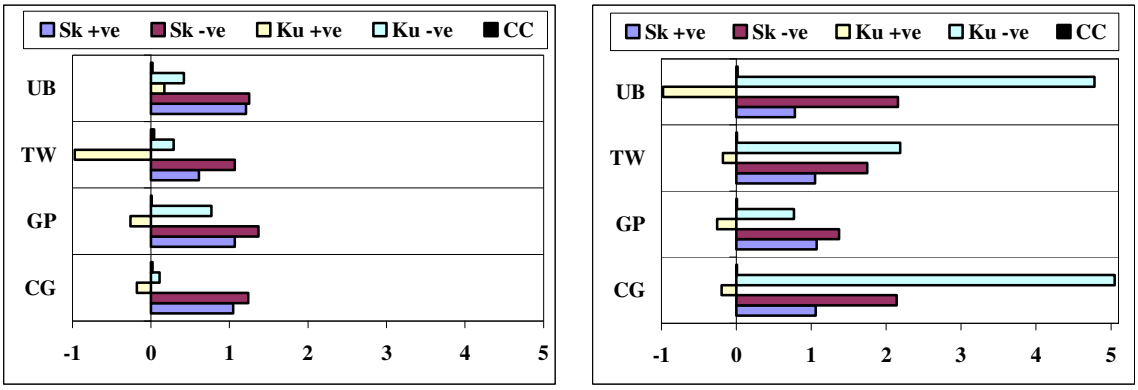

a). Atmospheric pressure: 100 kPa

b). Low pressure: 11.6 kPa

Figure 5.20: Statistical operators for mean PD magnitude against phase angle, $H_{qn}(\varphi)$

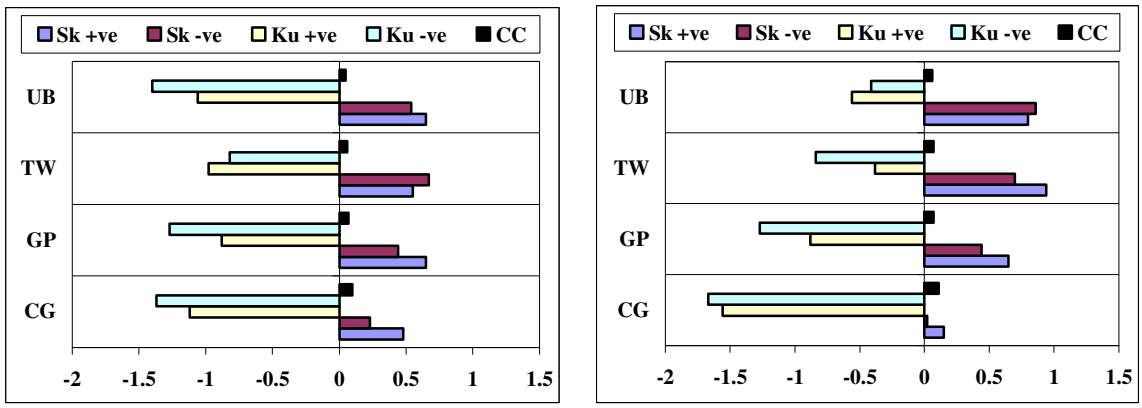

a). Atmospheric pressure: 100 kPa b). Low pressure: 11.6 kPa

Figure 5.21: Statistical operators for peak PD magnitude against phase angle, $H_{qmax}(\varphi)$

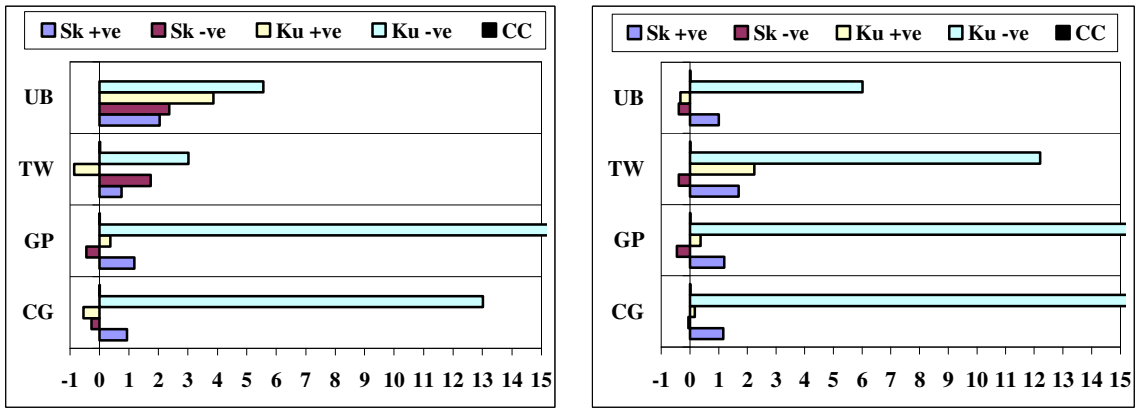

a). Atmospheric pressure: 100 kPa b). Low pressure: 11.6 kPa

Figure 5.22: Statistical operators for PD number against phase angle, $H_n(\varphi)$

Based on [68] a PD fingerprint exhibiting positive values of *Skewness* (when analysing the discharge magnitude as in Figures 5.20 and 5.21), is an indication of discharges taking place in multiple cavities within the insulation. On the other hand if *Skewness* is very near zero or if it is negative, this is an indication of surface discharges, or narrow cavity, or treeing discharges. As far as *Kurtosis* is concerned, if this is negative (when analysing the PD number as in Figure 5.22), this is again an indication of treeing or multiple cavities. If *Kurtosis* is positive then discharges will occur in *"single discharge sites"* [68]. In addition if the *Cross Correlation* is near zero (when analysing the discharge

magnitude as in Figures 5.20 and 5.21), the cavity present is *"electrode-bounded"* [68]. If the *Cross Correlation* is large this is a sign of surface discharges taking place.

Using Figures 5.20-5.22, test results obtained for each configuration, can be compared at 100 kPa (atmospheric pressure at sea level) and at 11.6 kPa (at an altitude of 50,000 feet). From Figures 5.20 and 5.21 it can be observed that *Skewness* results are positive for both pressure levels. Thus, both distributions $H_{qn}(\varphi)$ and $H_{qmax}(\varphi)$ have an asymmetry to the left when compared to a normal distribution. From Figure 5.22, all *Kurtosis* results are positive during the negative half cycle indicating that $H_n(\varphi)$ distribution is relatively sharp. In general, at 11.6 kPa the distributions for all configurations are sharper than at 100 kPa. During the positive half cycle, CG and GP configurations have very small *Kurtosis* values and their distributions are very close to a normal distribution. UB has a sharper distribution at 100 kPa whereas TW has a sharper distribution at 11.6 kPa. *Cross Correlation* for all figures indicates that both positive and negative half cycles exhibit distinct patterns.

On the basis of this information gathered from the literature [68], when looking at Figures 5.20 and 5.21 it is obvious that the *Skewness* results at both 100 kPa and 11.6 kPa, are showing that there is a high possibility of discharges occurring in multiple voids/cavities under all different testing configurations. *Kurtosis* results are showing that for TW and CG configurations at 100 kPa, discharges in multiple cavities might be occurring during the positive half cycle of the test voltage. On the contrary *Kurtosis* is positive for UB and GP increasing the probability of single discharge sites being present. It is also worth noticing that even though *Kurtosis* is positive for GP, its value is very near to zero compared with the UB case. During the negative half cycle discharges are limited to single discharge sites for all configurations. *Cross Correlation* results indicate that all the discharges occurring are most likely to be electrode-bound. When discharges are electrode-bound, they occur between a conductor-insulation boundary between which an airgap exists, which could be from the outer surface of the conductor to the inner surface of the insulation, or from the outer surface of the insulation to the earthed/grounded conductor.

When carrying out tests to determine PDIV values for different configurations, it is not important to examine what PD mechanisms are taking place. The only thing that matters is to determine which configuration results in the lowest PDIV to be on the safe side. However, PD analysis using the statistical operators can provide information on the PD mechanisms taking place. Furthermore from this information, the effect that the geometry of the cable system has on the PDIV can help to understand the behaviour of the system. At the beginning of this chapter it has been mentioned that when testing for PDIV for unscreened cables, all three types of discharges (cable to cable, cable to ground and void discharges), must be examined. This is because each type of partial discharge has a different inception voltage (PDIV). From tests carried out so far, the cables have been tested for PD between the cable and the ground and for void discharges. The analysis leads to the conclusion that electrode-bound airgap discharges occur at lower inception voltages than dielectric bound (void) airgap discharges for the pressure levels taken into consideration (100 kPa and 11.6 kPa). This also supports the results obtained in Chapter 3, where it was concluded that external airgap discharges occur at lower voltages than internal void discharges.

5.3.4 Average PD Repetition Rate

A parameter that also needs to be investigated is the PD Repetition Rate (*RR*). This quantity together with the PD magnitude plays an important role in determining the ageing of cable insulation [69]. These quantities affect the energy released in the insulation when PD takes place. The aim of this section is to make a comparison of the average *RR* obtained for all cable testing configurations when the PD inception voltage is reached and also at 20% above the inception voltage. In addition the results shown on Table 5.2 are going to be used in Chapter 6 to compare the PD rates when an AC and a DC voltage are applied across the cable test samples. It has to be noted that in these tests, the coupling capacitor was also included in the test circuit as it was included when the ROBINSON detector was used.

TABLE 5.2

AVERAGE PD REPETITION RATES FOR DIFFERENT CABLE TESTING CONFIGURATIONS: BY USING THE STRAIGHT DETECTION METHOD AND THE LEMKE PD DETECTOR AT 100 AND 11.6 kPa

Pressure	**Cable Configuration**	**Average PD Rate (PD/s) at Inception Voltage** **LEMKE – Straight PD Detection Method (including coupling capacitor)**	**Average PD Rate (PD/s) at 20% above Inception Voltage** **LEMKE – Straight PD Detection Method (including coupling capacitor)**
100 kPa	*CG*	*338*	*616*
	TW	*311*	*3783*
	UB	*203*	*476*
	GP	*118*	*1712*
11.6 kPa	*CG*	*146*	*168*
	TW	*244*	*812*
	UB	*189*	*406*
	GP	*315*	*658*

The LEMKE straight detection method was used to gather PD rate results, because by using the balanced circuit detection method, the data obtained would include information from discharges coming from both cable samples which were connected in parallel. The PD magnitude phase-resolved plots from the straight detection using the LEMKE device are shown in the appendix B.

Generally as it can be observed from the above table, the PD rate for each configuration at either the inception voltage or 20% above inception at 11.6 kPa, is lower with the exception of the GP case. In this case the PD rate is higher at 11.6 kPa. Furthermore, as expected the PD rates are larger at 20% above the PDIV. It is also worth mentioning that the GP configuration at the PDIV has a lower PD rate at 100 kPa than the UB configuration. However at 11.6 kPa, the GP configuration exhibits a higher PD rate than the UB configuration. The discussion is focused on the comparison between these two configurations because these configurations replicate in practice an actual aircraft electrical harness.

5.3.5 Summary of AC PD Results

The four different configurations that have been tested for PD seem to be undergoing a similar type of discharge. This happens even though the relevant magnitudes of the statistical operators vary from one configuration to the other. This might be due to the fact that different cable specimens of the same type were used to test the different configurations. There is a high probability that different cavity sizes exist between the stranded conductor and the inner insulation surface of the aerospace cable, or between the external insulation surface and the ground. Furthermore partial discharges of this type occur at lower voltages than dielectric bound discharges i.e. void discharges within the insulation.

It is also known from [5] that at high pressures (100 kPa at sea level), discharges occur at smaller airgap distances *'X'* mm. Thus if the system is operating at a lower pressure (at 11.6 kPa at 50,000 feet) and the cable configuration is as such that the maximum airgap distances are *'X'* mm, then discharges will occur at higher supply voltages. Thus the unscreened cables have to be configured so as to provide the necessary (possible in practice), airgap distances to obtain the lowest PDIV. Results show that the screened cable case (UB), provides the necessary airgap distances to test for PDIV at 100 kPa and at 11.6 kPa. This conclusion is drawn from the fact that at 100 kPa the inception voltages for the UB case, is the lowest. In addition, at 11.6 kPa PDIVs for UB and GP are approximately equal, with the GP case covering a larger range of airgap distances (0.05 mm up to 40 mm), between the outer insulation surface and the ground plane. As the UB cable configuration was examined, the airgap distance range from the outer insulation to the grounded braid varied approximately from 0.10 mm up to 0.40 mm. This depended on how tightly the braid was held around the insulation. Further work is required because it might be the case that at pressures lower than 11.6 kPa the airgap distance is not large enough to give the lowest possible PDIV.

At 11.6 kPa PDIV magnitudes for GP and TW have a difference of 4 % to 7% respectively, when compared with the UB case. The only exception is CG which is about 25% larger with respect to UB. At 100 kPa the PDIVs for all configurations are about 28%

larger with respect to UB. The PDIV magnitudes for all cases at 100 and at 11.6 kPa are again shown below in Table 5.3.

TABLE 5.3
AVERAGE PDIV FOR DIFFERENT CABLE TESTING CONFIGURATIONS: BY USING THE STRAIGHT DETECTION METHOD AND THE LEMKE PD DETECTOR AT 100 AND 11.6 KPA

Configuration	***PDIV at 100 kPa (kV)***	***PDIV at 11.6 kPa (kV)***
CG	*1.41*	*0.70*
TW	*1.40*	*0.63*
GP	*1.42*	*0.59*
UB	*1.10*	*0.56*

As far as the PD magnitudes are concerned, there is a significant difference between the different cable configurations. This statement applies at 100 kPa as well as at 11.6 kPa. With the exception of CG case, which shows a peak PD magnitude of 3000 pC, all the other cases have a peak magnitude less than 450 pC. At 11.6 kPa PD magnitudes are much bigger than at 100 kPa. For the CG case the peak magnitude doubles at 116 kPa whereas for all other cases the magnitudes increase tenfold. At both pressures there is a significant variation in the PD magnitudes when comparing the different configurations. PD rates differ especially for the GP case, where the rate is significantly larger at 11.6 kPa. This is an important result. For example for the GP case, this result shows that at 11.6 kPa, if the cable is operated at the inception voltage the cable insulation will age faster than at 100 kPa because of the larger PD magnitudes and the larger average PD rates.

Concluding from the results from this chapter, the different cable testing configurations undergo similar discharge processes when the voltage is raised up to the partial discharge inception voltage (PDIV). There is variation in the PD magnitudes but this might be due to the slight variation in PDIVs when comparing all four cable configurations. As far as the inception voltage is concerned, the configuration giving the lowest inception voltage at 100 as well as 11.6 kPa should be used to test the cable. At 100 kPa the configuration resulting in the lowest inception voltage is the UB case (which is

currently the method used in the standard [30]). At 11.6 kPa both UB and GP cases should be used. One advantage of the UB case is the fact that the whole of the insulation across the length of the cable is being tested for defects, since the screen uniformly surrounds the insulation in a relatively symmetric manner. In all other configurations only part of the outer cable insulation surface touches the grounded conductor and thus some defects might not be spotted and identified.

5.4 Calculated and Measured PDIV Comparison

A comparison is made in this section on the calculated PDIV results of different cables obtained using the methods explained in Chapter 3 and the PDIV results obtained from PD experimental tests as shown previously in Section 5.2. It has to be noted that 20% of the insulation of the cable tested in the previous sections consists of Polyimide according to [70]. For the calculations it has also been assumed that the cable has only one PTFE insulation layer uniformly distributed around a solid conductor, instead of a stranded conductor, to compare the effect of adding Polyimide.

The comparison of measured and calculated results is shown in Figures 5.23 and 5.24 for a pressure of 100 kPa and 11.6 kPa respectively. Colour codes are used to distinguish between the PDIV measured results of the different cable configurations. The black dashed line represents the calculated PDIV value based on a cable to plane discharge with a single PTFE insulation layer. The black dotted line represents the PDIV calculated value if 20% of the insulation thickness consists of Polyimide insulation and 80% consists of PTFE insulation (i.e. two different layers of insulation). It has to be noted that interfacial effects are not taken into consideration in the calculations. This is an area requiring further research.

It must be mentioned here that the cables have been tested at 100 kPa and at 11.6 kPa at an ambient temperature of 20 ^{o}C. These parameters have also been used to calculate the PDIV based on a void discharge within the cable insulation and an external airgap discharge, between the insulation and the ground. In order to calculate the inception voltage for a void discharge a coaxial field model was used (i.e. outer insulation fully

screened), and the void had to be determined. Since the void size is unknown, PDIV has been calculated for a range of void sizes to observe the effect of the void size.

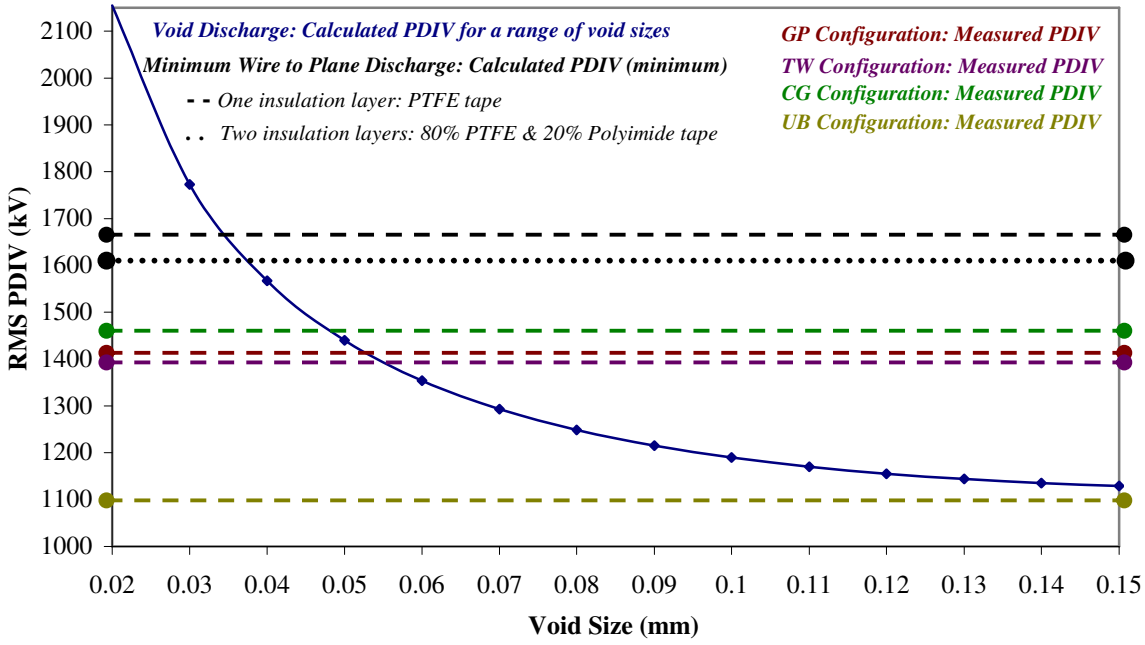

Figure 5.23: Comparison of measured and calculated PDIV results for the four different cable configurations that have been tested at 100 kPa (Altitude: Sea level)

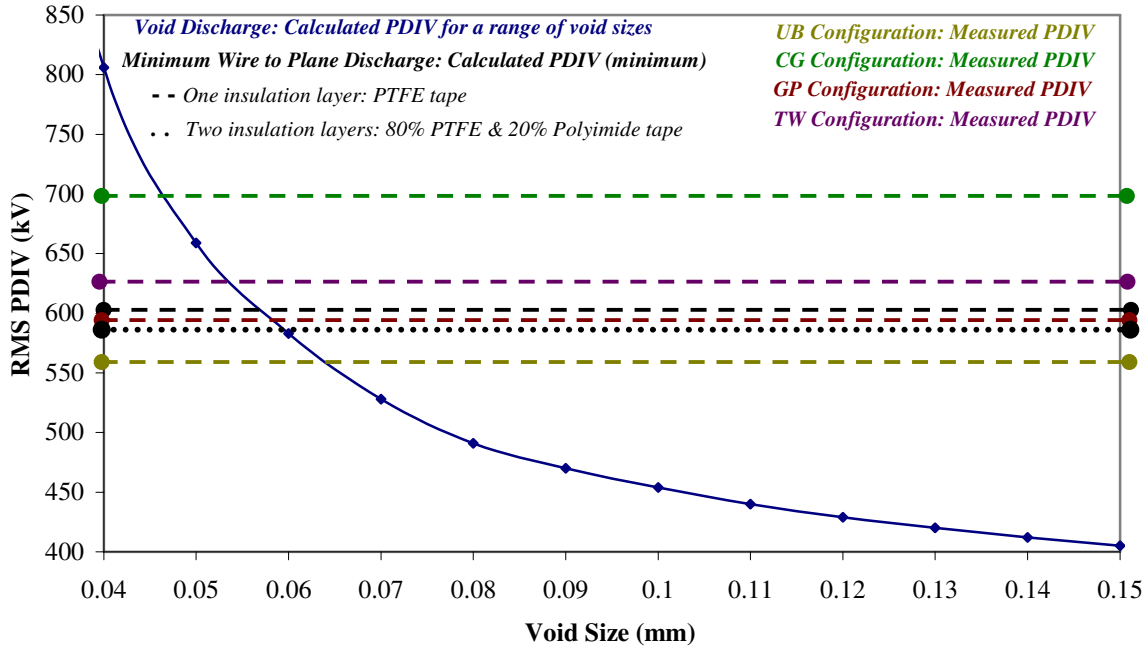

Figure 5.24: Comparison of measured and calculated PDIV results for the four different cable configurations that have been tested at 11.6 kPa (Altitude: 50,000 feet)

It is obvious from the results that at low pressure (11.6 kPa), the calculated PDIV values based on external airgap discharges, are more close to the actual measured PDIV values rather than at 100 kPa. At 11.6 kPa, the GP configuration measured results are closer to the calculated ones than any other configuration. It is questionable however, as to whether the discharges taking place when the experiments are carried out are due to external airgap discharges or void discharges. Analysis on statistical operators suggests that electrode bound discharges are taking place (i.e. airgap discharges), but this requires further investigation. Further experiments have to be performed on more cables of different type, consisting of different insulation materials and dimensions, to determine if voids are present.

In order to obtain a better comparison of calculated and measured results more cables have been tested. Due to time restrictions and limited equipment availability only another four types of cable were tested using the LEMKE straight detection method under the UB configuration. One of these cables was also tested under the GP configuration. Results are shown in the table below including the results for the GP and UB cases which have been shown in Figures 5.23 and 5.24. The calculated PDIV values are based only on external airgap discharges since the size of voids within the insulation is unknown.

TABLE 5.4

COMPARISON OF AVERAGE MEASURED RMS PDIV RESULTS AND CALCULATED PDIV RESULTS USING UNIFORM FIELD EQUATION MODELS AS IN CHAPTER 3

Cables	Insulation materials	Insulation Thickness (mm)	Conductor Radius (mm)	Cable Configuration	Measured RMS PDIV (kV) at 100 kPa	Measured RMS PDIV (kV) at 11.6 kPa	Calculated RMS PDIV (kV) at 100 kPa	Calculated RMS PDIV (kV) at 11.6 kPa	Percentage Difference (%) at 100 kPa	Percentage Difference(%) at 11.6 kPa
A	PTFE, $\varepsilon_r = 2.1$	0.23	1.04	GP	1.42	0.65	1.60	0.58	12.68	-10.77
	Polyimide Tape, $\varepsilon_r = 3.4$	0.06		UB	1.07	0.59			49.53	-1.69
				T P	2.45	0.84	2.37	0.79	-3.27	-5.95
B	Cross-linked extruded polyalkene, $\varepsilon_r = 2.25$	0.55	1.06	GP	1.96	0.78	2.33	0.77	18.88	-1.28
	Cross-linked extruded polyvinylidene fluoride, $\varepsilon_r = 3$	0.01		UB	1.29	0.94			80.62	-18.09
C	PTFE, $\varepsilon_r = 2.1$	0.30	1.83	UB	1.06	0.58	1.70	0.63	60.38	8.62
	Polyimide Tape, $\varepsilon_r = 3.4$	0.03								
D	PTFE, $\varepsilon_r = 2.1$	0.20	2.75	UB	1.87	0.80	1.91	0.67	2.14	-16.25
	Fibreglass Tape, $\varepsilon_r = 6.5$	0.45								
	Polyimide Tape, $\varepsilon_r = 3.4$	0.04								
E	PTFE, $\varepsilon_r = 2.1$	0.31	6.20	UB	1.68	0.83	2.28	0.76	35.71	-8.43
	Fibreglass Tape, $\varepsilon_r = 6.5$	0.53								
	Polyimide Tape, $\varepsilon_r = 3.4$	0.03								

Results in Table 5.4, show that the measured and the calculated RMS PDIV values at 11.6 kPa have an average percentage error of about -6.73%. At 100 kPa the average percentage error is about +32.08%. Cable D case appears to have the biggest percentage

error at 11.6 kPa but the smallest percentage error at 100 kPa. Four out of five cables that have been tested exhibited a negative sign on the percentage difference values, indicating that calculated PDIV results are smaller in magnitude than the actual measured results. (The exception is Cable C case). This leads to the argument made in Chapter 3, that uniform calculations provide rather conservative results. However at 100 kPa, all cables tested exhibit positive percentage difference values. This is a result which requires further investigation. More tests have to be carried out on different cable samples having different insulation thicknesses, different number of insulation layers and conductor sizes. The ideal case would be if many cable samples of the same type were available for testing, in different conductor sizes and insulation thicknesses. This way it would be possible to examine how the percentage difference varies with insulation thickness and conductor size. The drawback in this situation is the fact that different cable sizes of the same cable type are more probably to be composed of different insulation materials or having extra layers of different insulation due to mechanical considerations.

Comparing cables A and B, it can be observed that the GP configuration has smaller percentage differences at high pressure and at low pressure with the exception of cable A, when tested at 11.6 kPa under the UB configuration (-1.69%).

The TP configuration (twisted pair of cables of the same type) has a higher measured and calculated PDIV than the UB and the GP configurations. This is due to the presence of double the insulation thickness between the cable conductor connected at high voltage and the cable conductor connected to ground. The percentage difference is very small in both cases, when the pressure is 100 kPa and 11.6 kPa. PDIV results support the conclusion made in Chapter 3, which states that doubling the insulation thickness does not result in a double PDIV. At 100 kPa only PDIV tests using the GP configuration satisfy this conclusion. However at 11.6 kPa both configurations satisfy this conclusion.

It has to be noted that the accuracy of the calculated values depends on the values of relative permittivity of each insulation material which have been used in the uniform field equations. These values have been taken from literature and from cable specification datasheets. In addition the equations used do not take into account any interfacial/space charge effects as described in Chapter 2. The calculations used in Chapter 3 were used in

combination with Paschen's Law. Thus, it might also be the case that the percentage error is due to the Paschen's' Law data which was used in the calculations.

5.5 Summary

To begin with, a straight detection circuit for measuring PD at 100 kPa and at 11.6 kPa was constructed and the cables tested in different configurations. The model of the PD detection instrument which was used was called 'ROBINSON' type 700-Model 5. Furthermore a balanced PD detection circuit was used to reduce external noise and to compare and verify results. The instrument used in the balanced circuit detection method was the LEMKE LDS-6. PDIV and PDEV Results obtained with this model were different and thus the experiments using the straight detection method were repeated with the digital LEMKE model, to verify the PD results.

The aerospace cables have been tested in different configurations such as wrapping the cable around a hollow cylindrical grounded conductor (CG), laying the cable on a flat grounded plane (GP), having a bare cable wrapped around the insulated cable (TW) and finally adding a braid around the cable insulation (UB). In the last configuration, heat shrink insulation was also added to make sure the braid was held tightly around the cable insulation. Tests aimed to show the best way of testing cables for the aerospace industry based on practical applicability, on the lowest PDIV and on the consistency of the results.

PD magnitude-phase resolved plots and statistical operators (*Skewness, Kurtosis and Cross Correlation*) have been analysed to determine whether the discharges occurring in each configuration were in the airgap, or within a void in the insulation. In addition PD rates have been compared for all configurations. Finally measured and calculated PDIV results for different cable types have been compared using the UB and the GP configurations. It must be emphasized at this point, that in practice the voltage ratings should be based on the lowest PDEV. However, PDEV cannot be calculated using theoretical models. Thus PDIV values have been used for comparison.

In the next section DC PD tests are carried out to determine PDIV magnitudes, PD rates and PD magnitudes to compare them with the AC PD test results.

The phenomena associated with PD as well as PD testing, are very well understood for AC power systems on the ground. Even so, a Standard (BS EN 3475-307) [59] exists which describes the method for preparing aircraft cables for PD testing. It is not mentioned in literature why the method used in it for testing screened and unscreened cables is identical.

If you screen a cable, the cable is tested for PD either within the cable insulation for voids, or for PD occurring in the very small airgap between the outer insulation surface and the screen. However, according to Paschen's Law (also mentioned by Dunbar [5]), at a lower pressure, PD is most likely to occur with a relatively larger airgap distance. If the cable is to be installed without a screen, the airgap distances will certainly be much bigger than the airgap distance when the cable is screened.

Thus, the novelty of the work done in Chapter 5 is the testing of aircraft cables laid out in different configurations and the comparison of PD results including the PDIV with the configuration described in the Standard BS EN 3475-307. From the results it was concluded that the method of screening the cables according to the Standard, is satisfactory for a pressure as low as 11.6 kPa (up to an altitude of 50,000 feet). This was due to the fact that this method resulted in the lowest PDIV with a relatively low standard deviation of results.

What further needs to be examined is the case of aircraft flying at higher altitudes, where the pressure is lower than 11.6 kPa. In addition, analysis of PD results support the argument made in Chapter 3, that PD on unscreened cables at 11.6 kPa occurs outside the insulation, rather than inside the insulation within a void. A direct comparison of measured PDIV results with calculated PDIV results using the methodology in Chapter 3 was also carried out. From this comparison, the argument stated in Chapter 3, that calculations provide a conservative result, was confirmed. A comparison as such has not been found in literature.

Chapter 6

DC Partial Discharge Tests

As mentioned in Chapter 1, DC voltages used in aircraft electrical systems have increased through the years from 14.25 V in 1936 up to +/-270 V (540 V) up to date, due to the increase in the electrical power demand. Increased DC voltages are accompanied with an increased risk of DC partial discharges (PD). Since there is a lack of understanding of PD processes occurring under a DC voltage in an aircraft environment, research has to be carried out to investigate DC PD processes. PDs occurring under a DC rather than an AC supply voltage differ in PD magnitude and repetition rate (RR). As described in the previous chapters, under AC conditions the electric field distribution across the cable conductor and the insulation and across the airgap and the ground is determined by the relative permittivity of the materials, whereas under DC conditions the electric field is determined by the conductivity. Tests have been carried out, as they are explained in this chapter, to evaluate the differences between AC and DC PD results on specific unscreened aerospace cable having PTFE insulation with a small inner layer of polyimide tape. The same cable samples and configurations were used for testing as in chapter 5 (UB and GP).

6.1 Introduction

The principles for DC PD measurements are the same as for AC PD based on [50] and the straight detection circuit can be used in this case as well. However it is much more difficult to detect DC PD due to the fact that the repetition rate (RR) is very small compared to the AC case. Whilst RR, under AC conditions is governed by the frequency of the high voltage

applied (discharge reoccurs every half cycle) [19, 20], for DC it is dependent on the time constant 'τ' of the charging airgap or internal cavity, as given in Equation 2.22, in Chapter 2. The equation is shown again in Figure 6.1a together with the dielectric circuit used to analyse DC PD. The symbols used in the equation represent the electrical parameters shown on the dielectric circuit. Figure 6.1b shows a plot of the voltage across the cavity in the dielectric. All the diagrams shown below are taken from Morshuis and Smit [20].

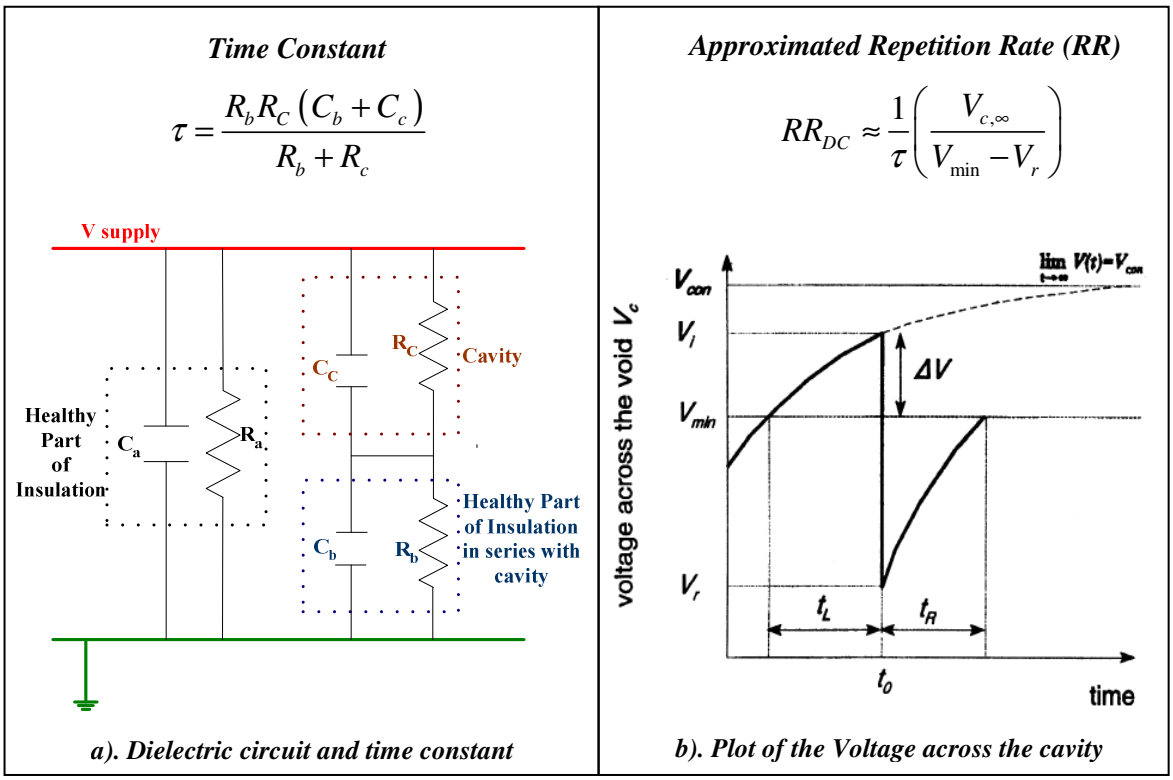

Figure 6.1: Figure showing a). Dielectric circuit used to analyse DC PD and b) Rough sketch of the voltage across the cavity Vs time. Diagrams include the equations for τ of the charging cavity and the *RR*

Because τ is very large, the time it takes for the voltage across the cavity to rise above the breakdown voltage of air in the cavity is also large. Consequently RR_{DC} can be as low as one discharge per minute [20]. The time at which this discharge occurs is also very random and this phenomenon makes the detection much more difficult and the whole test more vulnerable to external noise interference. Regarding DC PD magnitudes, these are dependent on the overvoltage 'ΔV' and the steepness of the overvoltage as shown in

Figure 6.1b [32, 71]. The larger the ΔV and the higher steepness, the larger the PD magnitude will be. ΔV is dependent on the statistical time lag 't_L'. The larger the t_L the larger the ΔV will be. According to Fromm [71], for DC voltages t_L can be several tens of ms, whereas for AC voltages t_L could be a maximum of 0.1 ms for Townsend discharges. However, the steepness of the AC overvoltage is several orders of magnitude bigger than the DC overvoltage resulting in much larger PD magnitudes.

6.2 External Noise Interference

Under AC conditions the PD occurs at specific points in time during the positive and the negative half cycle where dV/dt is the largest. In addition, PD magnitudes (*q in pC*) coming from the test samples are much larger than the Pico-coulomb values observed on the LDS-6 monitor, due to the propagation of noise through the testing circuit to the PD detector. It has also been shown in Chapter 5 that PD occurs in a certain phase range, during the positive and the negative half cycle. Thus, under AC conditions it is easy to distinguish the actual PD signals coming from the cable test samples, from external noise interference.

Under DC conditions it is very difficult to discriminate the actual PD signals. For example PD could occur at least once every minute. If during that time the lights are switched on in the laboratory, it would not be possible to determine whether the spike on the PD monitoring screen is due to an actual PD from the testing specimen, or whether it is caused from a voltage fluctuation from the mains, or from higher frequency noise signals in the area. In addition, at the inception voltage DC PD magnitudes can be very small (a maximum of 5 pC), compared with the AC PD magnitudes (several hundreds of pC). Thus, PD magnitudes cannot be used to distinguish the actual PD from external noise. Figure 6.2 shows all the possible noise sources from the testing circuit that was used.

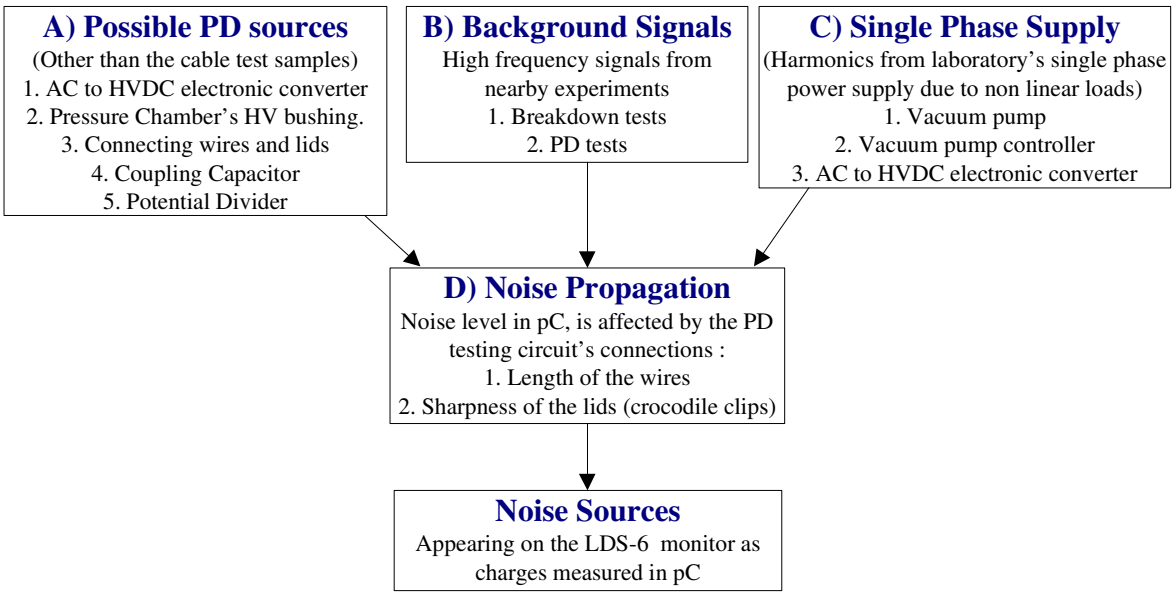

Figure 6.2: Possible sources of noise that manifest as a PD signal which is measured in Pico-Coulombs on the LDS-6 monitoring screen

In order to minimise the possible sources of noise, a balanced circuit was used to reduce background noise signals and possible harmonics coming from B and C as shown in Figure 6.2 above (noise level was reduced down to 2-4 pC). In addition the length of the connecting cables was reduced and any sharp connections were smoothed to account for D shown in Figure 6.2, to reduce the level of noise propagation.

6.3 Balanced PD Detection Circuit-LEMKE

Even though with the use of the balanced circuit (shown in Figure 6.3) background noise was reduced down to 2 - 4 pC, it was observed that interference from switching on the lights in the laboratory or interference coming from other test rigs in the area (mainly material breakdown test rigs), was still affecting the DC PD monitoring system. The only way to avoid this problem is to install the whole test rig in a grounded metal container. Due to time restrictions these actions were not carried out but instead the tests were carried out in times where no other tests were running in the laboratory. In addition tests were carried out to observe the magnitude and the shape of the false PD signals seen on the monitoring screen due to external interferences. For example it was observed that by switching on/off the lights a 3 -5 pC PD magnitude could be observed on the monitoring screen. When

breakdown tests were being carried out in the laboratory, every time there was a test sample breakdown, the false PD magnitude that was observed on the screen was again 5 pC. This way it was made easier to distinguish whether the data observed on the screen was false or whether the data was coming from PD occurring on the cable sample being tested.

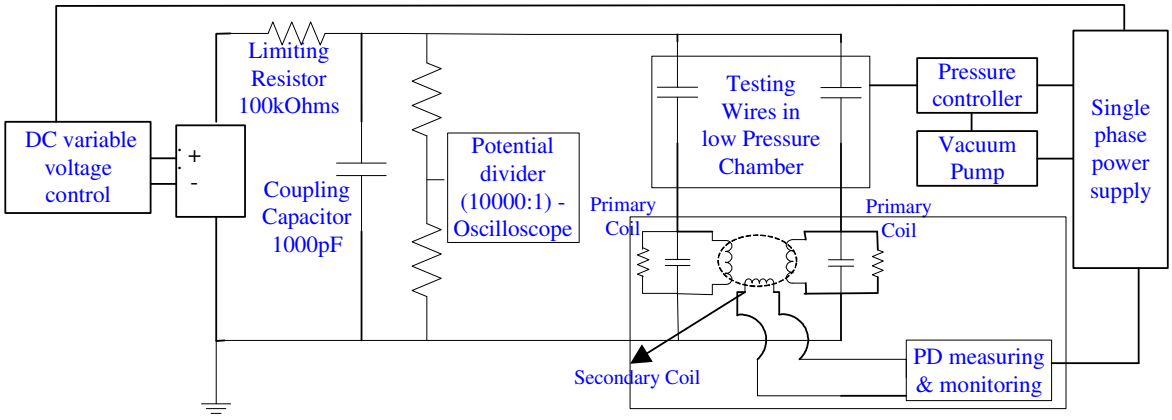

Figure 6.3: PD balanced detection circuit based on [30] with the addition of a vacuum chamber and a vacuum pump controller

6.3.1 Description of Testing Procedure

6.3.1.1 LABVIEW software development

DC PD tests were performed for the two different configurations GP and UB, at both high pressure (atmospheric pressure: 100 kPa) and at low pressure (50,000 feet: 11.6 kPa). Software was developed in LABVIEW to step up the DC voltage to determine the PDIV and then to step it down in order to determine the PDEV. The software was developed so that the step-up and the step-down voltages could be varied, as well as the time interval/delay (TD) between the voltage step changes at which the DC voltage was held constant at a specific level. Ideally a ramp should be used to determine the PDIV instead of using a step voltage to avoid the fast changes of voltages (high dV/dt) which can result in large PD spikes. However, even though a ramp function was firstly incorporated for the PD tests, it was observed that the voltage did not rise smoothly. Instead, it was kept constant

for a certain period of time and then rose in steps of 80 Volts. This was either due to the software not functioning properly, or due to the response of the AC to HVDC converter to the software.

As mentioned, during voltage step changes there is a high dV/dt. After a certain voltage level this high dV/dt can result in PD spikes as it will be observed in the figures that will be shown later on. In order to avoid the effect of the step changes the step-up and the step-down voltage was set at approximately 80 V. This was the step value observed when the ramp function was used. Furthermore the time delay (TD) was set at 120 seconds. Figure 6.4 shows a general preview of the test voltage generated using the LABVIEW software.

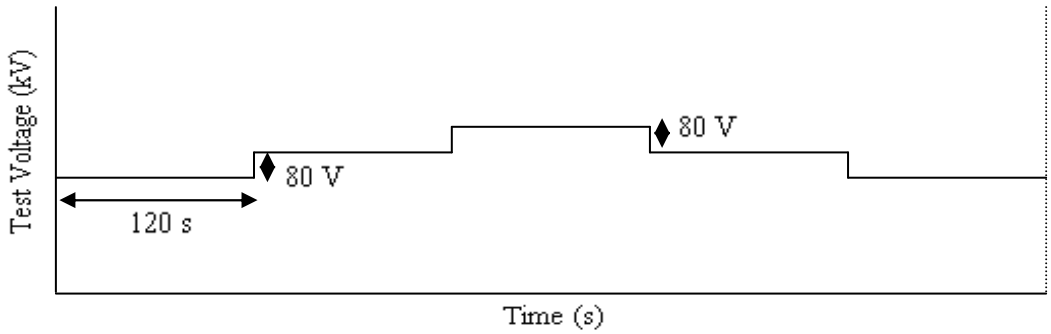

Figure 6.4: General preview of the test voltage applied across the test samples using the balanced PD detection method under DC conditions

The test voltage shown in Figure 6.4 was applied onto the test cable samples in a UB and in a GP configuration, at 100 kPa and at 11.6 kPa. Furthermore the tests were repeated using a different step-up and step-down voltage.

6.3.2 DC PD Results and Analysis

Figures 6.5 and 6.6 show the DC PD results of the GP and UB cable configurations at 100 kPa when the step voltage is 80 V. The GP case at 100 kPa is symbolised as GPHP and at 11.6 kPa it is symbolised as GPLP. Similarly UB at 100 kPa is symbolised as UBHP and at 11.6 kPa UBLP. It has to be noted that the starting voltage for all experiments was 0 V. However all figures shown below are a snapshot focusing at the voltage levels at which PD activity was observed on the monitoring screen.

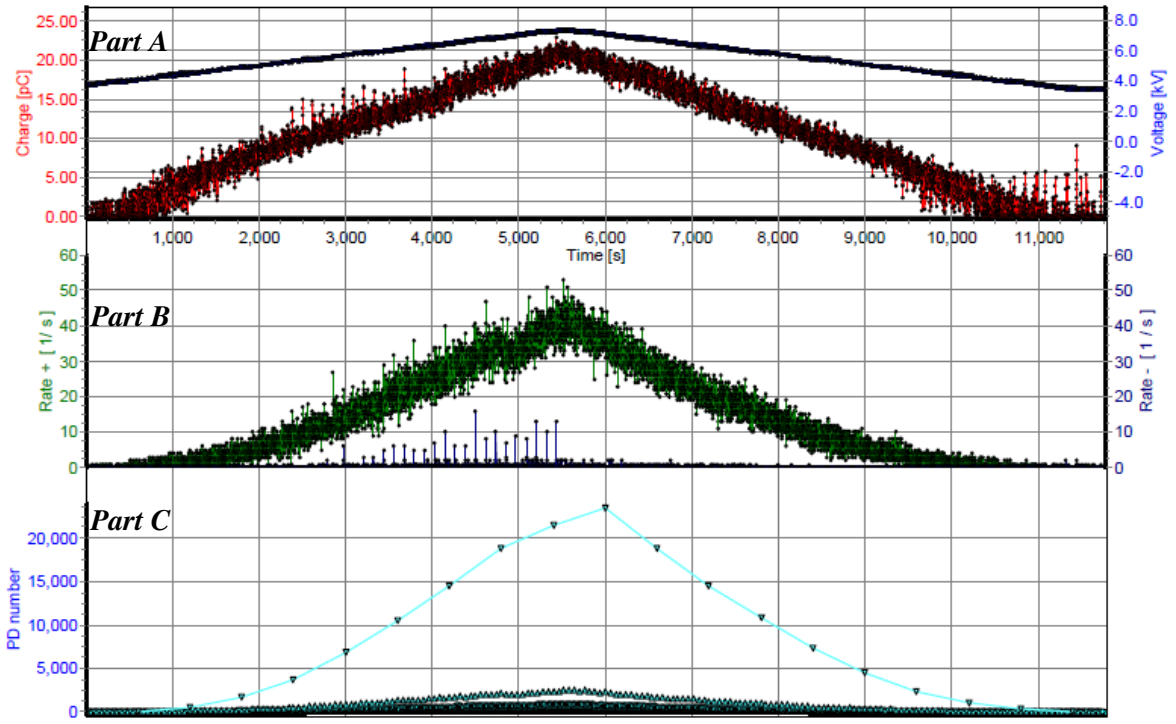

Figure 6.5: GPHP DC PD results using the balanced straight detection method with a step-up/step down voltage of 80 V and a TD of 120 seconds

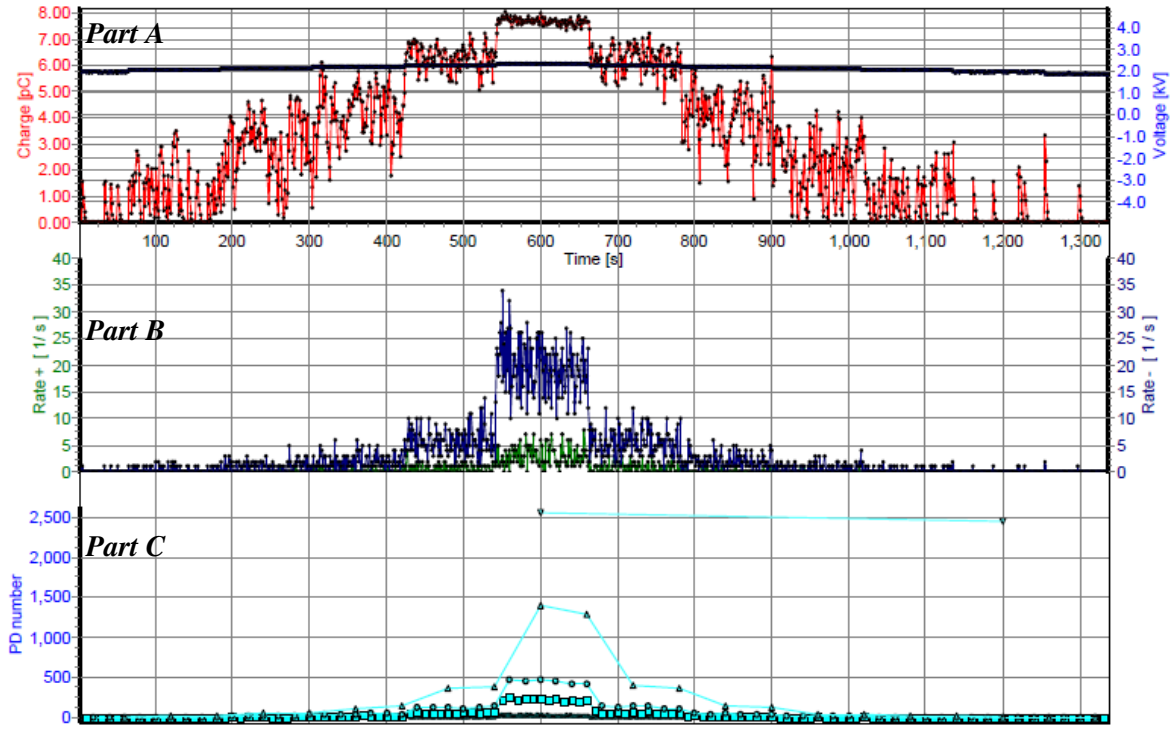

Figure 6.6: UBHP DC PD results using the balanced straight detection method with a step-up/step down voltage of 80 V and a TD of 120 seconds

Both GP and UB cable configurations exhibit different PD patterns at 100 kPa. For the GP case (look at Figure 6.5), the voltage was raised up to 7.2 kV, a voltage well above the AC PD inception voltage, to observe how the PD rate, the PD number and the PD magnitude are affected with the increase in the supply voltage. Results obtained agree with [20, 31, 71] which state that as the supply voltage is increased, the PD magnitude, the PD number and the PD rate increase.

It is arguable here whether the signals observed on the LDS-6 monitor is actual PD or noise. It must be noted that with the use of the balanced circuit the external noise was reduced down to 2 - 4 pC if 50 pC were injected into the balanced circuit (two parallel RLC impedance circuits, thus 25 pC should flow through each branch). Therefore the results obtained could be considered to be PD, only if by raising the voltage level up to 7.2 kV, the noise level does not increase above 50 pC. If for example the noise level increases up to 100 pC this would mean that the 2-4 pC of noise observed on the screen would also double to 4-8 pC etc. The external noise coming from background signals (electronic DC supply, vacuum pump, vacuum pump controller and signals intruding from other tests occurring near the testing area) should be constant. The only reason for the noise to increase would be the PD generation from other sources but from the testing cables. Looking again at Figure 6.5, the maximum PD magnitude observed is approximately 20 pC. This PD could originate from the cable and/or from the other PD sources listed in Figure 6.2. This PD could be generated from the bushing. If the noise level was reduced to 2 pC when 50 pC were injected across the parallel impedance branch, then the PD generated from the bushing would have to be approximately 500 pC to achieve a maximum PD magnitude of 20 pC on the LDS-6 screen.

The UB configuration has been tested up to 2.5 kV at 100 kPa (UBHP case) as is shown in Figure 6.6. GPHP results showed that there was no PD up to a voltage of 3.8 kV. Thus based on this observation it can be concluded that PD starts at a higher operating DC voltage when the cables tested are laid on a grounded plain (GP case), than when the cables tested are screened (UB case).

It can also be observed that in both configurations (GP and UB), there is some PD activity with small negative and positive PD rates respectively. This phenomenon requires further investigation. (The negative PD rate is most likely to originate due to the balanced circuit configuration. PD generated from one of the testing cables would appear on the output as negative PD and positive PD from the other cable. Thus PD rate from one of the cables would appear as negative and positive for the other). The PD number seems to increase with an increase in the DC supply voltage. For the GP case the supply voltage at which a +ve PD rate of 20 PD/s or 1200 PD/min is achieved, is larger than the UB case and thus the cables are exposed to an HV DC voltage for a longer period of time for the same TD (120 sec). Therefore the total PD number is also expected to be larger than the UB case.

At 11.6 kPa, Figures 6.7 and 6.8 which are shown below, illustrate that PD activity starts at about 1.2 kV for both configurations. PD rates and PD numbers show similar trends. However for the UB case, the +ve PD rate suddenly increases at 1.9 kV whereas for the GP case the PD rate increases gradually with the increase in supply voltage. Both testing configurations have similar –ve PD rates.

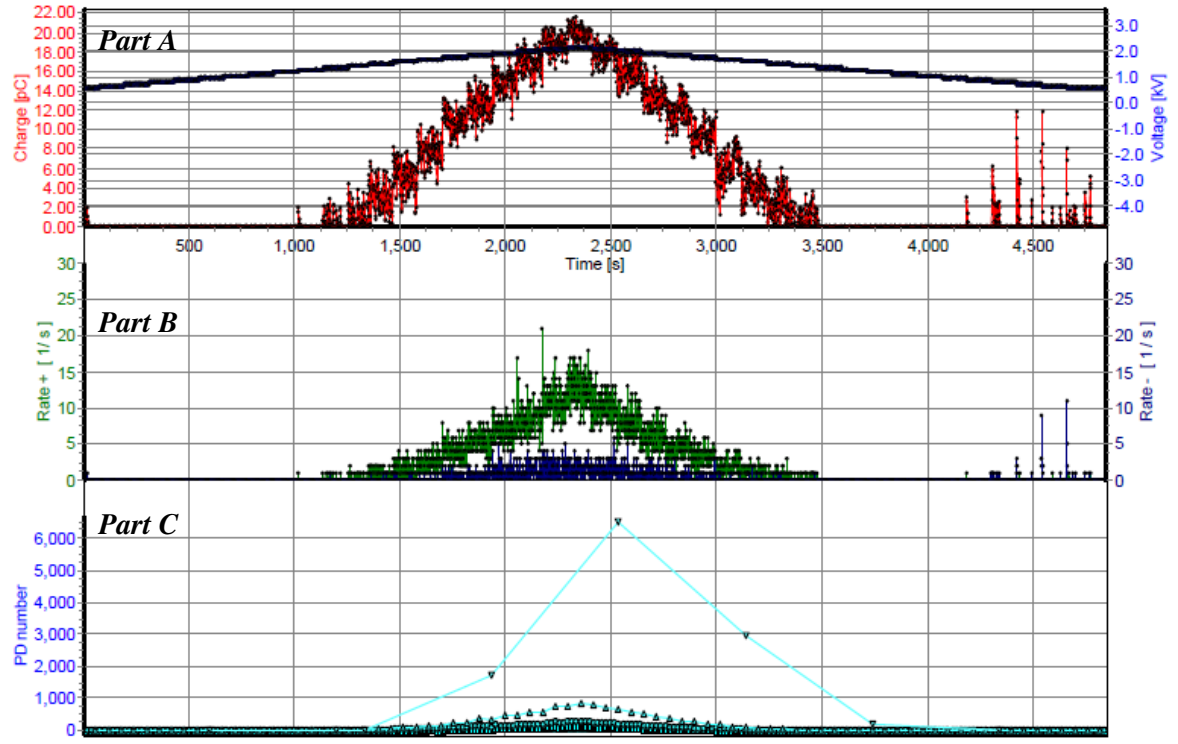

Figure 6.7: GPLP DC PD results using the balanced straight detection method with a step-up/step down voltage of 80 V and a TD of 120 seconds

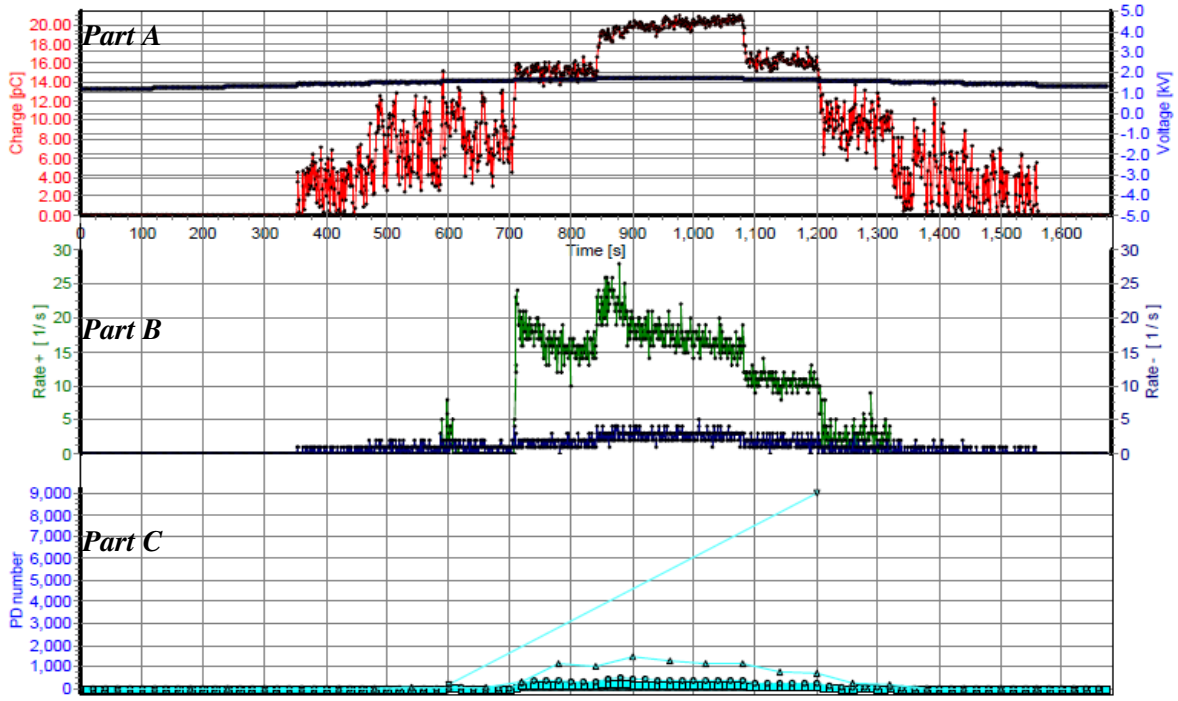

Figure 6.8: UBLP DC PD results using the balanced straight detection method with a step-up/step down voltage of 80 V and a TD of 120 seconds

The maximum PD magnitude reached is approximately the same for both cable configurations at about 2 kV. The differences in the PD results at low pressure are not as significant as high at high pressure but this is an area which requires further investigation. More tests are needed on cables of different conductor size and insulation thicknesses. The next section describes how the PDIV for each case was selected. In addition, Table 6.1 shown in the next section, summarizes all PD results at 100 kPa and at 11.6 kPa for both GP and UB configurations.

6.3.3 Average PDIV Results

In BS EN 60270 [30], it is stated that under AC conditions the test circuit and the equipment used to detect PD, should at least have a 5 pC sensitivity. This implies that the noise level should be lower than 5 pC and that when PD magnitudes equal or greater to 5 pC are detected, then the voltage at which this PD is generated should be regarded as the inception voltage (PDIV). For DC tests there is no reference regarding the sensitivity or the PD repetition rate and thus there is no reference on how to determine the PDIV under high voltage DC conditions. Kreuger [17] mentions however, that in the American society of testing and materials standards D1868-1973, it is stated that if the PD repetition rate reaches one PD/min, then the voltage at which this repetition rate is reached can be considered to be the PDIV. Thus, in this case the DC PDIV was selected based on a PD sensitivity of 5 pC having a sustained repetition rate of $RR_{DC} \geq 1$ PD/min.

The minimum PD detection level was set at 5 pC during the experiments. Even though the DC voltage was held constant at a specific level for two minutes no discharges were detected having a PD rate of one discharge per minute. Instead, after a certain voltage level, discharges of a very low magnitude (up to 2 pC) ignited suddenly having an average repetition rate of ≈11 PD/min (or ≈0.2 PD/s) for the GP case. This repetition rate kept increasing with increase in the DC supply voltage as it was shown in Figure 6.5 Part B. Figure 6.9 displays the results already shown in Figure 6.5 but zoomed in to show how the PDIV was determined.

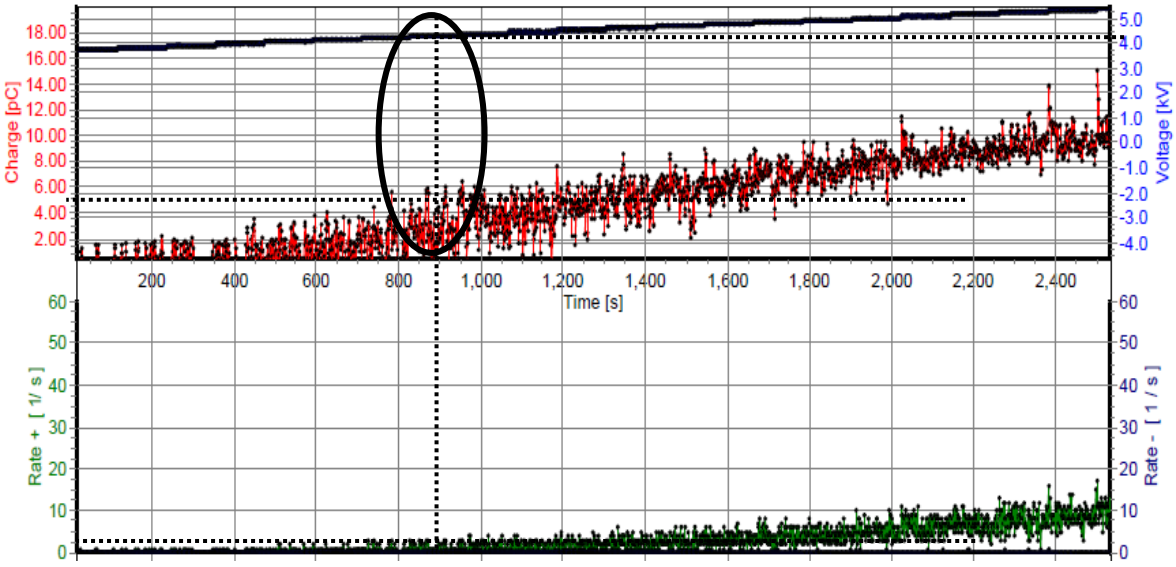

Figure 6.9: GPHP DC PD results (Zoomed in) using the balanced straight detection method with a step-up/step down voltage of 80 V and a TD of 120 seconds

It has to be mentioned that despite the fact that the detection level was set at 5 pC the software was still capturing PD data having a magnitude of ≤ 5 pC and displaying them on the graph as shown in figure 6.9. Nevertheless the PDIV was selected as soon as the 5 pC PD level was reached. Since a maximum of 5 pC is required in the standards for AC PD testing conditions, the same PD magnitude was chosen to determine the PDIV under DC conditions. Since the PD repetition rate is much less in the DC case, PD of the same magnitude should be less detrimental for the insulation under DC conditions than under AC conditions. The point which is circled on the graph in Figure 6.9 above, shows how a PDIV value of 4.25 kV was chosen when the PD rate was 7 PD/min (or 0.12 PD/s) when the GP cable configuration was tested at 100 kPa. Note that this PD rate value is not the same as the one shown in Figure 6.9 Part B. A PD rate of 7 PD/min was obtained by counting all the PD occurring during the TD of 120 seconds having a magnitude of ≥ 5 pC. The PD rate on the monitoring screen (Part B), includes smaller PD magnitudes as well. Figure 6.10 shows how a PDIV value of 2.0 kV was chosen when the PD rate was 102 PD/min (or 2.5 PD/s) for the UB cable configuration at 100 kPa. Similarly Figures 6.11 and 6.12 show how the PDIV values of 1.5 kV and 1.1 kV were chosen at 11.6 kPa for GP and UB respectively.

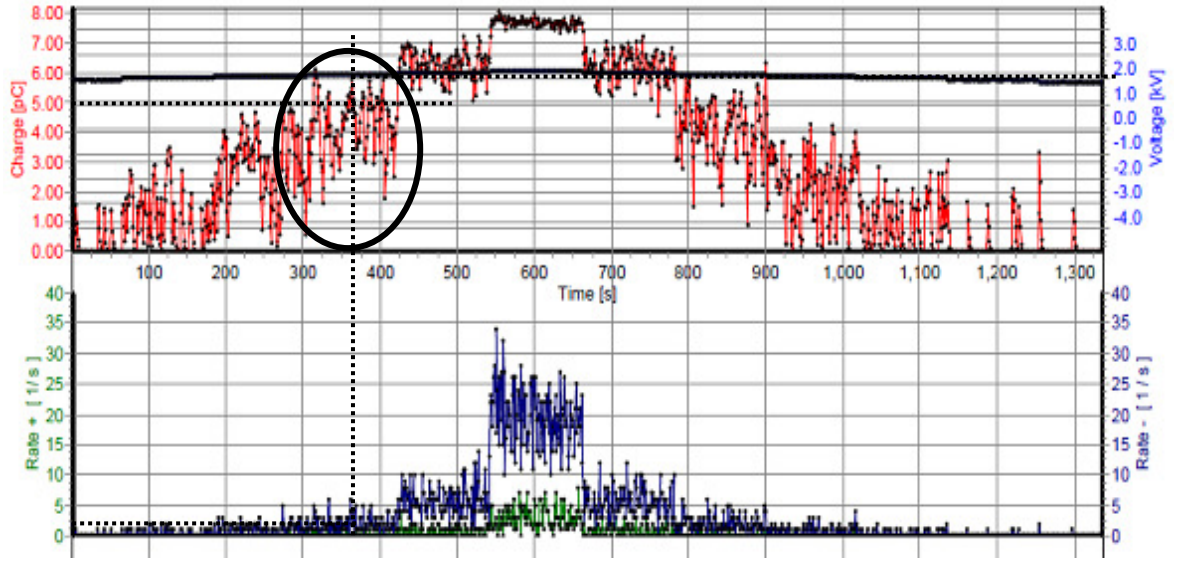

Figure 6.10: UBHP DC PD results using the balanced straight detection method with a step-up/step-down voltage of 80 V and a TD of 120 seconds

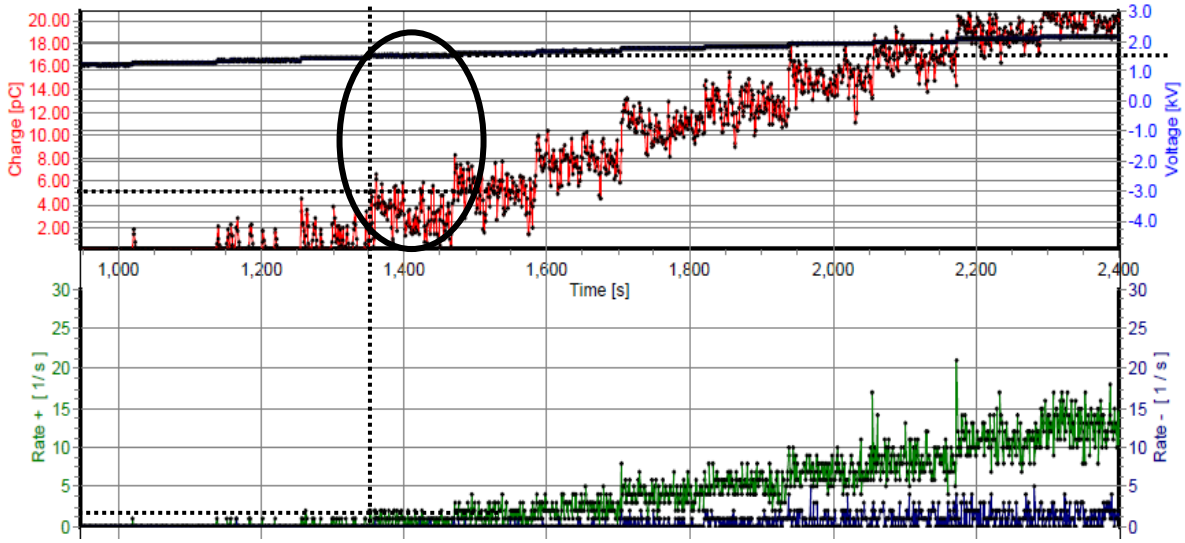

Figure 6.11: GPLP DC PD results (zoomed in) using the balanced straight detection method with a step-up/step-down voltage of 80 V and a TD of 120 seconds

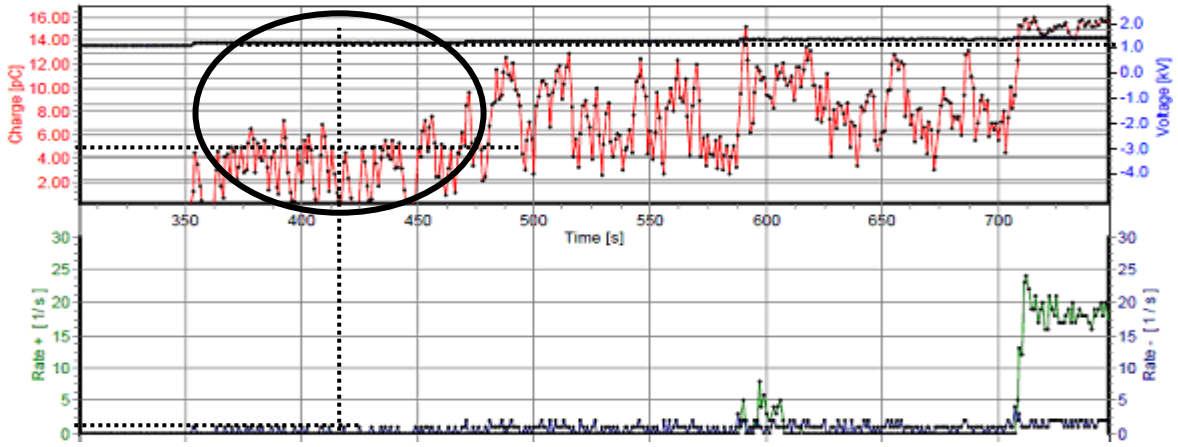

Figure 6.12: UBLP DC PD results (zoomed in) using the balanced straight detection method with a step-up/step-down voltage of 80 V and a TD of 120 seconds

Concluding, the PDIV for the GP cable case at 100 kPa (GPHP) is approximately 4.25 kV and this is significantly larger than the PDIV determined for the UB cable configuration which was found to be 1.9 kV. However at 11.6 kPa, both GP and UB cases result in lower PDIVs. It is uncertain whether the PDIVs obtained are for the cables that have been tested or for the high voltage bushing of the environmental chamber, or other possible PD sources which are listed in Figure 6.2. PD test results are shown below in Table 6.1. Some of these results are also listed in Table 6.3 in Section 6.4, where the PDIVs and the average PD rates determined under DC conditions, are compared with the corresponding results obtained under AC conditions.

TABLE 6.1

COMPARISON OF PD RESULTS FOR THE GP AND UB CABLE CONFIGURATIONS, FOR A STEP VOLTAGE OF 80V AT PRESSURE OF 11.6 KPA AND 100 KPA AND A TEMPERATURE OF 275 K

Configuration	***GP***		***UB***	
Pressure (kPa)	11.6	100	11.6	100
DC PDIV (kV)	1.5	4.25	1.1	1.9
Average PD Rate, RR_{DC} (PD/min) for a PD detection level of ≥ 5 pC	4.8	2.5	10.5	9.5
Average +ve PD Rate, RR_{DC} (PD/min)	108	75	0	75
Average -ve PD Rate, RR_{DC} (PD/min)	0	0	60	90
Average PD Magnitude (pC)	6	5.5	6.6	5.4
Average PD Number for a PD detection level of ≥ 5 pC	9.6	5	21	19

In general, the DC PDIV measured for the UB case at 100 kPa is only 42% of the PDIV obtained in the GP case. At 11.6 kPa the UB case PDIV is 73% of the GP PDIV value. UB PD rates are ≈2 and ≈3 times larger than the GP PD rates at 11.6 kPa and 100 kPa respectively. The total average PD number depends on the PD rate and the period of time that the cables are exposed to a high voltage (TD). Since TD is equal for both configurations, the PD numbers for the UB case will also be ≈2 and ≈3 times larger than the GP case.

It has to be mentioned that the +ve and -ve PD rates occur due to the arrangement of the balanced circuit with the two RLC impedance branches included into the circuit. PD generated from one cable will flow through one branch and it will appear with a +ve PD rate on the LDS-6 monitoring screen. PD generated from the second cable will flow through the second branch appearing with a -ve PD rate.

6.3.4 PDIV Results Using a Higher Step Voltage

In practice, DC loads in an aircraft electrical system are not constant during an aircraft flight. The voltage will have to be switched on or switched off depending on the operational loading conditions (load planning). Some loads operate at a higher voltage than others and thus they will require the voltage to be stepped up (switched on) at a higher level than others. The higher step-up voltage will affect the cables that connect these loads to the main distribution board/panel. This is another interesting area that requires further research. For example it is shown in Figures 6.13 and 6.14 that a higher voltage step change results in different PDIV values for the same test cable sample.

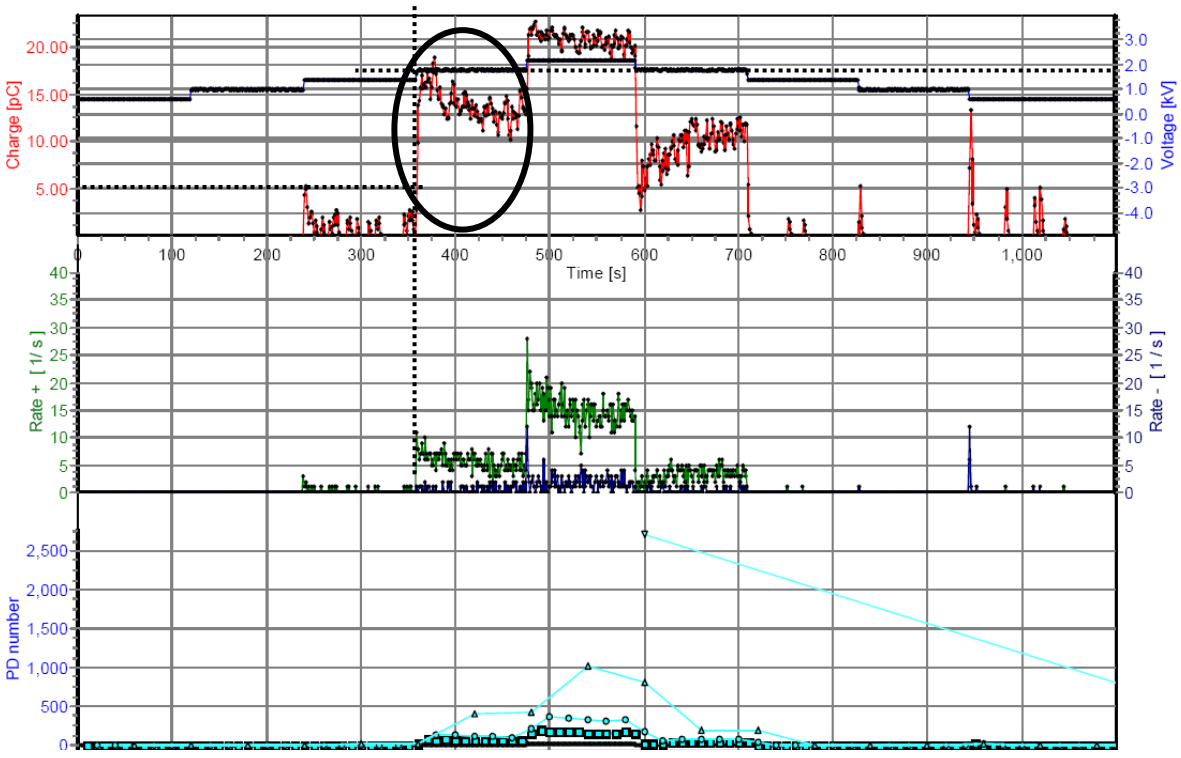

Figure 6.13: GPLP DC PD results using the balanced straight detection method with a step-up/step-down voltage of 375 V and a TD of 120 seconds

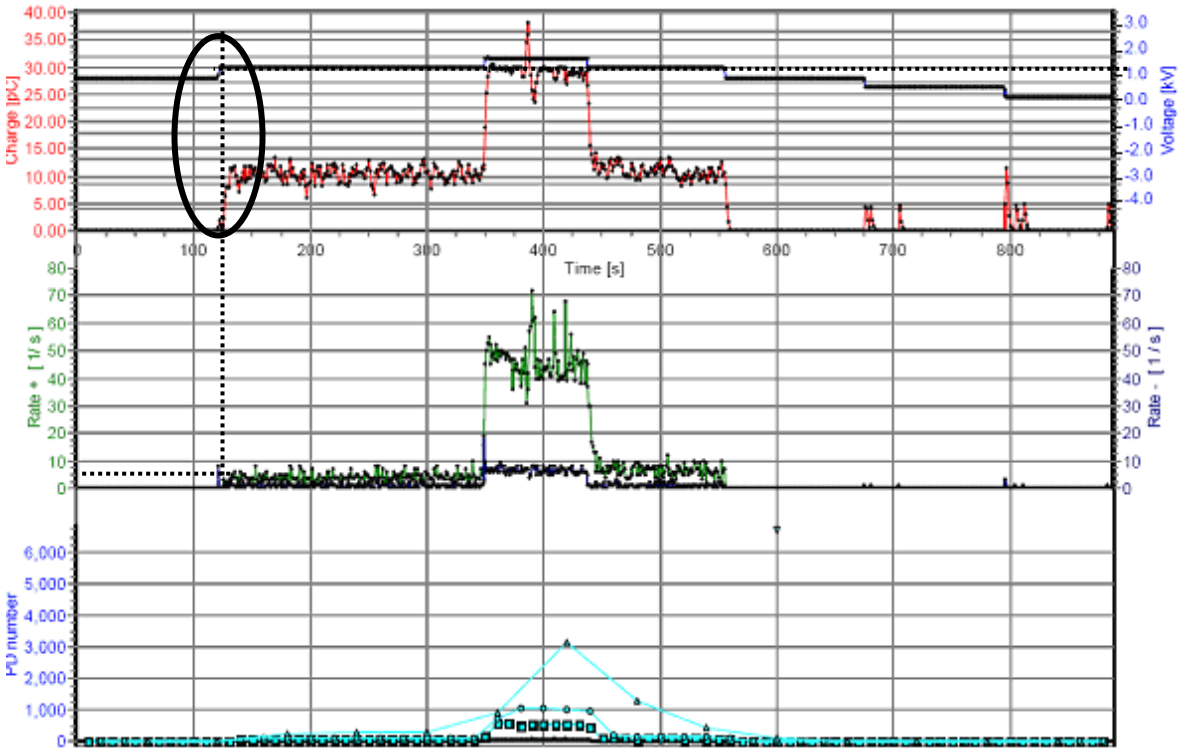

Figure 6.14: UBLP DC PD results using the balanced straight detection method with a step-up/step-down voltage of 375 V and a TD of 120 seconds

For example the aircraft loads could be switched on for the GP cable configuration at 11.6 kPa. If the step voltage is 375 V, the PDIV is approximately 1.75 kV instead of 1.5 kV, which was the PDIV determined when the step voltage was 80 V. It could be argued here since the step voltage is 375 V and the voltage does not increase gradually, going through the intermediate voltages of 1.5 kV and then 1.58kV and then 1.66 kV and so on. It increases suddenly from approximately 1.38 kV (a voltage value below the determined PDIV), to 1.75 kV. By looking at the PD rate and the PD magnitude results at the DC PDIV for GP case and the UB case at 11.6 kPa, some conclusions can be drawn. These results are summarised in Table 6.2 shown below.

TABLE 6.2
COMPARISON OF PD RESULTS FOR THE GP AND UB CABLE CONFIGURATIONS FOR DIFFERENT STEP VOLTAGES AT A PRESSURE OF 11.6 KPA AND AT A TEMPERATURE OF 275 K

Configuration	***GP***		***UB***	
Step Voltage (V)	80	375	80	375
DC PDIV (kV)	1.5	1.75	1.1	1.3
Average PD Rate, RR_{DC} (PD/min) for a PD detection level of ≥ 5 pC	4.8	360	10.5	225
Average +ve PD Rate, RR (PD/min)	108	360	0	225
Average -ve PD Rate, RR (PD/min)	0	75	60	120
Average PD Magnitude (pC)	6	15	6.6	10
Average PD Number for a PD detection level of ≥ 5 pC	9.6	250	125	240

If the DC PD rate and the DC PD magnitude results at a higher step voltage were lower, then it could be stated that indeed a different step voltage gives rise to higher PDIV values. However, this is not the case. What can be concluded from the results in Table 6.3 is that a bigger step voltage has a significant effect on the PD rate, the PD magnitude and thus the PD number during the TD period of 2 minutes.

By looking at the PD rates in the above table, some questions arise related with the determination of the PDIV. The PDIV was selected based on a step voltage of 80 V and

the average PD rate detected was 4.8 PD/min for the GP configuration for PD magnitudes ≥ 5 pC. If a smaller step voltage was used or a cable with thicker insulation, would it be the case that discharge rates of 1 PD/ min could be achieved? With an even smaller step voltage would the PDIV be smaller? Again, would using a smaller step voltage be a realistic approach to determine the true PDIV? Would it be better to use a ramp voltage to determine the PDIV and would this result in larger PDIVs? If so, could the loads be switched on by using a ramp function so that the PDIV of cables is bigger enhancing the capability of the cable? These are all questions that require further research.

One important difference in the conditions in which the experiments were carried out with a different step voltage is the time of exposure to relatively higher voltages when the step voltage was 80 V. This is due to the LABVIEW software which was designed to generate the supply voltage waveform. For example if the maximum voltage applied during the experiments is constant as well as the time delay, (TD – time during which DC voltage is constant), it will take less time to reach that maximum applied voltage if the step voltage is larger. In order to check if the period of time for which the cables are exposed to a HV DC voltage has an effect on the PDIV, the time delay (TD) should also be increased proportionately with the increase in the step voltage. For example if the voltage step is doubled, then TD should also double before and after the PDIV is reached, in order to have the cables exposed to these voltages the same period of time. This is another case which requires further investigation.

6.4 Comparison of AC and DC PD Results

The tables shown below list the average PD results measured under AC and DC conditions. Results displayed include PDIVs, PD magnitudes and PD rates at inception voltage and 20% above inception. A comparison is made between columns filled with the same colour code. For example the average PDIV under AC conditions (grey coloured column – Table 6.3A), is compared with the average PDIV under DC conditions (grey coloured column – Table 6.3B). The DC PD results which are displayed below are the results obtained when the step voltage was 80 V.

TABLE 6.3A

AVERAGE AC PD MEASURED RESULTS AT 100 KPA AND 11.6 KPA, FOR GP AND UB CONFIGURATIONS AT PDIV AND 20% ABOVE PDIV

Testing Conditions		**AC**				
Pressure (kPa)	**Configuration**	**PDIV (kV)**	**PD Magnitude (pC) at PDIV**	**Average PD Magnitude (pC) 20% above PDIV**	**PD Rates (1/s) at PDIV**	**PD Rates (1/s) 20% above PDIV**
100	*UB*	*1.10*	*98*	*610*	*203*	*476*
	GP	*1.42*	*120*	*1800*	*118*	*1712*
11.6	*UB*	*0.56*	*598*	*805*	*189*	*406*
	GP	*0.59*	*1010*	*2823*	*315*	*658*

TABLE 6.3B

AVERAGE DC PD MEASURED RESULTS AT 100 KPA AND 11.6 KPA, FOR GP AND UB CONFIGURATIONS AT PDIV AND 20% ABOVE PDIV

Testing Conditions		**DC**				
Pressure (kPa)	**Configuration**	**Average PDIV (kV)**	**Average PD Magnitude (pC) at PDIV**	**Average PD Magnitude (pC) 20% above PDIV**	**PD Rates (1/s) at PDIV**	**PD Rates (1/s) 20% above PDIV**
100	*UB*	*1.90*	*5.40*	*7.8*	*0.16*	*20.5*
	GP	*4.25*	*5.50*	*8.7*	*0.04*	*6.3*
11.6	*UB*	*1.10*	*6.60*	*15.4*	*0.18*	*17.5*
	GP	*1.50*	*6.00*	*13.3*	*0.08*	*5.4*

The first thing to notice from the table above is the large increase in PDIV if the tests are carried out under DC conditions. At 100 kPa, the DC PDIV is 1.7 times larger than the AC PDIV for the UB configuration. Similarly the DC PDIV is 3 times larger than the AC PDIV for the GP configuration. At 11.6 kPa, the DC PDIV is 2 times larger than the AC PDIV for the UB configuration and 2.5 times larger for the GP configuration. This information is very useful, since it can give an indication as to how much the operating voltage can be raised when using a DC instead of an AC operating voltage and consequently, give an indication of the enhancement in power transfer capability of an aircraft cable. As an alternative it can also give an indication on how much weight can be saved by using a smaller cable conductor, as a result of passing less current through the cable to achieve the same power transfer.

Based on the AC PD results, the PDIVs at 11.6 kPa for both configurations are approximately equal. At 100 kPa the AC PDIV obtained for the UB configuration is 77.5% of the AC PDIV measured for the GP case. However, DC PD results for the two cable configurations, exhibit a larger difference in PDIV at both 100 kPa, as well as at 11.6 kPa. As it is for the AC case, when comparing the two cable configurations at 11.6 kPa, the PDIV difference under DC conditions is much lower than at 100 kPa. However, this difference is much more significant than under AC conditions. The DC PDIV measured for the UB case at 100 kPa is only 42% of the PDIV obtained in the GP case. At 11.6 kPa the UB case DC PDIV is 73% of the GP PDIV value.

As far as PD rates at the PDIV are concerned, these are 3-4 orders of magnitude lower under DC conditions. At 20% above the PDIV, DC PD rates for GP are 2-3 orders of magnitude lower than the AC PD rates, whereas for UB the DC PD rates are 1-2 orders of magnitude lower. It can also be observed that the PD rates considering a sensitivity of 5 pC are generally lower at 11.6 kPa than at 100 kPa under AC conditions with the exception of the GP case. On the other hand PD rates are bigger at 11.6 kPa. At 20% above the PDIV, AC and DC PD rates follow similar trends at both pressure levels.

PD magnitudes obtained under AC conditions are much larger (≈ 1-2 orders of magnitude), than under DC conditions. At 11.6 kPa and 100 kPa, the PD magnitudes at the PDIV are approximately the same. As expected, at 20% above the PDIV the PD magnitudes are larger (≈ double). Under AC conditions PD magnitudes show a much stronger dependency on pressure.

The difference in AC and DC PD magnitudes is huge and consequently the long term deterioration of the cable insulation when it is operating under DC conditions should be much less. This result is of great importance for the lifetime of the cable since it might play a vital role in developing a new method in determining the PDIV of the cable operating under DC conditions. For example the PDIV determination could be based on the comparison of how a cable ages under AC and DC conditions. If the cable operating at the AC PDIV ages at certain rate, what would the equivalent DC PDIV that would result in the same aging rate.

Overall, from the results obtained it can be concluded that the PDIV for the cables tested is much higher at DC conditions than under AC conditions. However, it is not certain whether the results are due to other PD sources, as listed and explained in this chapter. The difficulty in DC PD measurements arises due to the very low DC PD rates (as low as 1 discharge per minute) and the very low DC PD magnitudes. Other tests have to be carried out to make sure that all the testing equipment used is free of PD for the required testing voltages.

6.5 Summary

Concluding, this chapter has been focused on DC PD testing of specific aerospace cables in two configurations (GP and UB). The balanced circuit was used in combination with the LDS-6 PD detector, to carry out the DC PD tests and furthermore to determine partial discharge inception voltages (PDIVs) at 100 kPa and at 11.6 kPa.

A description of the testing methodology has been described together with the difficulty in testing for PD under DC conditions. Possible noise and external PD sources have been identified and the actions taken to reduce these external interferences as much possible have been listed.

AC and DC PD measured results (PD rates, PD magnitudes and PD numbers), have been compared at the PDIV as well as 20% above inception. Furthermore, the measured DC PDIV results have also been compared with the PDIV theoretical calculation results as in chapter 3.

Unlike testing for PD under AC conditions, little work can be found in literature regarding testing for PD under DC conditions. Even so, the DC PD work found in literature is confined to ground power systems. With the development of the More Electric Aircraft (MEA) and the use of higher DC voltages past the minimum of Pachen's Law, it is necessary to carry out research in the field of DC PD, especially with an environment replicating the conditions of an aircraft at altitude.

As discussed, Chapter 6 points out the difficulties faced when it comes to testing for DC PD. Compared to other documents, journals or theses, the possible noise sources that can affect the PD results are listed and explained and the steps carried out to remove these noise sources are explained in detail.

A method for determining the PDIV of DC cables is also explained with the appropriate justification. By comparing the AC and the DC PD results at 100 kPa and at 11.6 kPa, it was concluded that PDIVs under DC conditions can be 2 to 3 times higher than under AC conditions. Despite the fact that there is an uncertainty as to where the PD obtained originates from (testing cables or PD occurring in other parts of the testing circuit), this PD was generated at higher voltages.

The DC voltage waveform applied to the testing cables was kept constant for 2 minutes and then stepped up in order to determine the PDIV. There is no reference in literature on the voltage waveform that should be used to test for DC PD. In addition, the case of raising the voltage using a higher step voltage was also examined to observe the differences in PD results. Again, unlike other research, this Chapter shows that the use of a higher step up voltage limits the operating voltage that can be applied on the cables.

An initial comparison between PD rates, PD magnitudes and PDIVs has been carried out; however more experiments are required to measure the PDIV, making sure that PD is generated from the testing cables.

Chapter 7

Conclusions and Further Work

7.1 Introduction

The aim of this thesis was to investigate the impact of increasing the operating voltage levels on different cable duct systems, on the More Electric Aircraft (MEA), taking into consideration volume and weight restrictions. A methodology was devised to determine the optimum Safe Operating Voltage (SOV) level at which these cable duct systems should be operated. The optimisation was based on uniform field calculations that have been used in literature to compute the partial discharge inception voltage (PDIV). In addition the uniform field calculation models have been used in combination with a finite element analysis tool to compare round cable systems and flat conductor systems in the form of a PCB. Furthermore AC and DC partial discharge (PD) tests have been carried out to measure PDIVs, PD rates and PD magnitudes at the inception voltage and 20% above inception, for a specific round aircraft cable. These measured results have been compared with the theoretical calculation results. This chapter summarises all the conclusions drawn from the research results and discusses further work that is required to expand this investigation.

7.2 Conclusions

7.2.1 Cable Duct System Optimisation

As it was described in the summary Section 3.7, Chapter 3 proposes two methodologies for optimising high voltage cable systems to be used in the MEA. This is an extension of the work carried out by Nelms [12] who performed optimisation on a cable system installed in

a fixed sized duct. The optimisation is based on selecting an appropriate voltage level for maximum power transfer with a minimum impact on system weight. In this thesis the possibility of bigger sized ducts has been examined and it was found that the maximum power to weight ratio of different cable systems does not increase if the diameter of the duct increases. In addition, a more practical methodology has been developed for cable system optimisation by starting from a fixed power demand (when the aircraft electrical loads are known), to determine the cable duct system resulting in less system weight. The new methods developed in Chapter 3 can be used by engineers to select exactly the cable they need, the cable system (AC/DC), the number of cables to use and at the same time figuring out how much space the cable system will occupy. The conclusions of Chapter 3 are described below in detail.

In chapter 3 the PDIV of certain cable systems was computed by using theoretical models and taking into consideration three types of discharges: void discharges, cable to ground airgap discharges and cable to cable airgap discharges. It was concluded that cable to cable airgap discharge, as opposed to the other types of discharges, was the determining type of discharge in computing the safe operating voltage of the cable installed in a bundle. The PDIV was higher due to double the insulation thickness between the cable conductors. However depending on the cable system, whether it was a grounded positive and negative DC system or a grounded three phase AC system, this PDIV had to be divided by 2 or by $\sqrt{3}$ to determine the voltage rating of a single cable. This rating was less than the voltage rating determined when a cable to ground airgap discharge and a void discharge were considered for calculating the PDIV.

A fixed duct size having a 30 mm diameter was used to calculate initially the optimal voltage based on the three types of discharges. For all the cable systems examined it was also concluded that maximum power transfer does not correspond to the system operating at maximum voltage. If the duct volume is fixed and the cable conductor decreases, there is more space to be filled by using thicker insulation and thus the voltage rating of the cable can be increased for fixed airgap distances between cables and the ground and cable to cable. However, as the conductor gets smaller the current rating

capability decrease dominates after a certain voltage increase and the maximum power transfer starts decreasing.

As far as the power to weight ratio against voltage rating curves are concerned, the maximum power to weight ratio occurs at higher voltages than the voltages at which maximum power transfer occurs. This shift in the optimal point occurs due to the lower power transfer capability of slightly higher voltages being compensated for by lower cable weights (i.e. less copper and more insulation).

Overall the analysis of both maximum power transfer capability and power to weight ratio show that the grounded positive and negative DC cable system appears to be the optimal choice for power distribution in an aircraft based on the criteria examined. The use of a DC system, where the insulation is utilised at its peak rating, gives good power transfer efficiencies. This is in contrast to the AC systems in which the power transfer capability is determined by the RMS voltage rating, this being 1.414 times lower than the maximum operating voltage. The use of a DC system where the conductors are allowed to float is not optimal, since each conductor has to be rated for the entire system voltage, even if it will not always operate at this value.

Using larger duct sizes does not result in an increase in the power to weight ratio optimal point. Even though larger ducts lead to larger conductor sizes and thicker insulation, they also lead to a significant increase in cable system weight, which compensates the increase in maximum power transfer.

However, it was observed that duct sizes having a diameter <30 mm, can achieve significantly larger power to weight ratios. Even though the maximum power transfer is less, the reduction in the cable system weight is much more resulting in an increase in the power to weight ratio. This is an interesting result since this allows the possibility to replace larger duct systems with multiple smaller ones, in an attempt to achieve the same power transfer with a reduction in cable system weight. The grounded positive and negative DC case, which was found to be the optimal system in terms of maximum power transfer and power to weight ratio, was investigated to examine this possibility. Even though this was proven to be possible, it was also found that the increase in resistive losses

and in voltage drops were significant. Thus it would not be beneficial to replace larger duct systems with multiple smaller ones.

The process of calculating the optimal voltage was also reversed in order to establish the optimal insulation thickness if the electrical power required is known. This is actually a more practical approach, since the loads in an aircraft electrical system are known. Results have shown that for a load of 250 kVA, which is the maximum power generated from one generator (as in BOEING 787) and for the cable clearance criteria taken into consideration, the optimal duct diameter is 25 mm for a grounded positive and negative DC cable system. In this case the optimal DC cable system consists of 4 cables with AWG 8 size conductors having an insulation thickness of 1.56 mm. In this case the voltage rating of the cable is 1.3 kV, with an approximate power to weight ratio of 610 kVA/ (kg/m).

7.2.2 PCBs VS Round Cables

Chapter 4 proposes a methodology for determining the SOV for a PCB model using theoretical calculations and FEA analysis. In addition, it shows that PCBs can replace round cable systems as means of transferring power around the aircraft. If appropriate dimensions are used for the conductor traces within the PCB and the insulation thickness, a PCB model can offer a bigger maximum power to weight ratio. No analysis as such has been made available in literature and the proposed methodology can be used by engineers to analyse a PCB system with various possible geometries. The PCB SOVs determination is unique because it is based on the PDIVs that can occur within a PCB or outside. The conclusions of Chapter 4 are described below in detail.

Results have shown that a three phase AC PCB system with flat AWG 16 conductors can be used in to replace the round AWG 16 cable system installed in a duct. In this case, the PCB system offers a power transfer enhancement of 13% when the cables are held in the middle of the duct with a certain clearance. Unfortunately it cannot be used to replace round cable systems consisting of larger AWG sized conductors due to the lower power transfer capability. However, if the cables are touching and sitting at the bottom of

the duct, there is a decrease in the current rating of the cables, which results in a lower power transfer capability. In this situation the PCB system offers a power transfer increase of about 39% with respect to the round cable case. In addition, for other round cable systems not consisting of the same conductor and insulation weight, like for example duct systems consisting of AWG 14 or AWG 12 size conductors, then the power transfer enhancement offered by the AWG 16 PCB system is 22% and 5% respectively.

The power to weight ratio results for optimal PCB design, as shown in Chapter 4, is larger than the power to weight ratio of the round cable duct systems consisting of conductors AWG 6, AWG 14 and AWG 16. On the other hand if the cables are touching, sitting at the bottom of the duct, then the PCB has a better power to weight ratio than all the AWG sizes that have been examined.

There is an optimum insulation thickness between the PCB traces & between the PCB traces & the surrounding duct giving a maximum voltage rating. These thicknesses affect the current rating as well. It might be the case that the optimum power rating is not achieved at that optimum voltage point since the current might be decreasing or increasing more rapidly before or after that optimum voltage point.

7.2.3 Different Cable Configurations for PD Testing

As discussed in the summary in Section 5.5 in Chapter 5, the Standard BS EN 3475-307 [59] is incomplete and it fails to explain why the cable preparation methods for PD testing of screened and unscreened cables is identical. Chapter 5 shows PD test results for aircraft cables laid out in different configurations and compares PD results including the PDIV with the configuration described in the Standard BS EN 3475-307. Analysis of PD test results were also used to support the arguments made in Chapter 3; that PD on unscreened aircraft cables at 11.6 kPa occurs outside the insulation, rather than inside the insulation within a void and also that calculations carried out in Chapter 3 provide conservative results. Comparisons as such have not been found in literature. The conclusions of Chapter 5 are described below in detail.

AC and DC PD tests have been carried out to investigate whether different cable configurations provide different PD results. In addition, the test results were analysed to show the best way of testing cables for the aerospace industry based on practical applicability, on the lowest PDIV and on the consistency of the results. These cable configurations could replicate the way cables are installed in an aircraft. PD tests were carried out using the analogue ROBINSON PD detector and also by using a straight PD detection circuit as described in Chapter 5. It has been observed that the CG case (unscreened cable wrapped around a grounded cylinder), is more consistent at 100 kPa in terms of measurement PDIV results, than all the other methods. Nevertheless the UB case (unscreened cable with grounded braid held tightly around the cable insulation) shows lower standard deviations and exhibits a lower average PDIV. At 11.6 kPa, the onset to a stable PD pattern was more rapid than at 100 kPa. In this situation the GP case (cable laid on a grounded conductive plane) results exhibited relatively lower PDIV results of higher consistency, as well as relatively lower standard deviations. In addition to the PDIV differences, PD magnitude phase-resolved plots suggested that different PD mechanisms were taking place when different cable configurations were tested.

In general, recording the PDIV values was a difficult task due to the analogue circuitry of the PD detector and the sensitive response of the PD deflection needle with the slightest noise, coming from the surrounding environment (other tests in the area, measuring equipment etc.). Due to the uncertainty of the PDIV results, the same tests were repeated using the digital LEMKE digital PD detector and by using both the balanced and the straight detection methods. Results obtained using the LEMKE PD detector, were more consistent exhibiting lower standard deviations in all cable configurations. PD magnitude phase resolved plots showed variations from one cable configuration to the other. However, the analysis of the statistical operators (Skewness, Kurtosis and Cross Correlation), suggests that the same PD mechanisms are taking place. The discharges taking place are electrode bound discharges either occurring between conductor and inner surface of the insulation or the outer insulation surface and the ground. Furthermore partial discharges of this type occur at lower voltages than dielectric bound discharges i.e. void discharges within the insulation.

PD magnitudes vary from one configuration to the other, but this might be due to the variation in PDIVs when comparing all four cable configurations. At 11.6 kPa the PD magnitudes are considerably larger than at 100 kPa. Furthermore PD rates differ especially for the GP case, where the rate is significantly larger at 11.6 kPa. This is an important result. For example for the GP case, this result shows that at 11.6 kPa, if the cable is operated at the inception voltage the cable insulation will age faster than at 100 kPa because of the larger PD magnitudes and the larger average PD rate.

PDIV results show that the screened cable case (UB), provides the necessary airgap distances to test for PDIV at 100 kPa and at 11.6 kPa. This conclusion is drawn from the fact that at 100 kPa the inception voltages for the UB case, is the lowest. In addition, at 11.6 kPa PDIVs for UB and GP are approximately equal, with the GP case covering a larger range of airgap distances (0.05 mm up to 40 mm), between the outer insulation surface and the ground plane.

As the UB cable configuration was examined, the airgap distance range from the outer insulation to the grounded braid varied approximately from 0.05 mm up to 0.40 mm. This depended on how tightly the braid was held around the insulation. Further work is required because it might be the case that at pressures lower than 11.6 kPa the airgap distance is not large enough to give the lowest possible PDIV. Nevertheless, the configuration giving the lowest inception voltage at 100 as well as 11.6 kPa should be used to test the cable. At 100 kPa the configuration resulting in the lowest inception voltage is the UB case (which is currently the method used in the standard. At 11.6 kPa both UB and GP cases should be used. One advantage of the UB case is the fact that the whole of the insulation across the length of the cable is being tested for defects, since the screen uniformly surrounds the insulation in a relatively symmetric manner. In all other configurations only part of the outer cable insulation surface touches the grounded conductor and thus some defects might not be spotted and identified.

The measured PDIVs have also been compared with the calculated PDIVs using the same uniform field methods as in Chapter 3. This was done for several cables having different types of insulation and different number of layers. In general, the percentage difference of the measured and the calculated PDIVs at 100 kPa is significantly larger than

at 11.6 kPa. In addition it is important to note the percentage differences at 11.6 kPa where negative, showing that the calculated results underestimate the true PDIV. This implies that the calculation results are conservative, providing a safe operating voltage. On the other hand, at 100 kPa results are overestimating the true PDIV.

PD tests under DC conditions have also confirmed the fact that under different cable configurations PD results differ. The difference in PDIVs between the UB and GP configurations is much more at DC than at AC conditions, both at 100 kPa and at 11.6 kPa. PD rates and magnitudes also differ. However, it has to be noted that there is no standard way of figuring out the DC PDIV. The step voltage was set to be very low at around 80 V. The PDIV was selected when PD magnitudes of $\geq$ 5pC where detected, when the PD rate was $\geq$ 1 PD/min.

It has to be noted that there is a big uncertainty in the DC PD results due to the very low PD magnitudes and PD rates. It is due to this fact that it is much more difficult to test for PD under DC than under AC conditions. The slightest noise can provide misleading results even with the use of the balanced circuit. Nevertheless, even if the PD was being generated from other PD sources rather than the cables being tested, the PDIVs were much higher at DC conditions.

7.2.4 AC and DC PD Comparison

Little work can be found in literature regarding testing of aircraft cabling for PD under DC conditions. With the development of the MEA, higher DC voltages have been introduced for transferring electrical power in aircraft and this has resulted in an increased risk of PD. Thus, it is necessary to carry out research in this field. Chapter 6 points out the difficulties faced (when it comes to testing for DC PD), identifies and explains the possible PD noise sources that can affect results and describes the steps carried out to remove these noise sources. A method for determining the PDIV of DC cables is also explained with the appropriate justification. Even though there is an uncertainty as to whether the PD results obtained are from the testing cables or other parts of the testing circuit, PD was generated at higher voltages under DC conditions than under AC conditions. A DC voltage waveform

to be applied for DC PD testing is also proposed. There is no reference in literature on the testing voltage that should be applied for DC PD. In addition, the case where the DC supply voltage might be switched on with a higher step value has been also examined. The use of a higher step up voltage limits the operating voltage that can be applied on the cables. An initial comparison between PD rates, PD magnitudes and PDIVs has been carried out; however more experiments are required to measure the PDIV, making sure that PD is generated from the testing cables. The conclusions of Chapter 6 are described below in detail.

Under DC conditions only one cable type was tested under the UB and GP configurations. As opposed to AC PD tests, DC PD test results have shown that the percentage difference is much bigger, but negative for both configurations at 100 kPa as well as at 11.6 kPa. This suggests that the standard, AS50881: "Wiring Aerospace Vehicle" [11], is not satisfactory for DC cable systems, since it makes no distinction in the determination of a cable's safe operating voltage between AC and DC cable systems.

As shown in Chapter 6, PDIVs are much larger at 100 kPa as well as at 11.6 kPa. This is true for both configurations. PD rates as well as PD magnitudes have been approximately found to be two orders of magnitude smaller under a DC test voltage than under an AC test voltage. This is a positive result, since the use of DC systems can significantly increase the power transfer capability as well as the power to weight ratio of the cable distribution system. In Chapter 3, calculations have shown that the positive and negative DC system is the optimal cable system offering higher power transfer capability and power to weight ratio. The equations used for the DC PDIV calculation were exactly the same as for the AC PDIV calculation. If the PDIV is significantly higher in reality then the DC calculated PDIV results greatly underestimate the true DC PDIV and furthermore greatly underestimate the power transfer capability of the DC system and the power to weight ratio.

7.3 Further Work

The research carried out in all chapters has raised some questions that need to be answered. Several assumptions have also been taken into consideration and the viability of these has to be examined further.

Firstly, voltage optimisation has been carried out without considering the weight of the duct itself. In addition skin and proximity effects were neglected when calculating the current rating of conductors, since the frequency was assumed to be less than 800 Hz. These effects should be taken into consideration at higher operating frequencies, since the use of frequencies up to 1 kHz and possibly greater will become more common. Insulation interfacial effects as well as space charge effects were also ignored when the optimal voltages for the DC cable duct systems were calculated.

Furthermore the increased number of ions in the airgap due to metal ion release due to cosmic radiation has not been taken into account. This phenomenon can be taken into account by considering Townsend's secondary ionisation coefficient.

The impedances and thus the resistive and the reactive losses and voltage drops have to be determined for each cable system that has been examined. As an example the losses for the DC system have been evaluated. This has to be done for all AC systems as well.

The optimisation process has to include the effect of loads and other power system equipment, like for example transformers, power electronic converters etc. If the higher voltage levels selected from the cable system optimisation process result in the use of equipment (circuit breakers, transformers and converters) with thicker insulation and increased weight or volume, then these results have to be compared so that an optimal electrical system voltage is chosen. In addition, with increased DC voltages there are other issues arising related to power system stability, quality and faults.

The optimisation process can be used to assess cables with other conductor and insulation materials installed in different configuration (for example cables installed in a duct of different shape). It must be noted that when larger duct sizes were examined, the

same clearances were assumed between cables. As a result the cable bundle radius was less than 75% of the duct radius. This implies that the cables sizes that can fit into the duct could be made larger that the ones that have been calculated by considering a 4 mm clearance.

When the PCB Vs round cable assessment was carried out in Chapter 4, only the AWG 16 round cable duct system has been compared. Larger conductor systems have to be examined using the same methodology. In addition, the fact that the electric field does not vary linearly with the increase in voltage, has to be incorporated in to the finite element analysis software. For example in *Opera: Vector Fields*, if the boundary condition on the conductor traces is set to be 1 volt, the electric field resulting from that voltage will have a specific value. If the voltage is doubled, the electric field will be doubled. In practice the relationship is not linear and an appropriate formula has to be defined for use in the software. Furthermore the same procedure has to be carried out for DC systems and other AC systems, as the ones that have been investigated in Chapter 3. The design of a PCB with more traces and more layers should also be investigated to observe not only the voltage and electric field distribution, but also the effect that the increased number of traces and layers have on the current rating of the PCB.

PD Tests have to be carried out on similar PCB designs to compare with the theoretical results and the simulations in Opera vector fields. As far as aerospace cables are concerned, AC and DC PD tests have been carried out on one specific type of cable. Ideally the research would have been more complete if cables of the same type but different conductor size and insulation thickness had been tested as well. This way, a relationship could have been obtained between PDIV and cable size. A better comparison between experimental data and measured data would then be possible.

For both AC and PD tests, Results have to be obtained when there is a variation in the ambient as well as in the conductor operating temperature. This would allow the researcher to observe how the PDIV, PD rate and the PD number, is affected with temperature. Under DC conditions the operating temperature would play a vital role in the PDIV, since the resistivity of the insulation changes and thus the voltage across the insulation and across the gap.

An initial research has been carried out by using the same methodology as in Chapter 3, to calculate the DC PDIV. However, calculations have to be adjusted for the DC case because it is the resistivity of the insulation and of the air in the gap that must be used to obtain the fraction of the voltage across the gap and not the relative permittivity.

References

[1] M. Howse, "All electric aircraft," *Power Engineer,* vol. 17, pp. 35-37, 2003.

[2] J. A. Weimer and A. Patterson, "Past, Present and Future of Aircraft Electrical Power Systems,"*39th Aerospace Sciences Meeting and Exhibit* Reno, Nevada: American Institute of Aeronautics and Astronautics (AIAA), 2001.

[3] I. Moir and A. Seabridge, *Aircraft Systems: Mechanical, Electrical and Avionics Sub-Systems Integration*, 2nd ed.: Professional Engineering Publishing, UK, 2001.

[4] B. G. Moffat, E. Abraham, M. P. Y. Desmulliez, D. Koltsov, and A. Richardson, "Failure mechanisms of legacy aircraft wiring and interconnects," *Dielectrics and Electrical Insulation, IEEE Transactions on,* vol. 15, pp. 808-822, 2008.

[5] W. G. Dunbar, "High Voltage Design Criteria," NASA Centre D180-15179-1, NASA-CR-149341, 1972.

[6] Boeing_Commercial_Airlines, "Boeing Aero Magazine QTR_04 07." Issue. 28, 2007.

[7] A. K. Hyder, "A Century of Aerospace Electrical Power Technology," *Propulsion and Power,* vol. 19, No. 16, pp. 1155-1178, 2003.

[8] N. L. Allen and J. Kong, "Effects of Temperature on Corona Onset Characteristics," in *Proceedings of the 14th International Conference on Gas Discharges and their Applications*, Liverpool, 2002.

[9] A. Brockschmidt, "Electrical environments in aerospace applications," in *Electric Machines and Drives, 1999. International Conference IEMD '99*, 1999, pp. 719-721.

[10] W. Khachen, J. Suthar, A. Stokes, R. Dollinger, and W. G. Dunbar, "Aerospace-specific design guidelines for electrical insulation," *IEEE Transactions on Electrical Insulation,* vol. 28, pp. 876-886, 1993.

[11] SAE_Aerospace, "AS50881: Wiring Aerospace Vehicle," Issued 1998-04 and revised 2006-10.

[12] A. J. Nelms, "Electrical Discharge in the More Electric Aircraft Power System", Electrical and Electronic Engineering, The University of Manchester for the degree of Doctor of Philosophy, 2007.

[13] J. P. O'Connor, "A Method for Establishing the Best Voltage Levels for Future Naval Aircraft," Naval Research Laboratory Washington DC 5611, 1961.

[14] D. K. Kelly and J. R. Jancauskas, "Cable sizing-avoid shortcuts and do it right," in *Energy Conversion Engineering Conference, 1996. IECEC 96. Proceedings of the 31st Intersociety*, 1996, pp. 2341-2346

[15] R. J. Van Brunt, "Stochastic properties of partial-discharge phenomena," *Electrical Insulation, IEEE Transactions on,* vol. 26, pp. 902-948, 1991.

[16] G. G. Raju, *Dielectrics in Electric Fields*: CRC Press., 2003.

[17] F. H. Kreuger, *Partial Discharge Detection in High Voltage Equipment*, 2nd ed.: Butterworth & Co. (Publishers) Ltd, 1989.

[18] S. Rowland, "EEPS05: Power System Plant,"*MEng. and MSc. Lectures in Electrical Power Engineering* The University of Manchester, 2006.

[19] T. Blythe and D. Bloor, *Electrical Properties of Polymers*, 2nd ed.: Cambridge University Press, 2005.

[20] P. H. F. Morshuis and J. J. Smit, "Partial discharges at DC voltage: their mechanism, detection and analysis," *Dielectrics and Electrical Insulation, IEEE Transactions on,* vol. 12, pp. 328-340, 2005.

[21] N. H. Malik, A. A. Al-Arainy, and M. I. Qureshi, *Electrical Insulation in Power Systems*: CRC Press, 1997.

[22] E. Kuffel, W. S. Zaengl, and J. Kuffel, *High Voltage Engineering Fundamentals*, 2nd ed.: Butterworth Heinemann, 2000.

[23] R. N. Hampton, "Some of the considerations for materials operating under high-voltage, direct- current stresses," *Electrical Insulation Magazine, IEEE,* vol. 24, pp. 5-13, 2008.

[24] J. V. Hughes and H. L. Armstrong, "The Dielectric Constant of Dry Air," *Journal of Applied Physics,* vol. 23, May 1952.

[25] J. Williams D. Callister, *Material Science and Engineering, An Introduction*, 3rd ed.: John Wiley & Sons, Inc., 1994.

[26] A. Tzimas, "Identification of AC Electro-Thermal Ageing Markers from Artemis Cable Feelings", Engineering, University of Leicester for the degree of Doctor of Philosophy, 2008.

[27] S. Deipino, D. Fabiani, G. C. Montanari, C. Laurent, G. Teyssedre, P. H. F. Morshuis, R. Bodega, and L. A. Dissado, "Polymeric HVDC cable design and space charge accumulation. Part 2: insulation interfaces," *Electrical Insulation Magazine, IEEE,* vol. 24, pp. 14-24, 2008.

[28] G. J. Anders, *Rating of Electric Power Cables in Unfavorable Thermal Environment*: John Wiley & Sons, Inc., 2005.

[29] R. Bartnikas, "Detection of partial discharges (Corona) in electrical apparatus," *Electrical Insulation, IEEE Transactions on,* vol. 25, pp. 111-124, 1990.

[30] BSI, "BS EN 60270: High Voltage Test Techniques-Partial Discharge Measurements," 2001.

[31] U. Fromm, "Interpretation of partial discharges at dc voltages," *Dielectrics and Electrical Insulation, IEEE Transactions on,* vol. 2, pp. 761-770, 1995.

[32] F. H. Kreuger and U. Fromm, "Partial Discharges in Gaseous Voids for DC Voltage," *Jpn. J. Appl. Phys.,* vol. 33, Part 1, No. 2, pp. 1079-1084, 1994.

[33] A. N. Hammoud, M. W. Stavnes, J. L. Suthar, W. Khachen, and J. R. Leghari, "Testing of cable insulation for aerospace applications," in *Electrical Insulation, 1994., Conference Record of the 1994 IEEE International Symposium on*, 1994, pp. 174-177.

[34] J. C. Chan, P. Duffy, L. J. Hiivala, and J. Wasik, "Partial discharge. VIII. PD testing of solid dielectric cable," *Electrical Insulation Magazine, IEEE,* vol. 7, pp. 9-16, 1991.

[35] M. J. P. Jeroense and P. H. F. Morshuis, "Electric fields in HVDC paper-insulated cables," *IEEE Transactions on Dielectrics and Electrical Insulation,* vol. 5, pp. 225-236, 1998.

[36] C. K. Eoll, "Theory of Stress Distribution in Insulation of High-Voltage DC Cables: Part I," *Electrical Insulation, IEEE Transactions on,* vol. EI-10, pp. 27-35, 1975.

[37] P. Morshuis, M. Jeroense, and J. Beyer, "Partial discharge. Part XXIV: The analysis of PD in HVDC equipment," *Electrical Insulation Magazine, IEEE,* vol. 13, pp. 6-16, 1997.

[38] C. K. Eoll, "Theory of Stress Distribution in Insulation of High-Voltage DC Cables Part II," *Electrical Insulation, IEEE Transactions on,* vol. EI-10, pp. 49-54, 1975.

[39] FAA, "Aircraft Electrical Wiring Interconnect System Best Practises: Job Aid Revision 2.0."

[40] FAA and AC43.13-1B, "Federal Aviation Administration, Ch.11: Aircraft Electrical Systems ", 1998.

[41] S. Ghosh and N. K. Kishore, "Modelling partial discharge inception and extinction voltages of sheet samples of solid insulating materials using an artificial neural network," *Science, Measurement and Technology, IEE Proceedings -,* vol. 149, pp. 73-78, 2002.

[42] D. A. Nattrass, "Partial discharge measurement and interpretation," *Electrical Insulation Magazine, IEEE,* vol. 4, pp. 10-23, 1988.

[43] M. C. Halleck, "Calculation of Corona-Starting Voltage in Air-Solid Dielectric Systems," *Power Apparatus and Systems, Part III. Transactions of the American Institute of Electrical Engineers,* vol. 75, pp. 211-216, 1956.

[44] P. Kemp, "The Dielectric Circuit." vol. XVI, H. P. Young, Ed.: The Whitefriars Press Ltd., 1960.

[45] N. H. Malik, A. A. Al-Arainy, A. M. Kailani, and M. J. Khan, "Discharge Inception Voltages Due to Voids in Power Cables," *Electrical Insulation, IEEE Transactions on,* vol. EI-22, pp. 787-793, 1987.

[46] D. Robert, "NASA's Flat Conductor: Wiring for the future?," in *Popular Science*, 1975.

[47] R. Herndon, "Flat Conductor Cable Development," NASA: Marshall Space Flight Center 1973.

[48] AVX, "History of FFC/FPC," ELCO, Available: http://www.avx.com/docs/catalogs/ffchist.pdf.

[49] Clarydon, "Why a Flexible PCB?,"*accessed om Nov. 2010, available at: http://www.clarydon.com/flexible-pcb:* Clarydon Electronic Services Ltd. , 2010.

[50] L. Yun, "On current carrying capacities of PCB traces," in *Electronic Components and Technology Conference, 2002. Proceedings. 52nd*, 2002, pp. 1683-1693.

[51] T. F. Lemczyk, B. Mack, J. R. Culham, and M. M. Yovanovich, "PCB trace thermal analysis and effective conductivity," in *Semiconductor Thermal Measurement and Management Symposium, 1991. SEMI-THERM VII. Proceedings., Seventh Annual IEEE*, 1991, pp. 15-22.

[52] IPC, "IPC-2221A: Generic Standard on Printed Board Design," Association Connecting Electronics Industries, 2003.

[53] IPC, "IPC-2223B: Sectional Design Standard for Flexible Printed Boards," A. C. E. Industry, Ed., 2008.

[54] IPC, "IPC-2222A: Sectional Design Standard for Rigid Organic Printed Boards," Association Connecting Electronics Industries, 2010.

[55] G. Hillman, R. Esser, and J. Mcleish, "Failure Mechanisms in High Voltage Printed Circuit Boards,"*DFR Solutions: White Paper, Available: http://www.dfrsolutions.com/uploads/white-papers*.

[56] J. Duncan Glover and M. S. Sarma, *Power System Analysis and Design*, 3rd ed.: THOMSON LEARNING, 2002.

[57] S. Black, "Composite PCBs,"*Composites Technology, Available: http://www.compositesworld.com/articles/update-composite-pcbs*, 2006.

[58] G. J. Anders, *Rating of Electric Power Cables: Ampacity Computations for Transmission, Distribution and Industrial Applications*: IEEE Press and MCGraw-Hill Companies Inc., 1997.

[59] BSI, "BS EN 3475-307: Cables, electrical, aircraft use. Test methods. Corona extinction voltage," 2005.

[60] M. Vakilian, T. R. Blackburn, O. H. N. Johnson, and B. T. Phung, "Investigation of partial discharge propagation on compact three phase XLPE cables," in *Power Engineering Conference, 2008. AUPEC '08. Australasian Universities*, 2008, pp. 1-6.

[61] M. S. Xin Liu, "Partial Discharge Detection and Analysis in Low Pressure Environments", The Ohio State University for the degree of Doctor of Philosophy, 2006.

[62] S. Bahadoorsingh, "Asset Management and the Role of Power Quality on Electrical treeing in Epoxy Resin", School of Electrical and Electronic Engineering, The University of Manchester for the degree of Doctor of Philosophy, 2009.

[63] Doble_Lemke, "LDS-6 User Manual: Digital Partial Discharge Monitoring System," 2008.

[64] N. Wang, "Partial Discharge Measurement", School of Electrical and Electronic Engineering, The University of Manchester for the degree of Master of Science, 2005.

[65] E. Gulski, "Computer-Aided Registration and Analysis of Partial Discharge in High Voltage Insulation," in *IEE Internatrional Coneference on Partial Discharge*, Canterbury, UK, 1993.

[66] J. Yun, M. Hong, L. Junhua, L. Yu, J. Xiaojuan, X. Rong, and L. Wenjie, "Partial Discharge Pattern Characteristic of HV Cable Joints with Typical Artificial Defect," in *Power and Energy Engineering Conference (APPEEC), Asia-Pacific*, 2010, pp. 1-4.

[67] A. Krivda, "Automated Recognition of Partial Discharges," *IEEE Transactions on Dielectrics and Electrical Insulation,* vol. 2, pp. 796-821, 1995.

[68] T. Tanaka, "PD pulse distribution pattern analysis," in *Properties and Applications of Dielectric Materials, 1994., Proceedings of the 4th International Conference on*, 1994, pp. 662-665 vol.2.

[69] L. Wang, A. Cavallini, G. C. Montanari, L. Testa, and T. Spa, "Patterns of partial discharge activity in XLPE: From inception to breakdown," in *Solid Dielectrics (ICSD), 10th IEEE International Conference on*, 2010, pp. 1-4.

[70] Tyco_Electronics, "Specification Control Drawing: RCW5986, Revision D," 2008.

[71] U. Fromm, *Partial Discharge and Breakdown Testing at High DC Voltage*: Delft University Press, 1995.

Appendix A: List of Publications

A.1 Journal Papers:

[1]. I. Christou, I. Cotton, A. Nelms and Mark Husband, "Choice of Optimal Voltage for More Electric Aircraft Wiring Systems", IET Electrical Systems in Transportation, 2010.

A.2 Conference Papers:

[1]. I. Christou, I. Cotton, "Methods for Partial Discharge Testing of Aerospace Cables", Electrical Insulation (ISEI), Conference Record of the 2010 IEEE International Symposium on Electrical Insulation, June 2010.

[2]. I. Christou, I. Cotton, "Partial Discharge Behaviour of Aircraft Wiring", SAE International: Power Systems Conference, November 2010.

Appendix B: AC PD Test Results Using the Lemke LDS-6

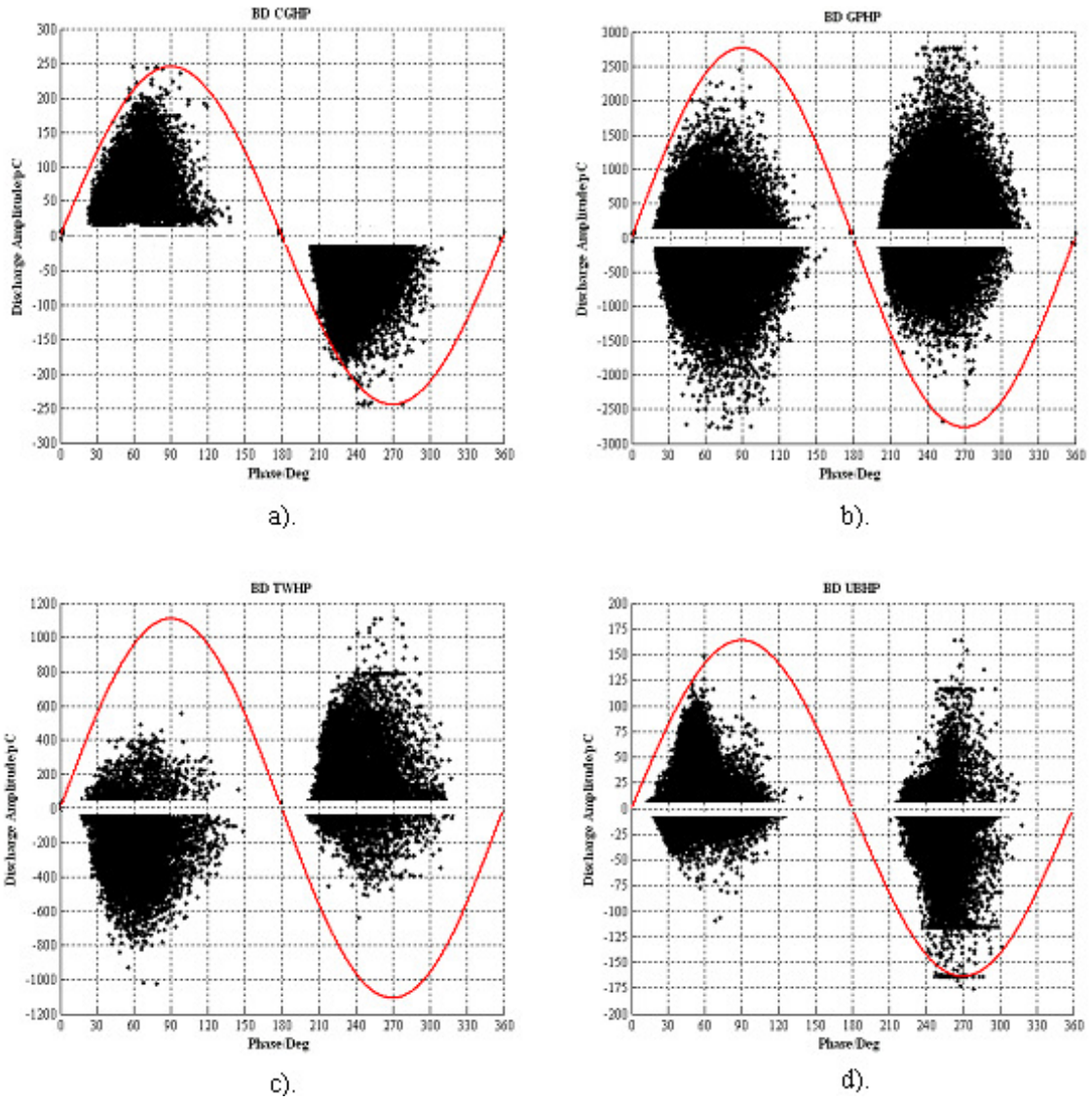

Figure B1.1: PD magnitude phase-resolved plots at 100 kPa for: a). CG, b). GP, c) TW and d). UB cable configurations with the use of a balanced PD detection circuit, including a 1000 pF coupling capacitor

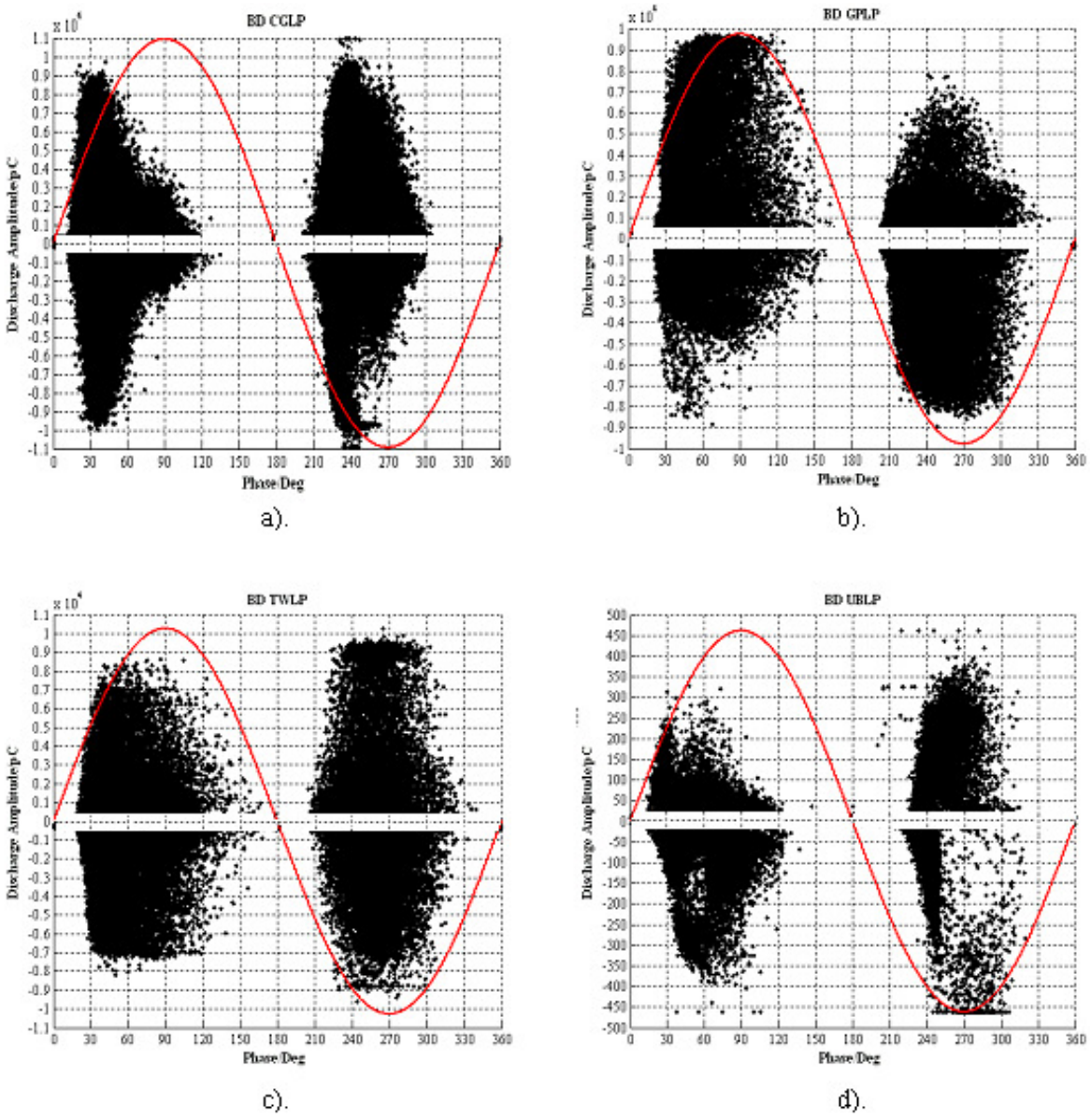

Figure B1.2: PD magnitude phase-resolved plots at 11.6 kPa for: a). CG, b). GP, c) TW and d). UB cable configurations with the use of a balanced PD detection circuit, including a 1000 pF coupling capacitor

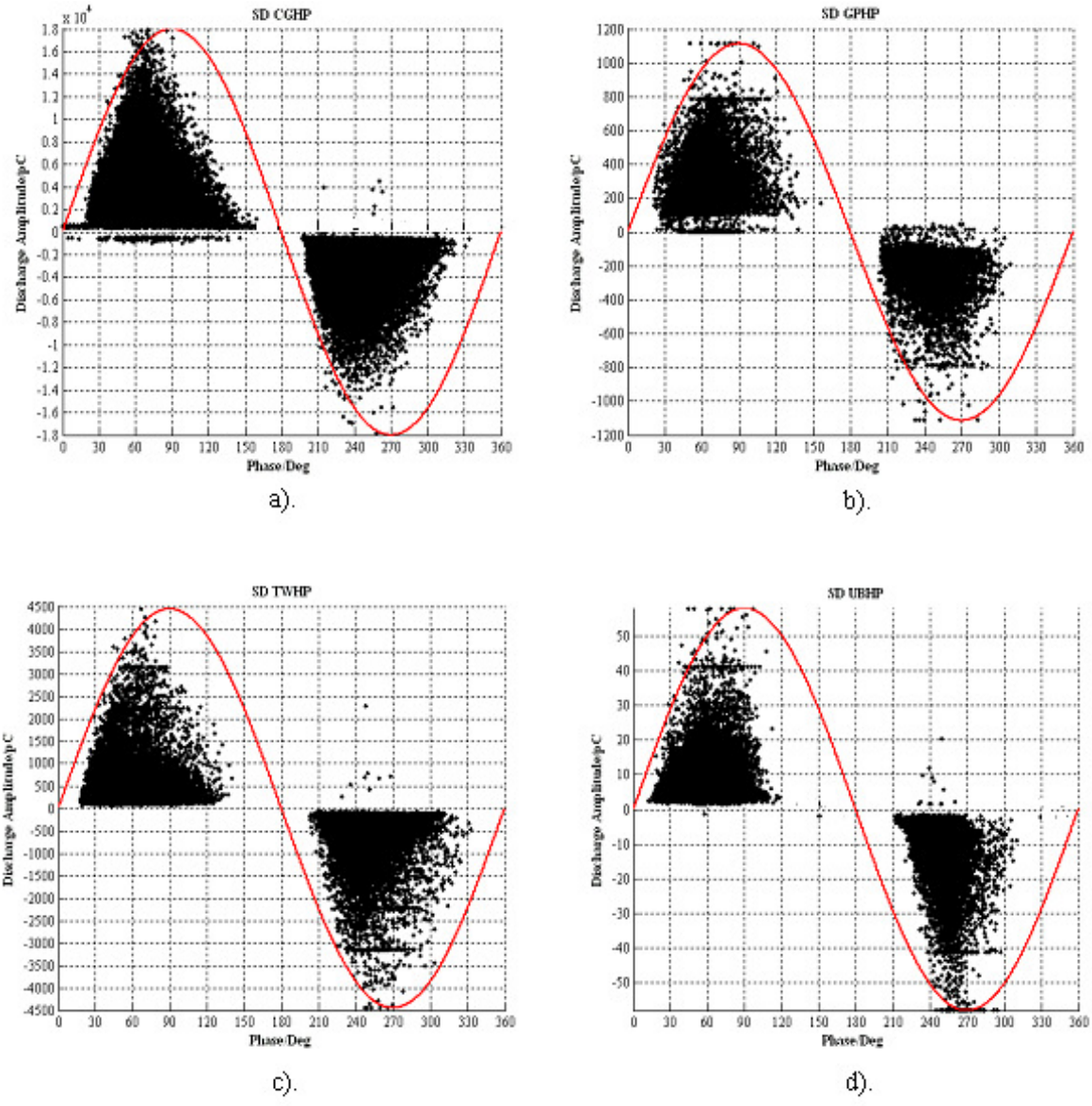

Figure B2.1: PD magnitude phase-resolved plots at 100 kPa for: a). CG, b). GP, c) TW and d). UB cable configurations with the use of a straight PD detection circuit

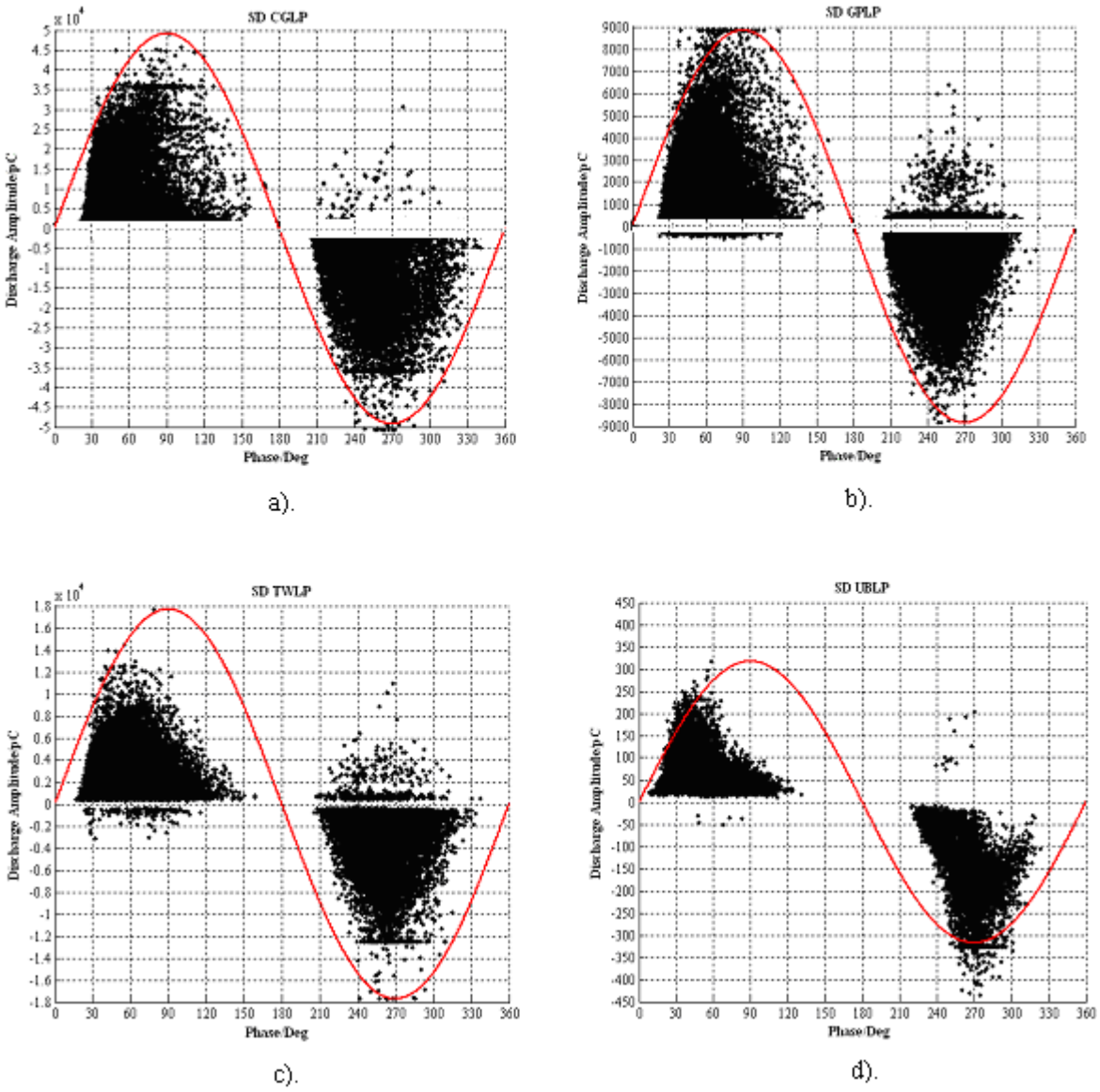

Figure B2.2: PD magnitude phase-resolved plots at 11.6 kPa for: a). CG, b). GP, c) TW and d). UB cable configurations with the use of a straight PD detection circuit

Appendix C-1:

Derivation of Equations for Calculating Maximum Cable Size in a Duct

Three Cables in a Duct

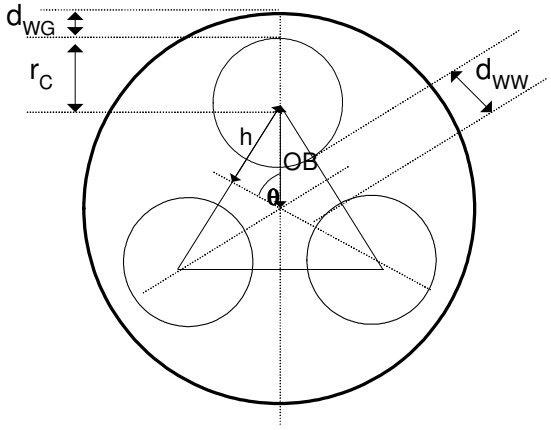

Derivation of Equation

$$r_{duct} = OB + r_C + d_{WG}$$

$$OB = ?, \theta = 60^o$$

$$\Rightarrow OB = \frac{h}{\sin 60^o}$$

$$\Rightarrow h = r_C + \frac{d_{WW}}{2}$$

$$\Rightarrow OB = \left(\frac{r_C + {d_{WW}}/{2}}{\sin 60^o} \right) = \frac{r_C + {d_{WW}}/{2}}{{\sqrt{3}}/{2}} = \frac{2r_C + d_{WW}}{\sqrt{3}}$$

$$\Rightarrow r_{duct} = \left(\frac{2r_C + d_{WW}}{\sqrt{3}} \right) + r_C + d_{WG}$$

$$\Rightarrow r_{duct} = r_C \left({2}/{\sqrt{3}} + 1 \right) + \left({1}/{\sqrt{3}} \right) d_{WW} + d_{WG}$$

$$\Rightarrow r_C = \frac{r_{duct} - \left({1}/{\sqrt{3}} \right) d_{WW} - d_{WG}}{\left({2}/{\sqrt{3}} + 1 \right)}$$

Four Cables in a Duct

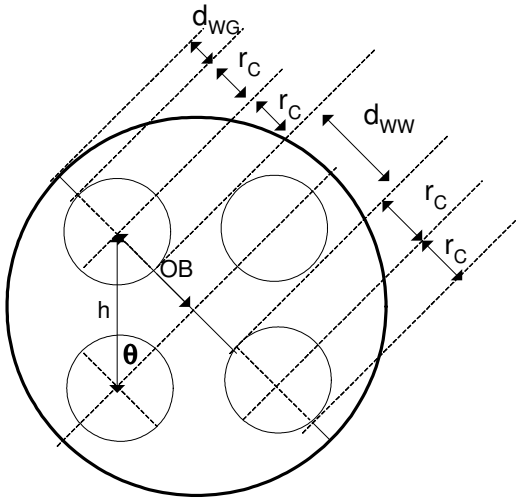

Derivation of Equation

$$r_{duct} = OB + 2r_C + d_{WG}$$

$$OB = ?, \theta = 45^o$$

$$\Rightarrow OB = h \times \sin 45^o$$

$$\Rightarrow h = 2r_C + d_{WW}$$

$$\Rightarrow OB = \left(\frac{2r_C + d_{WW}}{\sqrt{2}} \right)$$

$$\Rightarrow r_{duct} = \left(\frac{2r_C + d_{WW}}{\sqrt{2}} \right) + r_C + d_{WG}$$

$$\Rightarrow r_{duct} = r_C \left(1 + \sqrt{2} \right) + \left({1}/{\sqrt{2}} \right) d_{WW} + d_{WG}$$

$$\Rightarrow r_C = \frac{r_{duct} - \left({1}/{\sqrt{2}} \right) d_{WW} - d_{WG}}{\left(1 + \sqrt{2} \right)}$$

Six Cables in a Duct

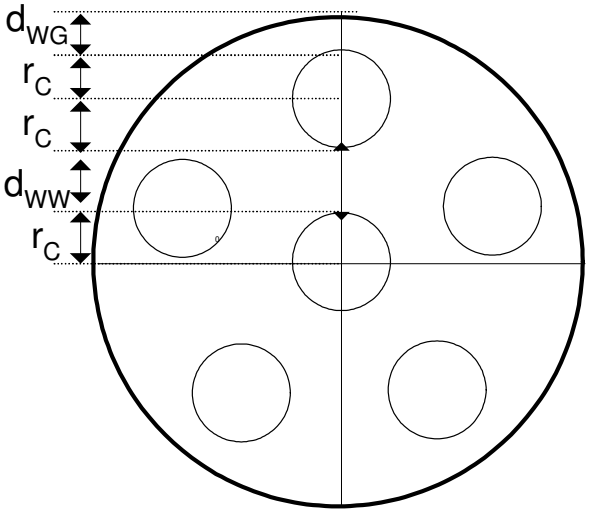

Derivation of Equation

$$r_{duct} = 3r_C + d_{WW} + d_{WG}$$
$$\Rightarrow r_C = \frac{r_{duct} - d_{WW} - d_{WG}}{3}$$

Seven Cables in a Duct

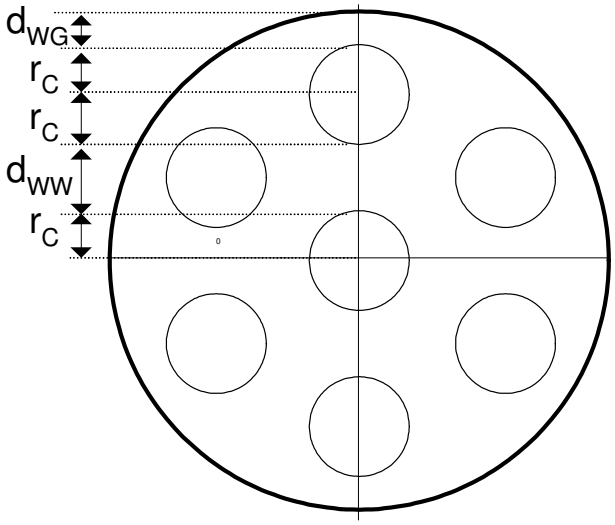

Derivation of Equation

$$r_{duct} = 3r_C + d_{WW} + d_{WG}$$
$$\Rightarrow r_C = \frac{r_{duct} - d_{WW} - d_{WG}}{3}$$

Appendix C-2:

Derivation of Equation for Analysing Different PCB Geometries

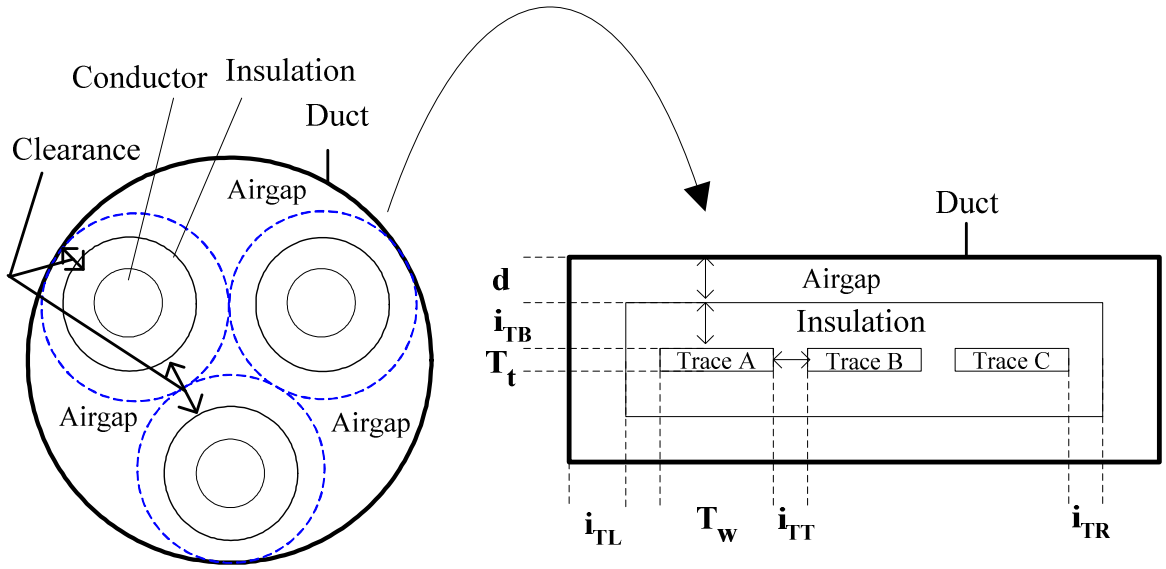

In order to analyse the PCB system and to compare it with a round cable system in a duct, certain assumptions have been taken into account:

1. *Total cross sectional area of round cable conductors = total cross sectional area of trace conductors in the PCB*
2. *Total cross sectional area of insulation in round cable system = total cross sectional area of insulation in the PCB. The area total cross sectional area of the insulation is symbolised as* i_A
3. $i_{TT} = \lambda i_{TB}$
4. $i_{TB} = i_{TL} = i_{TR}$
5. $N_{T(TB)}$ = *Number of Traces along the thickness of the PCB* (PCB_t)
6. $N_{T(LR)}$= *Number of Traces along the width of the PCB* (PCB_W)

Taking into consideration the above assumptions the total PCB insulation cross sectional area can be expressed as in Equation (1):

$$\begin{aligned} i_A &= (i_{TT}T_t)\left(N_{T(LR)}-1\right)\left(N_{T(TB)}\right)+2(i_{TB}T_t)\left(N_{T(TB)}\right)+..... \\ &.....2i_{TB}^2\left(N_{T(TB)}+1\right)+(i_{TB}T_W)\left(N_{T(TB)}+1\right)\left(N_{T(LR)}\right)+..... \\ &.....(i_{TT}i_{TB})\left(N_{T(LR)}-1\right)\left(N_{T(TB)}+1\right) \end{aligned} \quad (1)$$

Since $i_{TT} = \lambda i_{TB}$ substitute into the equation to get:

$$\begin{aligned} i_A &= (\lambda i_{TB}T_t)\left(N_{T(LR)}-1\right)\left(N_{T(TB)}\right)+2(i_{TB}T_t)\left(N_{T(TB)}\right)+..... \\ &.....2i_{TB}^2\left(N_{T(TB)}+1\right)+(i_{TB}T_W)\left(N_{T(TB)}+1\right)\left(N_{T(LR)}\right)+..... \\ &.....(\lambda i_{TB}^2)\left(N_{T(LR)}-1\right)\left(N_{T(TB)}+1\right) \end{aligned} \quad (2)$$

Simplify Equation (2) by sorting the coefficients of i^2_{TB} and i^2_{TB} to get:

$$\begin{aligned} i_A &= i_{TB}^2\left[2\left(N_{T(TB)}+1\right)+\lambda\left(N_{T(TB)}+1\right)\left(N_{T(LR)}-1\right)\right]+..... \\ &....i_{TB}\left[\lambda T_t\left(N_{T(LR)}-1\right)\left(N_{T(TB)}\right)+2T_t\left(N_{T(TB)}\right)+T_W\left(N_{T(TB)}+1\right)\left(N_{T(LR)}\right)\right] \end{aligned} \quad (3)$$

Simplify the coefficient of i^2_{TB} to get:

$$\left[2\left(N_{T(TB)}+1\right)+\lambda\left(N_{T(TB)}+1\right)\left(N_{T(LR)}-1\right)\right]=\left(N_{T(TB)}+1\right)\left(2+\lambda\left(N_{T(LR)}-1\right)\right)$$

Furthermore divide every part Equation (3) by the coefficient of i^2_{TB} to get Equation (4):

$$\begin{aligned} &i_{TB}^2+\left[\frac{\lambda T_t\left(N_{T(LR)}-1\right)N_{T(TB)}+2T_tN_{T(TB)}}{\left(N_{T(TB)}+1\right)\left(2+\lambda\left(N_{T(LR)}-1\right)\right)}+\frac{T_W}{\left(2+\lambda\left(N_{T(LR)}-1\right)\right)}\right]i_{TB}-..... \\ &.....\frac{i_A}{\left(N_{T(TB)}+1\right)\left(2+\lambda\left(N_{T(LR)}-1\right)\right)}=0 \end{aligned} \quad (4)$$

Simplify equation (4) to get equation (5):

$$i_{TB}^2+\left[\frac{\lambda T_t\left(N_{T(LR)}-1\right)N_{T(TB)}+2T_tN_{T(TB)}}{\left(N_{T(TB)}+1\right)\left(2+\lambda\left(N_{T(LR)}-1\right)\right)}+\frac{T_WN_{T(LR)}}{\left(2+\lambda\left(N_{T(LR)}-1\right)\right)}\right]i_{TB}-.....$$
$$.....\frac{i_A}{\left(N_{T(TB)}+1\right)\left(2+\lambda\left(N_{T(LR)}-1\right)\right)}=0 \quad (5)$$

Simplify the numerator of one of the coefficients of i^2_{TB}, the one that is circled in Equation (5) to get:

$$\lambda T_t\left(N_{T(LR)}-1\right)N_{T(TB)}+2T_tN_{T(TB)}=T_tN_{T(TB)}\left(2+\lambda\left(N_{T(LR)}-1\right)\right)$$

Furthermore simplify the circled part of Equation (5) to get Equation (6):

$$i_{TB}^2+\left[\frac{T_tN_{T(TB)}}{\left(N_{T(TB)}+1\right)}+\frac{T_WN_{T(LR)}}{\left(2+\lambda\left(N_{T(LR)}-1\right)\right)}\right]i_{TB}-\frac{i_A}{\left(N_{T(TB)}+1\right)\left(2+\lambda\left(N_{T(LR)}-1\right)\right)}=0 \quad (6)$$

Remember that $N_{T(TB)}$ represents the number of traces from the top to the bottom of the PCB, i.e. along the thickness of the PCB. Also $N_{T(LR)}$ represents the number of traces left to the right, along the width of the PCB. In this thesis a simple model PCB geometry has been used, consisting of $N_{T(TB)} = 1$ and $N_{T(LR)} = 3$ (i.e. 1 layer of 3 traces in the PCB model). Thus, Equation (6) simplifies to Equation (7) which is actually Equation 4.1 shown in Chapter 4, Section 4.2 in this thesis:

$$i^2_{TB}+\frac{1}{2}\left(T_t+\frac{3T_W}{1+\lambda}\right)i_{TB}-\frac{1}{4}\left(\frac{i_A}{1+\lambda}\right)=0 \quad (7)$$